STATE-BASED SIMULATIONS OF TUMOR RESPONSE TO RADIOTHERAPY

A Dissertation presented to the Faculty of the Graduate School
University of Missouri

In Partial Fulfillment
Of the Requirements for the Degree

Doctor of Philosophy

by
JEHO JEONG

Dr. Joseph O. Deasy and Dr. Sudarshan K. Loyalka,
Dissertation Supervisors

MAY 2012

The undersigned, appointed by the Dean of the Graduate School, have examined the dissertation entitled

STATE-BASED SIMULATIONS OF TUMOR RESPONSE TO RADIOTHERAPY

Presented by Jeho Jeong

A candidate for the degree of Doctor of Philosophy

And hereby certify that in their opinion it is worthy of acceptance.

Dr. Joseph O. Deasy

Dr. Sudarshan K. Loyalka

Dr. Tushar K. Ghosh

Dr. Mark A. Prelas

Dr. Dharanipathy Rangaraj

Dr. Michael R. Lewis

To my devoted parents, supportive wife,
and precious daughters, Grace and Sarah…

ACKNOWLEDGEMENTS

I would like to thank all of those who provided academic education to me during my graduate study. I would especially like to express my sincere gratitude and appreciation to my wonderful advisors, *Dr. Joseph O. Deasy* and *Dr. Sudarshan K. Loyalka,* for their guidance, encouragement, and assistance in the completion of my degree. Their devoted support and care always helped me to face both scientific and personal challenges successfully. I also want to thank all my committee members, *Dr. Mark A. Prelas*, *Dr. Tushar K. Ghosh*, *Dr. Dharanipathy Rangaraj,* and *Dr. Michael R. Lewis*, for their support and valuable suggestions in my research work.

I am thankful for the kind support from the staff, *Latrícia Vaughn* and *James Bennett*, and fellow students of the Nuclear Science and Engineering Institute (NSEI). Also, I want to thank *Gail Countie* at Washington University in St. Louis for her assistance.

I would like to express my earnest gratitude to my parents for their love and sacrifice. I want to thank my sister for supporting me in many ways. I want to thank my wife, *Misook Kim*, for her patience, support, and being there for me through difficult times. Finally, I want to thank my daughters *Grace* and *Sarah* for making me laugh and forget about my worries.

TABLE OF CONTENTS

LIST OF FIGURES

Figure **Page**

LIST OF TABLES

Table **Page**

STATE-BASED SIMULATIONS OF TUMOR RESPONSE TO RADIOTHERAPY

Jeho Jeong

Dr. Joseph O. Deasy and Dr. Sudarshan K. Loyalka,
Dissertation Supervisors

ABSTRACT

A tumor is comprised of biologically different subdivisions and microenvironmental factors affect the treatment response to radiation therapy (RT). In this work, a state-based tumor response model was developed based on well-established radiobiological principles to evaluate the treatment response for various microenvironmental conditions. Clinically important phenomena, including the interplay between proliferation and hypoxia, were evaluated and the results suggest the existence of an optimal fractionation schedule depending on microenvironmental factors. Including the cell cycle effect into the model, the treatment efficacy of hypofractionated radiotherapy was explored. The evaluated efficacy was underestimated compared to the observed high local control rates, which implies alternative effects in the hypofractionated RT. Based on the clinically observed adverse outcome of high FDG uptake, possible FDG uptake mechanism was also explored, which was evaluated to be associated with metabolically-viable hypoxic cells. This mathematical framework can contribute as a useful tool in testing the common radiobiological assumptions with clinical data and generating hypothesis.

CHAPTER 1

INTRODUCTION

1.1. Nature of the problem

In cancer treatment, radiation therapy (RT) has played a crucial role. Nowadays, almost two-thirds of all cancer patients are treated by RT as definite or adjuvant therapy[1]. There were a lot of efforts to increase the accuracy and the effectiveness of RT in cancer treatment. For example, three dimensional conformal radiation therapy (3DCRT), four dimensional radiation therapy (4DRT), intensity-modulated radiation therapy (IMRT), image-guided radiation therapy (IGRT), tomo-therapy, and arc-therapy are the results of the efforts and have changed the world of RT (Bucci *et al*., 2005). However, the treatment plan is still based on the concepts of gross tumor volume (GTV), clinical tumor volume (CTV), planned tumor volume (PTV), and organ at risk (OAR), which do not consider the variations of radiobiological factors in the target volume. The treatment plans of RT are usually generated to deliver the maximally achievable uniform dose to the target volume until the doses to the surrounding OARs do not exceed the dose constraints. This is based on the belief that the uniform dose distribution is desirable, since the highest tumor control was thought to be acquired when the dose is spatially uniform (Webb *et al*., 1994). Also, the understanding about the inhomogeneity throughout the target volume was insufficient without molecular imaging technique. In clinic, the dose to

[1] Based on the fast facts about radiation therapy, ASTRO website: http://www.astro.org/PressRoom/FastFacts/documents/FFAboutRT.pdf

the tumor is determined by the clinical experiences, depending mainly on conventional prognostic factors such as site, size, and stage.

However, the long clinical experiences with the uniform dose distribution have shown that there exist significant variations in the outcome, even when similar outcomes were expected considering those conventional prognostic factors and treatment regime. The cause of these variations could be explained with the advances of molecular imaging and histophatologic analysis (Shields *et al*., 1998; Varia *et al*., 1998; Pugachev *et al*., 2005; Krohn *et al*., 2008). With the aid of those techniques, it was revealed that a significant level of heterogeneity exists in a tumor, which might affect the tumor response to radiation therapy. A tumor is comprised of biologically different subdivisions; the most well-known factors for this heterogeneity are hypoxia, proliferation, and glucose metabolism (Marusyk & Polyak, 2009).

These heterogeneity factors have attracted attention as indices for outcome prediction and therapeutic decision-making. Many researchers have performed survival analysis based on the PET images with the various biomarkers such as ^{18}F-FDG, ^{18}F-FLT, ^{18}F-FMISO and ^{60}Cu-ATSM (Chen *et al*., 2005; Thorwarth *et al*., 2005; Rajendran *et al*., 2006; Kidd *et al*., 2007; van Baardwijk *et al*., 2007; Dehdashti *et al*., 2008; Xie *et al*., 2009). The results have shown that the enhanced uptake of these biomarkers has adverse effects on the tumor response to the RT and the outcome. Other researchers have shown that the recurrence often occurs in the high FDG uptake region in a tumor (Soto *et al*., 2008; Sura *et al*., 2008). Considering the heterogeneity of the tumor, it is believed that the dose boosting can significantly increase the tumor control probability (TCP) when the boost dose is assigned to biologically more malignant region of the tumor (Tomé &

Fowler, 2000; Bentzen, 2005). These days, many researchers are investigating the effectiveness of selective dose boosting or dose redistribution based on PET images. Several planning studies have demonstrated that the PET image-based selective dose boosting can improve the effectiveness of the treatment (Popple *et al*., 2002; Das *et al*., 2004; Vanderstraeten *et al*., 2006; Madani *et al*., 2007a; Thorwarth *et al*., 2007).

The capability to accurately deliver ionizing radiation in cancer therapy has amazingly increased with the recent advances in RT techniques. More attention should be paid to the biologically relevant target definition and more efficient therapeutic strategy considering the tumor heterogeneity and microenvironment.

1.2. Background

1.2.1. Tumor heterogeneity

Tumors are comprised of biologically different subdivisions (Heppner, 1984; Marusyk & Polyak, 2009). This intra-tumor heterogeneity is thought to be caused by the adaptation process of cancer cell to the microenvironment. Several heterogeneous factors, such as hypoxia, proliferation and metabolism, attracted attention as indices for the outcome prediction and therapeutic decision-making.

Hypoxia is one of the most important and well-known factors of tumor heterogeneity. Hypoxia arises from the uncontrolled growth of a tumor (Höckel & Vaupel, 2001b). Since the tumor usually grows faster than the vascular supply, the cells distant from the vascular structure become deficient of oxygen and nutrients, forming a hypoxic region. At a greater distance from the blood vessel, tumor necrosis may occur.

The hypoxia has long been considered as a negative prognostic factor. Many studies have shown that the level of hypoxia is a predictive factor for local control and survival (Dehdashti *et al*., 2003; Thorwarth *et al*., 2005; Rajendran *et al*., 2006; Dehdashti *et al*., 2008). This is not only because the hypoxic cells are more resistant to nonsurgical radiotherapy and chemotherapy (Brown, 1999; Brown, 2002; Brown & Wilson, 2004), but also because the hypoxic cells are known to promote malignant progression by stimulating angiogenesis, proliferation and metastasis (Höckel & Vaupel, 2001a; Vaupel & Mayer, 2007). It is found that the hypoxia-inducible factor 1 (HIF-1) is the main cause of the malignant progression of hypoxic tumor and inhibition of the HIF-1 can be a possible target of cancer treatment (Semenza, 2003).

The radiation dose necessary to achieve the same biologic effect, known as the oxygen enhancement effect, is about three times higher in the absence of oxygen than in the normal oxygen level (Hall & Giaccia, 2006). This implies that more aggressive therapy for the hypoxic region may improve the outcome. Several planning studies showed that the therapeutic response might be improved by selectively boosting the dose to the hypoxic region identified by PET imaging (Popple *et al*., 2002; Thorwarth *et al*., 2007).

It is important to identify the level of hypoxia in a tumor and the spatial location of hypoxic region for both the estimation of the prognosis and the effective therapy. The level of hypoxia is difficult to predict by other tumor parameters such as tumor size, grade, and level of necrosis. Instead, immunohistochemical staining with pimonidazole or EF5 and non-invasive PET imaging with different biomarkers, such as FMISO and Cu-ATSM, can be used for this purpose (Varia *et al*., 1998; Padhani, 2006; Krohn *et al*., 2008; Scigliano *et al*., 2008; Carlin *et al*., 2009; Wang *et al*., 2009). The oxygen level has

been observed to be fluctuating throughout the tumor and several studies have shown that the resulting intermittent hypoxia increases the aggressiveness of the tumor (Graeber *et al*., 1996; Cairns *et al*., 2001; Martinive *et al*., 2006; Cárdenas-Navia *et al*., 2008).

Tumor cell proliferation is generally decreasing as the distance from vascular structure to the cell increases, which is the opposite of the hypoxia. It has been shown that the level of proliferation is reduced in the hypoxic cells (Kennedy *et al*., 1997; Evans *et al*., 2001). The proliferation index also has been regarded as a negative prognostic factor for many different tumors (Ishida *et al*., 1993; Larsson *et al*., 1993; Müller *et al*., 1996; Viberti *et al*., 1997; Hoos *et al*., 2001; Valera *et al*., 2005). The level of proliferation can be visualized by the immunohistochemical staining with Ki-67 or by FLT-PET imaging (Shields *et al*., 1998; Buck *et al*., 2003; Been *et al*., 2004; Chen *et al*., 2005; Yamamoto *et al*., 2007).

The increased level of proliferation had been thought to be a cause of tumor repopulation, which can be beneficial from accelerated hyperfractionated radiotherapy (Kim & Tannock, 2005). However, clinical studies showed the opposite result: that less proliferating tumors benefit from the acceleration (Sakata *et al*., 2000; Wilson *et al*., 2006).

Most tumors have shown increased glucose uptake as a result of upregulated glycolysis (Gatenby & Gillies, 2004). Enhanced glycolysis might be a result of hypoxia, because hypoxic cells produce energy through glycolysis without oxygen. However, it is known that tumor cells showed increased glycolysis even in the presence of oxygen, known as Warburg effect (Warburg, 1956). This aerobic glycolysis is thought to be caused by a number of genetic changes in a malignant tumor (Dang & Semenza, 1999; Kim & Dang, 2006; Heiden *et al*., 2009).

The pattern of glucose uptake in a tumor also has a spatial variation and can be seen by ^{18}F-fluorodeoxyglucose (FDG) positron emission tomography (PET) imaging. The FDG-PET has become an important clinical tool for cancer detection, staging, and monitoring of response after therapy. Although there are several contrary results (Vesselle *et al*., 2007; Agarwal *et al*., 2009), many clinical studies have shown that the uptake of FDG, usually measured as a standardized uptake value (SUV), is a significant predictor of prognosis (Ahuja *et al*., 1998; Vansteenkiste *et al*., 1999; Dhital *et al*., 2000; Jeong *et al*., 2002; Downey *et al*., 2004; Borst *et al*., 2005; Cerfolio *et al*., 2005; Sasaki *et al*., 2005; Xue *et al*., 2006; Kidd *et al*., 2007; van Baardwijk *et al*., 2007; Casali *et al*., 2009; Chen *et al*., 2009; Xie *et al*., 2009). Also, the FDG uptake pattern after therapy correlates with the tumor response and the survival rate (Grigsby *et al*., 2003; Mac Manus *et al*., 2003; Grigsby *et al*., 2004; Mac Manus *et al*., 2005; Kong *et al*., 2007; Schwarz *et al*., 2007; van Loon *et al*., 2009).

Based on the hypothesis that the level of glucose uptake is indicative of the level of malignancy and resistance to the therapy, the FDG based dose boosting method is under study (Das *et al*., 2004; Vanderstraeten *et al*., 2006; Petit *et al*., 2009; Feng *et al*., 2009). Also the FDG based GTV delineation is thought to be a better method for target definition than conventional CT for some types of tumor and the standardization of the method is under investigation (Bradley *et al*., 2004; Daisne *et al*., 2004; Biehl *et al*., 2006; van Baardwijk *et al*., 2006; Janssen *et al*., 2009; Zhong *et al*., 2009).

The underlying mechanism of glucose uptake in a tumor is still unclear and there are many studies that have been carried out to correlate FDG uptake with other physiological parameters, such as hypoxia, proliferation, blood flow, histology, and differentia-

tion, using PET, immunostaining method, and histology (Vesselle *et al*., 2000; Rajendran *et al*., 2004; Pugachev *et al*., 2005; Hara *et al*., 2006; Zimny *et al*., 2006; Kelly *et al*., 2007; Yamamoto *et al*., 2007; Buchmann *et al*., 2008; Dierckx & Van De Wiele, 2008; Vesselle *et al*., 2008; Bruechner *et al*., 2009). Although many studies found the relationship between the FDG uptake and hypoxia (Rajendran *et al*., 2004; Pugachev *et al*., 2005; Zimny *et al*., 2006; Kelly *et al*., 2007; van Baardwijk *et al*., 2007), there may be many other factors that affect the glucose uptake. Recently, it is found that lactate, a byproduct of glycolysis in hypoxic cells, is used as a fuel for the oxidative metabolism in normoxic cells and the inhibition of lactate-fueled respiration seems to have a potential for cancer therapy (Semenza, 2008; Sonveaux *et al*., 2008).

1.2.2. TCP model

In order to evaluate the effectiveness of the RT plan, the tumor control probability (TCP) is widely used as an index. The TCP, as the term itself implies, is the probability that all the clonogenic cells in the target are controlled or destroyed by the therapy. Based on the TCP, the tumor response and the prognosis can be predicted and the treatment regime can be chosen. When the estimated TCP of a treatment plan seems too low for a patient, for example, the plan can be altered to be more aggressive by manipulating the dose and/or fractionation, so that the chance of control can be increased.

The TCP model can be divided into two categories, the empirical and mechanistic (Goitein, 2008). The empirical TCP models, such as probit and logistic TCP models, are based on the dose-response curve derived from the clinical outcome data, which have a typical sigmoid shape. These models are basically a curve-fitting of the clinical data and

fully determined by two parameters, the median response dose and a parameter related to the slope of the curve at this median dose. The probit and logistic models are almost identical and the difference is not distinguishable in the clinical level (Schultheiss *et al*., 1983). The logistic TCP model is given in the following form:

$$TCP(D) = \frac{1}{1 + \left(\frac{TD_{50}}{D} \right)^{4\gamma_{50}}} \tag{1.1}$$

where TD_{50} is the tumor dose at which 50% of TCP is expected and γ_{50} is the slope of the curve at TD_{50}. The empirical TCP models are simple and convenient for estimating the tumor response in terms of radiation dose, but they have no radiobiological basis and therefore the estimated parameters have no biological interpretation (Joiner & Kogel, 2009).

The mechanistic TCP models try to describe the basic biological mechanism of the tumor response to the radiation therapy from the cellular level. Although some minor variants exist, there is basically only one mechanistic TCP model. This model is based on both Poisson statistics for the probability calculation of local control and the linear-quadratic cell-kill model for the estimation of survival fraction (Brenner, 1993; Niemierko & Goitein, 1993; Webb & Nahum, 1993). The main assumption of the model is that the tumor consists of a large number of clonogens which do not interact with each other and the tumor control is obtained when all the clonogenic cells are sterilized. The probability of tumor control (TCP) can be expressed with binomial statistics as the following equation:

$$TCP = \left(1 - SF(D)\right)^{N} \tag{1.2}$$

where N is the number of initial clonogens and $SF(D)$ is the survival fraction as a function of dose. Since the survival fraction becomes very small at the end of cancer treatment, this binomial equation can be approximated to the Poisson equation as the following:

$$TCP = \exp\left(-N \cdot SF(D)\right) \tag{1.3}$$

The survival fraction is estimated from the well-known linear-quadratic model of cell survival as the following equation:

$$SF(D) = \exp\left[-\alpha D\left(1 + \frac{\beta}{\alpha} d\right)\right] \tag{1.4}$$

where α and β are the radiosensitivity parameters, D is the total dose and d is fractional dose. By implementing the survival fraction into the equation, the TCP can be expressed as the following equation:

$$TCP = \exp\left\{-N \cdot \exp\left[-\alpha D\left(1 + \frac{\beta}{\alpha} d\right)\right]\right\} \tag{1.5}$$

This Poisson TCP equation is the basis of the mechanistic TCP model. Although the shape of the plot for this model is the same sigmoidal curve as the empirical models, the parameters used in this model (α and β) have radiobiological meaning and represent

the radiosensivity of a specific type of tumor. Also, the α/β ratio of a specific tumor has implications about the dose fraction effect to the TCP (Thames *et al*., 1990). However, the slope of the curves obtained from the equation is much steeper than those from clinical dose-response data, which was attributed to the inter-tumor (patient-to-patient) heterogeneity in radiosensitivity. By incorporating a distribution of the radiosensitivity values, reasonable TCP curves can be generated (Bentzen, 1992; Suit *et al*., 1992; Niemierko & Goitein, 1993; Webb & Nahum, 1993; Keall & Webb, 2007). Webb and Nahum (1993) also investigated the effect of non-uniform clonogen density and non-uniform dose distribution on the TCP. They incorporated these non-uniformities to the model by dividing a tumor into small tumorlets within which the clonogen density and dose become almost uniform. The total TCP can be estimated from the product of the TCPs of each tumorlet, also known as voxel control probability (VCP). This is based on the reasonable assumption that the control probability of a tumorlet is independent of all the others and can be expressed as the following equation (Sanchez-Nieto & Nahum, 1999; Buffa & Nahum, 2000):

$$TCP_{total} = \prod_i TCP_i = \prod_i \exp\left(-\rho_i \cdot v_i \cdot SF(d_i)\right) \tag{1.6}$$

where TCP_i is the control probability of i^{th} tumorlet, ρ_i and v_i are the clonogen density and the volume of the tumorlet and $SF(d_i)$ is the survival fraction of a tumorlet with the radiation dose of d_i. Based on this equation, the TCP of a heterogeneous tumor treated by non-uniform dose distribution can be estimated. An important feature of the TCP model can be deduced from this equation: the total TCP can never exceed the control probability

of an individual tumorlet. When the same level of survival fraction and the clonogen density are assumed, the TCP is decreasing as the number of tumorlets increases and this can explain the observed tumor volume effect on the tumor control probability (Agren Cronqvist *et al*., 1995; Johnson *et al*., 1995; Bentzen & Thames, 1996; Buffa *et al*., 2000).

The Poisson TCP model discussed so far has an important practical limitation in that it does not take into account the clongen repopulation during the course of radiation therapy. The repopulation of the tumor might occur during the radiation therapy and is considered as one of the critical factors of treatment failure (Kim & Tannock, 2005). After radiation therapy, the proliferation rate of the surviving cells becomes faster than before, known as accelerated repopulation (Joiner & Kogel, 2009). Also, the prolongation of the overall treatment time is known to cause the loss of local control (Bentzen *et al*., 1991; Fowler & Chappell, 1994; Hendry *et al*., 1996). To take into account this repopulation phenomenon during radiation therapy, many authors introduced the repopulation term into the TCP model as shown in the following equation (Travis & Tucker, 1987; Fowler, 1989; Sanchez-Nieto & Nahum, 2000; Tomé & Fowler, 2000; Tomé & Fowler, 2003; Carlone *et al*., 2006; Søvik *et al*., 2007; South *et al*., 2008):

$$TCP = \exp\left\{-N \cdot \exp\left[-\alpha D\left(1+\frac{\beta}{\alpha}d\right)+\gamma T\right]\right\} \tag{1.7}$$

where $\gamma = ln2/T_d$ is the proliferation rate of the clonogens per day, T_d is the average doubling time of the clonogens in days, and T is the overall treatment time. The overall time, T, can be replaced by $(T-T_k)$ to take into account the lag time which is often observed in

clinical data (Withers *et al*., 1988), where T_k is the kick-off time in days at which the repopulation starts after the beginning of therapy. Considering that the proliferation rate is known to change during treatment, this simple exponential repopulation term with a constant rate can only be a rough approximation (Thames *et al*., 1990). Several authors tried to develop a better model that deals more rigorously with the repopulation effect during the radiation therapy (Tucker *et al*., 1990; Zaider & Minerbo, 2000; Stavreva *et al*., 2003; McAneney & O'Rourke, 2007).

Parallel to the TCP modeling, the tumor growth models have been developed to mathematically describe the growth pattern of a tumor. As a simple empirical equation, the Gompertzian model has successfully described the tumor growth (Norton, 1988; Marusic *et al*., 1994). Cell cycle kinetics models have been developed as theoretical explanations for the Gompertzian tumor growth and the important parameters for the tumor growth kinetics have been derived, such as potential doubling time (T_{pot}), cell cycle time (T_c), growth fraction (GF), and cell loss factor (CLF) (Gyllenberg & Webb, 1989; Tubiana, 1989; Deasy *et al*., 2003; Kozusko & Bajzer, 2003). Recently, several authors have adopted the cell cycle kinetic models into the TCP model for better representation of repopulation phenomena during radiation therapy (O'Donoghue, 1997; Dionysiou *et al*., 2004; Dawson & Hillen, 2006; Titz & Jeraj, 2008).

1.3. The organization of the dissertation

This dissertation has been organized into four chapters, which are self-contained and planned to submit for separate publication. In Chapter II, a state-based tumor response model for fractionated radiotherapy was developed, in which the impact of micro-

environmental condition can be simulated. A detailed model description was presented and tumor response to the conventional fractionated radiotherapy was simulated for head and neck squamous cell carcinoma (HNSCC) using relevant parameter values.

In Chapter III, the cell cycle effect on the fraction size was additionally incorporated into the developed state-based tumor response model to explore tumor response to the hypofractionated radiation therapy (or SBRT), where the effect is believed to be significant. The fraction size dependent effective radiosensitivity and effective OER were estimated and the treatment response of lung cancer to the hypofractionated radiation therapy was simulated.

In Chapter IV, the effect of FDG uptake on tumor response was explored. First, the required boost dose for high FDG uptake tumor was estimated for head and neck squamous cell carcinoma (HNSCC) from clinical outcome data. Then, the potential relationship between FDG uptake and classical radiobiological mechanisms was explored using the state-based tumor response model.

In Chapter V, a computer program, named 'PIH' code, was developed for the state-based tumor response model. The structure of the code and direction for execution of the code were described.

Chapter VI gives a brief summary and conclusion of the research work and some suggestions for future study.

CHAPTER 2

A STATE-BASED MODEL OF TUMOR RESPONSE TO RADIOATHERAPY

2.1. Introduction

Tumor control probability (TCP) estimations, or surrogates for TCP, have been widely used to analyze fractionation schedules and dose distribution differences. Usually, the linear-quadratic (L-Q) model has been combined with a simplified kick-off to exponential clonogen accumulation (Travis & Tucker, 1987). For a better representation of the effect of proliferation/repopulation, some authors adopted the tumor growth kinetics into the L-Q model (O'Donoghue, 1997; Dawson & Hillen, 2006; McAneney & O'Rourke, 2007). Others have included hypoxic effect in the tumor response model based on the oxygenation enhancement ratio (OER) of hypoxic subpopulations (Buffa *et al*., 2001; Nahum *et al*., 2003; Wang *et al*., 2006).

Given our current knowledge of tumor heterogeneity, a TCP model is required which can reflect the intra-tumor heterogeneity and can evaluate the effect of various micro-environmental factors on the treatment response. Several models used in the selective dose painting or dose redistribution are the examples that employed such intra-tumor heterogeneity into the model (Suit *et al*., 1992; Popple *et al*., 2002; Søvik *et al*., 2007). However, those models are focused mainly on hypoxia. Recently, several researchers have developed stochastic computer simulation models for the evaluation of tumor response, in which various biological processes are implemented in three-dimension (Borkenstein *et al*., 2004; Dionysiou *et al*., 2004; Titz & Jeraj, 2008).

In this chapter, a compartmental TCP model was developed, along the lines of ecological matrix models (Caswell, 2001) or other matrix models developed in radiotherapy (Roti Roti & Dethlefsen, 1975a; Roti Roti & Dethlefsen, 1975b). This novel computational formulation allows us to flexibly add or subtract effects, states, and state transitions. The objective of this work was to build a model, which is conceptually simple but powerful enough to capture the clinically observed phenomena and the accepted (though difficult to measure) interplay between proliferation and hypoxia. The model includes three compartments with different levels of proliferation, hypoxia, and cell death. A 'doomed' sub-compartment was incorporated into each compartment for a more realistic representation of cell-kill phenomena and cell removal lysis during tumor reoxygenation and regression. Initial proliferation and hypoxia apportionments were estimated based on the growth fraction (GF) and the cell loss factor (CLF) for a PET-voxel-comparable size of tumorlet. The response for a larger, homogeneous tumor is then easily computed. In this work, we do not address the important issue of intra-tumor heterogeneity, which is a straightforward extension of the model. The treatment response for a range of schedules was simulated.

We will add cell cycle effects to the model in Chapter 3, which focuses on hypofractionated response (1-3 fxs), where we believe such effects cannot be ignored. In this chapter we focus on response from 5 fractions up to standard 2 Gy/day treatments. As part of this project, the resulting computer code is described in Chapter 5, which will be made publicly available and open-source.

2.2. Methods and materials

2.2.1. The assumption of blood supply invariance

In the absence of good evidence to the contrary, we take the simplest assumption that each tumor sub-volume (a particular group of cells and their progeny, defined at the outset of therapy) has a constant blood (oxygen and nutrient) supply over a course of radiotherapy. This simplifies the model, and allows us to introduce the fundamental idea of the model, which is that every tumorlet sub-volume (which may shrink or grow during therapy) has an inherent blood supply available, and therefore an inherent proliferative cell capacity. We do not consider here the potential (but probably unimportant) case where one tumorlet has shrunk so much that its excess blood supply becomes available to surrounding tumorlets by diffusion.

Note that the tumorlets we study do not need to conserve volume. Although they generally shrink in size over a course of radiotherapy, they could theoretically increase in size. This is therefore not, strictly speaking, a 'voxel' simulation, except in the sense of a tumorlet being identified with a given voxel at treatment planning.

2.2.2. The three basic compartments: Proliferative, Intermediate, and Hypoxic

To align the application of the model with the interpretation of clinical PET imaging, our model focuses on a small tumorlet that has comparable size to a voxel of typical PET image ($4\times4\times4$ mm^3) and it is quite reasonable to assume that the tumorlet consists of three different types of microscopic regions having different nutrient availability and microenvironment as shown in histochemical studies (Ljungkvist *et al*., 2006; Hoogsteen *et al*., 2007; Wijffels *et al*., 2008). In order to focus on effects of the microenvironment, the

tumorlet is considered in isolation and the interactions between adjacent tumorlets are not considered for the current study.

The model includes three compartments considering two micro-regional factors, proliferation and hypoxia, which are thought to be the most important factors in the tumor growth and response to the RT (Hoogsteen *et al*., 2007; Wijffels *et al*., 2008). This classification is consistent with the study performed by Kiran *et al*. (Kiran *et al*., 2009), in which avascular tumor growth was simulated with three different zones. Based on the diffusion and consumption of two principal nutrients, glucose and oxygen, and cell death processes, the model could predict the size of each zone and showed excellent agreement with experimental data. Some growth pattern similarities were also reported between the avascular tumor and a tumorlet supported by a single blood vessel inside a vascular tumor (Roose *et al*., 2007).

The three compartments are denoted Proliferative (*P*), Intermediate (*I*), and Hypoxic (*H*) compartments. The *P*-compartment is comprised of cells that have a sufficient oxygen and glucose supply to proliferate. Considering the gradient and pulsed nature of the blood supply (Nilsson *et al*., 2002; Cárdenas-Navia *et al*., 2008), only a fraction of cells in *P* are assumed to be in the cell cycle at any time. For simplicity, the fraction was set to be 50% for a fully occupied *P*-compartment. However, as the total number of cells decreases over the course of radiotherapy and becomes less than the capacity of the *P*-compartment, the fraction of cells in proliferation is assumed here to linearly increase to unity due to less competition for oxygen and nutrients (Ljungkvist *et al*., 2006). The *I*-compartment is a mildly hypoxic compartment that is assumed to have an adequate glucose supply. Without enough oxygen, cells in the *I*-compartment will not proliferate but

can still survive as metabolically active cells outside the cell cycle (Hlatky *et al*., 1988). No cell loss is assumed to take place in the *I*-compartment. On the other hand, the *H*-compartment is filled with cells that are extremely hypoxic, with inadequate glucose and a non-zero death rate even in the absence of radiation. Nevertheless, the viable (non-doomed) cells in the *I*- and *H*-compartments are thought to have a latent capability to proliferate if they eventually reach the *P*-compartment where a sufficient oxygen and glucose supply exists (Hoogsteen *et al*., 2005). A schematic diagram of the model is shown in Figure 2-1.

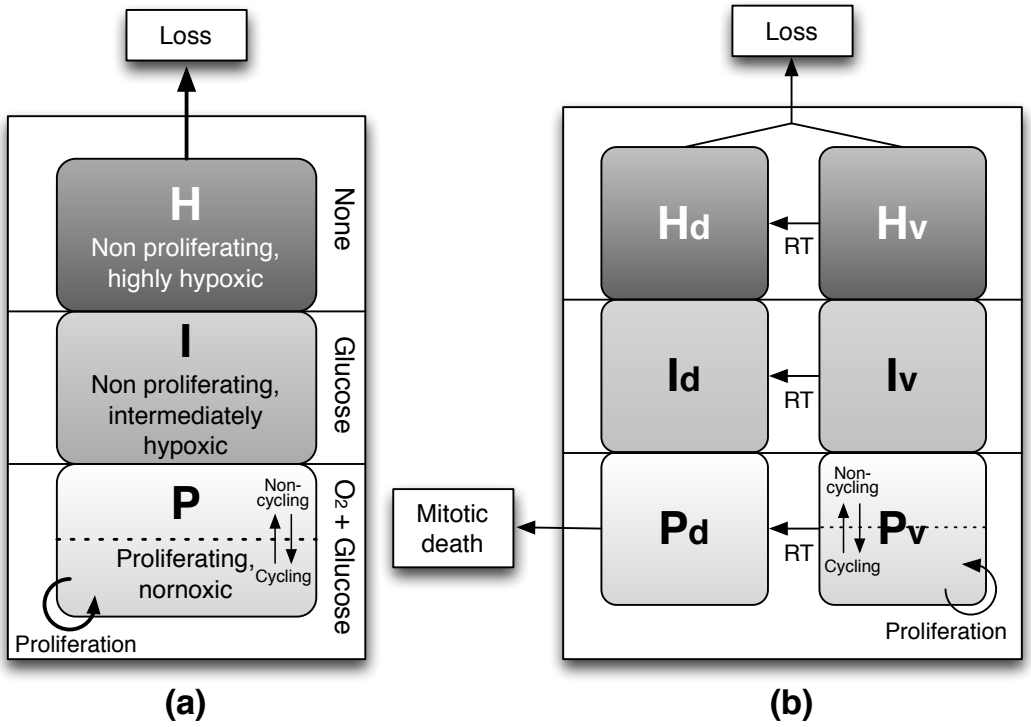

Figure 2-1. Schematic diagram of the model: (a) just prior to the initiation of radiation therapy and (b) after radiation therapy begins, with doomed sub-compartments in each compartment. The dotted lines and arrows in both directions in the *P*- and P_V-compartments indicate that only a fraction of the cells in the compartment are in cell cycle and proliferating, on average, due to the gradient and pulsed nature of tumor blood supplies.

In this model, the transition of cells from one compartment to another is not determined by 'transfer rates', which is commonly used in other compartmental models. Rather, the cells in the tumorlet are thought to behave like water in a water reservoir that has three divisions along its height as shown in Figure 2-1(a). When the number of cells in a compartment reaches the maximum, the extra cells are pushed up to the next compartment (i.e., *P* to *I* or *I* to *H*). Conversely, if there is room available in a better oxygenated compartment, cells fill in without any assumed delay. In other words, the transition of cells between compartments is governed by the inherent capacity of each compartment.

2.2.3. Proliferation and cell loss

Since each proliferating cell produces two progenies after a cell division, in the absence of other effects, the number of proliferating cells would double in one cell cycle time (T_C). Therefore, the proliferation of a given tumorlet depends on both the size of the *P*-compartment and the fraction of cells in cell cycle (f_{pro}^{P}) at any given time. The change in number of cells with time in the *P*-compartment due to proliferation can be calculated as follows:

$$N_v^P(t+\Delta t) = N_v^P(t) \times \exp\left(f_{pro}^{P} \frac{\ln 2}{T_C} \Delta t \right) \tag{2.1}$$

where N_v^P is the number of viable cells in *P-compartment;* f_{pro}^{P} is the fraction of cells in active proliferation in the *P-compartment;* T_C is the cell cycle time; and Δt is the time step of the calculation. The resulting number of cells might exceed the capacity of the *P*-

compartment and these extra cells are pushed up to the *I*-compartment, through a recompartmentalization process as discussed further in section 2.2.6.

Extremely hypoxic cells in the *H*-compartment undergo cell loss, which might be caused by various processes, such as tissue or cellular necrosis, apoptosis, metastasis, and any other type of shedding. Among these, necrotic cell death is thought to be a major factor due to the insufficient oxygen and nutrient supply in the compartment (Joiner & Kogel, 2009). Similarly to Chvetsov *et al.* (Chvetsov *et al*., 2008), cell loss was assumed to follow exponential decay with a cell loss half-time ($T_{1/2,loss}$), as shown in Equation 2.2.

$$N^H(t+\Delta t) = N^H(t) \times \exp\left(-\frac{\ln 2}{T_{1/2,loss}}\Delta t\right) \tag{2.2}$$

where N^H is total number of cells in the *H*-compartment (viable or doomed), and $T_{1/2,loss}$ is the cell loss half-time in the *H*-compartment. Equations 2.1 and 2.2 are discrete functions and the number of cells in each compartment is updated with a small time step of Δt (taken to be a quarter of an hour as default).

2.2.4. Growth fraction and cell loss factor for micro-environmental conditions

Because the input parameters of growth fraction (GF) and cell loss factor (CLF) have often been measured experimentally (Steel, 1977), we elected to work from those parameters as model inputs, to help estimate the initial distribution of cells in each compartment, although there is currently little data connecting both of these. GF is defined as the fraction of viable cells in active cell division at a given time. CLF is defined as the

rate of overall cell loss in the absence of radiotherapy (due directly to cell death or migration of cells out of the tumor), expressed as a fraction of excess cells measured relative to the rate of cell number increase due to mitotic divisions (Hall & Giaccia, 2006).

The GF directly determines the number of cells in the *P*-compartment. Since the fraction of actively dividing cells in the *P*-compartment is assumed to be half (initially with a full *P*-compartment), the fraction of the cells in the *P*-compartment is taken as twice the GF[2]. When the GF is 0.2, for example, the fraction of cells in the *P*-compartment becomes 40%. The CLF is used to calculate the size of the remaining compartments (*I* and *H*) together with the GF, based on the rates of proliferation and cell loss (see Appendix). For a given GF, we assume that the relative distribution in the *I*- vs. *H*-compartments results in the given CLF.

The CLF also determines the rate of overall growth of the tumorlet. The rate of volume increase can be expressed as the volume doubling time (T_D), which represents the time required for a tumor to double in volume (Joiner & Kogel, 2009). For a given GF and CLF, the volume doubling time becomes $T_C / \left[(1 - CLF) GF \right]$ (see Appendix A.2 for detail).

The volume increase of a tumorlet probably involves a relative increase of vascular delivery capability through angiogenesis. However, the change in vasculature was not considered in the current study, since the model simulation began with a tumorlet identified with a given voxel at treatment planning and the vasculature would not change significantly until the beginning of radiotherapy. Also, it is presumed that after a course of RT has begun, the process of angiogenesis does not significantly alter overall access to

[2] The precise value of this assumption has a modest effect on model predictions (see Appendix A.3).

nutrients. Clearly, this assumption may need to be revised if relevant data becomes available.

The GF and CLF parameters are used only to find the relevant initial distribution of cells in the tumorlet. After RT begins, the GF and CLF change with the updated cell distribution in each compartment. The GF increases and CLF decreases as the number of cells in the *I*- and *H*-compartments decreases.

2.2.5. Cell-kill model and oxygen enhancement ratio

Direct cell-kill from radiation is calculated based on the Linear-Quadratic (L-Q) model. However, cell-kill in this model does not imply a prompt death of the affected cells. The lethally damaged cells were assumed to become 'doomed' but able to survive metabolically, which are eventually dying during failed mitosis. Equations 2.3 and 2.4 represent the damage of viable cells and build-up of doomed cells in a compartment for a given fraction of RT:

$$N_v^X(t+\Delta t) = N_v^X(t) \times \exp\left(-\alpha_X d - \beta_X d^2\right) \tag{2.3}$$

$$N_d^X(t+\Delta t) = N_d^X(t) + N_v^X(t) \times \left[1 - \exp\left(-\alpha_X d - \beta_X d^2\right)\right] \tag{2.4}$$

where $N^X(t)$ and $N^X(t+\Delta t)$ are the number of viable or doomed cells in a certain compartment X (P, I or H) before and after RT fraction, respectively; α_X and β_X are the L-Q parameters for the X compartment; and d is the fractional dose. After several cell cycles, the doomed cells die through mitotic cell death and then are physically removed form the tumorlet through lysis process as discussed in the later section 2.2.7.

Hypoxic cells are known to be more difficult to sterilize than normoxic cells as expressed by the oxygen enhancement ratio (OER). The OER represents the ratio of dose required to achieve the same level of cell kill compared to that required for normoxic cells. The alpha and beta values of the L-Q cell-kill model were modified for different compartments as follows (Carlson *et al*., 2006):

$$\alpha_X = \alpha_P / OER_X \quad \text{and} \quad \beta_X = \beta_P / OER_X^2 \tag{2.5}$$

where α_X and β_X are the alpha and beta values for a given hypoxic compartment *X* (*I* or *H*), and α_P and β_P for the normoxic cells in the *P*-compartment.

2.2.6. Recompartmentalization and reoxygenation

After each fraction of RT, some viable cells become doomed. The doomed cells are metabolically alive but die out after few cell cycles. The main mechanism of doomed cell death is thought to occur through mitotic catastrophe or mitotic failure (Hall & Giaccia, 2006; Joiner & Kogel, 2009). Therefore, as the proliferation rate is higher for a compartment, the death rate of doomed cells becomes higher.

Mitotic death does not always occur in the first attempt and may occur after several subsequent attempts (Joiner & Kogel, 2009). Therefore, the survival probability of each progeny (k_m) after mitosis was applied to the calculation of mitotic cell death of doomed cells as shown in Equation 2.6. The zero survival probability of each progeny ($k_m = 0$) represents the mitotic death in the first attempt of mitosis with the half-life equivalent to

the doubling time of viable cells. Since the number of doomed cells increases after mitosis for k_m values larger than half, the probable range of k_m is thought to be 0.1~0.4.

$$N_d^P(t+\Delta t) = N_d^P(t) \times \exp\left(\left(2k_m - 1\right) f_{pro}^P \frac{\ln 2}{T_C} \Delta t \right) \tag{2.6}$$

As doomed cells die in the *P*-compartment, oxygen becomes available to other cells and a 'recompartmentalization' takes place as shown in Figure 2-2. In this process, reoxygenation of the hypoxic cells also occurs.

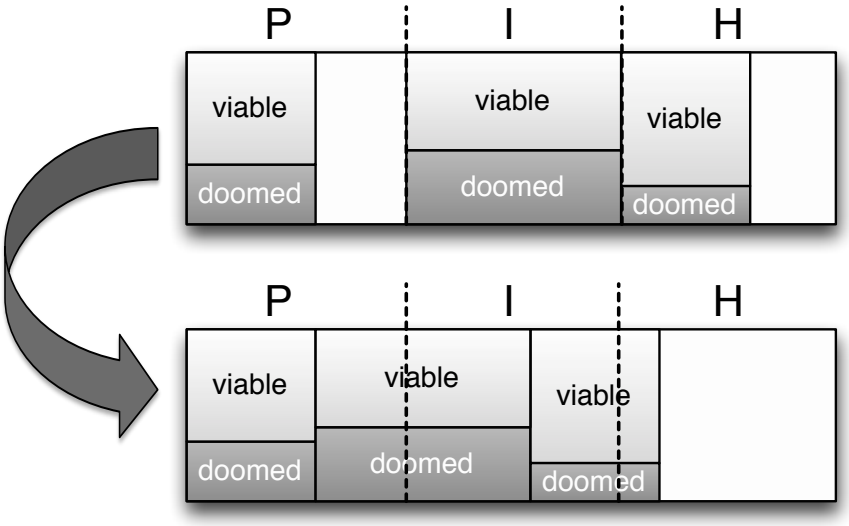

Figure 2-2. Recompartmentalization and reoxygenation pattern after mitotic death of doomed cells in the *P*-compartment. As long as cells are available, the *P*-compartment 'tops up' at each time step.

2.2.7. Programming and the parameter values

Simulation was performed using the Matlab® software system. The model program is comprised of two main parts. In the first part, the initial distribution of cells in the

compartments was determined based on the GF and CLF. In the second part, the RT began and the treatment response of the tumor was evaluated from the initial distribution. The model was applied to head and neck squamous cell carcinoma (HNSCC) and the parameters values used for the calculation are shown in Table 2-1.

Tumor growth is thought to depend on a small subset of tumor cells that have stem cell-like properties with great proliferative potential and self-renewal ability. This cancer stem cell hypothesis was applied for the model; the fraction of cells which are stem cells (i.e., have the clonogenic ability to repopulate a tumor) was set to be 0.01 (Hemmings, 2010). However, this number is poorly known and might vary widely. With a tumor cell density of 10^9 cm^{-3} of the model, the clonogenic (stem) cell density becomes 10^7 cm^{-3}, which corresponds to published values in the range of 10^6-10^8 cm^{-3}.

The radiosensitivity of the normoxic *P*-compartment was set to be 0.41 and 0.041 for α and β, respectively, based on data measured in the normoxic condition (Søvik *et al*., 2007). The OER of the extremely hypoxic *H*-compartment (OER_H) was assumed to be 1.37 based on the work of Chan *et al*. (2008), in which a reduced OER was observed for extremely hypoxic cells due to the decreasing availability of homologous recombination. Chan *et al.* also showed that the time of cells in hypoxic condition affected the OER: cells exposed to hypoxia for less time had a higher OER. Hence, the cells in the *I*-compartment might therefore have a higher OER than cells in the *H*-compartment. Because there is no clear guidance regarding the OER of the *I*-compartment cells (OER_I), three different values (1.2, 1.37 and 2.0) were evaluated. The resulting $TLCD_{50}$'s were judged to be much more realistic with an OER_I of 2.0, as further discussed below.

We assume that metabolically dead cells are not instantly removed from the tumor and require some time to physically disintegrate and be removed from the tumor through cell lysis. Cell lysis was assumed to follow an exponential decay with lysis half-time ($T_{1/2,lysis}$), which was assumed to be 3 days and was applied to all dead cells, either from cell loss in the *H*-compartment or from mitotic cell death in the *P*-compartment.

A time step (Δt) of 15 minutes was used, which is sufficiently small, compared the cellular processing time.

Table 2-1. The parameters used to demonstrate the model for HNSCC

Parameters	**Values**
Tumor cell density (ρ_t)	10^6 mm^{-3} (Zips, 2009)
Volume of a tumorlet (v_t)	64 mm^3 (typical PET voxel size)
Total number of cells in a tumorlet (n_t)	6.4×10^7 ($\rho_t \cdot v_t$)
Stem cell fraction (f_S)	0.01 (Hemmings, 2010)
Cell cycle time (T_C)	2 days (Joiner & Kogel, 2009)
Initial proliferation fraction in *P* (f_{pro}^P)	0.5[a]
Cell loss half-time in *H* ($T_{1/2,loss}$)	2 days (Ljungkvist *et al*., 2005)
Survival rate of progeny after mitosis (k_m)	0.3[a]
Linear radiosensitivity coefficient (α_P)	0.41 Gy^{-1} (Søvik *et al*., 2007)
Quadratic radiosensitivity coefficient (β_P)	0.041 Gy^{-2} (Søvik *et al*., 2007)
OER of *I*-compartment (OER_I)	1.2, 1.37 or 2.0[a]
OER of *H*-compartment (OER_H)	1.37 (Chan *et al*., 2008)
Lysis half-time ($T_{1/2,lysis}$)	3 days[a]
Time step of the calculation (Δt)	15 min

[a] Assumed parameters

2.2.8. Initial distribution based on GF & CLF

The number of cells in each compartment prior to RT was determined based on the growth fraction (GF) and cell loss factor (CLF), which represents the microenvironment of a tumorlet. As shown in the Appendix A.1, a CLF and GF, along with model assumptions, perhaps surprisingly, imply a unique distribution among the compartments. Put simply, a higher growth fraction always implies a higher fraction of cells in the *P*-compartment. Once this is fixed, variations in cell loss factor determine the fractions of cells in the *I*- and *H*- compartments.

In Figure 2-3, the initial distributions are shown for various GFs and CLFs. Clinically relevant values for GF and CLF are thought to be around 0.2 and 0.9, respectively. The distribution significantly differs for different GFs, since the number of cells in the *P*-compartment is directly determined by the GF. The size of the *H*-compartment became smaller as the CLF decreased, due to reduced cell loss from the *H*-compartment. Compared to the effect of GF, the initial distribution is less sensitive to the CLF and the difference between the CLF=0.9 and 0.8 was not substantial for GF of 0.2.

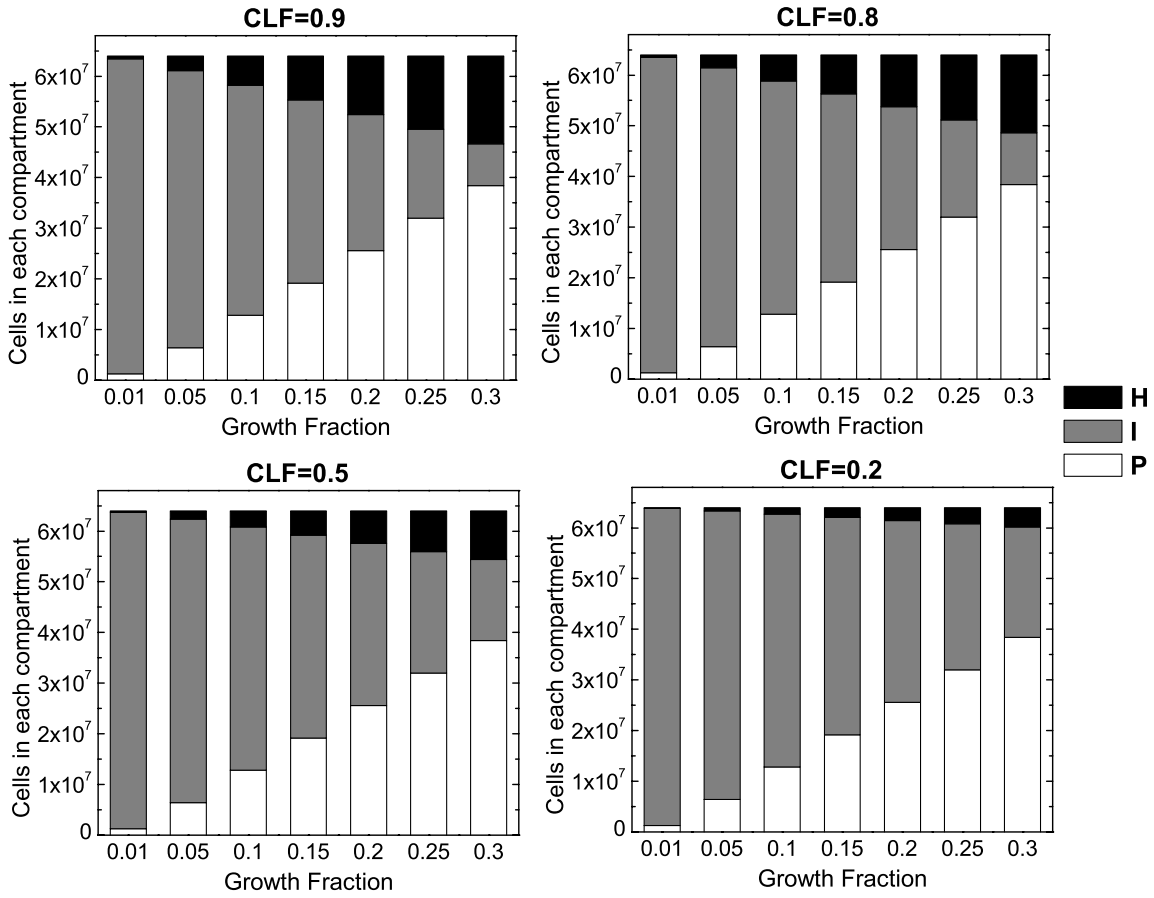

Figure 2-3. The initial number of cells in each compartment before RT begins based on various growth fractions (GFs) and 4 different cell loss factors (CLFs) for a tumorlet voxel with size of 4×4×4 mm^3.

2.3. Simulation results for conventional fractionated RT

2.3.1. Response of a tumorlet

Tumorlet response was evaluated based on the calculated initial clonogen distribution. The results presented in this section focus on the variation of GF and fraction size with a fixed CLF of 0.9 and an OER_I of 2.0. The effect of CLF and OER_I are evaluated and discussed in the next section 2.3.2.

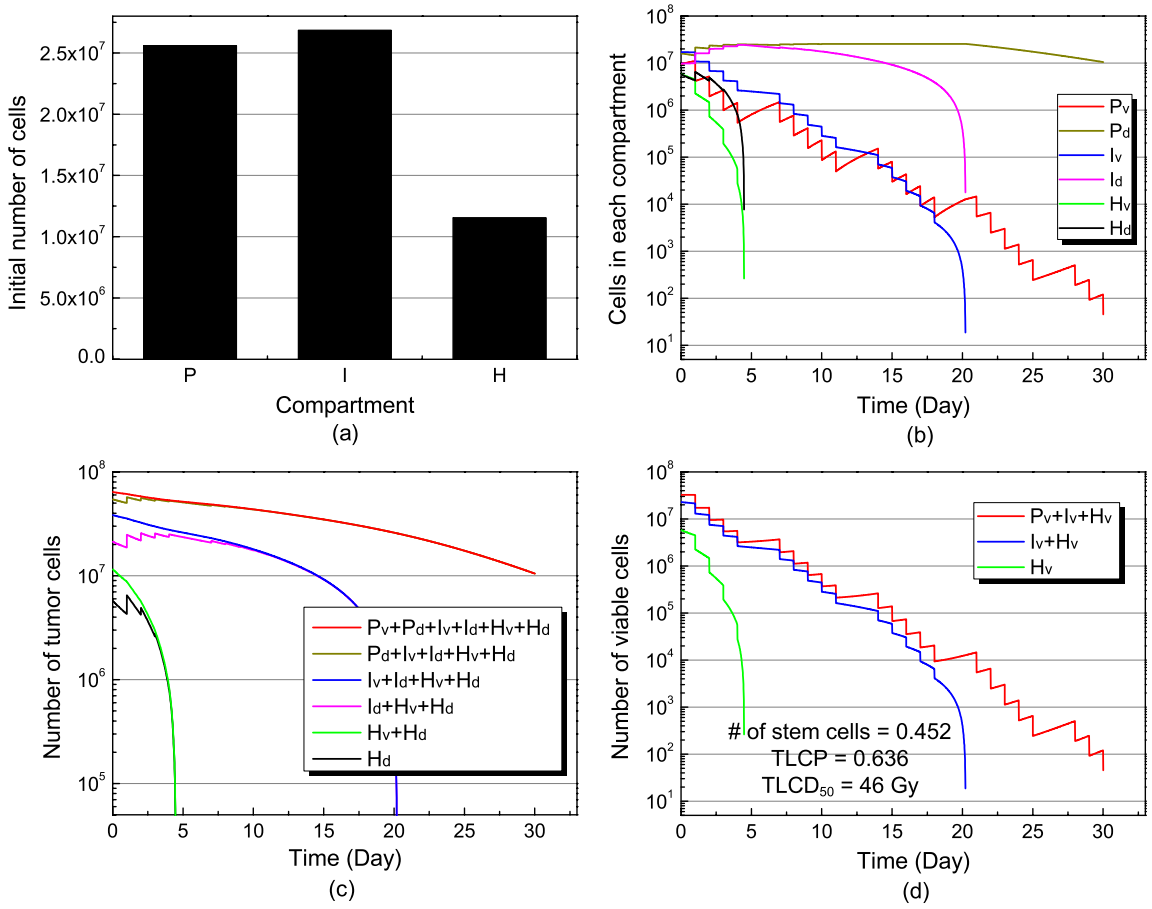

Figure 2-4. Example of simulation result with a growth fraction of 0.2 and a cell loss factor of 0.9 for the conventional fraction size of 2 Gy/fx: (a) the initial cell distribution for three compartments, (b) the number of cells in each compartment during the course of RT, (c) the cumulative number of cells in a tumorlet during the course of RT (from which the tumor regression pattern and reoxygenation time can be estimated), and (d) the cumulative viable cells in a tumorlet during the course of RT (from which TCP can be estimated).

Simulation results are shown in Figure 2-4 Figure 2-5 for fraction size of 2 and 5 Gy/fx, respectively. Beginning with the initial distribution calculated for the growth fraction of 0.2 and the cell loss factor of 0.9, the change in the number of cells in each compartment was simulated during the course of radiation therapy. For the conventional fraction size of 2 Gy/fx (Figure 2-4), the tumorlet dose for 50% of control ($TLCD_{50}$) was estimated to be 46 Gy, which is thought to be an appropriate value for a small tumorlet (see

discussion for more detail). After a few days, the doomed cells comprise the majority and determine the regression pattern of the tumorlet. It took less than 5 days for the *H*-compartment to empty and the overall reoxygenation time, when all the hypoxic cells in the *I*- and *H*-compartments are completely removed from the tumorlet, was found to be about 20 days from the inception of RT. After this time, all the cells are in the *P*-compartment and the regression of the tumorlet becomes faster.

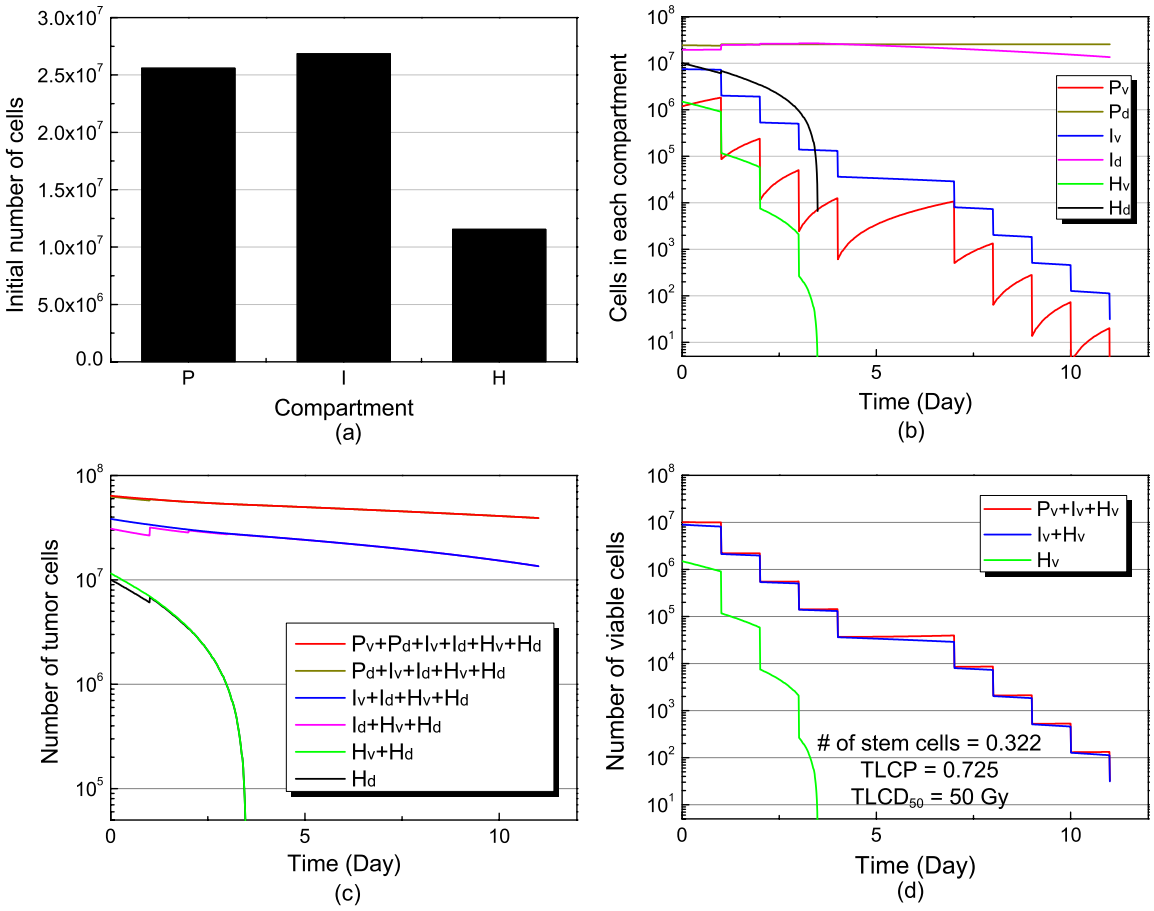

Figure 2-5. Example of simulation result with a growth fraction of 0.2 and a cell loss factor of 0.9 for the hypo-fractionation with 5 Gy/fx: (a) the initial cell distribution for three compartments, (b) the number of cells in each compartment during the course of RT, (c) the cumulative number of cells in a tumorlet during the course of RT (from which the tumor regression pattern and reoxygenation time can be estimated), and (d) the cumulative viable cells in a tumorlet during the course of RT (from which TCP can be estimated).

For the hypo-fractionation case shown in Figure 2-5, a faster cell kill effect was observed with the larger fraction size of 5 Gy/fx. In spite of faster cell kill, however, the estimated $TLCD_{50}$ was still higher than for the conventional fraction size of 2 Gy/fx (50 vs. 46 Gy). This is because the tumorlet is not reoxygenated until it achieves 50% of tumorlet control probability (TLCP) without enough time for the doomed cells to be cleared out from the tumorlet.

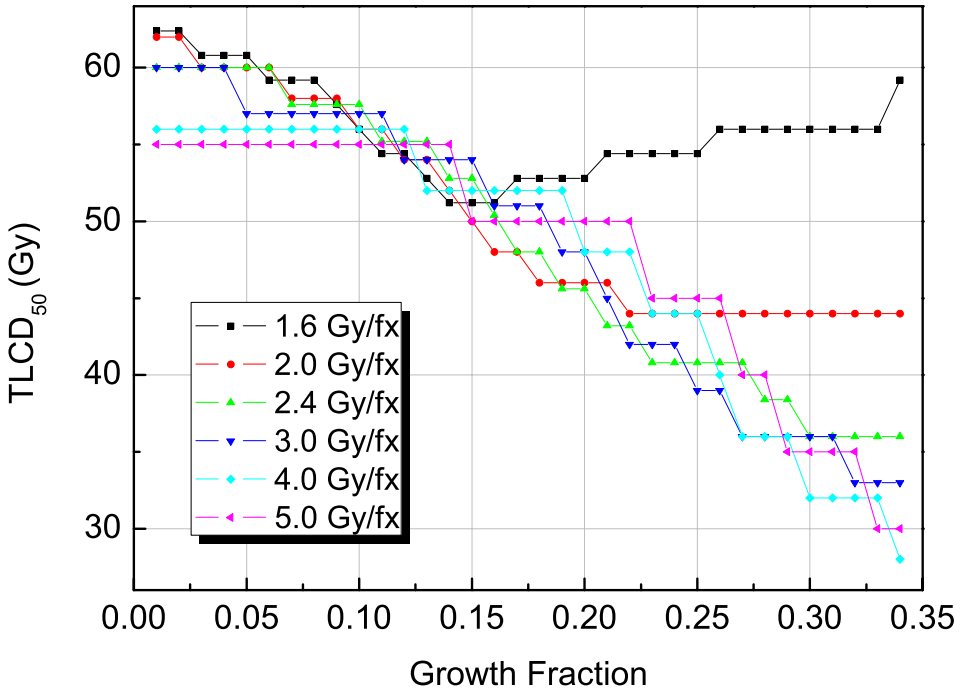

Figure 2-6. Model predicted tumorlet dose required to achieve at least 50% TLCP ($TLCD_{50}$) vs. the growth fraction (GF) for several different daily fraction sizes with a cell loss factor (CLF) of 0.9.

To compare the effect of various GF and fraction sizes on tumorlet response, the $TLCD_{50}$ was found for each initial distribution with different fraction sizes. Note that the TLCP cannot be exactly 50% in the calculation due to the discrete nature of the fractionation. A typical case is shown in the Figure 2-6. We could observe the interplay between

hypoxia and proliferation from the result. In general, a higher GF tumorlet requires less dose, mainly because the ratio of radio-resistant hypoxic cells in the tumorlet decreases as the GF increases. Also, reoxygenation occurs faster with a higher GF, since the size of the *P*-compartment, where the mitotic cell death of doomed cells takes place, is proportional to GF. For smaller fraction sizes (1.6-2.4 Gy/fx), however, the $TLCD_{50}$ did not keep decreasing but rather increased after a certain GF, because the proliferation capacity also increases with GF and the smaller daily fraction size was not effective for higher GFs.

Interestingly, larger fraction sizes were not always more effective and conventional smaller fraction sizes (2-2.4 Gy/fx) resulted in smaller $TLCD_{50}$ values than higher fraction sizes (4-5 Gy/fx) for the GF values of around 0.2 (0.15-0.23), due to the advantage in reoxygenation. Considering that the biologically relevant GF is likely around 0.2, the result supports the current fractionation scheme.

The reoxygenation time was calculated depending on the GF for the fraction size of 2 Gy/fx and CLF of 0.9, as shown in Table 2-2. It was found in two different ways. First, the time was found when the change of total number of hypoxic cells has a maximum curvature on a semi-log plot. Second, the full-reoxygenation time was found, when all the hypoxic cells are removed from the tumorlet. These two values were not significantly different, with only about 0.7 days difference. The reoxygenation time decreased as the growth fraction of a tumorlet increased, due to higher cell death and clearance capacity with the larger *P*-compartment. For growth fractions of 0.01 and 0.05, the reoxygenation time exceeded 100 days, due to the very small size of the *P*-compartment.

Table 2-2. Model predicted reoxygenation times for fraction size of 2 Gy/fx (CLF=0.9).

Growth fraction	By maximum curvature[a] (Day)	Full reoxygenation[b] (Day)
0.01	705.1	705.8
0.05	127.8	128.5
0.1	55.6	56.3
0.15	31.6	32.3
0.2	19.5	20.2
0.25	12.2	12.9
0.3	7.3	8.0

[a] when the total number of hypoxic cells curve (I_v+I_d+H_v+H_d) has the maximum curvature in semi-log plot [refer to Figure 2-4(c) and Figure 2-5(c)]
[b] when all the hypoxic cells are removed from the tumorlet

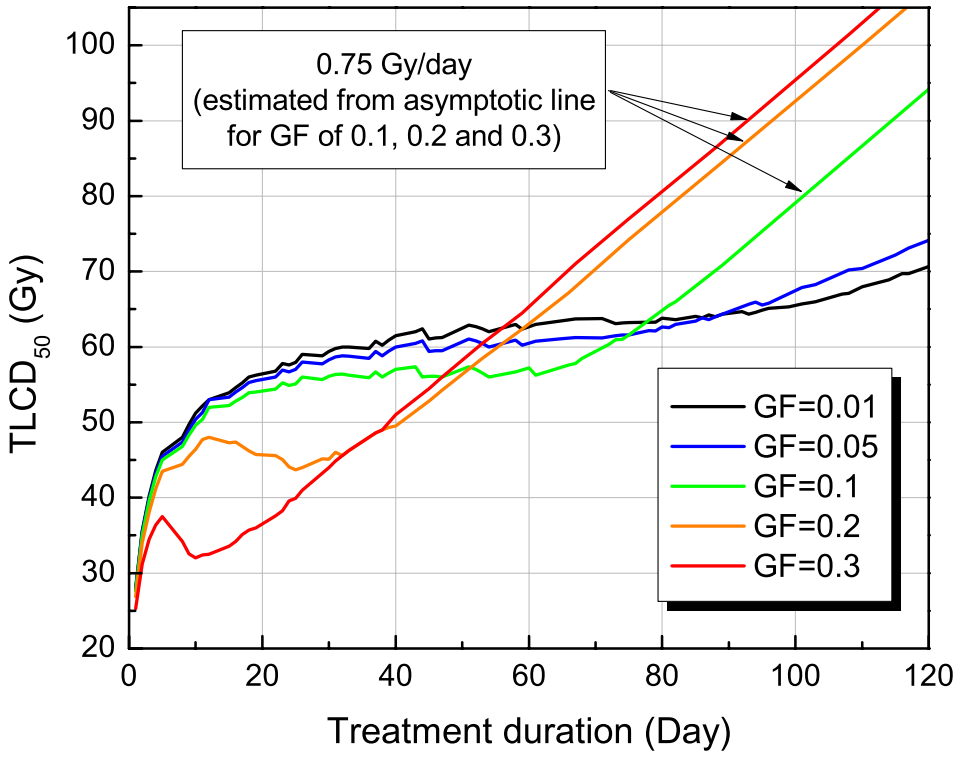

Figure 2-7. Tumorlet dose required to achieve at least 50% TLCP ($TLCD_{50}$) vs. the treatment duration assuming one fraction per day (5 days per week) for several different growth fractions (GFs) with a cell loss factor (CLF) of 0.9.

$TLCD_{50}$ was also evaluated for various overall treatment durations, simulated by manipulating the fraction size for a given GF. For all cases, one fraction per day (5 days per week) was simulated. The results are affected by both reoxygenation and repopulation patterns as shown in Figure 2-7. The $TLCD_{50}$ for a GF of 0.2 was lowest at 25 days. Before this optimal time, there was not enough time for the doomed cells to be cleared out, resulting in poor reoxygenation. After the optimal time, the repopulation affects the required $TLCD_{50}$. An asymptotic line is found for GFs of 0.1 to 0.3 and the slope of the line was found to be about 0.75 Gy/day, which implies the extra dose required to overcome the loss of local control due to the prolongation of the treatment time.

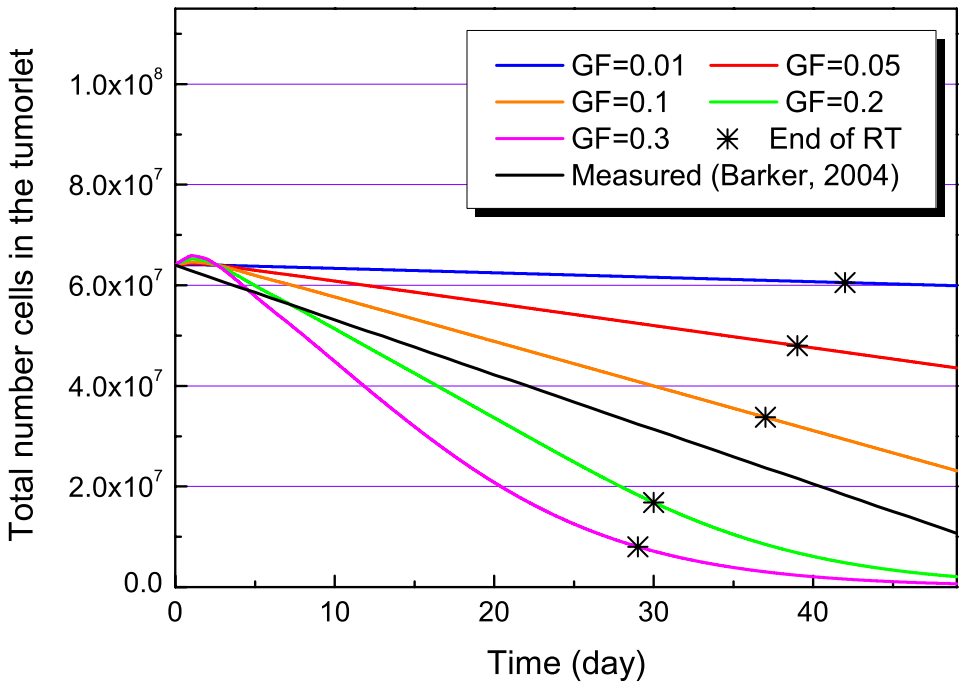

Figure 2-8. Model predicted tumor regression pattern of the tumorlet depending on the growth fraction (GF). The star signs (✳) indicate the time when the RT has been finished with $TLCD_{50}$ for each GF. For all cases, the CLF was set to be 0.9 and the fractional dose was 2 Gy/fx.

Tumorlet regression patterns were simulated depending on the GF for a fraction size of 2 Gy/fx. The basic assumption is that the volume of a tumorlet is proportional to the total number of cells in the tumorlet. In addition to the doomed cells, the cells in lysis after mitotic death or cell loss from the *H*-compartment were also considered. In Figure 2-8, the tumorlet regression pattern is shown for several different GF values for a fraction size of 2 Gy/fx and a CLF of 0.9. It is shown that the regression of the tumorlet becomes faster with a higher GF. The black linear line in the figure is the median regression rate of H/N cancer, which was clinically measured during fractionated RT (Barker Jr *et al*., 2004). It is shown that the regression pattern for a GF of 0.1-0.2 agreed with clinically observed rate.

2.3.2. Effect of OER of I-compartment and CLF on tumorlet response

To examine the effect of OER of the *I*-compartment, the simulation was repeated for different OER_I values (1.2 and 1.37) and the results were compared with that in the previous section, in which an OER_I of 2.0 was used.

To verify the hypoxic effect of different OER_I values, the $TLCD_{50}$ was decomposed, as shown in Figure 2-9. The proliferation effect on $TLCD_{50}$ was the same for all three OER_I values but the hypoxia effect was significantly different. For an OER_I of 1.2, about halfway between the normoxic *P*- and extremely hypoxic *H*-compartments, the $TLCD_{50}$ increased as GF increased, due to the larger effect of proliferation compared to hypoxia. For an OER_I of 1.37, the same OER value as the *H*-compartment, the evaluated $TLCD_{50}$ was almost flat for various GF values, since the effect of proliferation and hy-

poxia cancel each other out. Compared to an OER_I of 2.0, these two OER_I values seemed to underestimate the effect of hypoxia.

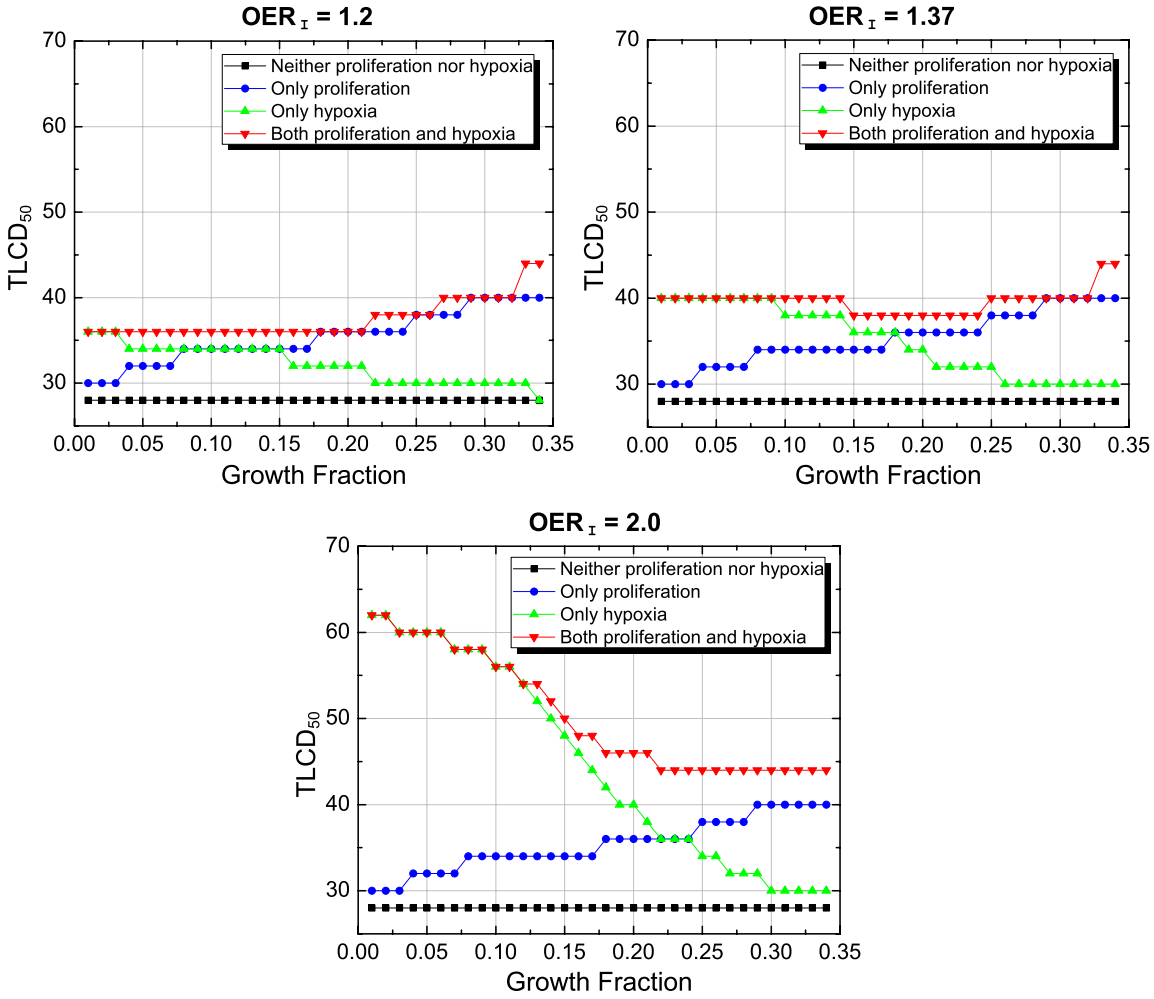

Figure 2-9. Effect of hypoxia and proliferation on $TLCD_{50}$ for various OER values of the *I*-compartment cells for 2 Gy/fx.

The effect of different CLF values on tumorlet response was also evaluated. As the CLF decreased, the $TLCD_{50}$ increased due to the relative increase in the *I*-compartment cells, which are more radioresistant than the extreme *H*-compartment and do not undergo

cell loss, as shown in Figure 2-10. However, changes in CLF had only a small effect on the $TLCD_{50}$. For a GF of 0.2, the $TLCD_{50}$ was unaffected for both 2 and 5 Gy/fx.

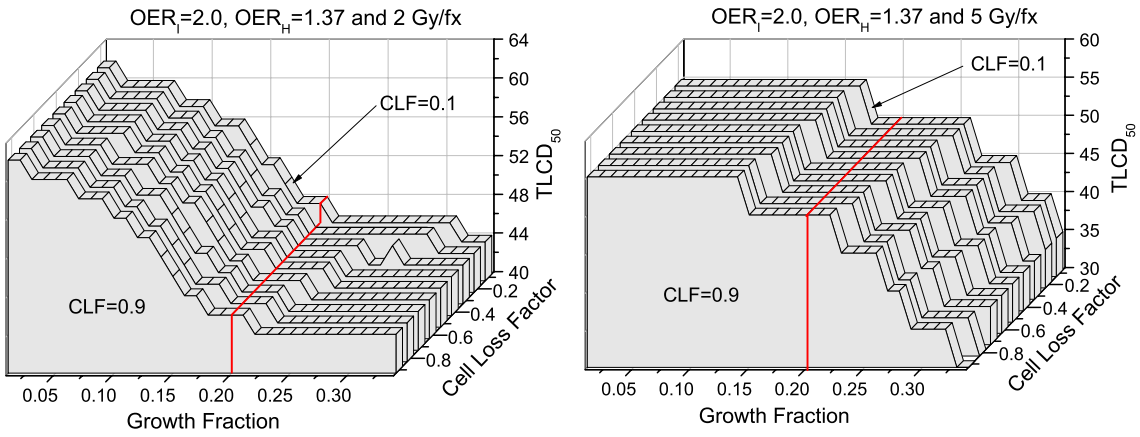

Figure 2-10. The effect of cell loss factors (CLF) on $TLCD_{50}$ for two different fraction sizes (2 and 5 Gy/fx) with the red line along a GF of 0.2.

An increase in reoxygenation time and the resulting reduced tumor regression were observed with a decreased CLF, due to the size decrease of the *H*-compartment, where cell loss in the absence of therapy takes place. The effect was more significant for higher GF values, since the size decrease of the *H*-compartment is more significant for higher GFs, as can be seen in Figure 2-3.

Neither the change in OER_I nor CLF significantly affected the estimation of the extra dose required to overcome the loss of local control due to the prolongation of the treatment time, which remains almost the same with the value of 0.75 Gy/day. Once reoxygenation has occurred, the rate of "dose loss" per day is determined by the *P*-compartment parameters along with the radiosensitivity parameters that set the dose scale.

2.3.3. Response of a homogeneous tumor

For a more direct comparison with clinical results, the response of a homogeneous tumor was also evaluated for various tumor sizes. The tumor dose for 50% control (TCD_{50}) can be estimated assuming the total TCP of a tumor is the product of the TCPs of each tumorlet (or TLCP), as shown in Equation 2.7 (Sanchez-Nieto & Nahum, 1999; Buffa & Nahum, 2000).

$$TCP_{total} = \prod_i TLCP_i \tag{2.7}$$

Table 2-3. Model predicted tumorlet dose required to achieve at least 50% local control, depending on tumor size for a GF of 0.2, a CLF of 0.9 and a fraction size of 2 Gy/fx.

Tumor diameter (cm)	Tumor volume[a] (cc)	Required TLCP[b]	TCD_{50} (Gy)
1	0.52	0.918766	54
2	4.19	0.989465	60
3	14.14	0.996867	66
4	33.51	0.998677	68
5	65.45	0.999322	70
6	113.10	0.999608	74
7	179.59	0.999753	76

[a] A tumor volume was calculated assuming the tumor is spherical.
[b] The required VCP was calculated from Equation 2.7.

In the Table 2-3, the variation of the required tumorlet dose was shown depending on the tumor size. Since all the tumorlets in the tumor were dealt as identical and the interaction between adjacent tumorlets was not considered, the result is just an estimation.

However, this rough estimation can be a reasonable approximation if the parameters used are representative of the whole tumor behavior. Note that this is not intended to reproduce an entire clinical dose response curve; consequently inter-tumor-heterogeneity is neglected.

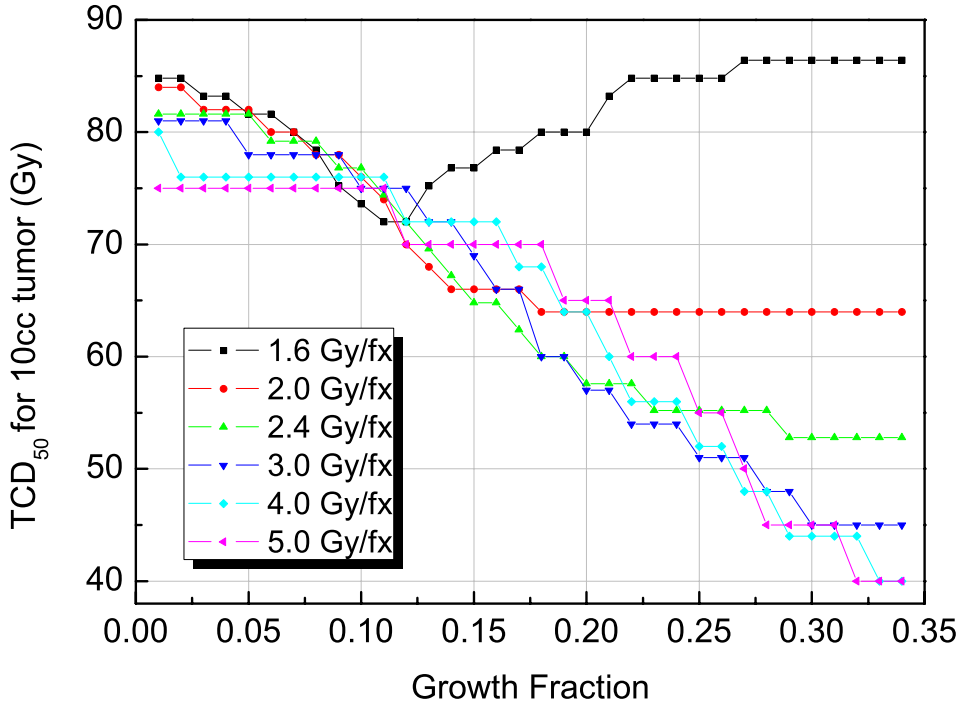

Figure 2-11. Model predicted tumor dose required to achieve at least 50% TCP (TCD_{50}) for a 10 cc tumor vs. the growth fraction (GF) for several different fraction sizes with the cell loss factor (CLF) of 0.9 (OER_I=2.0).

In Figure 2-11, the TCD_{50} values were shown in terms of GF and fraction size for a 10 cc tumor. The plot showed a similar pattern to the $TLCD_{50}$ plot shown in Figure 2-6 and the required dose is 64 Gy for a GF of 0.2 and a fraction size of 2 Gy/fx.

Since the tumor was comprised of homogeneous tumorlets, only the total dose for 50% control was increased compared to the tumorlet response. The reoxygenation time,

the extra dose required to overcome the longer schedule, and the tumor regression pattern remained the same as for the tumorlet.

2.4. Discussions

A mechanistic compartmental TCP model was developed, which can evaluate the treatment response of a tumorlet having various microenvironmental conditions. Three theoretical compartments were modeled based on the level of proliferation and hypoxia, which is determined by the GF and CLF of a voxel-sized tumorlet.

To make the model biologically reasonable, the following features were incorporated into the model: The transfer of cells between compartments was determined by the maximum size of each compartment, not by a fixed transfer rate. We hypothesize that this is a more realistic representation of the transition of tumor cells between compartments than using fixed transfer rates between compartments, considering the actual continuum nature of the tumor cell conditions. With the OER based alpha and beta values, different radiosensitivities were applied for each compartment. Also, the doomed sub-compartment was included for each compartment, which enables to describe the cell death caused by irradiation. This makes the model describe both reoxygenation and regression patterns.

The size of the tumorlet was determined to have comparable size to a typical PET voxel, because the PET-voxel is currently the smallest unit that can reveal the microenvironment from the *in-vivo* molecular imaging. Also, the information acquired from the PET image with various biomarkers can be used as input parameters for the model. Fur-

thermore, the heterogeneous dose distribution based on the PET image can be easily evaluated with this setting.

It is a strength of the model that the initial (relative) clonogen distributions are completely fixed by knowing the CLF together with the GF. Conversely, a simpler model would not be able to naturally integrate CLF and GF values. The size of the *P*-compartment is proportional to the GF and the size of the *H*-compartment is proportional to the product of the GF and the CLF. The *I*-compartment, of course, is the remainder.

The estimated $TLCD_{50}$ for a GF of 0.2 and a CLF of 0.9 was 46 Gy with the conventional fraction size of 2 Gy/fx. This corresponded to 64 Gy for a 10 cc homogeneous tumor, as shown in Figure 2-11, which is thought to be in the clinically relevant range of dose for the size. Except for the fraction size of 1.6 Gy/fx or very high GFs and 2.0 Gy/fx, the model predicted $TLCD_{50}$ value decreases as the GF increases, implying that a more proliferative tumor might have a more favorable prognosis compared to hypoxic tumors. The prognostic value of proliferation for head and neck cancer measured by Ki-67 labeling index (LI) is still controversial (Pich *et al*., 2004). Also, several authors have reported that the high proliferation correlates with a favorable response when treated with radiation therapy (Kropveld *et al*., 1998; Raybaud *et al*., 2000). Considering the critical importance of hypoxia in RT, higher proliferation, according to this model, implies less intermediately hypoxic cells, and more rapid reoxygenation.

Since the extremely hypoxic *H*-compartment is assumed to have a modest OER value of 1.37, and the cells in the *H*-compartment vanish relatively rapidly (less than 5 days for a GF of 0.2, Figures 2-4 and 2-5), the *I*-compartment is more important to RT response. The effect of different OER values of the *I*-compartment (1.2, 1.37 and 2.0)

was significant. For OER_I values of 1.2 and 1.37, the hypoxic effect was smaller than the proliferation effect in magnitude and the dose required for a hypoxic tumor (lower GF) was evaluated to be smaller than an oxic tumor (high GF), as shown in Figure 2-9. From clinical observations, it is known that hypoxic tumors require more dose for control and an OER_I of 2.0 seems to be more clinically relevant. For a 10 cc tumor with an OER_I of 2.0 (Figure 2-11), the dose difference (Δ) between hypoxic and oxic condition for 2 Gy/fx was about 20 Gy.

The fraction size effect was evaluated for various GFs. TCD_{50} is predicted to be relatively insensitive to fractionation, except when reoxygenation occurs before the end of therapy. For a small (10 cc) tumor, this only happens with high GF values and 2.0 Gy/fx or at lower GF values for 1.6 Gy/fx. For larger tumors (not shown), reoxygenation is likely to occur well before a tumoricidal dose is obtained, and hypofractionation may be an advantage, as proposed by Fowler *et al*. (Fowler *et al*., 2004).

The effect of overall treatment time on $TLCD_{50}$ was evaluated. The pattern was again closely related to reoxygenation as dose loss due to clonogen proliferation. The dependence of overall time on total dose, for tumorlets with a large enough growth fraction, shows a shape that might be identified as the "Withers dog-leg effect" (Withers *et al*., 1988). Accelerated clonogen proliferation after a certain "kick-off time" (often modeled by assuming a kickoff time of 2-4 weeks) arises naturally from this simple model and thus explains the kick-off time in terms of more fundamental radiobiological concepts. The result suggests that there might exist an optimal fractionation schedule if the GF were known. The extra dose required to compensate the loss of local control due to the longer treatment time was estimated to be 0.75 Gy/day and is driven by the kinetic and

radiosensitivity parameters. When the total dose is normalized to 2 Gy-fractionation (NTD_2), the extra dose per day was evaluated to be 0.69 Gy/day (data not shown), which agrees with the clinically observed value of 0.64 Gy/day (95%CL [0.42; 0.86]), which was estimated from a review of studies for head and neck cancer (Hendry *et al*., 1996).

The change in GF (0.1-0.3), OER_I, CLF, or tumor size showed little effect on the estimated extra dose required to overcome the longer schedule, which remained almost the same for those variations. At the end of the RT, when the success or failure of the treatment is determined, all the viable cells are in the *P*-compartment for the longer schedule. Therefore, the extra dose per day depends on the cell proliferation capacity of the *P*-compartment, which is unaffected with those parameters. Also, the failure of local control occurs in the *P*-compartment for the conventional fractionation schedule. This could be a possible explanation for the observed accelerated repopulation and fast relapse of the tumor after finishing the radiation therapy (Withers *et al*., 1988).

By incorporating a doomed sub-compartment, clinically realistic tumor regression patterns emerge. Reoxygenation takes place as doomed cells are removed from the tumorlet and the cells in the hypoxic compartments return to the (intermittently) normoxic *P*-compartment. Since the rate of doomed cell death increases as the GF increases, resulting in a larger *P*-compartment, reoxygenation becomes faster. In this model, the reoxygenation phenomenon is explicitly described based on a constant oxygenation capacity of a tumorlet, compared to other models in which the reoxygenation is modeled by assuming either a constant hypoxic fraction (Popple *et al*., 2002) or a constant reoxygenation rate (Søvik *et al*., 2007).

The regression pattern also depends on the removal of the doomed cells and was evaluated by incorporating mitotic cell death of doomed cells and the subsequent lysis mechanism. A tumorlet having a GF of 0.1-0.2, which is thought to be the most clinically relevant range, showed great agreement with clinical observations, as shown in Figure 2-8. The regression pattern was not significantly different for different fractional sizes (data not shown). Like the reoxygenation, the delayed clearance of the doomed cells seems to determine the rate of regression, which is mainly governed by the size of the *P*-compartment or the GF. Some researchers have developed tumor regression models based on the half-life of doomed cell disintegration (Chvetsov *et al*., 2008; Chvetsov *et al*., 2009; Huang *et al*., 2010). Chvetsov *et al.* (Chvetsov *et al*., 2009) evaluated the clinical data for HNSCC and found that the half-life of normoxic doomed cells is about 18 days. In our model, the disintegration of doomed cells consists of two steps–mitotic cell death and lysis– and the effective half-life was found to be about 15 days, which is similar to Chvetsov's result. This tumor regression pattern is important for modeling the interaction between tumorlets. Also, this pattern provides valuable information for inter-fractional adaptive RT (Chvetsov *et al*., 2008).

In the current study, the initial distribution of cells in each compartment was derived from the GF and CLF and the feasibility of the model was investigated. The method to produce the initial distribution from the PET image should be developed, so that this model can be used for the adaptive radiation therapy in which a boost dose is given in voxel dimension.

The current model is based on a tumorlet and this model should be expanded to the whole tumor to describe the whole tumor response to the radiation therapy. For this pur-

pose, the interaction between the adjacent tumorlets should be considered for the realistic description of the growth and regression pattern of a tumor. The change in blood supply during the RT should also be considered to improve the model, which was assumed to be fixed for the current work.

The feasibility of the voxel-based dose boosting is still controversial, but basically IMRT is thought to be capable of it. After the modeling of a whole tumor is completed and clinically validated, this model can be used to verify a treatment plan representing the TCP of each voxel. Further, the model can be helpful in the optimization of non-uniform dose distribution for voxel-based adaptive radiation therapy, considering the micro-regional factors in a heterogeneous tumor.

2.5. Conclusions

A tumor is a biologically heterogeneous entity and the micro-environmental factors such as hypoxia and proliferation are thought to significantly affect the treatment response to the RT. This heterogeneity of a tumor should be considered to increase the therapeutic effectiveness of the treatment. In this work, a compartmental TCP model was developed, in which the impact of various microenvironmental conditions on the treatment response can be evaluated. This model has three compartments based on the proliferation and hypoxia and focused on a small tumorlet having the size of a typical PET voxel. The initial distribution of the cells in the compartments was found based on various GFs and CLFs. The treatment response to the RT was demonstrated for HNSCC. The tumor dose required to achieve 50% of TCP (TCD_{50}) was found for various GFs and the fraction size effect was evaluated. The reoxygenation time for a given GF was estimated

and the effect of overall treatment time on the TCD_{50} was also evaluated. The model also predicted seemingly realistic tumor regression patterns, based on post-mitotic cell death and cell lysis. Although this model has minimum mathematical complexity, it yielded clinically relevant results and could successfully capture the clinically observed phenomena, such as fraction size effect, reoxygenation, the treatment time effect, and the tumor regression pattern. This flexible model provides an idealized prediction of how complex microenvironmental conditions are likely impacting local control rates, and can be used to generate hypotheses about potential fractionation changes. When the PET-derived information is integrated, this model can be used to design personalized RT strategies.

CHAPTER 3

CAN THE STATE-BASED MODEL EXPLAIN HIGH LOCAL CONTROL RATES FOR HYPOFRACTIONATED RADIOTHERAPY?

3.1. Introduction

Recently, hypofractionated stereotactic body radiation therapy (SBRT) has been widely accepted as an alternative treatment option for several types of tumors (Khrizman *et al*., 2010; Benedict *et al*., 2010; Chang *et al*., 2011). Most of its applications are for non-surgical lung cancer, for which clinical outcomes have shown much better local control rates when compared to conventional radiation therapy with acceptable toxicity (Chang & Timmerman, 2007; Chi *et al*., 2011).

SBRT uses a small number of fractions (usually less than 5 fx) with larger fraction sizes, ranging from 8 to 30 Gy/fx. With advanced localization and immobilization techniques, highly conformal radiation dose is delivered to the target volume, while exposure to the surrounding normal tissues is reduced by rapidly dropping the dose at the edge of the tumor.

Although SBRT has shown promising results, radiobiological understanding is still insufficient (Benedict *et al*., 2010; Chi *et al*., 2011). Clinical outcomes of SBRT are usually analyzed in terms of biologically effective dose (BED), which is based on the linear-quadratic model (L-Q model). The quantity is used to evaluate the treatment efficacy of SBRT by comparing with the dose response relationships of conventional radiation ther-

apy, which are well established in clinical experiences. However, this quantity does not consider all of the radiobiological differences between the conventional and SBRT fractionations.

In radiobiology, the four "R"s (repair of sublethal damage, repopulation, reassortment of cells within the cell cycle, and reoxygenation) are considered the basis of understanding the efficacy of fractionated radiation therapy (Hall and Giaccia, 2006). Conventional radiation therapy and SBRT depend on different radiobiological mechanisms: the conventional fractionation benefits from the reassortment and reoxygenation that accompanies that technique's small dose and long schedule, whereas SBRT benefits from the lesser sublethal damage repair and repopulation with its larger dose and shorter schedule. Therefore, when the outcomes of SBRT are compared with conventional radiation therapy, all these mechanisms should be considered.

The BED only considers the first "R", repair of sublethal damage: as the fractional dose increases, sublethal damage accumulates and results in higher cell death, as expressed in terms of relative effectiveness $\left[1+d\left(\alpha/\beta\right)\right]$. Sometimes, the second "R", repopulation, is included in the BED calculation, based on the potential doubling time for schedules longer than the so-called "kick-off" time of 3 to 4 weeks. However, the other two "R"s (reassortment and reoxygenation), which are disadvantageous for SBRT, are not considered in the BED calculation. This might cause overestimation of the treatment efficacy of SBRT and can possibly explain why the outcomes of SBRT are usually poorer than expected from the BED.

In the analyses of clinical outcomes of SBRT in terms of BED, several authors have concluded that the L-Q model overestimates cell killing, and they questioned the va-

lidity of the L-Q model for evaluating the high fractional dose used in SBRT (Timmerman *et al*., 2003; Chi *et al*., 2011). Taking hypoxia into consideration, however, other authors argued that the L-Q model is not sufficient enough to explain the high control rate and that other effects might be involved in SBRT (Brown & Koong, 2008; Brown *et al*., 2010; Carlson *et al*., 2011). These confusing conclusions are a result of the different radiobiological factors included in these studies. Therefore, it is necessary to consider all the radiobiological factors in evaluating the therapeutic efficacy of different fractionation schemes.

In this work, considering all the effects (the four "R"s), the treatment responses to different fractionation schemes were explored. A state-based tumor response model, in which the effects of proliferation, hypoxia and reoxygenation are already incorporated, was used to accommodate all the effects. Additionally, the cell cycle effect on different fraction sizes was included in terms of effective radiosensitivity and effective oxygen enhancement ratio (OER). A model predicted equivalent dose of 2 Gy/fx ($EQD_{2,model}$) was estimated using the resulting model and compared with BED-based NTD_2.

3.2. Methods and materials

3.2.1. Effective radiosensitivity based on cell cycle

The dependency of radiosensitivity on the cell cycle has long been recognized and is a well-known phenomenon (Madoc-Jones, 1964; Sinclair & Morton, 1966; Gillespie *et al*., 1975; Quiet *et al*., 1991; Biade *et al*., 1997). In general, the S-phase (especially late S-phase) is known to be the most radioresistant and cell cycles around mitosis (G2/M-phases) are known to be the most radiosensitive. Although the radiosensitivity of the ear-

ly G1-phase can be as high as that of the S-phase in some cells that have a long G1-phase time, the radiosensitivity of the G1-phase is known to be generally in between that of the S- and G2/M-phases.

To take the cell cycle dependency of radiosensitivity into account, the tumor population is divided into three subpopulations, based on cell cycle phases (G1, S and G2/M). The survival fraction (SF) of each cell cycle phase was calculated based on the L-Q model as follows:

$$SF = \exp\left(-\alpha d - \beta d^2\right) \tag{3.1}$$

The total survival fraction of the tumor is obtained as a summation of the survival fractions of the three cell cycle phases weighted by the cell cycle phase distribution. The effective radiosensitivity can be estimated based on the equivalent survival fraction, as shown in Equation 3.2. The effective radiosensitivity is dependent on both the fraction of cells and the radiosensitivity in each cell cycle.

$$\begin{aligned} SF_{pro} &= f_{G1}\exp\left(-\alpha_{G1}d - \beta_{G1}d^2\right) + f_S\exp\left(-\alpha_S d - \beta_S d^2\right) \\ &\quad + f_{G2/M}\exp\left(-\alpha_{G2/M}d - \beta_{G2/M}d^2\right) \\ &= \exp\left(-\alpha_{eff}d - \beta_{eff}d^2\right) \end{aligned} \tag{3.2}$$

where α_{eff} and β_{eff} are the effective L-Q parameters, d is the fractional dose, and f_X, α_X and β_X are the fraction of cells, linear parameter, and quadratic parameter for a given cell cycle X (G1, S or G2/M).

It is assumed that the cell distribution after a RT fraction returns to the previous distribution through reassortment (or redistribution) before the next fraction, which is reasonable, considering that usually there are two or more days of break between fractions in SBRT and that the desynchronization is a fast process.

3.2.2. Hypoxia and cell cycle

Tumor hypoxia is a general phenomenon for most human tumors, including lung cancer (Vaupel and Mayer, 2007). In the conventional fractionated RT (2 Gy/fx), the adverse hypoxic effect can be relieved by the reoxygenation process that accompanies its long schedule. In SBRT, however, the reoxygenation is not as effective as that in conventional fractionation due to SBRT's short schedule, and the hypoxic effect might be more significant. Increased radioresistance of hypoxic cells can be quantified in terms of the oxygenation enhancement ratio (OER), which is the ratio of the required dose in a hypoxic condition to the dose in a normoxic condition (Joiner & Kogel, 2009).

The OER of hypoxic cells is also known to be dependent on cell cycle phase. Palcic and Skarsgard found that the OER is dependent on dose (Palcic & Skarsgard, 1984; Révész & Palcic, 1985; Skarsgard & Harrison, 1991), and further research has shown this dependency of OER is a consequence of the variation of the OER with cell cycle phase. In their analysis, Freyer *et al.* (1991) found that the OER of CHO cells was evaluated to be highest for the S-phase (2.8-2.9) and lowest for the G1-phase (2.3-2.4). As the dose increases, the most resistant S-phase cells become dominant in the cell survival, and this causes an increase of the OER at a higher fractional dose.

Values for the OER are measured in *in vitro* experiments, in which a cell culture is usually exposed to nitrogen or argon gas for only a short time. In a tumor, however, the vast majority of hypoxic cells are thought to be in the quiescent phase, in which cells are arrested in the G0/G1-phase and cannot proliferate. The difference in cell cycle distribution between *in vivo* hypoxia (in a tumor) and *in vitro* hypoxia (in cell culture) might cause a significant discrepancy in OER values. Confluent (plateau phase) cell culture, in which nutrients or space is limited to imitate the *in vivo* condition of a tumor, has shown a decreased OER, with most hypoxic cells out of cell cycle (G0/G1-phase) (Berry *et al*., 1970; West *et al*., 1988). It has also been found that the cells in the G0-phase might be more sensitive to radiation damage, when compared with cells in the G1-phase (Luk *et al*., 1985; Wallen *et al*., 1985). Recently, it has been postulated that the repair mechanisms of hypoxic cells are less effective than normoxic cells (Zölzer & Streffer, 2002; Rothkamm *et al*., 2003; Chan *et al*., 2008; Chan *et al*., 2009).

In the current study, all the hypoxic cells are considered to be only in the G0/G1-phase and, therefore, a lower OER value was used. Since the hypoxic cells are in the same cell cycle, dose dependency does not exist with constant radiosensitivity. However, the OER changes as a function of dose, since normoxic radiosensitivity is changing. Like the reference radiosensitivity value, the OER values were applied to 2 Gy/fx and the effective OER (OER_{eff}) can be found as a function of fractional dose in the following equation:

$$SF_{hyp} = \exp(-\frac{\alpha_{eff}}{OER_{eff}}d - \frac{\beta_{eff}}{OER_{eff}^2}d^2) = \exp(-\frac{\alpha_{ref}}{OER}d - \frac{\beta_{ref}}{OER^2}d^2) \qquad (3.3)$$

where α_{eff} and β_{eff} are the effective L-Q parameters, OER_{eff} is the dose-dependent effective OER value, and α_{ref} and β_{ref} are the reference L-Q parameters at 2 Gy/fx.

3.2.3. State-based tumor response model

In order to evaluate the treatment response of various fractionation regimes, a state-based tumor response model, which incorporated all the effects of four "R"s, was used. A detailed description of the model has been given previously in Chapter 2. In brief, the model is comprised of three theoretical compartments (*P*-, *I*-, and *H*-compartments) and can evaluate treatment response of a small tumorlet having various microenvironments, including the interplay between hypoxia and proliferation. Proliferation takes place in the *P*-compartment and the cell loss takes place in the extremely hypoxic *H*-compartment. In the intermediate *I*-compartment, neither proliferation nor cell loss takes place. Unlike repopulation based on kick-off time, a fraction of the cells in the *P*-compartment of this model keep proliferating. With a doomed sub-compartment, reoxygenation takes place over a course of radiotherapy: following post-mitotic cell death and clearance of proliferating cells, intermediate cells move into the proliferative compartment and hypoxic cells move into the intermediate compartment. Cell-cycle-dependent radiosensitivity has been included in the model, and radiosensitivity of the hypoxic compartment was determined, as explained in the previous section.

3.2.4. Model-predicted equivalent dose of 2 Gy/fx ($EQD_{2,model}$)

The treatment efficacy of the SBRT regime was evaluated in terms of equivalent dose in 2 Gy/fx (5 fx/week) in order to compare with conventional RT. To estimate the

$EQD_{2,model}$, two separate simulations were performed: first, the cell survival fraction was estimated for the SBRT regime with the fraction-size-dependent effective radiosensitivity and then, a conventional 2 Gy-fraction was simulated to find the same level of survival fraction as the SBRT regime.

The estimated $EQD_{2,model}$ was compared with NTD_2 for various SBRT schedules which differed in either number of fractions or treatment duration. For several typical SBRT regimes, the $EQD_{2,model}$ was estimated and compared with NTD_2.

3.2.5. Model parameters for lung cancer SBRT

In the model, the degree of proliferation and hypoxia-caused cell death are determined by the size of each compartment, which is derived from the growth fraction (GF) and cell loss factor (CLF). GF and CLF values of 0.25 and 0.92, respectively, were used for simulation, based on the potential doubling time (8 days) and volume doubling time (100 days) measured for lung cancer (Tinnemans *et al*., 1993; Shibamoto *et al*., 1998). Cell cycle time (T_c) was assumed to be 2 days.

For simplicity, we assumed the α/β ratio to be 10 for all cases. The cell cycle distribution was assumed to be 78%, 12% and 10% for the G1-, S-, G2/M-phases, respectively, based on a flow cytometric analysis of 187 surgical specimens of non-small-cell lung cancer (Volm *et al*., 1985). Since the exact values for cell-cycle-dependent radiosensitivity are not available for lung cancer, the ratios of radiosensitivity of the G1- and G2/M-phases to the most resistant S-phase (α_{G1}/α_S and $\alpha_{G2/M}/\alpha_S$) were introduced and several sets of these ratios [α_{G1}/α_S, $\alpha_{G2/M}/\alpha_S$] were assumed, including [2, 3], which are thought to be relevant values for a human tumor. The radiosensitivity of each cell cycle phase was

derived from the reference radiosensitivity value (α_{ref} = 0.35) that was used at 2 Gy/fx (Mehta *et al*., 2001).

The hypoxic cells in the *I*- and *H*-compartments are considered to be only in the G0/G1-phase, which results in fraction-size-independent radiosensitivity. The OER values were assumed to be 2 and 1.4 for the *I*- and *H*-compartments, respectively, at 2 Gy/fx, considering the lower OER of the G0/G1 phase and reduced repair capability of a chronically hypoxic cell. The parameter values used for the model simulation are summarized in Table 3-1.

Table 3-1. Parameter values used for the model simulation for lung cancer

Parameter	Value
Growth fraction (GF)	0.25[a]
Cell loss factor (CLF)	0.92[a]
Cell cycle time (T_C)	2 days (Joiner & Kogel, 2009)
Fraction of cells in P compartment (f^P)	50 %[b]
G1-phase in P (f^P_{G1})	28 % (Volm *et al*., 1985)
S-phase in P (f^P_S)	12 % (Volm *et al*., 1985)
G2/M-phase ($f^P_{G2/M}$)	10 % (Volm *et al*., 1985)
Fraction of cells in I compartment (f^I)	27 %[b]
Fraction of cells in H compartment (f^H)	23 %[b]
Ratio of alpha of G1- to S-phase (α_{G1}/α_S)	1.5, 2 or 3[c]
Ratio of alpha of G2/M- to S-phase ($\alpha_{G2/M}/\alpha_S$)	2, 3 or 5[c]
Reference radiosensitivity at 2 Gy/fx (α_{ref})	0.35 Gy^{-1} (Mehta *et al*., 2001)
Alpha-beta ratio (α/β)	5 or 10 Gy[c]
OER of I compartment at 2 Gy/fx (OER_I)	2[c]
OER of H compartment at 2 Gy/fx (OER_H)	1.4 (Chan *et al*., 2008)

[a] estimated from potential doubling time and volume doubling time measured for lung cancer (Tinnemans *et al*., 1993; Shibamoto *et al*., 1998)
[b] estimated from GF and CLF of the model
[c] assumed parameters

3.3. Results

3.3.1. Effective radiosensitivity for proliferating tumor cells

For proliferating tumor cells, the radiosensitivity of each cell cycle phase was estimated from Equation 3.2 based on relevant distribution of cell cycle phases for lung cancer and reference radiosensitivity at 2 Gy/fx (Table 3-1). For three assumed ratios of radiosensitivities (α_{G1}/α_S and $\alpha_{G2/M}/\alpha_S$), the cell-cycle-dependent radiosensitivity values are calculated as shown in Table 3-2.

Table 3-2. Estimated radiosensitivity of each cell cycle phase for several assumed ratios of radiosensitivities with assumed cell cycle distribution (G1: 56%, S: 24% and G2/M: 20%) and reference alpha of 0.35 (assuming, α/β=10).

Cell cycle	The ratio of radiosensitivity [α_{G1}/α_S , $\alpha_{G2/M}/\alpha_S$]		
	[1.5, 2]	**[2, 3]**	**[3, 5]**
α_{G1}	0.3625	0.3759	0.3968
α_S	0.2417	0.1880	0.1323
$\alpha_{G2/M}$	0.4833	0.5639	0.6613

Using the calculated cell-cycle-dependent radiosensitivity values, the survival fraction of each cell cycle phase was estimated, as shown in Figure 3-1, along with the total survival fraction. As the fractional dose increases, relatively sensitive cells in the G2/M- and G1-phases are preferentially killed and then more resistant cells in the S-phase are controlled. The cells in the S-phase become dominant after about 5 Gy/fx, and the values for the total survival fraction follow those for the cycle's survival fraction.

In Figure 3-2, the effective alpha value was presented as a function of the fractional dose in Gy for three different sets of ratios of alpha values (α_{G1}/α_S and $\alpha_{G2/M}/\alpha_S$). As the fractional dose increases, the effective alpha values decrease and approach to the alpha value of the most resistant cell cycle phase (S-phase). As the variation of radiosensitivity increases throughout the cell cycle with increased ratios of alpha values (α_{G1}/α_S and $\alpha_{G2/M}/\alpha_S$), the decrease in effective radiosensitivity becomes more significant. Note that the effective radiosensitivity is identical for the reference radiosensitivity at 2 Gy.

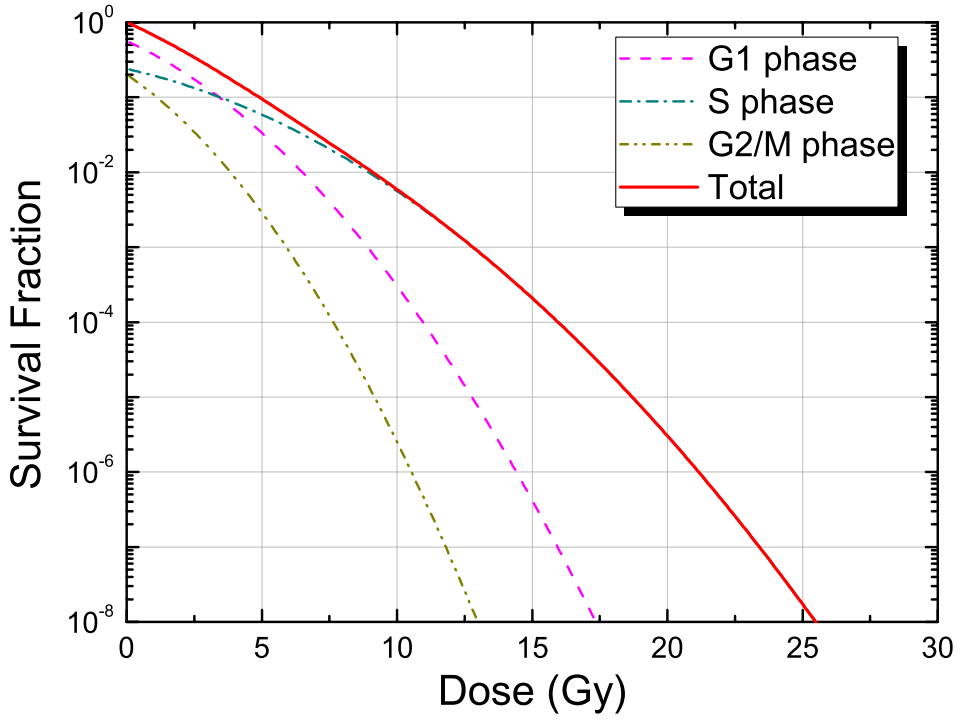

Figure 3-1. Survival fraction (SF) of each cell cycle phase and the total SF for proliferating cells in P compartment based on individual radiosensitivity values (α_{G1}/α_S=2 and $\alpha_{G2/M}/\alpha_S$=3) with assumed cell cycle distribution (G1: 56%, S: 24% and G2/M: 20%).

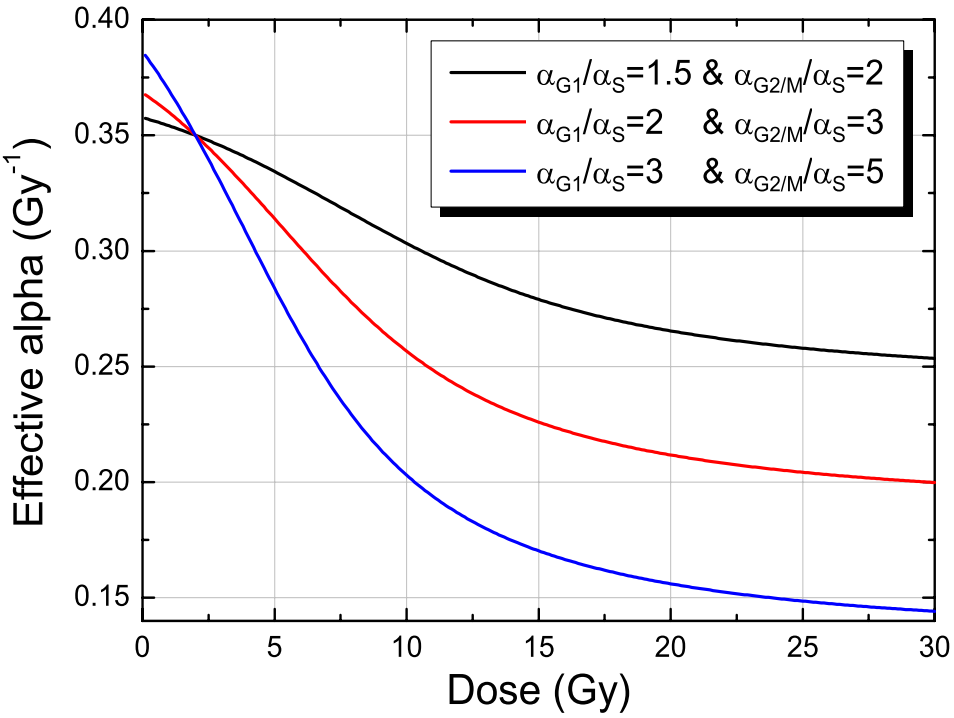

Figure 3-2. Effective alpha value as a function of fractional dose, estimated from the assumed cell cycle distribution (56% of G1-phase, 24% of S-phase and 20% of G2/M-phase) and cell-cycle-dependent radiosensitivity values (α_{G1}/α_S=2 and $\alpha_{G2/M}/\alpha_S$=3). At 2 Gy/fx, a reference alpha value of 0.35 was used.

3.3.2. Effective OER for hypoxic tumor cells

Hypoxia was considered in the model with two hypoxic compartments (*I*- and *H*-compartments). Since the cells in hypoxia were assumed to be only in G0/G1-phase, the survival fractions of the hypoxic compartments are determined by a single radiosensitivity value, whereas the survival fraction of the proliferating compartment is composed of three different cell cycle phases (G1, S and G2/M) with different radiosensitivity values. The survival fraction of each compartment is shown in Figure 3-3. Cell cycle distribution of 78%, 12% and 10% for G1-, S- and G2/M-phases, respectively, was used for the proliferating *P*-compartment with radiosensitivity ratios of α_{G1}/α_S =2 and $\alpha_{G2/M}/\alpha_S$ =3. Due to the relatively resistant S-phase in the *P*-compartment, the slope of the survival fraction of

the *P*-compartment becomes shallow as the fractional dose increases and becomes similar to the slope of the survival fraction of the *H*-compartment. Although the slope of the survival fraction of the *I*-compartment is still more shallow than that of the *P*-compartment, relative resistance decreases with increasing fraction dose. The effective OER values for hypoxic compartments are shown in Figure 3-4. The survival fraction and OER values for different radiosensitivity ratio values (α_{G1}/α_S and $\alpha_{G2/M}/\alpha_S$) are shown in Appendix A.4.

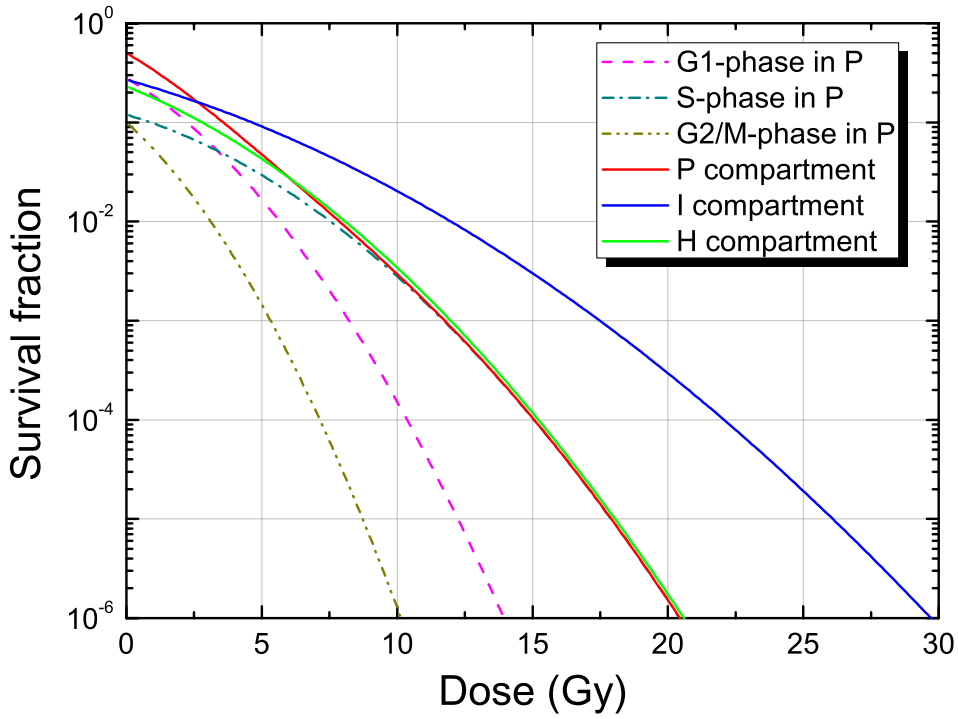

Figure 3-3. Survival fraction of each compartment including cell-cycle-phase-dependent SF in *P*-compartment for cell cycle distribution in *P*-compartment of 78%, 12% and 10% for G1-, S- and G2/M-phase, respectively, and radiosensitivity ratios of α_{G1}/α_S=2 and $\alpha_{G2/M}/\alpha_S$=3.

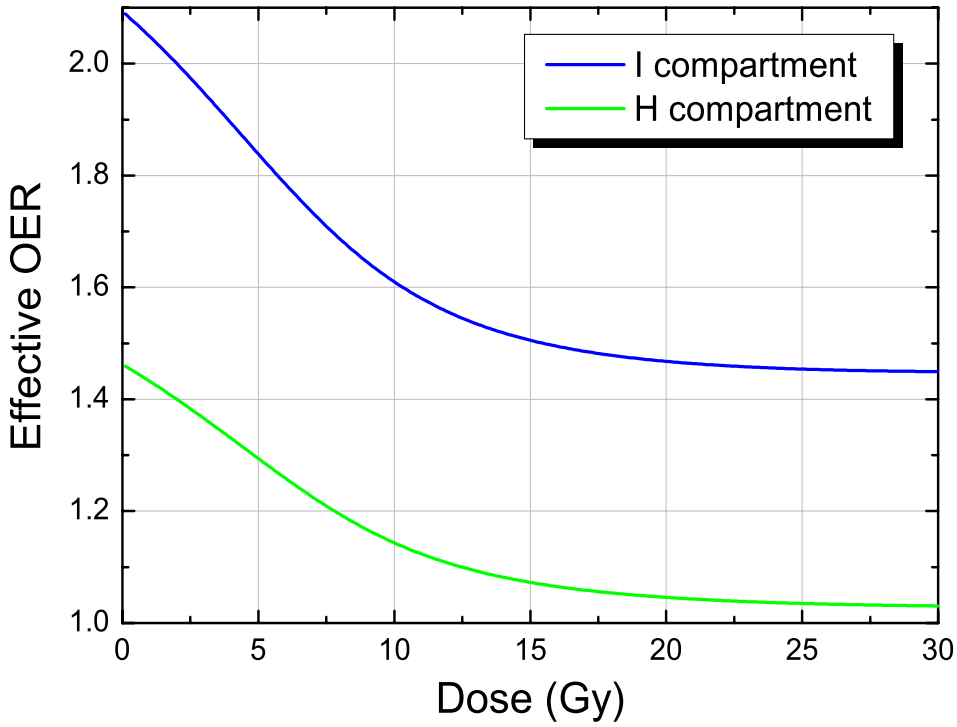

Figure 3-4. Effective OER values of *I*- and *H*-compartments as a function of fractional dose for cell cycle distribution in *P*-compartment of 78%, 12% and 10% for G1-, S- and G2/M-phase, respectively, and radiosensitivity ratios of α_{G1}/α_S=2 and $\alpha_{G2/M}/\alpha_S$=3.

3.3.3. Estimated $EQD_{2,model}$ and comparison with NTD_2 for SBRT regimes

An equivalent dose in 2 Gy/fx was estimated with the model for SBRT regimes. First, the survival fraction of a SBRT regime was predicted (Figure 3-5a) and then, the simulation in 2-Gy/fx RT was performed until the same level of survival fraction was achieved (Figure 3-5b). Note that the survival fractions are not exactly the same due to the discrete nature of the 2-Gy-fractionation and the exact $EQD_{2,model}$ should be between 64 Gy and 66 Gy for the example case shown in Figure 3-5. The survival fraction of SBRT was determined by hypoxic cells in the *I*-compartment without reoxygenation. The 2-Gy-fraction dealt with proliferating cells that exhibited accelerated repopulation after full reoxygenation at about two weeks.

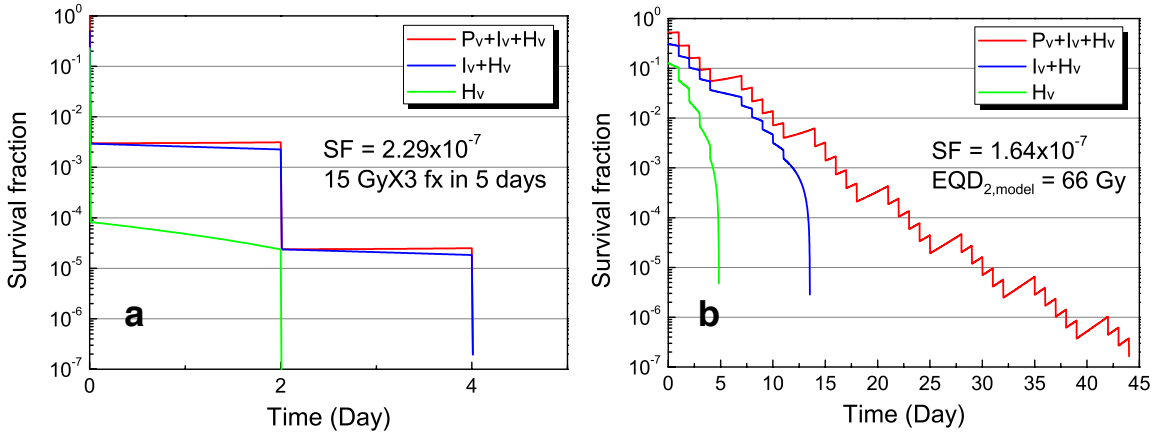

Figure 3-5. Example of estimating the $EQD_{2,model}$ based on survival fractions of (a) SBRT regimen (15Gy×3fractions) and (b) conventional 2-Gy fractionation using state-based mathematical tumor response model, in which fraction-size-dependent radiosensitivity (α_{eff} = 0.238 for 15 Gy/fx and 0.35 for 2 Gy/fx), proliferation and hypoxia effects are incorporated.

The $EQD_{2,model}$ was estimated for various SBRT regimes and compared with NTD_2. In Figure 3-6, three different daily fractionations are compared. As the number of fractions increased, treatment efficacy (in terms of the ratio $EQD_{2,model}/NTD_2$) increased due to cell cycle reassortment between fractions and increased reoxygenation with a longer schedule. In Figure 3-7, different treatment durations were compared for 3-fraction SBRT. As treatment duration increased, treatment efficacy increases with better reoxygenation. The increase of treatment efficacy was more significant for a 15-day schedule, and this seems to be related to full reoxygenation time, which is about 2 weeks. Note that cell cycle distribution of 78%, 12% and 10% for G1-, S- and G2/M-phases, respectively, was used for the proliferating *P*-compartment with radiosensitivity ratios of α_{G1}/α_S =2 and $\alpha_{G2/M}/\alpha_S$ =3. The results of different radiosensitivity ratio values (α_{G1}/α_S and $\alpha_{G2/M}/\alpha_S$) are shown in Appendix A.4.

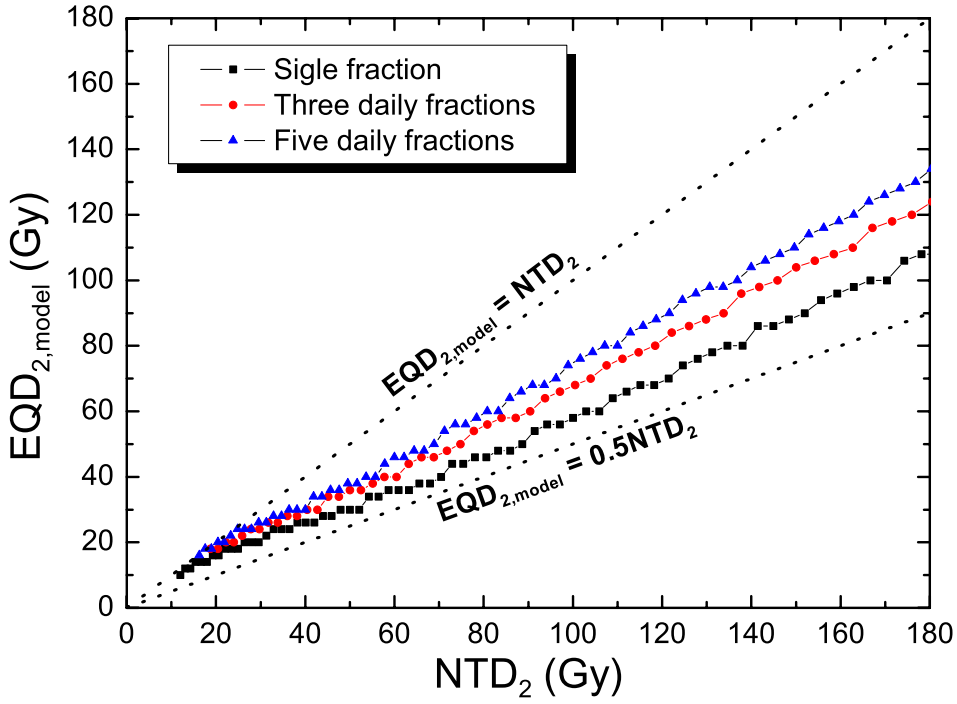

Figure 3-6. Model-predicted equivalent dose of 2 Gy/fx ($EQD_{2,model}$) vs. NTD_2 for several numbers of daily fractions.

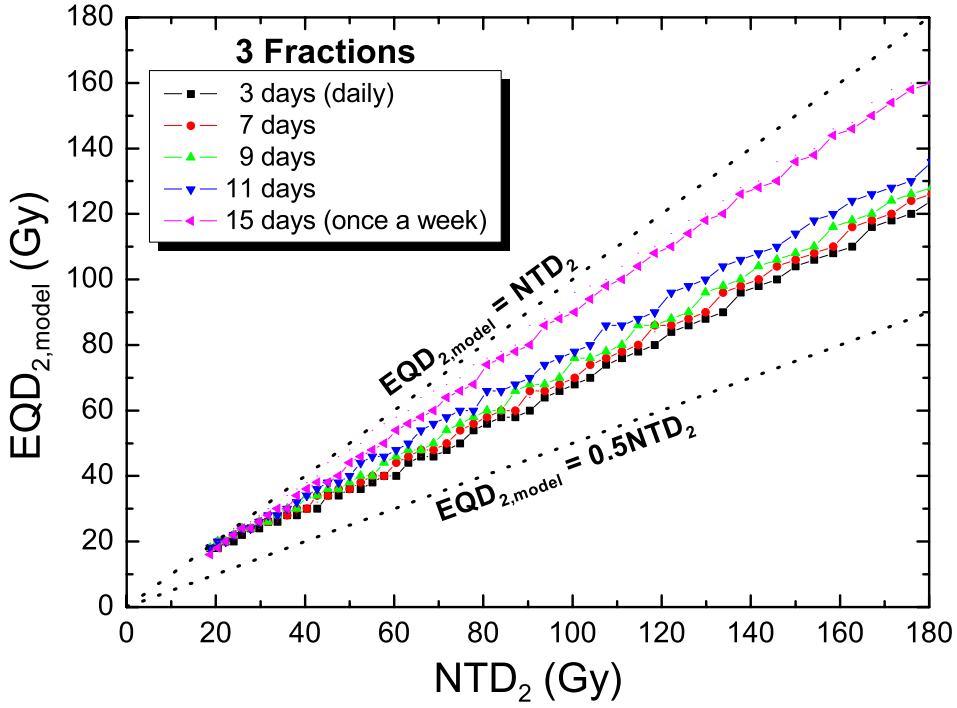

Figure 3-7. Model predicted equivalent dose of 2 Gy/fx ($EQD_{2,model}$) vs. NTD_2 for several treatment durations for 3-fraction SBRT.

For several typical SBRT regimens, the estimated $EQD_{2,model}$ and survival fraction (SF) at the end of therapy were evaluated for two different α/β ratio values (α/β=5 and 10). For the α/β ratio of 10, the result is shown in Table 3-3. The model-predicted $EQD_{2,model}$ was significantly less than the BED-based NTD_2, by 25% to 30 %. The treatment duration of SBRT affected the treatment efficacy and the ratio of $EQD_{2,model}/NTD_2$ was lowest for high-dose single-fraction SBRT (~60%). With the longer treatment duration, the $EQD_{2,model}$ increased and approached NTD_2, due to increased reoxygenation. For most evaluated SBRT regimens, predicted cell survival levels were too high to account for the high local control rates that have been reported for SBRT outcomes.

Table 3-3. The model-predicted equivalent dose in 2 Gy/fx ($EQD_{2,model}$) and survival fraction (SF) at the end of therapy for several typical SBRT regimes to achieve the same surviving fraction of viable cells at the end of radiotherapy (α/β = 10).

SBRT regimen (Gy×# fx)	Treatment duration (day)	BED (Gy)	NTD_2 (Gy)	$EQD_{2,model}$[a] (Gy)	$EQD_{2,model}/NTD_2$	Estimated SF at the end of RT
26×1	1	93.6	78	46	59 %	1.1×10^{-5}
30×1	1	120	100	58	58 %	8.2×10^{-7}
12×3	9	79.2	66	48	73 %	4.3×10^{-6}
15×3	5	112.5	93.75	66	70 %	2.3×10^{-7}
20×3	8	180	150	108	72 %	1.2×10^{-10}
22×3	8	211.2	176	126	72 %	5.4×10^{-12}
12×4	12	105.6	88	78	89 %	2.3×10^{-8}

BED: biologically effective dose, NTD_2: normalized total dose at 2 Gy fraction, SF: survival fraction
[a] model-predicted equivalent dose in 2 Gy/fx including cell cycle, proliferation and hypoxia effects

In Table 3-4, the estimated $EQD_{2,model}$ and survival fraction (SF) at the end of therapy were shown for the α/β ratio of 5. Due to increased quadratic radiosensitivity (β component of L-Q model), the cell kill effect was significantly increased, which resulted in higher NTD_2 and lower SF, compared to the result of α/β=10. With a lower α/β ratio (α/β=5), the treatment efficacy of SBRT was evaluated to be increased, and the ratio of $EQD_{2,model}/NTD_2$ was significantly increased.

Table 3-4. The model-predicted equivalent dose in 2 Gy/fx ($EQD_{2,model}$) and survival fraction (SF) at the end of therapy for several typical SBRT regimes to achieve the same surviving fraction of viable cells at the end of radiotherapy (α/β = 5).

SBRT regimen (Gy×# fx)	Treatment duration (day)	BED (Gy)	NTD_2 (Gy)	$EQD_{2,model}$[a] (Gy)	$EQD_{2,model}/NTD_2$	Estimated SF at the end of RT
26×1	1	161.2	115.1	76	66 %	3.9×10^{-8}
30×1	1	210	150	100	67 %	4.7×10^{-10}
12×3	9	122.4	87.4	68	78 %	1.0×10^{-7}
15×3	5	180	128.6	96	75 %	8.1×10^{-10}
20×3	8	300	214.3	164	77 %	5.7×10^{-15}
22×3	8	356.4	254.6	194	76 %	3.1×10^{-17}
12×4	12	163.2	116.6	108	93 %	1.0×10^{-10}

BED: biologically effective dose, NTD_2: normalized total dose at 2 Gy fraction, SF: survival fraction
[a] model predicted equivalent dose in 2 Gy/fx including cell cycle, proliferation and hypoxia effects

3.4. Discussion

In this work, the treatment efficacy of SBRT was evaluated by the state-based mathematical model, including the effects of cell cycle, hypoxic, proliferation, and reox-

ygenation. The effectiveness of SBRT was quantified in terms of equivalent dose in 2 Gy/fx ($EQD_{2,model}$), which yielded the same level of surviving fraction of viable cells as the SBRT regime at the end of radiotherapy. For various SBRT regimes, the $EQD_{2,model}$ was compared with the normalized total dose in 2 Gy/fx (NTD_2), which is usually used to evaluate the clinical outcomes of SBRT. Although there was variation in degree depending on the fraction size and schedule, in general, the BED-based NTD_2 was evaluated to overestimate the efficacy of SBRT by about 30% compared to the $EQD_{2,model}$.

Table 3-5. Effect of each factor (cell cycle effect, proliferation and hypoxia) on the model-predicted equivalent dose in 2 Gy/fx ($EQD_{2,model}$) for several typical SBRT regimes ($\alpha/\beta = 10$).

SBRT regimen (Gy×# fx)	NTD_2 (Gy)	$EQD_{2,model}$[a] (Gy)						
		C	P	H	C+P	C+H	P+H	All (C+P+H)
26×1 (1 day)	78	46	156	34	78	34	46	46
30×1 (1 day)	100	58	208	40	106	40	60	58
12×3 (9 days)	66	46	120	36	74	36	50	48
15×3 (5 days)	93.75	62	190	44	110	42	66	66
20×3 (8 days)	150	92	320	62	180	60	110	108
22×3 (8 days)	176	106	384	70	216	68	128	126
12×4 (12 days)	88	62	170	50	106	48	84	78

NTD_2: normalized total dose at 2 Gy fraction, C: cell cycle effect, P: proliferation, H: hypoxia
[a] model predicted equivalent dose in 2 Gy/fx including cell cycle, proliferation and hypoxia effects

To test the effect of each factor (cell cycle effect, proliferation and hypoxic), the $EQD_{2,model}$ was evaluated for all combinations of the factors as shown in Table 3-5 for

α/β=10. The result showed that the proliferation significantly increases the $EQD_{2,model}$, while the cell cycle effect and hypoxia decreases the $EQD_{2,model}$, which verifies that SBRT benefits from inhibiting proliferation but suffers from the lack of cell cycle redistribution and reoxygenation. Interestingly, the $EQD_{2,model}$ values with only cell cycle effect included (column 'C' in the table) was evaluated to be similar to the $EQD_{2,model}$ with all factors included (C+P+H). It seems that the adverse hypoxic effect is cancelled out by proliferation to a certain extent and the cell cycle effect is dominant until the BED is very high.

The direct comparison of the result with clinical outcome is not easy, since the SBRT technique is not standardized yet and there are many factors to consider in interpreting the clinical outcomes from different institutions, such as the immobilization and localization technique and the dose calculation algorithm.

Considering the reported high local control rates in SBRT, however, the classic radiobiological factors included in the model seems to be not enough to explain the clinical outcomes of SBRT, as other researchers have already concluded in the consideration of hypoxia (Brown & Koong, 2008; Brown *et al*., 2010; Carlson *et al*., 2011). There might be alternative mechanisms in the high fractional dose range used in SBRT, such as vascular endothelial cell apoptosis (Garcia-Barros *et al.*, 2003) and immune stimulation after tumor ablative SBRT (Lee *et al.*, 2009).

3.5. Conclusion

Based on the state-based model, in which well-established radiobiological principles are incorporated, the treatment efficacy of SBRT was evaluated in terms of the mod-

el predicted equivalent dose in 2 Gy/fx ($EQD_{2,model}$). It is verified that the treatment efficacy of SBRT estimated from BED is significantly overestimated compared to the model results and the SBRT schedule seems to affect the treatment efficacy. Considering the reported high local control rates of SBRT in clinical, non-classical biological or radiobiological principles are apparently at work in high-dose SBRT treatments.

CHAPTER 4

MODEL SIMULATIONS OF THE CORRELATION OF HIGH FDG-PET AND REDUCED LOCAL CONTROL: CAN THE STATE-BASED MODEL EXPLAIN CLINICAL OBSERVATION?

4.1. Introduction

As the most commonly used functional imaging modality, ^{18}F-fluorodeoxyglucose (FDG) positron emission tomography (PET) has played a valuable role in oncology since first synthesized in 1978 (Ido *et al*., 1978). The tumor cells exhibit an increased glucose uptake as a result of upregulated glycolysis (Gatenby & Gillies, 2004) and the FDG PET, as a glucose analogy, can show the spatial distribution of glucose uptake in a patient. The FDG-PET has become an important diagnostic tool for cancer detection, staging and target definition (Biehl *et al*., 2006; van Baardwijk *et al*., 2006; Janssen *et al*., 2009; Zhong *et al*., 2009), as well as for monitoring tumor response after treatment (Mac Manus *et al*., 2005; van Loon *et al*., 2009).

Although there are several contrary results (Vesselle *et al*., 2007; Agarwal *et al*., 2009), many clinical studies have shown that the uptake of FDG, usually measured as a standardized uptake value (SUV), is a significant predictor of prognosis (Ahuja *et al*., 1998; Vansteenkiste *et al*., 1999; Dhital *et al*., 2000; Jeong *et al*., 2002; Downey *et al*., 2004; Borst *et al*., 2005; Cerfolio *et al*., 2005; Sasaki *et al*., 2005; Xue *et al*., 2006; Kidd *et al*., 2007; van Baardwijk *et al*., 2007; Casali *et al*., 2009; Chen *et al*., 2009; Xie *et al*., 2009). Also, the region of high FDG uptake is known to be radioresistant and correlated

with increased local failure and shorter survival (Madani *et al*., 2007b; Soto *et al*., 2008; Abramyuk *et al*., 2009; Aerts *et al*., 2009).

Based on the clinical outcome, the FDG-avid region in a tumor is recognized as a possible target for dose escalation. Several planning and optimization studies have assessed the feasibility of dose boosting on the sub-volume of a tumor based on the FDG-PET image with the intensity modulated radiation therapy (IMRT) (Das *et al*., 2004; Vanderstraeten *et al*., 2006; Thorwarth *et al*., 2007; Thorwarth *et al*., 2008; Feng *et al*., 2009). In those studies, however, the extra dose was prescribed either by a uniform boost based on clinical experience or by the level of SUV with an arbitrarily determined maximum dose level. In either case, there is no clear basis for the determination of extra dose.

The enhanced glycolysis of tumor cells might be a result of hypoxia, because hypoxic cells produce energy through glycolysis without oxygen. However, it is also recognized that tumor cells showed increased glycolysis even in the presence of oxygen, known as Warberg effect (Warburg, 1956). This aerobic glycolysis is thought to be caused by a number of genetic changes in a malignant tumor (Dang & Semenza, 1999; Kim & Dang, 2006; Heiden *et al*., 2009). Many studies have been carried out to correlate FDG uptake with physiological parameters, such as hypoxia, proliferation, blood flow, histology and differentiation, using PET, immune histochemical method, and histology (Vesselle *et al*., 2000; Rajendran *et al*., 2004; Pugachev *et al*., 2005; Hara *et al*., 2006; Zimny *et al*., 2006; Kelly *et al*., 2007; Yamamoto *et al*., 2007; Buchmann *et al*., 2008; Dierckx & Van De Wiele, 2008; Vesselle *et al*., 2008; Bruechner *et al*., 2009). Although several studies have shown the relationship between the FDG uptake and hypoxia or proliferation, the underlying mechanism of FDG uptake in a tumor is still unclear.

In this study, the extra dose required to compensate for the worse outcome of FDG-avid tumor was explored. Based on the available published data for head and neck squamous cell carcinoma (HNSCC), the range of extra dose was estimated, which is required to equalize local control between FDG-avid and non-avid tumors. Also, the FDG uptake mechanism was explored using the state-based mathematical model for tumor response, in which classical radiobiological mechanisms were incorporated. Several different FDG uptake patterns were hypothesized and tested in the model to find a relevant FDG uptake mechanism, which is consistent with the clinical observation.

4.2. Methods and materials

4.2.1. Clinical outcome review and study criteria

A literature review was performed for radiation therapy (RT) for head and neck squamous cell carcinoma (HNSCC), in which RT outcomes were compared for high and low FDG uptake groups based on the maximum standardized uptake value (SUV_m). Among nine relevant trials (Minn *et al*., 1997; Brun *et al*., 2002; Kunkel *et al*., 2003; Allal *et al*., 2004; Schwartz *et al*., 2004; Kim *et al*., 2007; Roh *et al*., 2007; Machtay *et al*., 2009; Torizuka *et al*., 2009), four provided adequate data for analysis, based on the following criteria: (1) only RT patients were included or separate outcome comparison for the RT group was performed; (2) the endpoint of the analysis is either local control rate (LC) or disease-free survival (DFS); and (3) the administrated dose was reported. The trials included in this study are shown in Table 4-1.

Table 4-1. The trials included in this study.

Clinical data	Site	SUV_m cut-off	# patients	Disease-free Survival (%)		Local Control (%)		RT Dose
Roh *et al*., 2007	Larynx/ Hypo-pharynx	<8	23	54	3-year	74.4*	3-year	69.8 Gy (61.2-73.8)
		≥8	16	27	(p=0.002)	36.6*		
Kim *et al*., 2007	Orophar-ynx	<6	11	78	3-year	86	3-year	68.8 Gy (60.2-76.2)
		≥6	10	33		30	(p=0.039)	
Allal *et al*., 2004	Head and Neck	<5.5	73	79	4-year	88	4-year	69.9 Gy (69.8-74.4)
		≥5.5		40	(p=0.005)	58	(p=0.01)	
Brun *et al*., 2002	Head and Neck	<9.0	23			96	5-year	68 Gy (66-70)
		≥9.0	23			57	(p=0.003)	

* Estimated from disease-free survival (DFS) (refer section 4.2.2).

4.2.2. Estimate of local control rate from disease free survival

The endpoint used in the study was LC as a surrogate of tumor control probability (TCP). For the clinical data, in which only DFS was reported, the LC was estimated from DFS based on the meta-study that analyzed the 17 treatment-control comparisons (6515 patients) on the effect of altered-fractionation for HNSCC (Michiels *et al*., 2009). It was assumed that the change in LC (ΔLC) is proportional to the change in DFS (ΔDFS). The proportional coefficient between ΔLC and ΔDFS was found to be 1.4 and the ratio of LC/DFS at 3 years was also found to be 1.37 from the meta-analysis. Both factors were applied to DFS, and LC was estimated (Table 4-1).

4.2.3. Logistic TCP model and estimate of boost dose for high FDG uptake

The logistic TCP model was used to estimate the tumor dose for 50% of control (TD_{50}), as shown in the following equation (Schultheiss *et al*., 1983):

$$TCP = \frac{1}{1+\left(\frac{TD_{50}}{D}\right)^{4\gamma_{50}}} \tag{4.1}$$

where TCP is tumor control probability as a function of dose (D) and γ_{50} is normalized slope of the TCP curve at TD_{50}. For both high and low FDG SUV_m groups, the TD_{50} values were estimated from the reported prescribed dose and local control rates for several assumed γ_{50} values.

The boost dose required for the high FDG SUV_m group to achieve the same level of TCP as the low FDG SUV_m group was estimated from the ratio of TD_{50} values between the high and low FDG SUV_m groups ($TD_{50,high}/TD_{50,low}$). When the same slope (γ_{50}) was applied to both groups, the dose ratio between the high and low FDG SUV_m groups ($D_{50,high}/D_{50,low}$) for a given level of TCP remains unchanged, which is also equal to the ratio of $TD_{50,high}/TD_{50,low}$. Therefore, the dose required for high FDG SUV_m group was estimated from the product of prescribed dose and the ratio of $TD_{50,high}/TD_{50,low}$.

4.2.4. State-drive tumor response model for evaluation of FDG uptake pattern

To explore the potential relationship between FDG-PET uptake and classical radiobiological mechanisms, a previously developed state-based tumor response model was used. The model is comprised of three sub-populations of cells based on the level of pro-

liferation, hypoxia, and cell loss, which is thought to be related to the available amount of oxygen and glucose, as shown by Kiran *et al*. (Kiran *et al*., 2009). The model focused on a small tumorlet that has a comparable size to a typical PET voxel ($4\times4\times4$ mm^3), which is the smallest *in-vivo* imaging unit that can reveal the microenvironment within a tumor. Figure 4-1(a) shows three compartments before RT. Proliferation takes place only in the *P*-compartment and cell loss in the *H*-compartment. Cells in the *I*-compartment neither proliferate nor die. The transition of cells between compartments is determined by the size of each compartment, not by fixed transfer rates. After RT begins, the damaged cells (calculated by L-Q model) become doomed with compartment-specific radiosensitivity and mitotic cell death takes place in the P_d sub-compartment (Figure 4-1(b)). As doomed cells die out, the hypoxic cells move toward the *P*-compartment and, in this process, re-oxygenation occurs, while viable cells in the *P*-compartment still proliferate and cause repopulation.

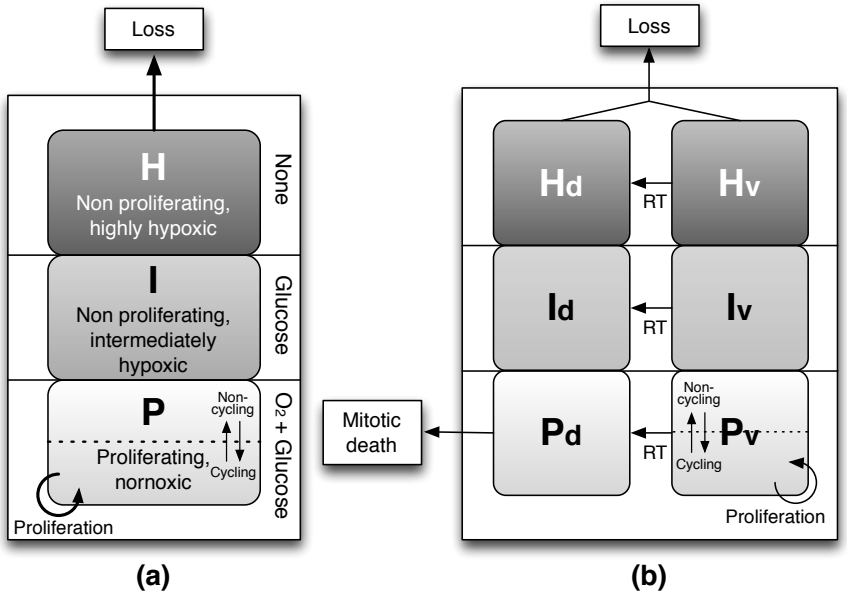

Figure 4-1. Schematic diagram of the model: (a) just prior to the initiation of radiation therapy and (b) after radiation therapy begins with doomed sub-compartment in each compartment.

4.2.5. Assumed FDG uptake pattern

The sub-populations of tumor cells in the model were distinguished based on oxygen and glucose availability (Kiran *et al*., 2009), and only the *P*- and *I*-compartments were thought to be associated with FDG uptake. Based on the correlation studies between FDG and physiological factors, three different potential relationships between FDG uptake and cell sub-populations were hypothesized: the FDG uptake is proportional to the total number of metabolically viable cells (*pattern I*); the FDG uptake is associated mainly with the proliferating cells with minor contribution from intermediate cells (*pattern II*); and, the FDG uptake is associated mainly with the intermediate cells with minor contribution from proliferating cells (*pattern III*). The contribution from extremely hypoxic cells in the *H*-compartment contribution was additionally tested (*uptake pattern IV*).

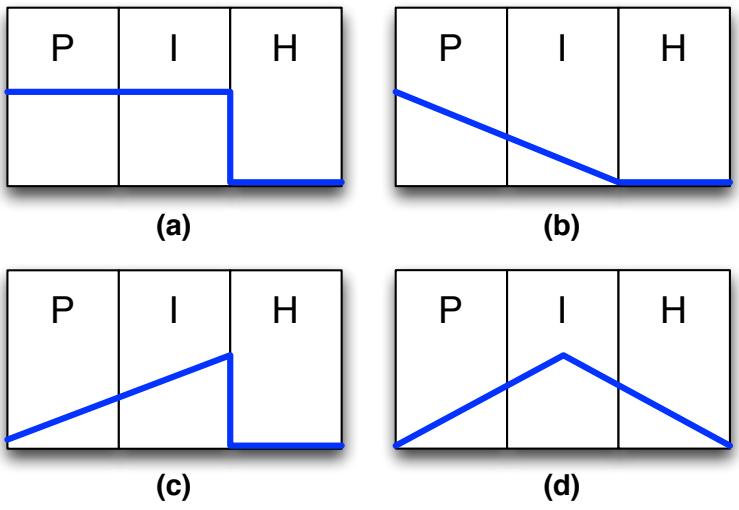

Figure 4-2. Assumed FDG uptake patterns in each compartment. The FDG uptake pattern was assumed to be: (a) proportional to the total number of viable cells (*pattern I*), (b) associated mainly with proliferation with minor contribution from intermediate hypoxia (*pattern II*), (c) associated mainly with intermediate hypoxia with minor contribution from proliferation (*pattern III*), and (d) associated mainly with intermediate hypoxia with minor contribution from proliferation and extreme hypoxia (*pattern IV*).

4.2.6. Estimation of FDG uptake and TD_{50} and the correlation

The model simulations were performed in 2 Gy/fx (5 fx/week) using relevant parameter values for head and neck squamous cell carcinoma (HNSCC), including radiosensitivity of the *P*-compartment (α_p=0.41 & α/β=10) (Søvik *et al*., 2007). The hypoxic cells in the *I*- and *H*-compartments are considered to be only in the G0/G1-phase and the OER values for the *I*- and *H*-compartments were assumed to be 2 and 1.4, respectively, considering the lower OER of the G0/G1-phase and reduced repair capability of a chronically hypoxic cell (Chan *et al*., 2008).

For each assumed FDG uptake pattern, the FDG uptake values were quantified for all possible initial distributions of cells in each compartment, which are determined based on growth fraction (GF) and cell loss factor (CLF). The tumor dose for 50% control (TD_{50}) was also estimated for all initial distribution and correlated with the quantified FDG uptake values. After linear regression, the coefficient of determination (R^2) was found for each hypothesized uptake pattern.

4.3. Results

4.3.1. Estimate of boost dose required to compensate for high FDG uptake in HNSCC

The boost dose required to compensate for the worse outcome of the high FDG uptake group was found based on the logistic TCP model (Equation 4.1). With a γ_{50} of 2, which is thought to most likely represent the clinical reality, the estimated boost doses were in the range of 16-30 Gy. Considering the prescribed dose was about 70 Gy, the re-

quired total dose for the high FDG uptake group was in the range of 85-98 Gy. In Figure 4-3, the estimated boost dose is shown for each clinical trial with a γ_{50} of 2.

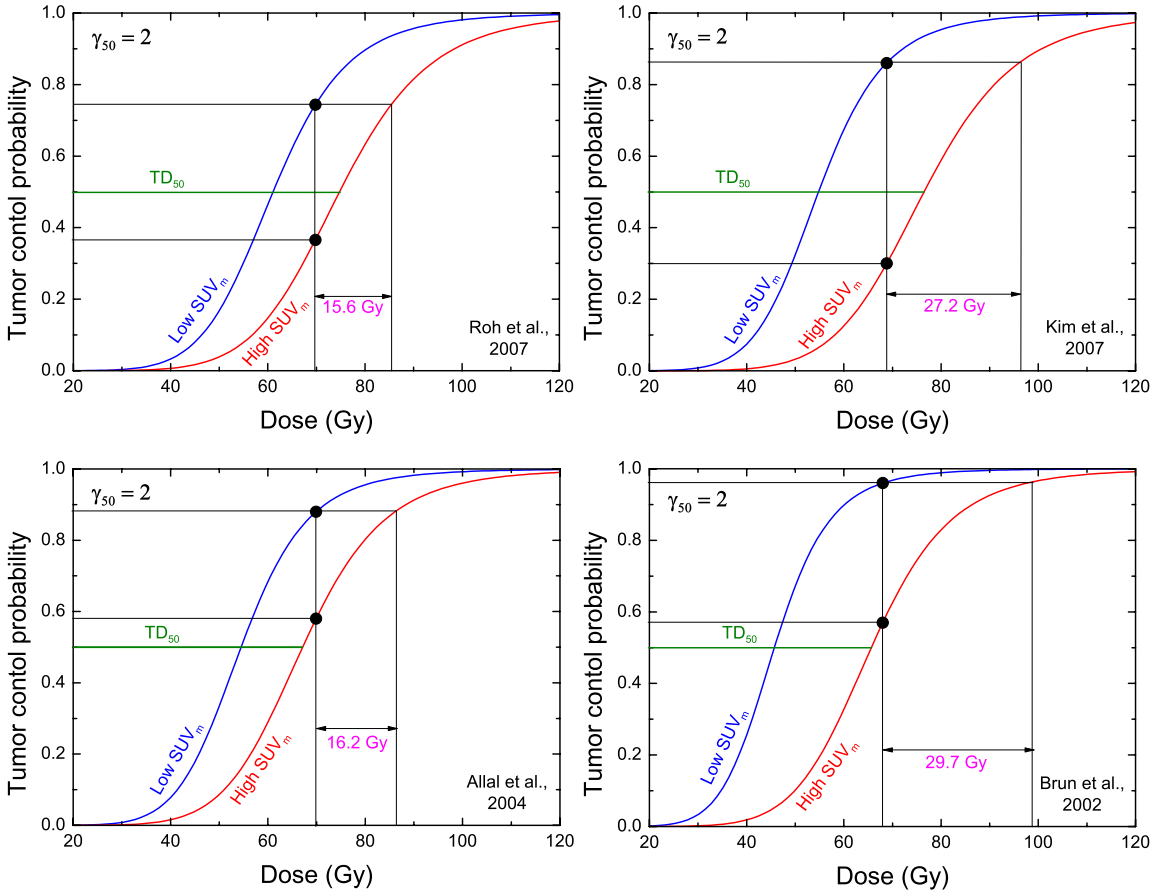

Figure 4-3. Estimated boost dose to equalize the TCP of high FDG uptake group to that of low FDG uptake group for each clinical trial data, based on logistic TCP model with γ_{50}=2.

The TD_{50} values for the high and low FDG uptake groups were estimated for each trial with three different γ_{50} values (γ_{50}=1, 2, and 4), as shown in Table 4-2. The estimated TD_{50} was significantly lower for the low FDG uptake group than the high FDG uptake group and the difference was larger for a smaller γ_{50} value (shallower slope of the TCP curve). For a clinically relevant γ_{50} =2, TD_{50} for the low FDG uptake group ($TD_{50,low}$) was

in the range of 46-61 Gy, while TD_{50} of the high FDG uptake group ($TD_{50,high}$) was 66-77 Gy.

The ratio of TD_{50}'s for the high and low FDG uptake groups ($TD_{50,high}/TD_{50,low}$) was also calculated and shown in Table 4-2. Estimated $TD_{50,high}/TD_{50,low}$ ratios were found to be in the range of 1.11~2.06, with decreasing tendency as the presumed slope of the dose-response relationship (γ_{50}) increased up to 4. With γ_{50}=2, which is thought to most likely represent the clinical reality, the derived ratios ($TD_{50,high}/TD_{50,low}$) were 1.22, 1.40, 1,23, and 1.44 for each clinical data.

Table 4-2. Estimated TD_{50} values for each group and the ratios of TD_{50} between high and low SUV_m groups ($TD_{50,high}/TD_{50,low}$) for three different γ_{50} values for HNSCC.

Clinical data	SUV_m cut-off	TD_{50}		
		γ_{50} = 1	γ_{50} = 2	γ_{50} = 4
Roh *et al*., 2007	< 8	53.5	61.1	65.3
	≥ 8	80.1	74.8	72.2
	Ratio	1.50	1.22	1.11
Kim *et al*., 2007	< 6	43.7	54.8	61.4
	≥ 6	85.0	76.5	72.5
	Ratio	1.95	1.40	1.18
Allal *et al*., 2004	< 5.5	42.5	54.5	61.7
	≥ 5.5	64.5	67.1	68.5
	Ratio	1.52	1.23	1.11
Brun *et al*., 2002	< 9.0	30.7	45.7	55.8
	≥ 9.0	63.4	65.7	66.8
	Ratio	2.06	1.44	1.20

Considering all the data included in this study, the TCP curves for the high and low FDG uptake groups were evaluated by logistic regression analysis with γ_{50}=2, as shown in Figure 4-4. The estimated TD_{50} values were 55 Gy for the low FDG uptake group and

71 Gy for the high FDG uptake group. The ratio of $TD_{50,high}/TD_{50,low}$ was 1.29, which means the high FDG uptake group requires about 29% of extra dose to equalize the TCPs between low and high FDG uptake groups.

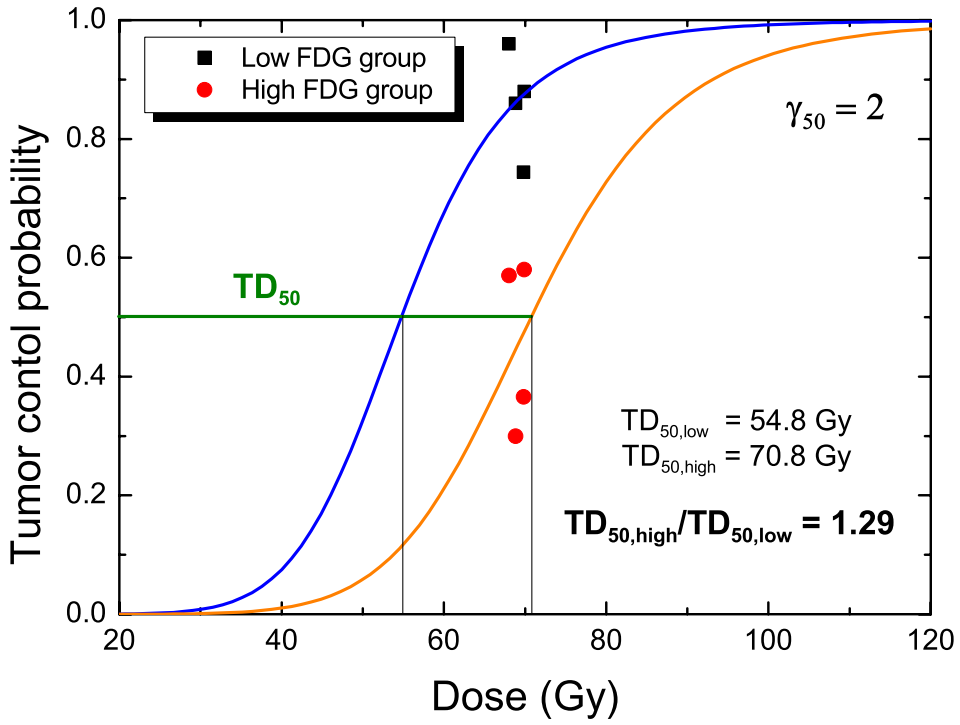

Figure 4-4. TCP curves for high and low FDG uptake groups evaluated by logistic regression analysis and the estimated TD_{50} value for each group with the ratio of $TD_{50,high}/TD_{50,low}$ for γ_{50}=2.

4.3.2. Correlation between FDG uptake and model predicted TD_{50}

TD_{50} values were calculated for all possible initial conditions of the model, which is determined by the growth fraction and cell loss factor. The estimated TD_{50} values for all conditions are shown in Figure 4-5. TD_{50} increases as the growth fraction decreases, with a larger fraction of cells in hypoxic compartments. The TD_{50} decreased as the cell

loss factor increased but the dependency of TD_{50} on the cell loss factor was much less significant than the growth fraction.

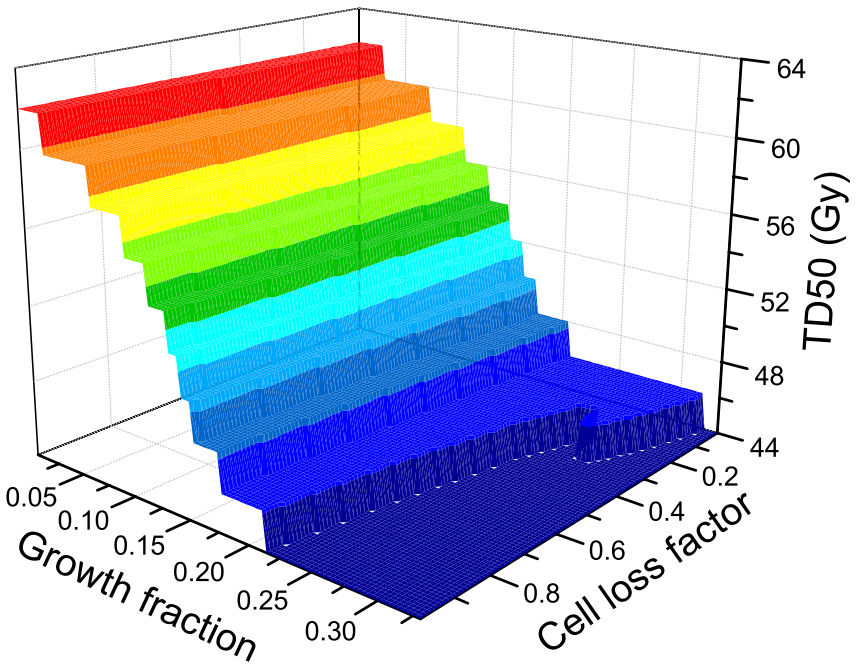

Figure 4-5. Model predicted tumor dose for 50% control (TD_{50}) in 2 Gy/fx for all possible initial conditions given by growth fraction (GF) and cell loss factor (CLF).

The FDG uptake value was quantified for each initial condition based on the hypothesized FDG uptake pattern and compared with the required TD_{50} for the initial condition. The correlations between FDG uptake and TD_{50} were shown in Figure 4-6 for four different hypothetical FDG uptake patterns.

For the first assumed pattern (*pattern I*), where the FDG uptake was assumed to be proportional to the total number of viable cells, only weak positive correlation was observed with a coefficient of determination (R^2) of 0.38. When the uptake pattern was assumed to be mainly associated with cell proliferation with minor contribution from intermediate cells (*pattern II*), significant negative correlation existed between FDG uptake

and TD_{50} ($R^2 = 0.76$), which is opposed to the clinical observation. For the hypothesis that metabolically-viable hypoxic cells in the *I*-compartment are avid for FDG uptake (*pattern III*), a strong positive correlation was acquired ($R^2 = 0.85$), which is consistent with the clinical observation. Inclusion of the contribution from extremely hypoxic cells in the *H*-compartment (*pattern IV*) yielded almost the same result as *uptake pattern III*, with a slightly higher value of coefficient of determination ($R^2 = 0.86$).

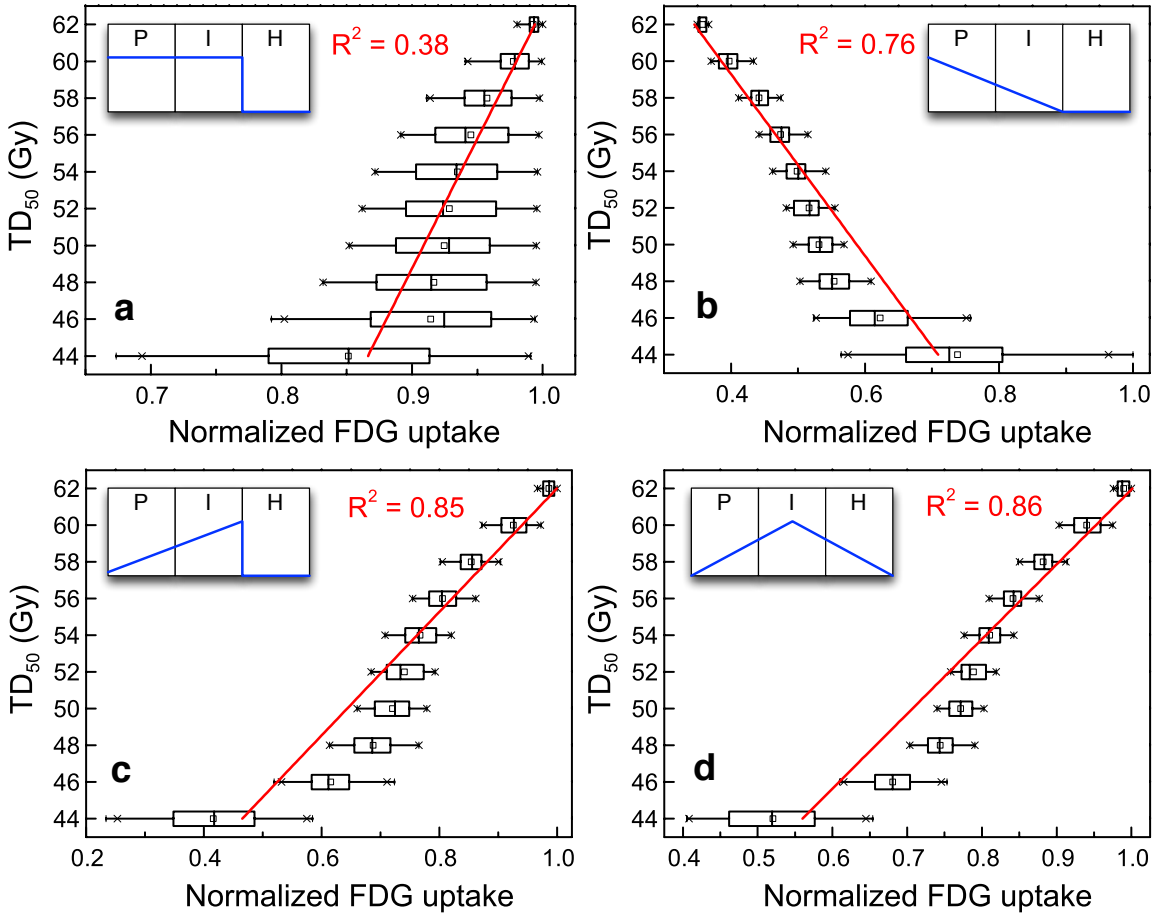

Figure 4-6. Model predicted tumor dose for 50% control (TD_{50}) in 2 Gy/fx vs. FDG uptake (normalized to maximum) for four different hypothetical uptake patterns: (a) proportional to the total number of viable cells, (b) associated mainly with proliferation with minor contribution from intermediate hypoxia, (c) associated mainly with intermediate hypoxia with minor contribution from proliferation, and (d) associated mainly intermediate hypoxia with minor contribution from proliferation and extreme hypoxia.

To explore the relationship between FDG uptake and growth fraction (GF), the correlation between FDG uptake (for *pattern IV*) and TD_{50} was evaluated for a fixed cell loss factor of 0.9, as shown in Figure 4-7. For the assumed uptake pattern, the FDG uptake was inversely correlated with the GF.

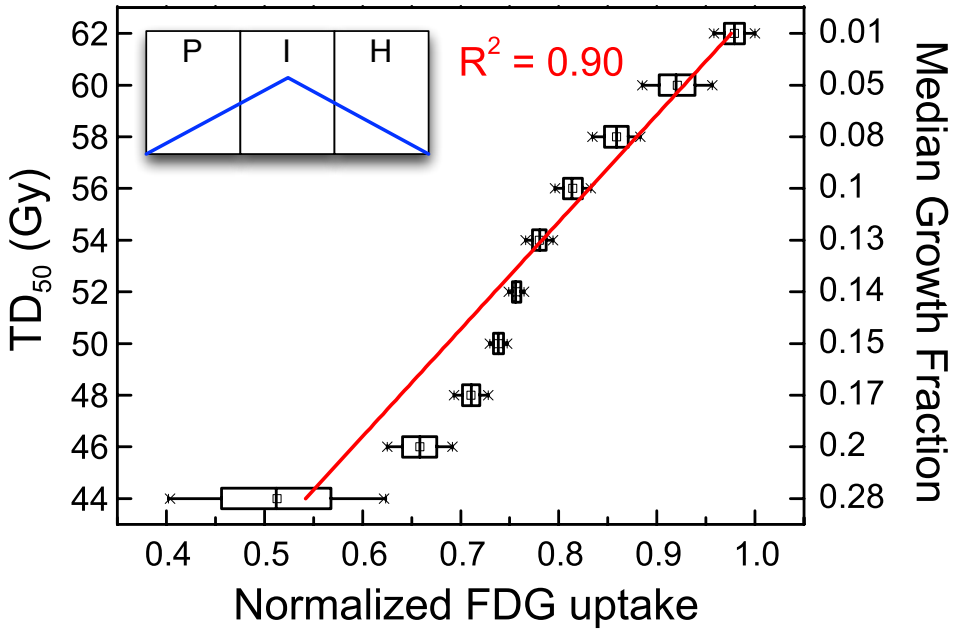

Figure 4-7. Model predicted tumor dose for 50% control (TD_{50}) in 2 Gy/fx vs. FDG uptake (normalized to maximum) with median growth fraction value for each TD_{50} group (right axis) for FDG uptake pattern IV with fixed cell loss factor of 0.9.

4.4. Discussion

Despite of the well-known relationship between a high FDG uptake and increased local failure, there was no effort to derive the boost dose for an adverse high FDG uptake tumor from the clinical outcomes. In this work, the boost dose was estimated from available clinical outcome data. With the same assumed slope of TCP curve (γ_{50}) for both groups, the boost dose required for the high FDG uptake group to achieve the same level

of TCP can be directly calculated from the ratio of $TD_{50,high}/TD_{50,low}$ for any TCP level. For the total data set, the ratio of $TD_{50,high}/TD_{50,low}$ was estimated to be 1.29 with $\gamma_{50}=2$, which implies 29% of extra dose for the high FDG uptake group. Assuming a non-boost dose of 70 Gy, the most likely boost dose becomes about 90 Gy (84-98 Gy for each data set). Considering the possible variation of the γ_{50} value, however, the values between 78 Gy and 144 Gy cannot be ruled out.

In the absence of an established cut-off for the FDG-PET SUV_m, different institutes used their own best discriminative SUV_m cut-off value. The relationship between the ratio of $TD_{50,high}/TD_{50,low}$ and the cut-off SUV_m could not be found from this study, as shown in Figure 4-8.

This analysis was performed for the dichotomous groups (high vs. low SUV_m) without group mean value. If this analysis would be performed for the several stratified groups with group mean value, the relationship between the SUV_m and required extra dose might be also found. Although conclusive results cannot be obtained with the few available data, this study provides a proper approach to derive the prescription function from clinical data. Also, these estimates provide a rational starting point for clinical trials to test the usefulness of IMRT boots for FDG-avid tumors.

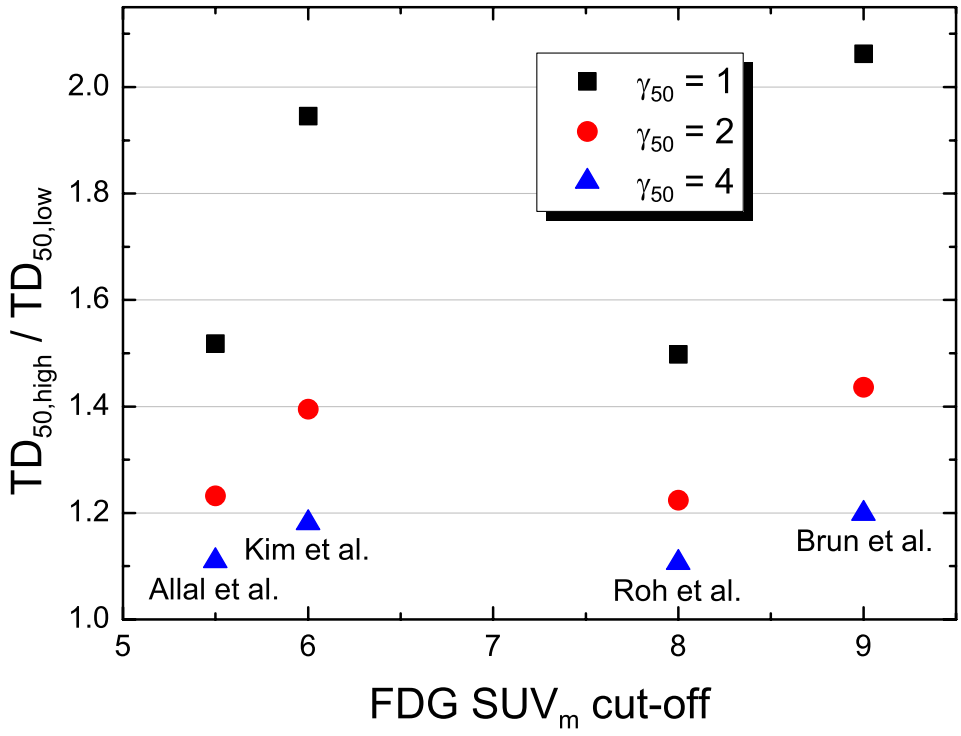

Figure 4-8. The ratios of TD_{50} between high and low FDG uptake groups ($TD_{50,high}/TD_{50,low}$) for three different γ_{50} values with respect to FDG SUV_m cut-off values.

In this work, the FDG uptake mechanism was also explored using a state-based mathematical model for tumor response, in which classical radiobiological mechanisms were incorporated. Three different FDG uptake patterns were hypothesized based on published correlation studies, in which the number of viable cells, proliferation, or hypoxia was observed to correlate with the FDG uptake tumor. For each assumed FDG uptake pattern, the model simulation was performed to find a relevant FDG uptake mechanism, which is consistent with the clinically observed radioresistance of a high FDG uptake. Among the assumed FDG uptake patters, only for the metabolically-viable hypoxia with minor contribution from proliferation (uptake pattern III, Figure 4-6(c)) was a significant positive correlation between FDG uptake and required TD_{50} observed (R^2=0.85), which implies that the number of metabolically hypoxic cells (in the *I*-compartment of the mod-

el) is responsible for the increased radioresistance and is therefore associated with FDG uptake.

Since one of the basic assumptions of the model was that the FDG uptake takes place only in the *P*- and *I*-compartments, the contribution of cells in the *H*-compartment was not evaluated. When the total number of cells in each hypoxic compartment (*I*- or *H*-compartment) was correlated with the required TD_{50} values, a strong positive correlation was observed for the *I*-compartment ($R^2 = 0.86$), but a weak negative correlation for the *H*-compartment ($R^2 = 0.38$), as shown in Figure 4-9.

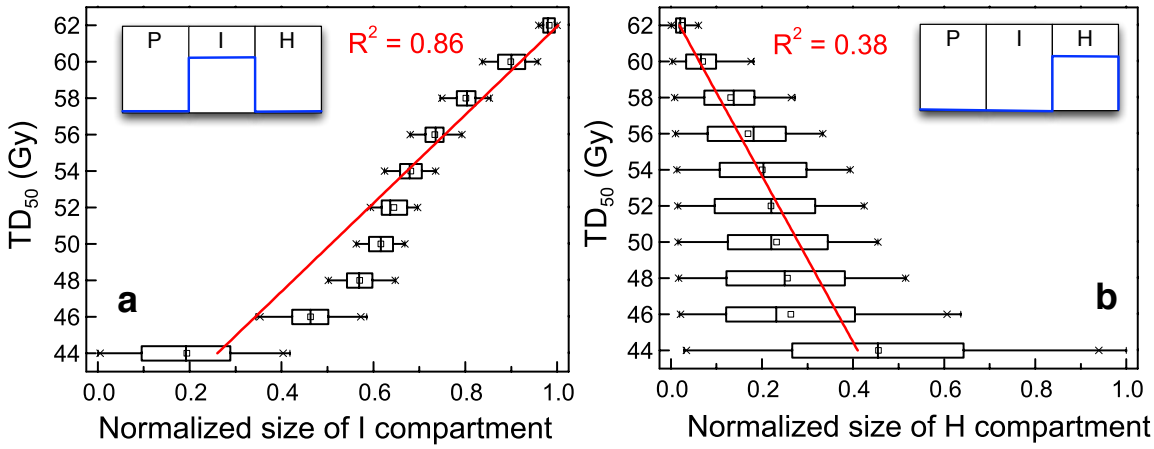

Figure 4-9. Model predicted tumor dose for 50% control (TD_{50}) in 2 Gy/fx vs. the number of cells in I compartment (a) or H compartment (b) (normalized to maximum).

This implies that the extremely hypoxic cells in the *H*-compartment do not exhibit the increased radioresistance. This might be caused by the lower OER value of the *H*-compartment used for the model simulation ($OER_H = 1.37$), compared to the OER of the *I*-compartment ($OER_I = 2$). Therefore, higher values of OER_H ($OER_H = 2$ or 3) were simulated and the results were shown in Table 4-3. Although the significance of the correlation was slightly reduced as the OER_H increased, the same relationships were observed.

Even when the OER_H was assumed to be 3, the strong correlation between the required TD_{50} and the intermediate hypoxia in the *I*-compartment was conserved (R^2=0.83).

Table 4-3. Dependency of OER of *H*-compartment on the correlation between hypothesized FDG uptake pattern and required TD_{50} (OER_I = 2).

OER of *H*-compartment	Correlation coefficient, R (coefficient of determination, R^2)			
	Pattern I	**Pattern II**	**Pattern III**	**Pattern IV**
1.4	0.62 (0.38)	-0.87 (0.76)	0.92 (0.85)	0.93 (0.86)
2	0.62 (0.38)	-0.88 (0.77)	0.93 (0.86)	0.93 (0.87)
3	0.59 (0.35)	-0.87 (0.75)	0.90 (0.82)	0.91 (0.83)

The result suggests that the total number of metabolically-viable hypoxic cells (in *I*-compartment of the model) is a deterministic factor in tumor response and this sub-population might be associated with FDG uptake, which exhibits clinically adverse effects. This result is consistent with the voxel-by-voxel correlation studies performed by Pugachev *et al*. (2005) and Rajendran *et al*. (2004), in which the microregional relationship between FDG and hypoxia was observed. Also the result supports the study of Wouters and Brown, in which the importance of the cells at intermediate oxygen level was emphasized (Wouters & Brown, 1997).

4.5. Conclusion

In this work, the implication of FDG uptake in tumor control was explored in two ways: first, the range of extra dose required to compensate for high FDG uptake was estimated from clinical data; second, the potential relationship between FDG-PET uptake and classical radiobiological mechanisms was explored using a mathematical framework. The boost dose mostly likely required to compensate for radioresistant FDG-avid tumors is estimated to be about 90 Gy, assuming a non-boost dose of 70 Gy, although values between 78 Gy and 144 Gy cannot be ruled out. These estimates provide a rational starting point for clinical trials to test the usefulness of IMRT boost for FDG-avid tumors. Also, several different FDG uptake patterns were hypothesized and the estimated FDG uptake values were correlated with tumor dose for 50% control (TD_{50}) using the state-based tumor response model. Given the established clinical fact that FDG uptake correlates to a requirement of higher dose to achieve local control, the results support a potential avidity of FDG for cells in the intermediate stress state between being well-oxygenated (and proliferating) and very poorly oxygenated (extremely hypoxic).

CHAPTER 5

AN IN-DEPTH LOOK AT THE STATE-BASED MODEL AND ASSOCIATED USER INTERFACE

5.1. Introduction

A mechanistic compartmental TCP model was developed in Chapter 2, which can evaluate the treatment response of a tumorlet having various microenvironmental conditions. Three theoretical compartments (proliferative, intermediate, and hypoxic compartments) were included in the model, which represent cell subpopulations in different states. A distribution of the number of cells in each compartment corresponds to a specific microenvironmental condition in terms of the levels of proliferation, hypoxia, and cell loss, which is determined by a growth fraction (GF) and a cell loss factor (CLF) of a voxel-sized tumorlet. Based on the model, treatment response to conventional fractionated radiation therapy was evaluated for many aspects, including tumor dose required for 50% control for various microenvironments and fraction sizes, the reoxygenation time, the effect of overall treatment time, and the tumor regression pattern.

The cell cycle effect on the fraction size was additionally included into the model in Chapter 3. The fraction size dependent radiosensitivity values and oxygen enhancement ratio (OER) were estimated and the treatment response to hypofractionated radiation therapy (or SBRT) was evaluated in terms of model predicted equivalent dose in 2 Gy/fx ($EQD_{2,model}$), which implies the tumor dose (in conventional 2 Gy/fx) required to achieve the same level of cell kill as the hypofractionated radiation therapy (or SBRT).

The FDG uptake mechanism was also explored using the model in Chapter 4 to find a relevant FDG uptake mechanism, which is consistent with the clinically observed radioresistance of a high FDG uptake. Three different FDG uptake patterns were hypothesized and the model simulation was performed to correlate the tumor response with the FDG uptake value for each assumed uptake pattern.

These various analyses involving many simulations throughout this project were integrated into a model software, called 'PIH' code (named after the initials of each compartment). This code enables one not only to reproduce the simulation results discussed in the previous chapters, but also to easily evaluate different parameter settings using the convenient graphical user interface. As a time discretized simulation algorithm, the code can execute fast and efficient simulations, and also allows us to flexibly add or subtract effects, states, and state transitions. This code will be made publicly available and open-source.

5.2. The Matlab Graphical User Interface (GUI)

The PIH code was built using the Matlab® mathematics software package (The Mathworks, Inc.: www.mathworks.com), which provides one of the most efficient matrix computation environments with simple syntax and a rich set of intrinsic functions. Also, Matlab offers intuitive graphical user interface (GUI) tools, which provides the PIH code with easy and interactive control of the simulation. The GUI of PIH code contains all components (simulation type selection, input parameters and the result plots) required for simulation in a window, as shown in Figure 5-1.

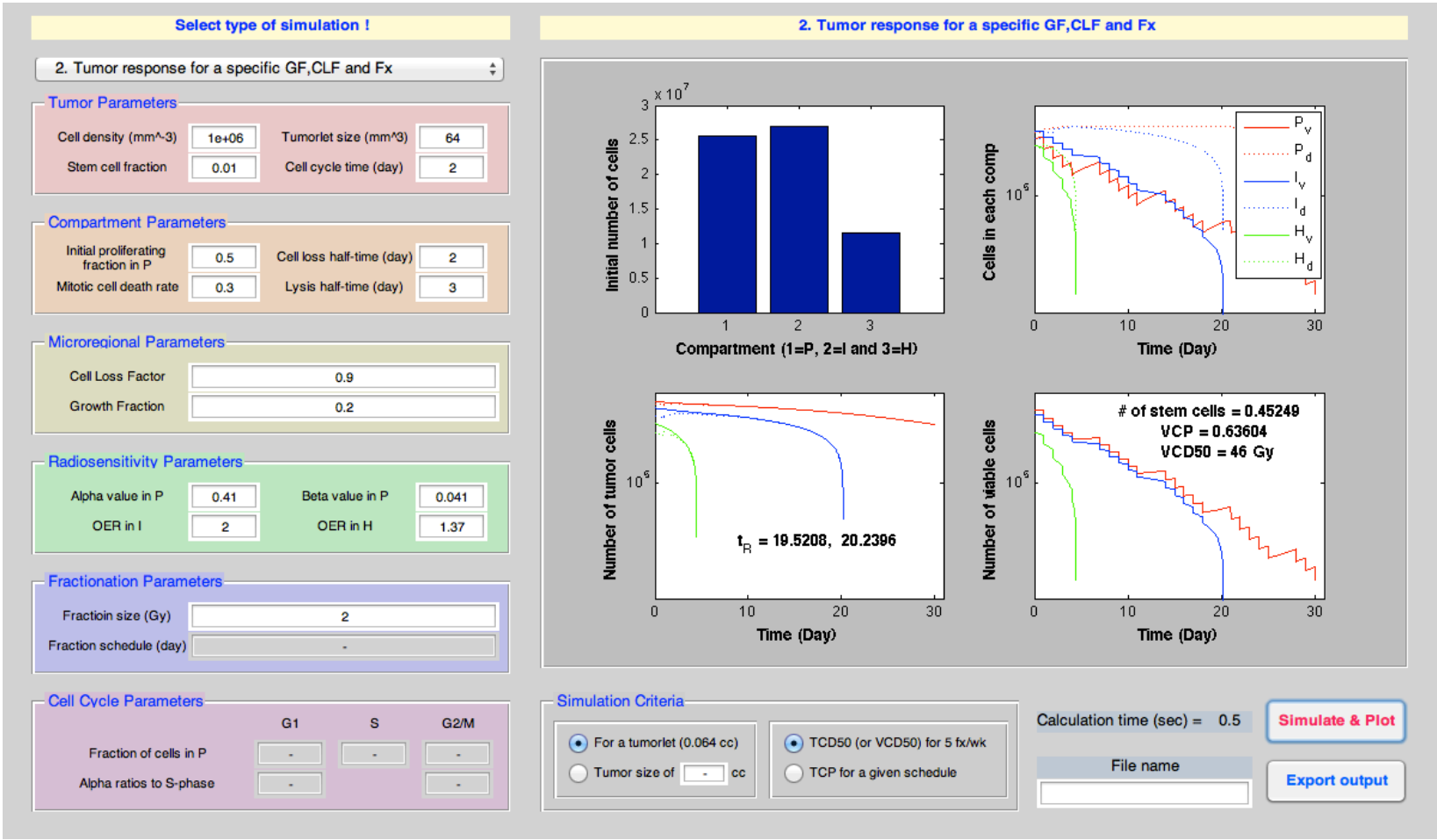

Figure 5-1. PIH code graphical user interface

5.3. Models

A detailed model description was presented in each relevant chapter (Chapter 2: model description, Chapter 3: cell cycle effect, Chapter 4: FDG uptake pattern). Here, the equations and algorithms used in the model code are presented with a simple explanation in the order of the simulation algorithm procedure. The description of variables used in the code is given in section 5.6.

Initial distribution

The initial number of cells in each compartment (N^P, N^H and N^I) was calculated based on the growth fraction (GF) and the cell loss factor (CLF) as follows:

$$N^P(t) = \frac{GF}{f_{pro}^P} \cdot N^{total}(t) \tag{5.1}$$

$$N^H(t) = CLF \cdot GF \cdot \frac{T_{1/2,loss}}{T_C} \cdot N^{total}(t) \tag{5.2}$$

$$N^I(t) = \left[1 - GF\left(\frac{1}{f_{pro}^P} + CLF \cdot \frac{T_{1/2,loss}}{T_C}\right)\right] N^{total}(t) \tag{5.3}$$

Cell kill model

After irradiation, the lethally damaged viable cells become doomed and the number of doomed cells in each compartment is determined based on the fractional dose and the compartment-specific radiosensitivity values, depending on the oxygenation enhancement ratio (OER) as follows:

$$N_v^X(t+\Delta t) = N_v^X(t) \times \exp\left(-\alpha_X d - \beta_X d^2\right) \tag{5.4}$$

$$N_d^X(t+\Delta t) = N_d^X(t) + N_v^X(t) \times \left[1 - \exp\left(-\alpha_X d - \beta_X d^2\right)\right] \tag{5.5}$$

$$\alpha_X = \alpha_P / OER_X \quad \text{and} \quad \beta_X = \beta_P / OER_X^2 \tag{5.6}$$

For the evaluation of SBRT regimes, cell cycle dependent effective radiosensitivity (α_{eff} & β_{eff}) and OER (OER_{eff}^{I} & OER_{eff}^{H}) were used, which were estimated based on the equivalent survival fraction as follows:

$$\begin{aligned} SF_{pro} &= f_{G1} \exp\left(-\alpha_{G1} d - \beta_{G1} d^2\right) + f_S \exp\left(-\alpha_S d - \beta_S d^2\right) \\ &\quad + f_{G2/M} \exp\left(-\alpha_{G2/M} d - \beta_{G2/M} d^2\right) \\ &= \exp\left(-\alpha_{eff} d - \beta_{eff} d^2\right) \end{aligned} \tag{5.7}$$

$$SF_{hyp} = \exp\left(-\frac{\alpha_{eff}}{OER_{eff}} d - \frac{\beta_{eff}}{OER_{eff}^2} d^2\right) = \exp\left(-\frac{\alpha_{ref}}{OER} d - \frac{\beta_{ref}}{OER^2} d^2\right) \tag{5.8}$$

Proliferation and cell loss

Only a fraction of viable cells in the *P*-compartment (f_{pro}^{P}) proliferate as shown in Equation 5.9. Extremely hypoxic cells in the *H*-compartment undergo cell loss with a cell loss half-time ($T_{1/2,loss}$), as shown in Equation 5.10. Mitotic cell death takes place for doomed cells in the *P*-compartment with the survival probability of each progeny (k_m) after mitosis, as shown in Equation 5.11.

$$N_v^P(t+\Delta t) = N_v^P(t) \times \exp\left(f_{pro}^P \frac{\ln 2}{T_C} \Delta t \right) \tag{5.9}$$

$$N^H(t+\Delta t) = N^H(t) \times \exp\left(-\frac{\ln 2}{T_{1/2,\,loss}} \Delta t \right) \tag{5.10}$$

$$N_d^P(t+\Delta t) = N_d^P(t) \times \exp\left((2k_m - 1) f_{pro}^P \frac{\ln 2}{T_C} \Delta t \right) \tag{5.11}$$

Cell lysis

Metabolically dead cells are not instantly removed from the tumor and require some time to physically disintegrate and be removed from the tumor through cell lysis. The cell lysis was assumed to follow exponential decay with a lysis half-time ($T_{1/2,\,lysis}$) as follows:

$$N^{lysis}(t+\Delta t) = N^{lysis}(t) \times \exp\left(-\frac{\ln 2}{T_{1/2,\,lysis}} \Delta t \right) \tag{5.12}$$

Recompartmentalization

As the doomed cells are dying in the *P*-compartment, the oxygen and glucose, which had supported the doomed cells, become available to the cells outside of the *P*-compartment. The recompartmentalization of the cells takes place as shown in Figure 2-2 and, through this process, reoxygenation of the hypoxic cells also occurs.

TLCP and TCP

The Poisson TCP equation was used to calculate the control probability of a tumor-let (TLCP) based on the total number of viable cells ($N_v^P + N_v^I + N_v^H$) in the tumorlet, as

shown in Equation 5.13. The tumor control probability of a homogeneous tumor (TCP), which is comprised of multiple equivalent tumorlets, was calculated from Equation 5.14.

$$TLCP = \exp\left[-\left(N_v^P + N_v^I + N_v^H\right)\right] \tag{5.13}$$

$$TCP_{total} = \prod_i TLCP_i \tag{5.14}$$

5.4. Simulation procedure in PIH code

The "PIH" code is composed of a main program file and several subroutine files (Appendix A.5). The code GUI is run in the Matlab environment by opening the main program file (pih.m). After GUI loads, the user can select a type of simulation from the popup menu located in the top left corner of the GUI window. When a type of simulation is selected, the default input parameter values are loaded into the input parameter panels, located in the left side of the GUI window. The user can customize the parameter values and select the simulation criteria located in the bottom center of the GUI window before clicking the 'Simulate & Plot' button for the start of the simulation. After finishing the simulation, the result plot relevant to the type of simulation is displayed in the plot area. The result data can be exported into a text file format with an assigned file name by clicking the 'Export output' button. A simplified flow chart of the PIH code is shown in Figure 2-1.

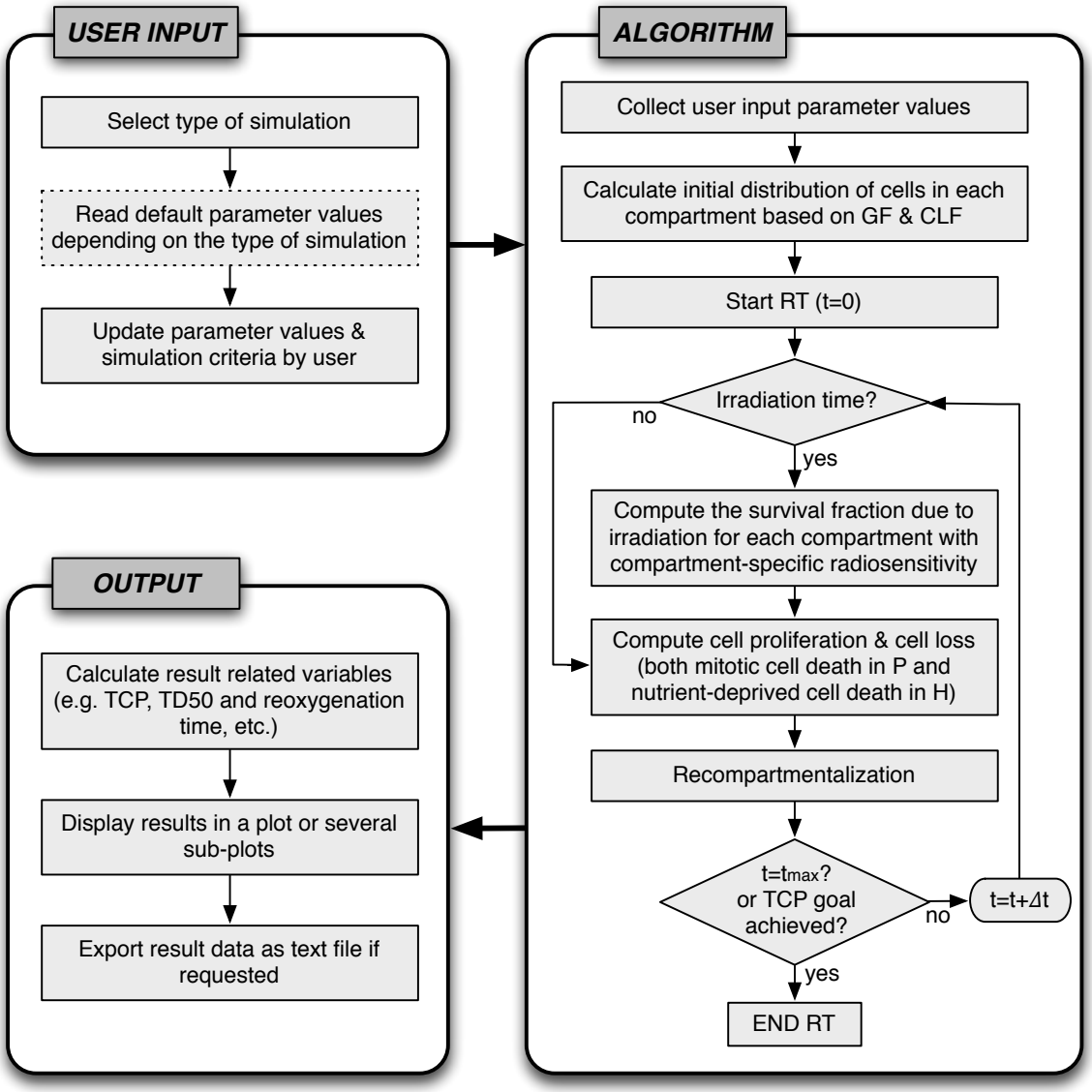

Figure 5-2. Simplified flow chart of the simulation procedure in the PIH code.

5.5. Type of simulations

The "PIH" code is composed of a total of eleven different types of simulations, which are divided into three groups, as shown in Figure 5-3. For the first group, seven different simulations were implemented to evaluate various aspects of the tumor response to the conventional radiotherapy without cell cycle effect. For the second group, three different simulations were implemented to evaluate SBRT regimes with cell cycle effect, where the effect is thought to be significant. The simulation for the FDG uptake pattern was also implemented into the model. A detailed description of each type of simulation was shown in Table 5-1.

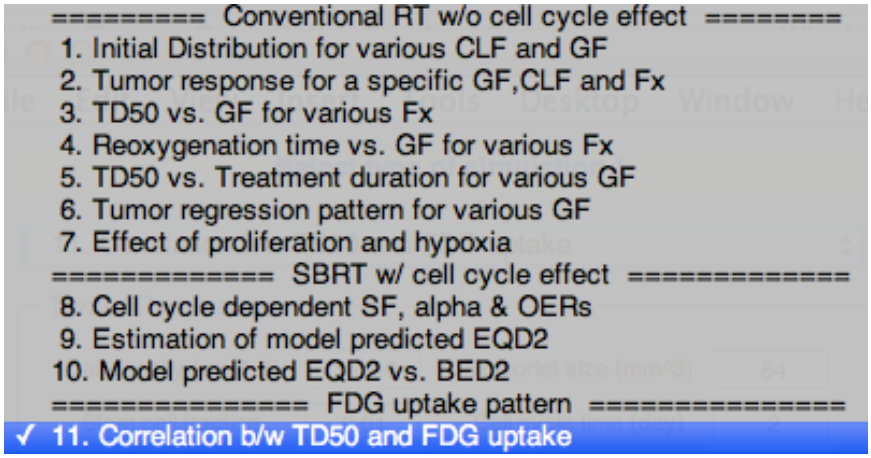

Figure 5-3. Popup menu for the selection of simulation type in the PIH code GUI

Table 5-1. Description of each type of simulation implemented into the PIH code

Type of simulation	Description
Conventional RT without cell cycle effect (Chapter 2)	
1. Initial distribution for various CLF and GF	Find the initial number of cells in each compartment for various cell loss factors and growth fractions
2. Tumor response for a specific GF, CLF and Fx	Simulate the response of tumorlet (or a tumor with a specific size) for a specific growth fraction and cell loss factor with a given fraction size
3. TD50 vs. GF for various FX	Find tumor dose required for 50% control (TD_{50}) with respect to growth fraction for several fraction sizes with a fixed cell loss factor
4. Reoxygenation time vs. GF for various Fx	Find reoxygenation time in two ways (full reoxygenation and maximum curvature) with respect to growth fraction for several fraction sizes with a fixed cell loss factor
5. TD50 vs. Treatment duration for various GF	Find tumor dose required for 50% control (TD_{50}) for various treatment durations by varying the fraction size for several growth fractions (extra dose required to compensate for the longer schedule (Gy/day) is also reported)
6. Tumor regression pattern for various GF	Find the tumor regression pattern based on the total number of cells in the tumor for various growth fractions
7. Effect of proliferation and hypoxia	Find the contribution of proliferation and hypoxia effect in the tumor response with respect to growth fraction for a fixed cell loss factor and fraction size
SBRT with cell cycle effect (Chapter 3)	
8. Cell cycle dependent SF, alpha & OERs	Find the cell cycle dependent survival fraction for each compartment, alpha value and oxygen enhancement ratio (OER) as a function of fraction size
9. Estimation of model predicted EQD2	Estimate the model predicted EQD_2 ($EQD_{2,\ model}$) for a given SBRT regime, which achieves the same surviving fraction of viable cells at the end of radiotherapy
10. Model predicted EQD2 vs. BED2	Compare the model predicted EQD_2 ($EQD_{2,\ model}$) with BED_2, considering proliferation, hypoxia, and cell cycle effects
FDG uptake pattern (Chapter 4)	
11. Correlation b/w TD50 and FDG uptake	Find the correlation between tumor dose for 50% control (TD_{50}) and FDG uptake value for several assumed FDG uptake patterns (viable cells, proliferation and hypoxia)

5.6. Input parameters

In the model, many parameters are involved. All the input parameters are assessable through the input parameter panels in the code GUI, as shown in Figure 5-1, which are classified into six groups (tumor parameters, compartment parameters, microenvironmental parameters, radiosensitivity parameters, fractionation parameters, and cell cycle parameters). When a type of simulation is selected, the default input parameter values are loaded into each input parameter panel and the user can modify these values. Refer to Chapters 2 and 3 for a detailed description of each parameter. In Table 5-2, a simple description and a default value for each parameter are presented.

Table 5-2. Descriptions and default values of input parameters used in the PIH code

Symbol	Description	Default values
Tumor parameters		
ρ_t	tumor cell density (mm^{-3})	10^6 mm^{-3} (Joiner & Kogel, 2009)
v_t	volume of a tumorlet (mm^3)	64 mm^3 (typical PET voxel size)
f_S	stem cell fraction	0.01 (Hemmings, 2010)
T_C	cell cycle time (day)	2 days (Joiner & Kogel, 2009)
Compartment parameters		
f_{pro}^P	initial proliferation fraction in *P*	0.5[a]
$T_{1/2,loss}$	cell loss half-time in *H* (day)	2 days (Ljungkvist *et al*., 2005)
k_m	survival rate of progeny after mitosis	0.3[a]
$T_{1/2,lysis}$	lysis half-time (day)	3 days[a]
Microenvironmental parameters		
CLF	cell loss factor	H/N: 0.9[a], Lung: 0.92[b]
GF	growth fraction	H/N: 0.2[a], Lung: 0.25[b]
Radiosensitivity parameters		
α_P	linear coefficient (Gy^{-1})	H/N: 0.41 Gy^{-1} (Søvik *et al*., 2007) Lung: 0.35 Gy^{-1} (Mehta *et al*., 2001)
β_P	quadratic coefficient (Gy^{-2})	H/N: 0.041 Gy^{-2} (Søvik *et al*., 2007) Lung: 0.035 Gy^{-2} (Mehta *et al*., 2001)
OER_I	OER of *I*-compartment	2.0[a]
OER_H	OER of *H*-compartment	1.37 (Chan *et al*., 2008)
Fractionation parameters		
fx	fraction size (Gy)	varies
tx	fraction schedule (day)	varies
Cell cycle parameters (only for cells in P-compartment)		
f_{G1}^P	fraction of cells in G1-phase	0.56 (Volm *et al*., 1985)
f_S^P	fraction of cells in S-phase	0.24 (Volm *et al*., 1985)
$f_{G2/M}^P$	fraction of cells in G2/M-phase	0.20 (Volm *et al*., 1985)
α_{G1}/α_S	ratio of alpha of G1- to S-phase	2[a]
$\alpha_{G2/M}/\alpha_S$	ratio of alpha of G2/M- to S-phase	3[a]
System parameters		
Δt	time step of the calculation (min)	15 min

[a] assumed parameters
[b] estimated from potential doubling time and volume doubling time measured for lung cancer (Tinnemans *et al*., 1993; Shibamoto *et al*., 1998)

5.7. Output

Depending on the type of simulation, relevant simulation results are presented. All the outputs are displayed graphically in a plot or several subplots, sometimes with text information inserted into the plot. Also, the output data can be exported as a text format (.txt) for further analysis or data processing. A simple example of the exported output file is shown in Figure 5-4 for the reoxygenation time simulation. In Figure 5-5, examples of output plots are shown for several selected types of simulation.

```
    4. Reoxygenation time vs. GF for various Fx

Computing time [sec]:  3.28

Proliferation fraction of P compartment:  0.50
Cell death half time of H compartment [day]:  2.00
Cell density [#/(mm^3)]: 1.00e+06
Voxel size [mm^3]: 64.00
Stem Cell Fraction:  0.01
Cell cycle time [day]:  2.00
Calculation time interval [min]: 15.00
Mitotic death rate: 0.30
Lysis time [day]: 3.00
OER of I: 2.00
OER of H: 1.37
VCP goal: 0.50000
Cell loss factor: 0.90
Growth fraction: 0.05 ~ 0.30


Fx = 2.0

 GF   Reox_time  Reox_time2
0.05   128.51    127.79
0.10    56.34     55.64
0.15    32.28     31.57
0.20    20.24     19.52
0.25    12.96     12.25
0.30     8.01      7.29
```

Figure 5-4. Example of exported output file in text format (.txt)

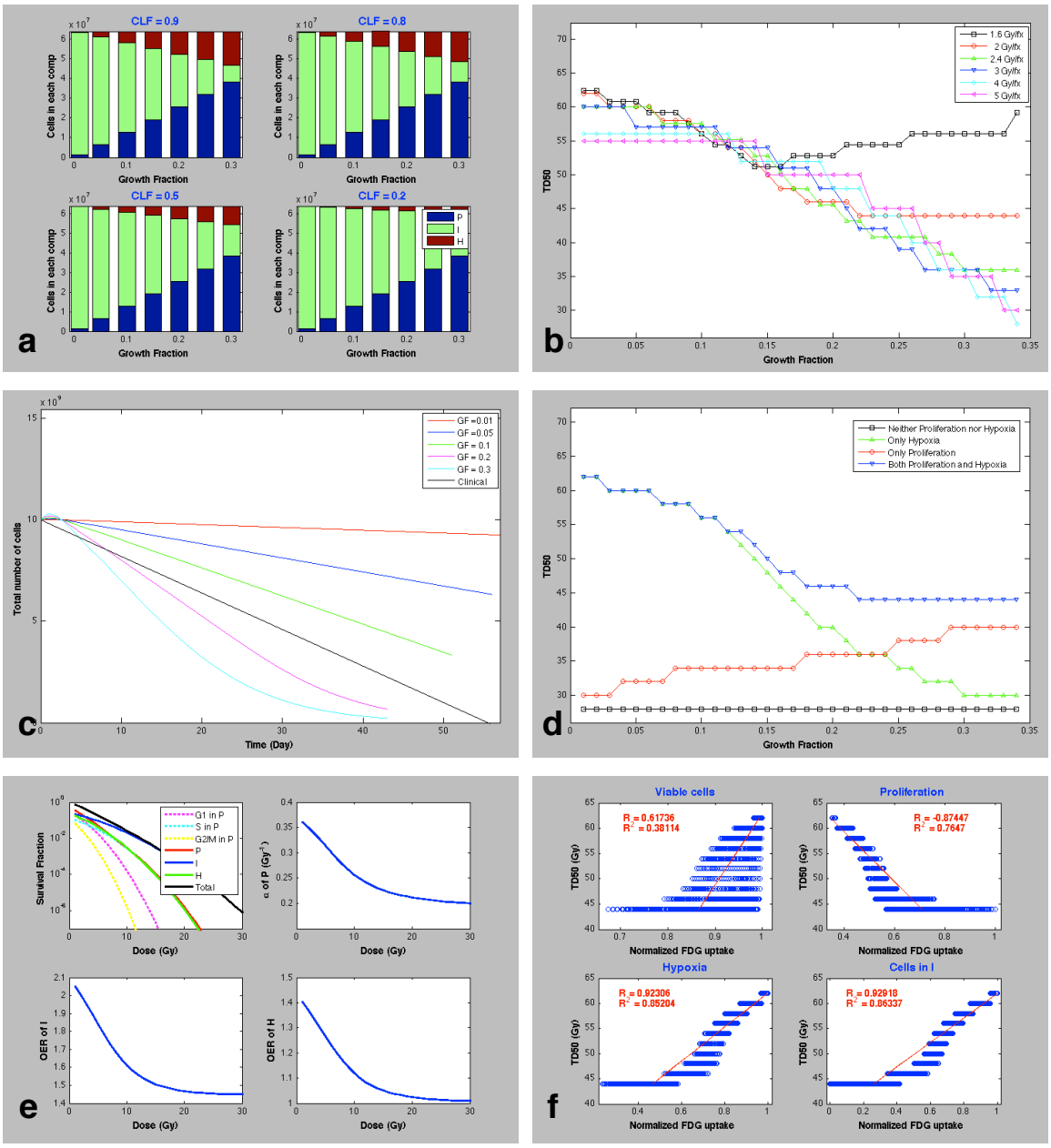

Figure 5-5. Example output plots for several selected types of simulation: (a) Initial Distribution for various CLF and GF; (b) TD50 vs. GF for various Fx; (c) Tumor regression pattern for various GF; (d) Effect of proliferation and hypoxia; (e) Cell cycle dependent SF, alpha & OERs; and (f) TD50 vs. FDG uptake.

5.8. Summary

A simulation software, PIH code, was built to evaluate tumor response depending on microenvironmental conditions. A total of eleven different types of simulations were integrated into the code to explore various aspects of tumor response. Using the Matlab GUI, various parameter settings can be easily simulated and the raw output data can be exported as a text file for further analysis. With its modularized structure, additional effects, which might be identified to be important in tumor response, can be easily incorporated into the code and this code will be made publicly available and open-source.

CHAPTER 6

SUMMARY AND SUGGESTIONS FOR FUTURE WORK

6.1. Summary and conclusion

A tumor is comprised of biologically different subpopulations of cells, known as tumor heterogeneity. The microenvironmental factors of a heterogeneous tumor, such as hypoxia and proliferation, are known to significantly affect the treatment response to radiation therapy.

A state-based tumor response model was developed based on basic, well-established radiobiological principles. Comprised of three theoretical compartments, the model can evaluate the treatment response of a small tumorlet having various microenvironments, including the interplay between hypoxia and proliferation. The initial distribution of the cells in the compartments was found based on the growth fraction and cell loss factor, which represents the microenvironment of the tumorlet. The treatment response to the conventional fractionated radiation therapy was demonstrated for HNSCC. The model could successfully capture the clinically observed phenomena, such as the fraction size effect, the reoxygenation, the treatment time effect, and the tumor regression pattern. The model provides an idealized prediction of how complex microenvironmental conditions are likely impacting local tumor control, and can be used to generate hypotheses about potential fractionation changes.

To evaluate the treatment response to hypofractionated radiotherapy (or SBRT), the cell cycle effect, which affects the radiosensitivity and oxygenation effect depending on

the fractional dose, was incorporated into the model. The equivalent dose in 2 Gy/fx was estimated for several typical SBRT regimes. The treatment efficacy of SBRT estimated from BED is significantly overestimated compared to the model results, and the SBRT schedule seems to affect the treatment efficacy. It was verified that the classic radiobiological factors are not enough to explain the clinical outcomes of SBRT and there might be alternative mechanisms in the high fractional dose range used in SBRT.

The implication of FDG uptake in tumor control was explored. The range of extra dose required to compensate for high FDG uptake was estimated from clinical data. The boost dose mostly likely required to compensate for radioresistant FDG-avid tumors is estimated to be about 90 Gy, assuming a non-boost dose of 70 Gy. These estimates provide a rational starting point for clinical trials to test the usefulness of IMRT boost FDG-avid tumors. Also, several different FDG uptake patterns were hypothesized and tested in the model to investigate the potential relationship between FDG uptake and classical radiobiological mechanism. Given the established clinical fact that FDG uptake correlates to a requirement of a higher dose to achieve local control, the results support a potential avidity of FDG for cells in the intermediate stress state, between well-oxygenated (and proliferating) and extremely hypoxic states.

These various analyses involving many simulations throughout this project were integrated into a model software, called 'PIH' code (named after the initials of each compartment). This code enables one not only to reproduce the simulation results discussed in the previous chapters, but also to easily evaluate different parameter settings using the convenient graphical user interface.

The model software, PIH code, was developed in the Matlab environment. Using the code, the simulation results discussed in this dissertation can be reproduced. Also, different parameter settings can be easily explored with the convenient graphical user interface.

By incorporating basic, well-established radiobiological principles, the developed state-based model can be used to predict response where the principles are known to be valid and also to test the model in regimes where alternative effects might be important, including hypofractionated radiotherapy. The model is only complicated enough to incorporate well-established principles such as cell loss, growth fraction, cellular radiosensitivity, and hypoxia. It therefore provides a mathematical framework for investigating the way in which common radiobiological assumptions lead to results that agree or disagree with clinical data.

6.2. Future study

The model has very wide applicability because it incorporates basic cellular response to local microenvironmental conditions. Key areas for future validation work include tests of the assumption of relatively constant blood delivery to tumorlets over a course of therapy. This is currently being tested via perfusion imaging in MRI and CT protocols. The PIH model could be further validated based on the response of preclinical small animal xenograft models to radiation. A key development in medical physics in the last ten years has been the design of micro-irradiators ('microRT') that can be used to deliver scaled-down, human-like dose distributions.

Possible extensions of this work include:

1. Integrating over heterogeneous tumorlet responses to create expected tumor responses. We have resisted doing this at the outset primarily because, as radiotherapy becomes more of an image-driven treatment modality, understanding the relationship between local response, local image characteristics, and 'local radiobiological' becomes more important. Nonetheless, this would be an area for potential future development.

2. Implications of the 'PIH' model for evaluating treatment plans. The PIH model could be applied to the evaluation of treatment plans, in the role of a traditional TCP model.

3. Describing the outcome implications of advanced imaging results. The PIH model could be used in conjunction with advanced imaging, such as dynamic-contrast enhanced MRI, computed tomography imaging, or FDG-PET, to convert such images into maps of predicted tumor response. Obviously, this would require pre-clinical and clinical validation studies.

APPENDIX

A.1. Analytic solution for initial distribution

Given the model assumptions, the initial distributions of cells in each compartment can be analytically derived based on the growth fraction (GF) and cell loss factor (CLF). The CLF is defined as the rate of cell loss from a tumor, as a proportion of the rate at which cells are being added to the tumor by mitosis:

$$CLF = \frac{\text{rate of cell loss}}{\text{rate of proliferation}} \tag{A.1}$$

Proliferation only takes place in the *P*-compartment, for a fraction of cells in active proliferation. Cell loss only occurs in the *H*-compartment following exponential decay with cell loss half-time. The rates of proliferation and cell loss can be expressed as follows:

$$\begin{aligned} \text{rate of proliferation} &= \frac{dN^P(t)}{dt} = f_{pro}^P \frac{\ln 2}{T_C} N^P(t) \\ \text{rate of cell loss} &= \frac{dN^H(t)}{dt} = \frac{-\ln 2}{T_{1/2,loss}} N^H(t) \end{aligned} \tag{A.2}$$

From the definition of CLF (Equation A.1) and rates of proliferation and cell loss (Equation A.2), the number of cells in the *H*-compartment (N^H) can be expressed in terms of the number of cells in the *P*-compartment (N^P) in terms of CLF as follows:

$$N^H(t) = CLF \times f_{pro}^P \frac{T_{1/2,loss}}{T_C} N^P(t) \tag{A.3}$$

It can be seen that the number of cells in the *H*-compartment (N^H) is proportional to the number of cells in the *P*-compartment (N^P) and the proportional constant can be directly determined from the CLF, the fraction of cells in active proliferation in the *P*-compartment, and the ratio of cell death half-time and cell cycle time.

The number of cells in the *P*-compartment (N^P) is defined based on the growth fraction (GF), as a fraction of the total number of cells (N^{total}). From the relation between N^H and N^P (Equation A.3), the number of cells in the *H*- and *I*-compartments (N^H & N^I) can be calculated. The number of cells in each compartment satisfying a given GF and CLF are therefore as follows:

$$\begin{aligned} N^P(t) &= \frac{GF}{f_{pro}^P} \cdot N^{total}(t) \\ N^H(t) &= CLF \cdot GF \cdot \frac{T_{1/2,loss}}{T_C} \cdot N^{total}(t) \\ N^I(t) &= \left[1 - GF\left(\frac{1}{f_{pro}^P} + CLF \cdot \frac{T_{1/2,loss}}{T_C} \right) \right] N^{total}(t) \end{aligned} \tag{A.4}$$

A.2. Overall growth

When the CLF is less than 1, the total number of cells (N^{total}) increases and the rate of increase can be determined from the following rate equation:

$$\begin{aligned}\frac{dN^{total}(t)}{dt} &= \text{rate of proliferation - rate of cell loss} \\ &= \text{rate of proliferation - } CLF \times \text{rate of proliferation} \\ &= (1 - CLF) \times \text{rate of proliferation} \\ &= (1-CLF)\cdot f_{pro}^{P} \cdot \frac{\ln 2}{T_C} \cdot N^{P}(t) \\ &= (1-CLF)\cdot GF \cdot \frac{\ln 2}{T_C} \cdot N^{total}(t)\end{aligned} \tag{A.5}$$

Solve the differential equation with initial total number (N_0^{total}) and we get the following equation:

$$N^{total}(t) = N_0^{total} \cdot \exp\left[(1-CLF)\cdot GF \cdot \frac{\ln 2}{T_C} \cdot t \right] \tag{A.6}$$

From the above equation (A.6), the volume doubling time (T_D) can be found in terms of CLF, GF and T_C , assuming the tumor volume is proportional to the number of cells. The exponential term of Equation A.6 can be expressed as $2^{(1-CLF)\cdot GF\cdot t/T_C}$ and the volume doubling time can be found as the following equation:

$$T_D = \frac{T_C}{(1-CLF)\cdot GF} \tag{A.7}$$

A.3. Model sensitivity test

The model sensitivity was tested for several parameter values. A variation of ±20% was simulated for six model parameters (radiosensitivity, stem cell fraction, initial prolif-

erating fraction, cell loss half-time, cell cycle time, and mitotic cell death rate). The result is shown in Table A-1 for a GF of 0.2 with a fraction size of 2 Gy/fx. Among them, radiosensitivity (α) and the stem cell fraction (f_s) showed significant effects on the simulation result. A detailed plot is presented in Figures A-1~A-6 for each effect.

Table A-1. Model sensitivity test for several model parameters for a GF of 0.2 with 2 Gy/fx

Parameter values		$TLCD_{50}$ (Gy)				Slope of asymptotic line
		Both proliferation and hypoxia	Only hypoxia	Only proliferation	Neither proliferation nor hypoxia	
Default*		46	36	40	28	0.75
α	0.33	60 (30%)	48 (33%)	46 (15%)	36 (29%)	0.90 (20%)
	0.49	38 (-17%)	28 (-22%)	36 (-10%)	24 (-14%)	0.64 (-15%)
f_s	0.004	44 (-4%)	34 (-6%)	38 (-5%)	26 (-7%)	0.74 (-1%)
	0.0251	48 (4%)	38 (6%)	42 (5%)	30 (7%)	0.75
f_{pro}^P	0.4	44 (-4%)	38 (6%)	36 (-10%)	28	0.76 (1%)
	0.6	48 (4%)	34 (-6%)	44 (10%)	28	0.72 (-4%)
$T_{1/2,loss}$	1.6	46	36	40	28	0.75
	2.4	46	36	38 (-5%)	28	0.76 (1%)
T_C	1.6	48 (4%)	40 (11%)	36 (-10%)	28	0.92 (23%)
	2.4	46	34 (-6%)	42 (5%)	28	0.64 (-15%)
k_m	0.24	46	36	36 (-10%)	28	0.75
	0.36	48 (4%)	36	44 (10%)	28	0.71 (-5%)

* default parameter values: $\alpha = 0.41$, $f_s = 0.01$, $f_{pro}^P = 0.5$, $T_{1/2,loss} = 2$ days, $T_C = 2$ days and $k_m = 0.3$

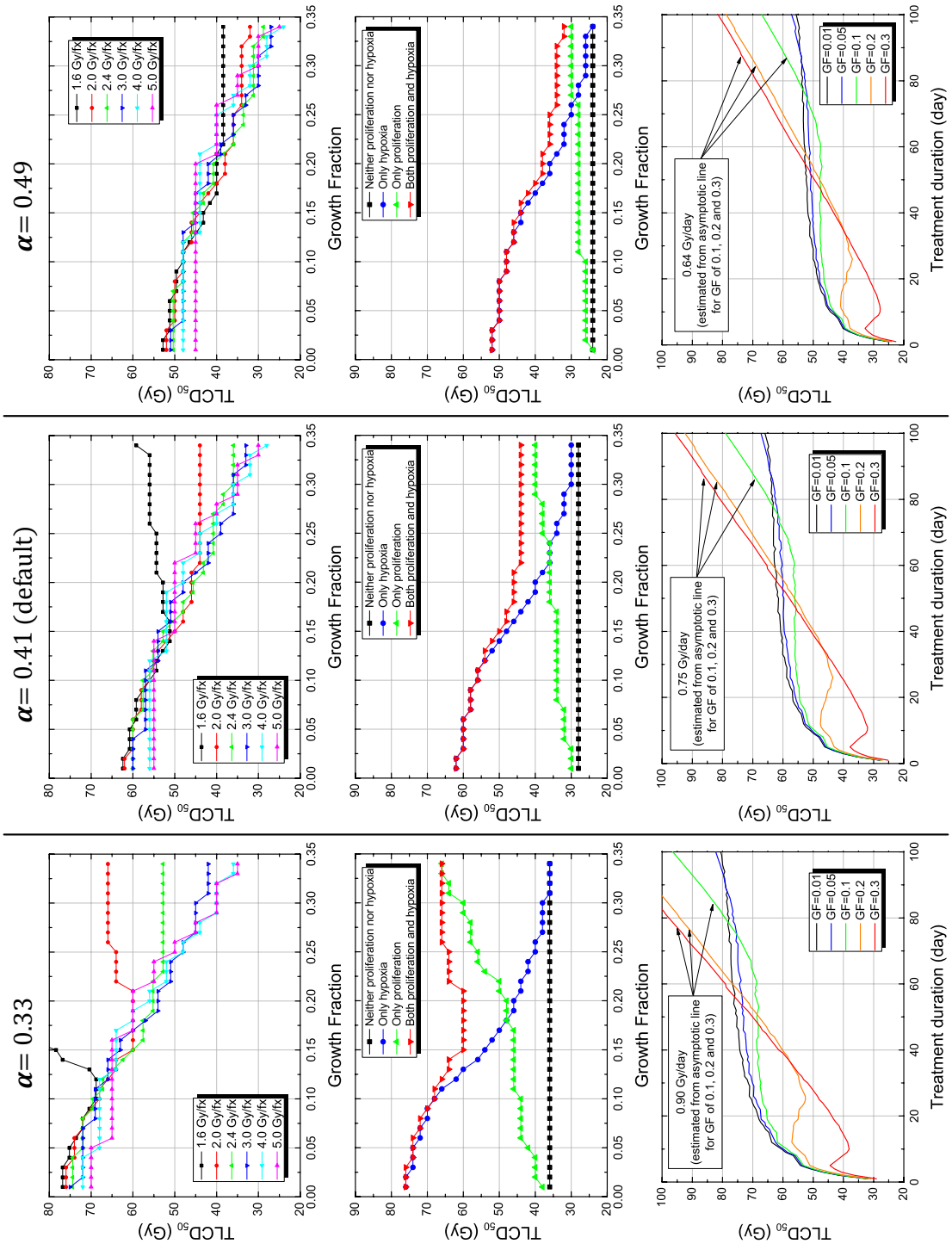

Figure A-1. Model sensitivity test for the variation of radiosensitivity value (α)

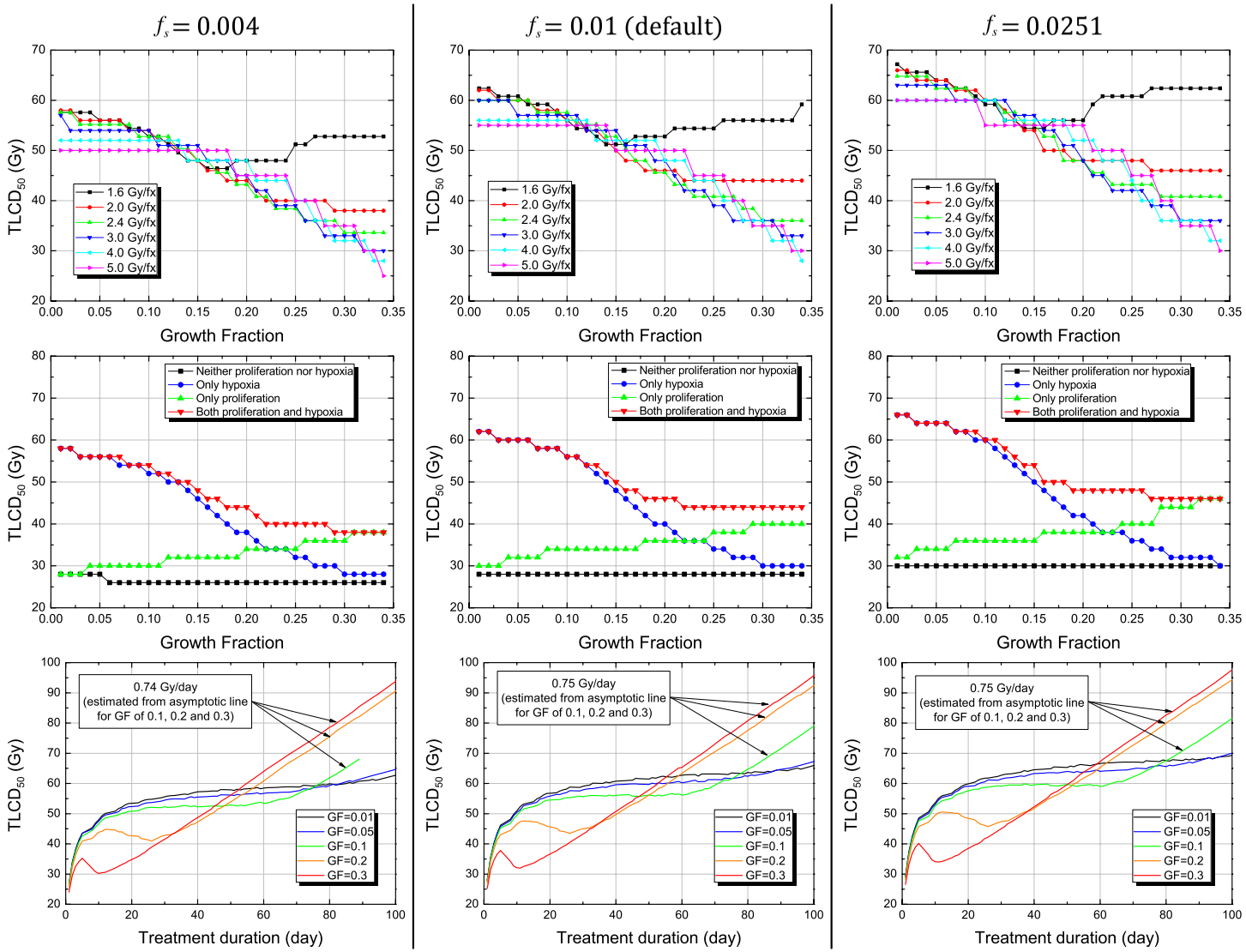

Figure A-2. Model sensitivity test for the variation of stem cell fraction (f_s)

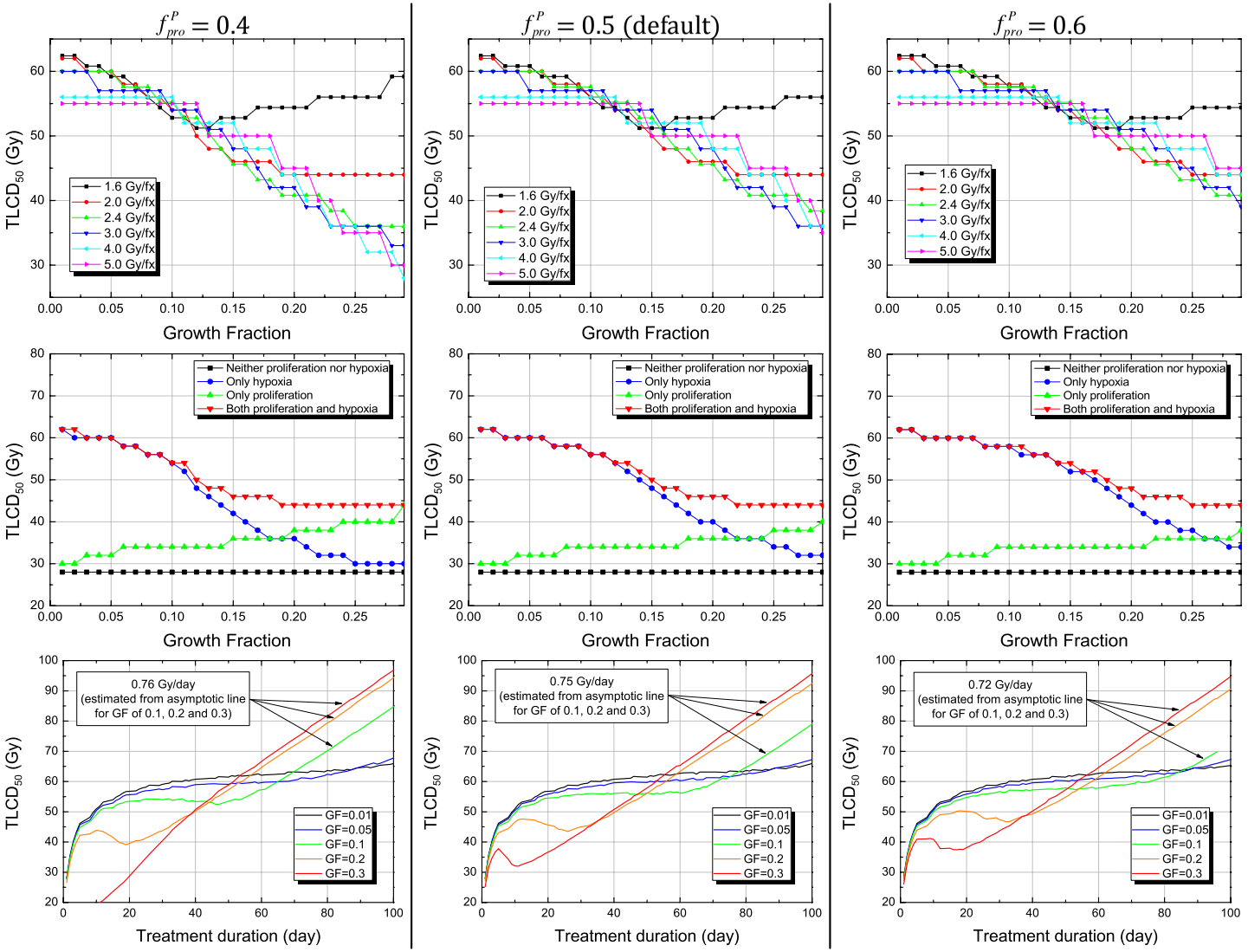

Figure A-3. Model sensitivity test for the variation of initial fraction of proliferating cells in *P*-compartment (f_{pro}^{P})

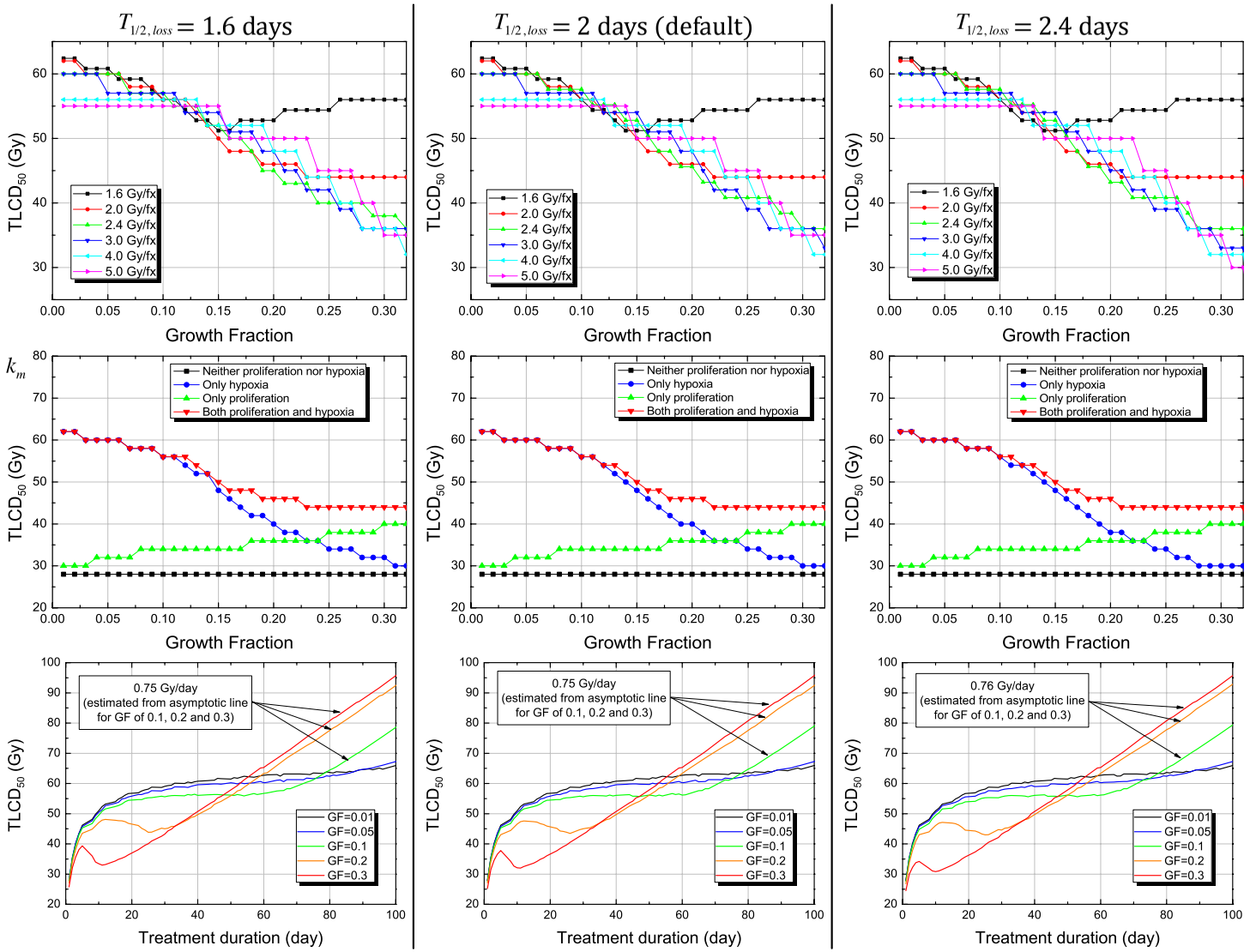

Figure A-4. Model sensitivity test for the variation of cell loss half-time ($T_{1/2,\ loss}$)

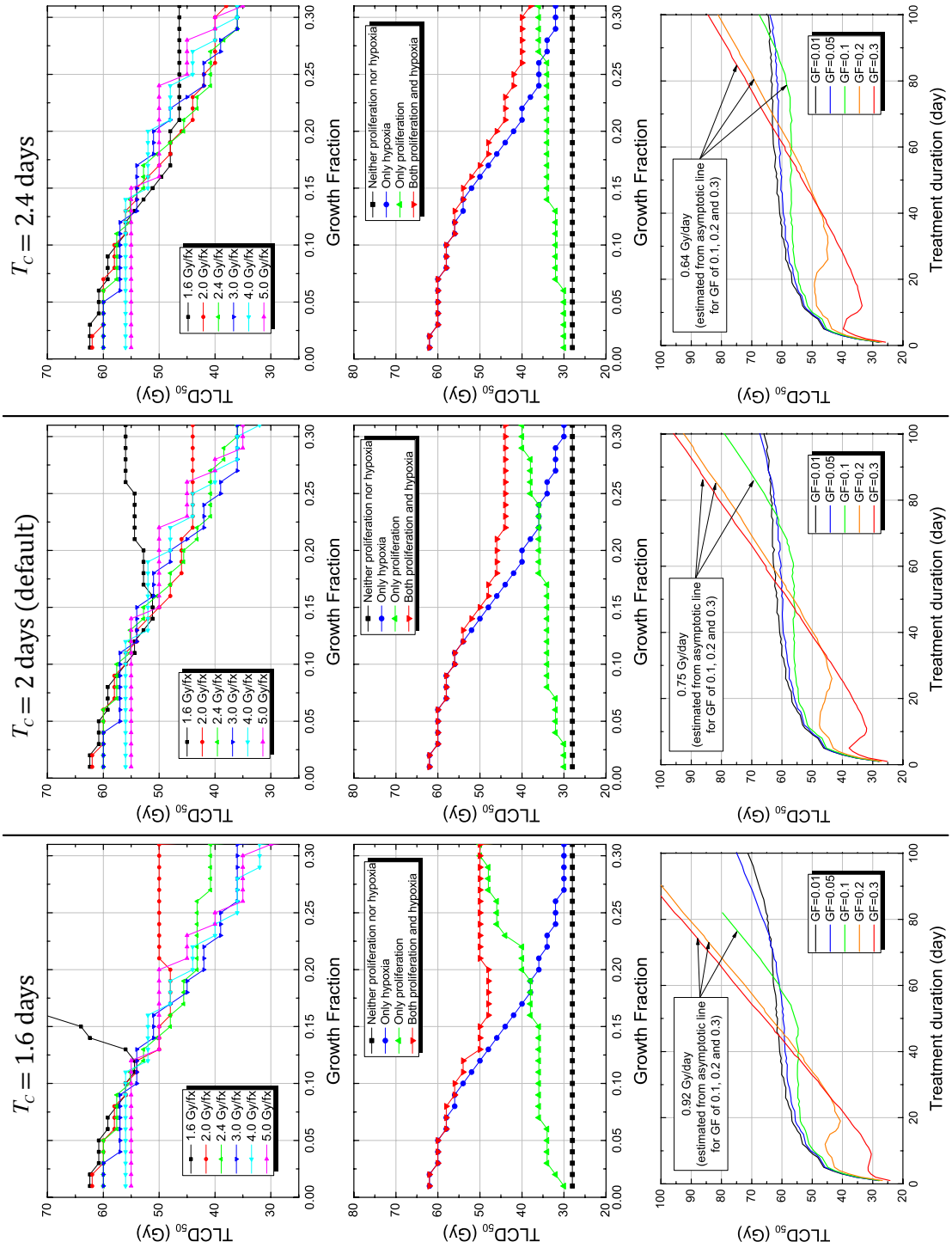

Figure A-5. Model sensitivity test for the variation of cell cycle time (T_c)

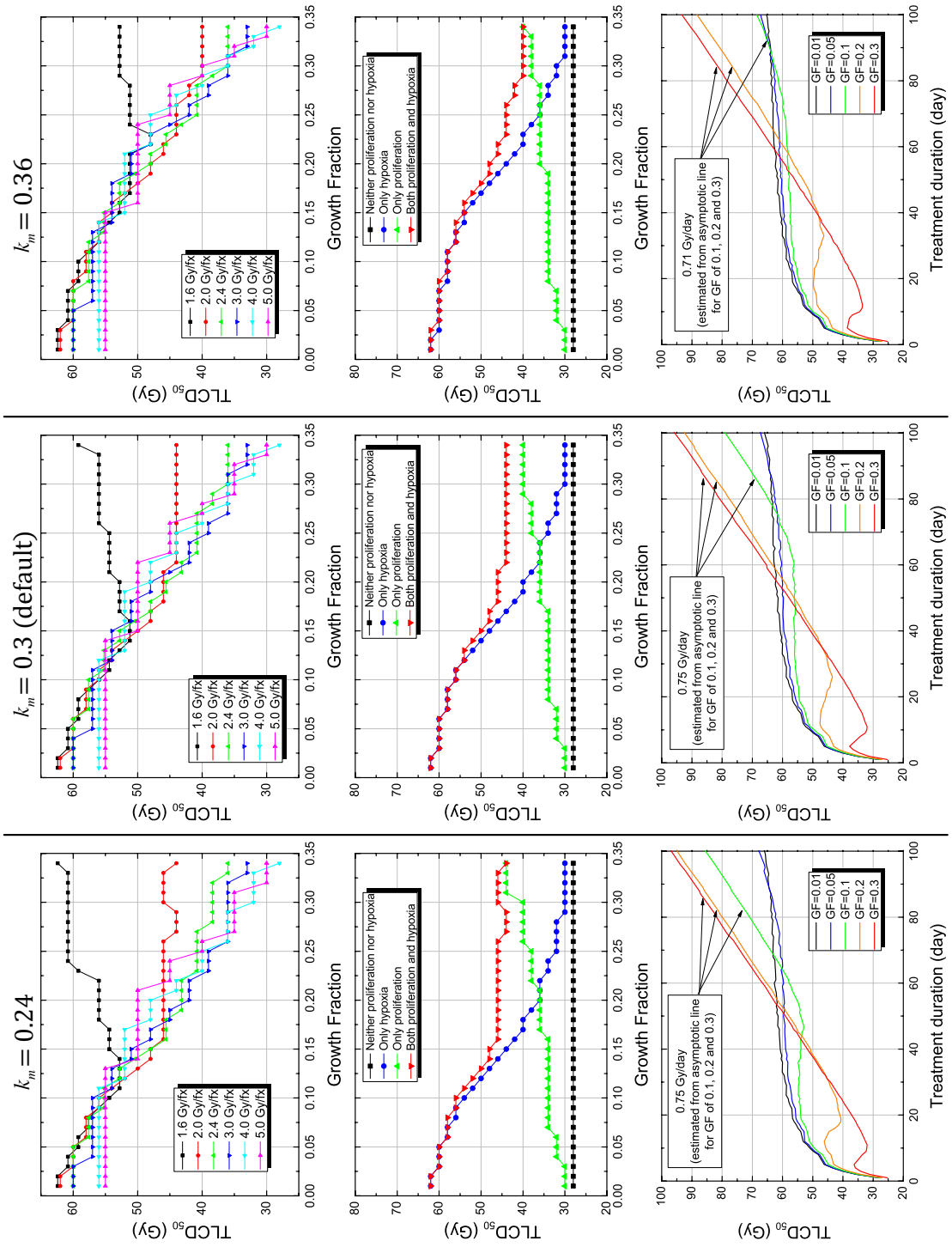

Figure A-6. Model sensitivity test for the variation of mitotic cell death rate (k_m)

A.4. SF, OER_{eff} and $EQD_{2,model}$ vs. NTD_2 for different alpha ratio values

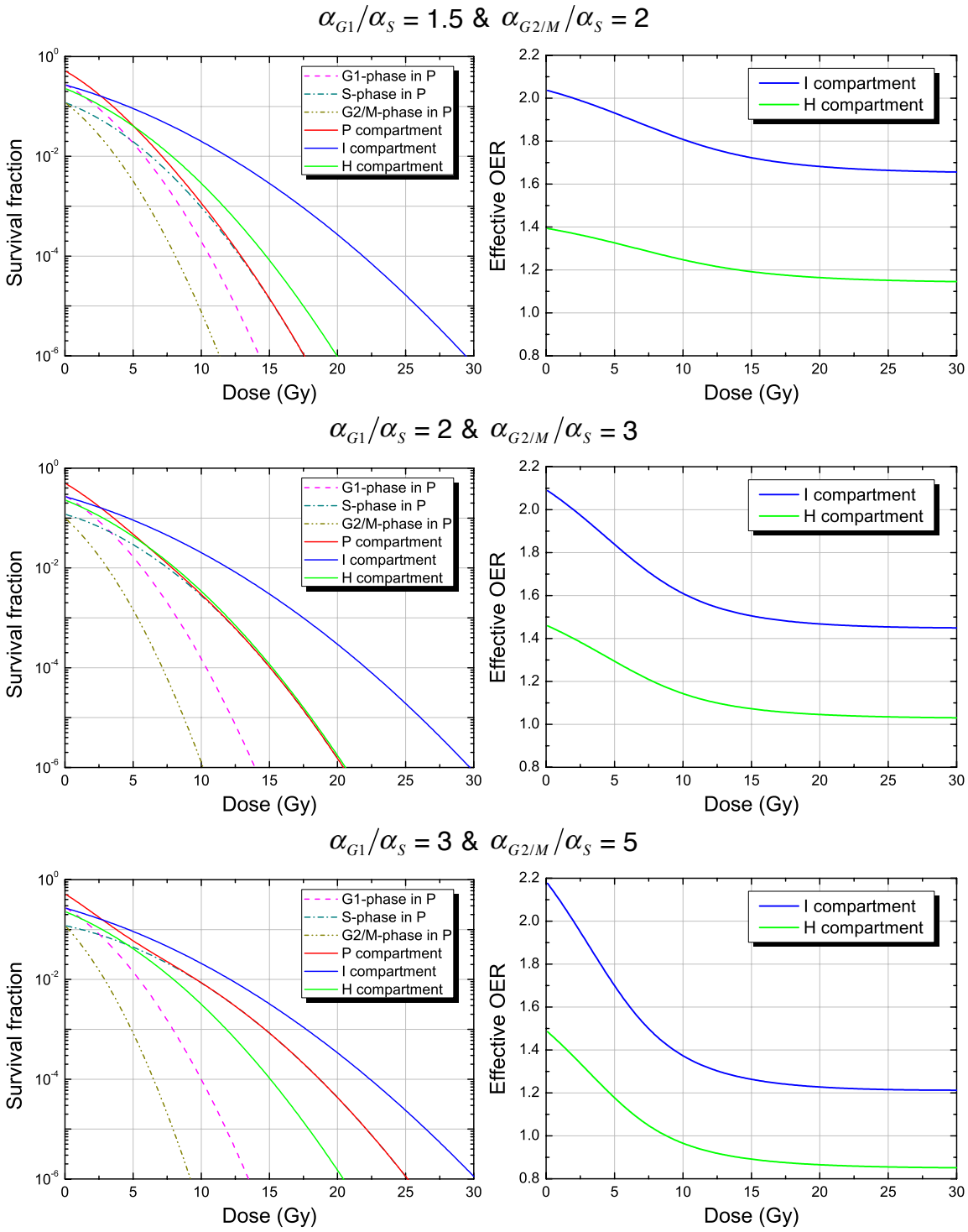

Figure A-7. Survival fraction (SF) of each compartment including cell cycle phase dependent SF in *P*-compartment (left column) and effective OER values of *I*- and *H*-compartments (right column) for three different alpha ratio values (α_{G1}/α_S & $\alpha_{G2/M}/\alpha_S$)

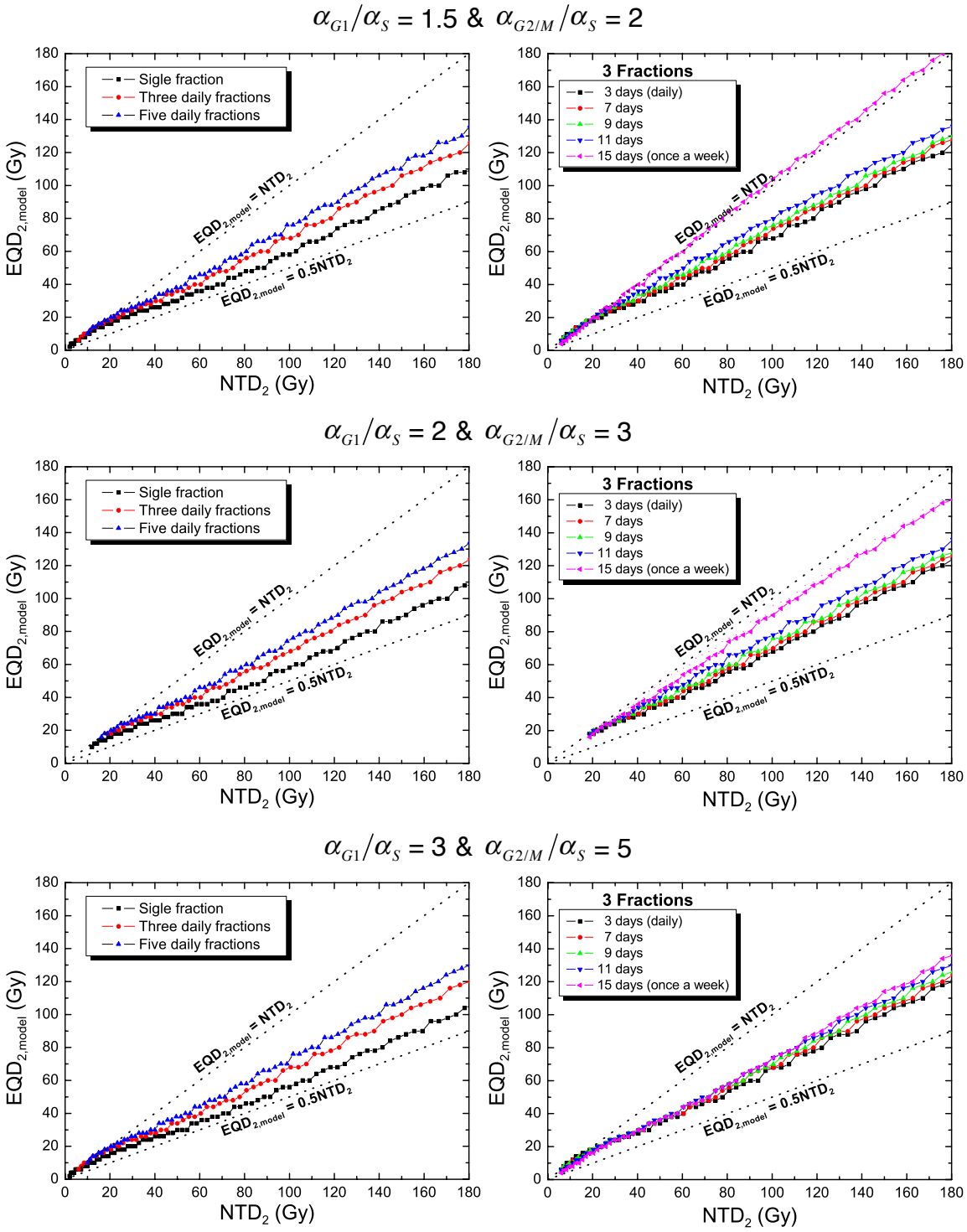

Figure A-8. Model predicted equivalent dose of 2 Gy/fx ($EQD_{2,model}$) vs. NTD_2 for three different alpha ratio values (α_{G1}/α_S & $\alpha_{G2/M}/\alpha_S$): for different numbers of daily fractions (left column) and for different treatment durations for three-fraction SBRT (right column).

A.5. PIH code – Matlab Program

The PIH code is composed of a main function file (PIH.m) and five subroutine script files (SR_initial_distribution.m, SR_RT.m, SR_RT_sbrt.m, SR_RT_eqd2.m and SR_Reox_time.m). The source codes of the main function and subroutines are presented in the following subsections.

A.5.1. Main PIH function (PIH.m)

```
function PIH
% State-driven tumor response model
% Main GUI-based program file
% Execute several types of simulations


%%  Declare global variables that might be used in sub-routines

% Tumor parameters
global rho_t v_t f_s t_c n_t;

% Compartment parameters
global f_p_pro_in ht_loss k_m ht_lys;

% RT parameters
global alpha_p beta_p alpha_i beta_i alpha_h beta_h oer_i oer_h;

% Cell cycle parameters
global F_p_cyc Alpha_ratio_p_cyc Alpha_p_cyc;

% Simulation parameters
global vcp_goal tumor_size tcp_goal ;

% Input parameters
global clf_in gf_in fx_in schedule_in d_t;

% general variables
global type clinical t_start t_cal IC TD50 Treat_duration vec_leng slope...
    terminated linearCoef SF Alpha_eff OERI_eff OERH_eff sf_sbrt ntd2 ...
    sf_eqd2 eqd2 NTD2 EQD2

% variables for initial distribution sub-routine
global f_p_pro comp_size;

% variables for RT sub_routine
global cell_dist t j add_time cum_cell_dist delta_t h_pre p_d_pre md...
    p_ex p_ratio p_def i_ex i_def i_ratio h_ratio Total_cell T_end no_pro

% variables for reoxygenation time sub-routine
global reox_time reox_time2 Reox_time Reox_time2 time T T1 T2 T3 ...
    C C1 C2 C3 a b c A crv abs_crv m;
```

```
% variables for SBRT sub-routine
global cum_cell_dist_sbrt t_sbrt time_sbrt

% variables for FDG uptake pattern
global fdg_via fdg_pro fdg_hyp fdg_mix fdg_idst nor_fdg_via nor_fdg_pro...
    nor_fdg_hyp nor_fdg_mix nor_fdg_idst td50 r_via r_pro r_hyp r_mix...
    r_idst R_sq_via R_sq_pro R_sq_hyp R_sq_mix R_sq_idst Via Pro Hyp...
    Mix Idst



%%  Create GUI figure

f = figure('NumberTitle','off',...
    'Position',[40,50,1200,700]);
set(f,'Name','State-driven tumor response model ("PIH" code)')



%%  Pop-up selection of type of calculation

color_0=[1 1 0.8];
htype_title = uicontrol('Style','text','String',...
    'Select type of simulation !','FontSize',10,'ForegroundColor','b',...
    'FontWeight','bold','BackgroundColor',color_0,...
    'Position',[25,670,400,20]);
htype_value = uicontrol('Style','popupmenu','FontSize',10,...
      'String',{...
      '=========  Conventional RT w/o cell cycle effect  ========',...
      ' 1. Initial distribution for various CLF and GF',...
      ' 2. Tumor response for a specific GF,CLF and Fx',...
      ' 3. TD50 vs. GF for various Fx',...
      ' 4. Reoxygenation time vs. GF for various Fx'...
      ' 5. TD50 vs. Treatment duration for various GF',...
      ' 6. Tumor regression pattern for various GF',...
      ' 7. Effect of proliferation and hypoxia',...
      '=============  SBRT w/ cell cycle effect  =============',...
      ' 8. Cell cycle dependent SF, alpha & OERs',...
      ' 9. Estimation of model predicted EQD2',...
      '10. Model predicted EQD2 vs. BED2',...
      '===============  FDG uptake pattern  ===============',...
      '11. Correlation b/w TD50 and FDG uptake',...
      },...
      'Position',[25,630,400,25],'Callback',{@type_Callback});

ha_title = uicontrol('Style','Text','String','',...
    'FontSize',10,'ForegroundColor','b','FontWeight','bold',...
    'BackgroundColor',color_0,'Position',[450,670,725,20]);

hinput = uipanel;
hinput2 = uipanel;
hinput3 = uipanel;
hinput4 = uipanel;
hinput5 = uipanel;
hinput6 = uipanel;
hinput7 = uipanel;



%% Assign parameter values depending on the type of simulation

function type_Callback(source,eventdata)
    str = get(source, 'String');
```

```
val = get(source,'Value');
set(ha_title,'String',str{val});
delete(hinput,hinput2,hinput3,hinput4,hinput5,hinput6,hinput7);
switch str{val};

    case ' 1. Initial distribution for various CLF and GF'
        rho_t=10^6;     v_t=4*4*4;      f_s=0.01;       t_c=2;
        f_p_pro_in=0.5; ht_loss=2;      k_m='-';        ht_lys='-';
        alpha_p='-';    beta_p='-';     oer_i='-';      oer_h='-';
        F_p_cyc=['-';'-';'-'];
        Alpha_ratio_p_cyc=['-';'-'];
        vcp_goal='-';   tumor_size='-'; tcp_goal='-';   d_t=15;
        clf_in=[0.9 0.8 0.5 0.2]; clf_in_st='0.9 0.8 0.5 0.2';
        gf_in=[0.01 0.05 0.1 0.15 0.2 0.25 0.3];
        gf_in_st='0.01 0.05 0.1 0.15 0.2 0.25 0.3';
        fx_in='-';fx_in_st='-';
        schedule_in='-';
        type=1;

    case ' 2. Tumor response for a specific GF,CLF and Fx'
        rho_t=10^6;     v_t=4*4*4;      f_s=0.01;       t_c=2;
        f_p_pro_in=0.5; ht_loss=2;      k_m=0.3;        ht_lys=3;
        alpha_p=0.41;   beta_p=0.041;   oer_i=2.0;      oer_h=1.37;
        F_p_cyc=['-';'-';'-'];
        Alpha_ratio_p_cyc=['-';'-'];
        tumor_size='-'; tcp_goal='-';
        vcp_goal=0.5;
        d_t=15;
        clf_in=0.9; clf_in_st='0.9';
        gf_in=0.2; gf_in_st='0.2';
        fx_in=2;fx_in_st='2';
        schedule_in='-';
        type=2;

    case ' 3. TD50 vs. GF for various Fx'
        rho_t=10^6;     v_t=4*4*4;      f_s=0.01;       t_c=2;
        f_p_pro_in=0.5; ht_loss=2;      k_m=0.3;        ht_lys=3;
        alpha_p=0.41;   beta_p=0.041;   oer_i=2.0;      oer_h=1.37;
        F_p_cyc=['-';'-';'-'];
        Alpha_ratio_p_cyc=['-';'-'];
        tumor_size='-'; tcp_goal='-';
        vcp_goal=0.5;
        d_t=15;
        clf_in=0.9; clf_in_st='0.9';
        gf_in=0.01:0.01:0.34; gf_in_st='0.01:0.01:0.34';
        fx_in=[1.6 2 2.4 3 4 5]; fx_in_st='1.6  2  2.4  3  4  5';
        schedule_in='-';
        type=3;

    case ' 4. Reoxygenation time vs. GF for various Fx'
        rho_t=10^6;     v_t=4*4*4;      f_s=0.01;       t_c=2;
        f_p_pro_in=0.5; ht_loss=2;      k_m=0.3;        ht_lys=3;
        alpha_p=0.41;   beta_p=0.041;   oer_i=2.0;      oer_h=1.37;
        F_p_cyc=['-';'-';'-'];
        Alpha_ratio_p_cyc=['-';'-'];
        tumor_size='-'; tcp_goal='-';
        vcp_goal='-';
        d_t=15;
        clf_in=0.9; clf_in_st='0.9';
        gf_in=[0.05 0.1 0.15 0.2 0.25 0.3];
        gf_in_st='0.05  0.1  0.15  0.2  0.25  0.3';
        fx_in=[1.6 2 2.4 3 4 5]; fx_in_st='1.6  2  2.4  3  4  5';
        schedule_in='-';
```

```
    type=4;

case ' 5. TD50 vs. Treatment duration for various GF'
    rho_t=10^6;     v_t=4*4*4;      f_s=0.01;       t_c=2;
    f_p_pro_in=0.5; ht_loss=2;      k_m=0.3;        ht_lys=3;
    alpha_p=0.41;   beta_p=0.041;   oer_i=2.0;      oer_h=1.37;
    F_p_cyc=['-';'-';'-'];
    Alpha_ratio_p_cyc=['-';'-'];
    tumor_size='-'; tcp_goal='-';
    vcp_goal=0.5;
    d_t=15;
    clf_in=0.9; clf_in_st='0.9';
    gf_in=[0.01 0.05 0.1 0.2 0.3];
    gf_in_st='0.01  0.05  0.1  0.2  0.3';
    fx_in=1.2:0.1:50; fx_in_st='varies';
    schedule_in='-';
    type=5;

case ' 6. Tumor regression pattern for various GF'
    rho_t=10^6;     v_t=4*4*4;      f_s=0.01;       t_c=2;
    f_p_pro_in=0.5; ht_loss=2;      k_m=0.3;        ht_lys=3;
    alpha_p=0.41;   beta_p=0.041;   oer_i=2.0;      oer_h=1.37;
    F_p_cyc=['-';'-';'-'];
    Alpha_ratio_p_cyc=['-';'-'];
    tumor_size='-'; tcp_goal='-';
    vcp_goal=0.5;
    d_t=15;
    clf_in=0.9; clf_in_st='0.9';
    gf_in=[0.01 0.05 0.1 0.2 0.3];
    gf_in_st='0.01  0.05  0.1  0.2  0.3';
    fx_in=2; fx_in_st='2';
    schedule_in='-';
    type=6;

case ' 7. Effect of proliferation and hypoxia'
    rho_t=10^6;     v_t=4*4*4;      f_s=0.01;       t_c=2;
    f_p_pro_in=0.5; ht_loss=2;      k_m=0.3;        ht_lys=3;
    alpha_p=0.41;   beta_p=0.041;   oer_i=2.0;      oer_h=1.37;
    F_p_cyc=['-';'-';'-'];
    Alpha_ratio_p_cyc=['-';'-'];
    tumor_size='-'; tcp_goal='-';
    vcp_goal=0.5;
    d_t=15;
    clf_in=0.9; clf_in_st='0.9';
    gf_in=0.01:0.01:0.34;
    gf_in_st='0.01:0.01:0.34';
    fx_in=2; fx_in_st='2';
    schedule_in='-';
    type=7;

case ' 8. Cell cycle dependent SF, alpha & OERs'
    rho_t=10^6;     v_t=4*4*4;      f_s=0.01;       t_c=2;
    f_p_pro_in=0.5; ht_loss=2;      k_m=0.3;        ht_lys=3;
    alpha_p=0.35;   beta_p=0.035;   oer_i=2.0;      oer_h=1.37;
    F_p_cyc=[0.56;0.24;0.2];
    Alpha_ratio_p_cyc=[2;3];
    tumor_size='-'; tcp_goal='-';
    vcp_goal='-';
    d_t='-';
    clf_in=0.92;  clf_in_st='0.92';
    gf_in=0.25; gf_in_st='0.25';
    fx_in=1:1:30; fx_in_st='1:1:30';
    schedule_in='-';
```

```
        type=8;

    case ' 9. Estimation of model predicted EQD2'
        rho_t=10^6;     v_t=4*4*4;      f_s=0.01;       t_c=2;
        f_p_pro_in=0.5; ht_loss=2;      k_m=0.3;        ht_lys=3;
        alpha_p=0.35;   beta_p=0.035;   oer_i=2.0;      oer_h=1.37;
        F_p_cyc=[0.56;0.24;0.2];
        Alpha_ratio_p_cyc=[2;3];
        tumor_size='-'; tcp_goal='-';
        vcp_goal='-';
        d_t=15;
        clf_in=0.92; clf_in_st='0.92';
        gf_in=0.25; gf_in_st='0.25';
        fx_in=15; fx_in_st='15';
        schedule_in=[1 3 5];
        type=9;

    case '10. Model predicted EQD2 vs. BED2'
        rho_t=10^6;     v_t=4*4*4;      f_s=0.01;       t_c=2;
        f_p_pro_in=0.5; ht_loss=2;      k_m=0.3;        ht_lys=3;
        alpha_p=0.35;   beta_p=0.035;   oer_i=2.0;      oer_h=1.37;
        F_p_cyc=[0.56;0.24;0.2];
        Alpha_ratio_p_cyc=[2;3];
        tumor_size='-'; tcp_goal='-';
        vcp_goal='-';
        d_t=15;
        clf_in=0.92; clf_in_st='0.92';
        gf_in=0.25; gf_in_st='0.25';
        fx_in=5:0.5:26; fx_in_st='5:0.5:26';
        schedule_in=[1 3 5];
        type=10;

    case '11. Correlation b/w TD50 and FDG uptake'
        rho_t=10^6;     v_t=4*4*4;      f_s=0.01;       t_c=2;
        f_p_pro_in=0.5; ht_loss=2;      k_m=0.3;        ht_lys=3;
        alpha_p=0.41;   beta_p=0.041;   oer_i=2.0;      oer_h=1.37;
        F_p_cyc=['-';'-';'-'];
        Alpha_ratio_p_cyc=['-';'-'];
        tumor_size='-'; tcp_goal='-';
        vcp_goal=0.5;
        d_t=15;
        clf_in=0.03:0.03:0.99; clf_in_st='0.03:0.03:0.99';
        gf_in=0.01:0.01:0.33; gf_in_st='0.01:0.01:0.33';
        fx_in=2; fx_in_st='2';
        schedule_in='-';
        type=11;

end


%%  First input panel (tumor parameters)

color_1=[0.9 0.75 0.75];
hinput = uipanel('Title','Tumor Parameters','FontSize',10,...
    'ForegroundColor','b','BackgroundColor',color_1,'Unit','pixels',...
    'Position',[25,540,400,85]);


    hcell_density_title = uicontrol('Parent',hinput,'Style','Text',...
        'String','Cell density (mm^-3)','BackgroundColor',color_1,...
        'FontSize',9,'Position',[10,35,120,20]);
    hcell_density_value = uicontrol('Parent',hinput,'Style','edit',...
```

```
        'FontSize',9,'String',rho_t,'Position',[130,35,60,25],...
        'BackgroundColor','white','Callback',{@cell_density_Callback});
    function cell_density_Callback(source,eventdata)
        str = get(source, 'String');
        rho_t = str2double(str);
    end


    hvoxel_size_title = uicontrol('Parent',hinput,'Style','Text',...
        'String','Tumorlet size (mm^3)','BackgroundColor',color_1,...
        'FontSize',9,'Position',[200,35,120,20]);
    hvoxel_size_value = uicontrol('Parent',hinput,'Style','edit',...
        'FontSize',9,'String',v_t,'Position',[320,35,60,25],...
        'BackgroundColor','white','Callback',{@voxel_size_Callback});
    function voxel_size_Callback(source,eventdata)
        str = get(source, 'String');
        v_t = str2double(str);
    end


    hscf_title = uicontrol('Parent',hinput,'Style','Text',...
        'String','Stem cell fraction','BackgroundColor',color_1,...
        'FontSize',9,'Position',[10,10,120,20]);
    hscf_value = uicontrol('Parent',hinput,'Style','edit',...
        'FontSize',9,'String',f_s,'Position',[130,10,60,25],...
        'BackgroundColor','white','Callback',{@scf_Callback});
    function scf_Callback(source,eventdata)
        str = get(source, 'String');
       f_s = str2double(str);
    end


    ht_cycle_title = uicontrol('Parent',hinput,'Style','Text',...
        'String','Cell cycle time (day)','BackgroundColor',color_1,...
        'FontSize',9,'Position',[200,10,120,20]);
    ht_cycle_value = uicontrol('Parent',hinput,'Style','edit',...
        'FontSize',9,'String',t_c,'Position',[320,10,60,25],...
        'BackgroundColor','white','Callback',{@t_cycle_Callback});
    function t_cycle_Callback(source,eventdata)
        str = get(source, 'String');
        t_c = str2double(str);
    end



%%  Second input panel (Compartment parameters)

color_2=[0.9 0.8 0.7];
hinput2 = uipanel('Title','Compartment Parameters','FontSize',10,...
    'ForegroundColor','b','BackgroundColor',color_2,'Unit','pixels',...
    'Position',[25,440,400,85]);


    hp_pro_title = uicontrol('Parent',hinput2,'Style','Text',...
        'String','Initial proliferating fraction in P',...
        'BackgroundColor',color_2,'FontSize',9,...
        'Position',[10,35,120,25]);
    hp_pro_value = uicontrol('Parent',hinput2,'Style','edit',...
        'FontSize',9,'String',f_p_pro_in,'Position',[130,35,60,25],...
        'BackgroundColor','white','Callback',{@p_pro_Callback});
    function p_pro_Callback(source,eventdata)
        str = get(source, 'String');
        f_p_pro_in = str2double(str);
```

```
    end


    hh_death_title = uicontrol('Parent',hinput2,'Style','Text',...
        'String','Cell loss half-time (day)',...
        'BackgroundColor',color_2,'FontSize',9,...
        'Position',[200,35,120,20]);
    hh_death_value = uicontrol('Parent',hinput2,'Style','edit',...
        'FontSize',9,'String',ht_loss,'Position',[320,35,60,25],...
        'BackgroundColor','white','Callback',{@h_death_Callback});
    function h_death_Callback(source,eventdata)
        str = get(source, 'String');
        ht_loss = str2double(str);
    end


    hk_m_title = uicontrol('Parent',hinput2,'Style','Text',...
        'String','Mitotic cell death rate',...
        'BackgroundColor',color_2,'FontSize',9,...
        'Position',[10,10,120,20]);
    hk_m_value = uicontrol('Parent',hinput2,'Style','edit',...
        'FontSize',9,'String',k_m,'Position',[130,10,60,25],...
        'BackgroundColor','white','Callback',{@k_m_Callback});
    function k_m_Callback(source,eventdata)
        str = get(source, 'String');
        k_m = str2double(str);
    end


    ht_lys_title = uicontrol('Parent',hinput2,'Style','Text',...
        'String','Lysis half-time (day)','BackgroundColor',color_2,...
        'FontSize',9,'Position',[200,10,120,20]);
    ht_lys_value = uicontrol('Parent',hinput2,'Style','edit',...
        'FontSize',9,'String',ht_lys,'Position',[320,10,60,25],...
        'BackgroundColor','white','Callback',{@t_lys_Callback});
    function t_lys_Callback(source,eventdata)
        str = get(source, 'String');
        ht_lys = str2double(str);
    end



%%  Third input panel (Microregional parameters)

 color_3=[0.85 0.85 0.7];
 hinput3 = uipanel('Title','Microregional Parameters','FontSize',10,...
     'ForegroundColor','b','BackgroundColor',color_3,'Unit','pixels',...
     'Position',[25,340,400,85]);


    hclf_title = uicontrol('Parent',hinput3,'Style','Text',...
        'String','Cell Loss Factor','BackgroundColor',color_3,...
        'FontSize',9,'Position',[10,35,120,20]);
    hclf_value = uicontrol('Parent',hinput3,'Style','edit',...
        'String',num2str(clf_in_st),'Position',[130,35,260,25],...
        'FontSize',9,'BackgroundColor','white',...
        'Callback',{@clf_Callback});
    function clf_Callback(source,eventdata)
        str = get(source, 'String');
        clf_in = str2num(str);
    end
```

```
    hgf_title = uicontrol('Parent',hinput3,'Style','Text',...
        'String','Growth Fraction','BackgroundColor',color_3,...
        'FontSize',9,'Position',[10,10,120,20]);
    hgf_value = uicontrol('Parent',hinput3,'Style','edit',...
        'String',num2str(gf_in_st),'Position',[130,10,260,25],...
        'FontSize',9,'BackgroundColor','white',...
        'Callback',{@gf_Callback});
    function gf_Callback(source,eventdata)
        str = get(source, 'String');
        gf_in = str2num(str);
    end



%%  Fourth input panel (Radiosensitivity parameters)

color_4=[0.7 0.9 0.7];
hinput4 = uipanel('Title','Radiosensitivity Parameters',...
    'FontSize',10,'ForegroundColor','b','BackgroundColor',color_4,...
    'Unit','pixels','Position',[25,240,400,85]);


    halpha_p_title = uicontrol('Parent',hinput4,'Style','Text',...
        'String','Alpha value in P','BackgroundColor',color_4,...
        'FontSize',9,'Position',[10,35,120,20]);
    halpha_p_value = uicontrol('Parent',hinput4,'Style','edit',...
        'FontSize',9,'String',alpha_p,'Position',[130,35,60,25],...
        'BackgroundColor','white','Callback',{@alpha_p_Callback});
    function alpha_p_Callback(source,eventdata)
        str = get(source, 'String');
        alpha_p = str2double(str);
    end


    hbeta_p_title = uicontrol('Parent',hinput4,'Style','Text',...
        'String','Beta value in P','BackgroundColor',color_4,...
        'FontSize',9,'Position',[200,35,120,20]);
    hbeta_p_value = uicontrol('Parent',hinput4,'Style','edit',...
        'FontSize',9,'String',beta_p,'Position',[320,35,60,25],...
        'BackgroundColor','white','Callback',{@beta_p_Callback});
    function beta_p_Callback(source,eventdata)
        str = get(source, 'String');
        beta_p = str2double(str);
    end


    hoer_i_title = uicontrol('Parent',hinput4,'Style','Text',...
        'String','OER in I','BackgroundColor',color_4,...
        'FontSize',9,'Position',[10,10,120,20]);
    hoer_i_value = uicontrol('Parent',hinput4,'Style','edit',...
        'FontSize',9,'String',oer_i,'Position',[130,10,60,25],...
        'BackgroundColor','white','Callback',{@oer_i_Callback});
    function oer_i_Callback(source,eventdata)
        str = get(source, 'String');
        oer_i = str2double(str);
    end


    hoer_h_title = uicontrol('Parent',hinput4,'Style','Text',...
        'String','OER in H','BackgroundColor',color_4,...
        'FontSize',9,'Position',[200,10,120,20]);
    hoer_h_value = uicontrol('Parent',hinput4,'Style','edit',...
        'FontSize',9,'String',oer_h,'Position',[320,10,60,25],...
```

```
        'BackgroundColor','white','Callback',{@oer_h_Callback});
    function oer_h_Callback(source,eventdata)
        str = get(source, 'String');
        oer_h = str2double(str);
    end


%%  Fifth input panel (Fractionation parameters)

color_5=[0.7 0.7 0.9];
hinput5 = uipanel('Title','Fractionation Parameters','FontSize',10,...
    'ForegroundColor','b','BackgroundColor',color_5,'Unit','pixels',...
    'Position',[25,140,400,85]);


    hfx_title = uicontrol('Parent',hinput5,'Style','Text',...
        'String','Fractioin size (Gy)','BackgroundColor',color_5,...
        'FontSize',9,'Position',[10,35,120,20]);
    hfx_value = uicontrol('Parent',hinput5,'Style','edit',...
        'String',num2str(fx_in_st),'Position',[130,35,260,25],...
        'FontSize',9,'BackgroundColor','white',...
        'Callback',{@fx_Callback});
    function fx_Callback(source,eventdata)
        str = get(source, 'String');
        fx_in = str2num(str);
    end


    hschedule_title = uicontrol('Parent',hinput5,'Style','Text',...
        'String','Fraction schedule (day)','BackgroundColor',...
        color_5,'FontSize',9,'Position',[10,10,120,20]);
    hschedule_value = uicontrol('Parent',hinput5,'Style','edit',...
        'String',num2str(schedule_in,'%5.2g'),...
        'Position',[130,10,260,25],'FontSize',9,...
        'BackgroundColor','white','Callback',{@schedule_Callback});
    function schedule_Callback(source,eventdata)
        str = get(source, 'String');
        schedule_in = str2num(str);
    end


%%  Sixth input panel (Cell cycle parameters)

color_6=[0.8 0.7 0.8];
hinput6 = uipanel('Title','Cell Cycle Parameters','FontSize',10,...
    'ForegroundColor','b','BackgroundColor',color_6,'Unit','pixels',...
    'Position',[25,25,400,100]);


    cell_cycle_g1 = uicontrol('Parent',hinput6,'Style','Text',...
        'String','G1','BackgroundColor',color_6,...
        'FontSize',9,'Position',[180,60,70,20]);
    cell_cycle_S = uicontrol('Parent',hinput6,'Style','Text',...
        'String','S','BackgroundColor',color_6,...
        'FontSize',9,'Position',[250,60,70,20]);
    cell_cycle_g2m = uicontrol('Parent',hinput6,'Style','Text',...
        'String','G2/M','BackgroundColor',color_6,...
        'FontSize',9,'Position',[320,60,70,20]);


    hf_p_title = uicontrol('Parent',hinput6,'Style','Text',...
```

```
        'String','Fraction of cells in P','BackgroundColor',color_6,...
        'FontSize',9,'Position',[10,35,170,20]);
    hf_p_g1_value = uicontrol('Parent',hinput6,'Style','edit',...
        'FontSize',9,'String',F_p_cyc(1),'Position',[185,35,60,25],...
        'BackgroundColor','white','Callback',{@f_p_g1_Callback});
    function f_p_g1_Callback(source,eventdata)
        str = get(source, 'String');
        F_p_cyc(1) = str2double(str);
    end


    hf_p_s_value = uicontrol('Parent',hinput6,'Style','edit',...
        'FontSize',9,'String',F_p_cyc(2),'Position',[255,35,60,25],...
        'BackgroundColor','white','Callback',{@f_p_s_Callback});
    function f_p_s_Callback(source,eventdata)
        str = get(source, 'String');
        F_p_cyc(2) = str2double(str);
    end


    hf_p_g2m_value = uicontrol('Parent',hinput6,'Style','edit',...
        'FontSize',9,'String',F_p_cyc(3),'Position',[325,35,60,25],...
        'BackgroundColor','white','Callback',{@f_p_g2m_Callback});
    function f_p_g2m_Callback(source,eventdata)
        str = get(source, 'String');
        F_p_cyc(3) = str2double(str);
    end


    halpha_title = uicontrol('Parent',hinput6,'Style','Text',...
        'String','Alpha ratios to S-phase','BackgroundColor',...
        color_6,'FontSize',9,'Position',[10,10,170,20]);
    halpha_g1_value = uicontrol('Parent',hinput6,'Style','edit',...
        'FontSize',9,'String',Alpha_ratio_p_cyc(1),...
        'Position',[185,10,60,25],'BackgroundColor','white',...
        'Callback',{@alpha_g1_Callback});
    function alpha_g1_Callback(source,eventdata)
        str = get(source, 'String');
        Alpha_ratio_p_cyc(1) = str2double(str);
    end


    halpha_g2m_value = uicontrol('Parent',hinput6,'Style','edit',...
        'FontSize',9,'String',Alpha_ratio_p_cyc(2),...
        'Position',[325,10,60,25],'BackgroundColor','white',...
        'Callback',{@alpha_g2m_Callback});
    function alpha_g2m_Callback(source,eventdata)
        str = get(source, 'String');
        Alpha_ratio_p_cyc(2) = str2double(str);
    end



%%  Seventh input panel (Simulation criteria)

color_7=[0.78 0.78 0.78];
hinput7 = uipanel('Title','Simulation Criteria','FontSize',10,...
    'ForegroundColor','b','BackgroundColor',color_7,'Unit','pixels',...
    'Position',[450,25,400,100]);
    htumor = uibuttongroup('Parent',hinput7,'Unit','pixels',...
        'Position',[10,10,170,65],'FontSize',9,...
        'BackgroundColor',color_7);
    tumorlet = uicontrol('Parent',htumor,'Style','Radio','String',...
```

```
    'For a tumorlet (0.064 cc)','FontSize',9,...
    'BackgroundColor',color_7,'Position',[10,35,160,20]);
tumor = uicontrol('Parent',htumor,'Style','Radio','String',...
    'Tumor size of                cc','FontSize',9,...
    'BackgroundColor',color_7,'Position',[10,10,160,20]);
set(htumor,'SelectionChangeFcn',@selcbk);

function selcbk(source,eventdata)
    if strcmp(get(get(source,'SelectedObject'),'String'),...
            'For a tumorlet (0.064 cc)')==1
        tumor_size='-';
        tcp_goal='-';
        vcp_goal=0.5;
        set(htumor_size_value,'String','-');
    else
        tcp_goal=0.5;
        tumor_size=10;
        vcp_goal = tcp_goal^(v_t/(tumor_size*1000));
        set(htumor_size_value,'String',num2str(tumor_size,'%3.0f'));
    end
end

htumor_size_value = uicontrol('Parent',htumor,'Style','edit',...
    'FontSize',9,'String',tumor_size,'Position',[105,10,40,20],...
    'BackgroundColor','white','Callback',{@tumor_size_Callback});
function tumor_size_Callback(source,eventdata)
    str = get(source, 'String');
    tumor_size = str2double(str);
    tcp_goal = 0.5;
    vcp_goal = tcp_goal^(v_t/(tumor_size*1000));
end

if type == 2 || type == 9 || type == 10
    hcriteria = uibuttongroup('Parent',hinput7,'Unit','pixels',...
        'Position',[190,10,200,65],'FontSize',9,...
        'BackgroundColor',color_7);
    tcd50 = uicontrol('Parent',hcriteria,'Style','Radio',...
        'String','TCD50 (or VCD50) for 5 fx/wk','FontSize',9,...
        'BackgroundColor',color_7,'Position',[10,35,180,20]);
    schedule = uicontrol('Parent',hcriteria,'Style','Radio',...
        'String','TCP for a given schedule','FontSize',9,...
        'BackgroundColor',color_7,'Position',[10,10,180,20]);
    set(hcriteria,'SelectionChangeFcn',@selcbk2);
else if type==3 || type==5 || type==6 || type==7 || type==11
    hcriteria = uibuttongroup('Parent',hinput7,'Unit','pixels',...
        'Position',[190,10,200,65],'FontSize',9,...
        'BackgroundColor',color_7);
    tcd50 = uicontrol('Parent',hcriteria,'Style','Radio',...
        'String','TCD50 (or VCD50) for 5 fx/wk','FontSize',9,...
        'BackgroundColor',color_7,'Position',[10,35,180,20]);
    set(hcriteria,'SelectionChangeFcn',@selcbk2);
    else
        @selcbk2;
    end
end
function selcbk2(source,eventdata)
    if get(source,'SelectedObject')=='For a tumorlet (0.064 cc)'
        tumor_size='-';
        tcp_goal='-';
    else
        tcp_goal=0.5;
        tumor_size=10;
        vcp_goal = tcp_goal^(v_t/(tumor_size*1000));
```

```
                set(htumor_size_value,'String',num2str(tumor_size,'%3.0f'));
            end
        end


        if type==1
            set(halpha_p_value,'BackgroundColor',[0.8 0.8 0.8]);
            set(hbeta_p_value,'BackgroundColor',[0.8 0.8 0.8]);
            set(hoer_i_value,'BackgroundColor',[0.8 0.8 0.8]);
            set(hoer_h_value,'BackgroundColor',[0.8 0.8 0.8]);
            set(hfx_value,'BackgroundColor',[0.8 0.8 0.8]);
            set(hschedule_value,'BackgroundColor',[0.8 0.8 0.8]);
            set(hf_p_g1_value,'BackgroundColor',[0.8 0.8 0.8]);
            set(hf_p_s_value,'BackgroundColor',[0.8 0.8 0.8]);
            set(hf_p_g2m_value,'BackgroundColor',[0.8 0.8 0.8]);
            set(halpha_g1_value,'BackgroundColor',[0.8 0.8 0.8]);
            set(halpha_g2m_value,'BackgroundColor',[0.8 0.8 0.8]);
        end
        if type==2||type==3||type==4||type==5||type==6||type==7||type==11
            set(hschedule_value,'BackgroundColor',[0.8 0.8 0.8]);
            set(hf_p_g1_value,'BackgroundColor',[0.8 0.8 0.8]);
            set(hf_p_s_value,'BackgroundColor',[0.8 0.8 0.8]);
            set(hf_p_g2m_value,'BackgroundColor',[0.8 0.8 0.8]);
            set(halpha_g1_value,'BackgroundColor',[0.8 0.8 0.8]);
            set(halpha_g2m_value,'BackgroundColor',[0.8 0.8 0.8]);;
        end
        if type==8
            set(hinput7,'Visible','off');
        end
        if type==5
            set(hfx_value,'BackgroundColor',[0.8 0.8 0.8]);
        end

end



%% Simulation & Plot

%  Pushbuttons

ha=uipanel('Unit','pixels','Position',[450,145,725,510]);
color_7=[0.7 0.75 0.8];


ht_cal_title = uicontrol('Style','Text','FontSize',10,...
    'String','Calculation time (sec) = ','Position',[865,91,140,18],...
    'BackgroundColor',color_7);
ht_cal_value = uicontrol('Style','Text','String',' ','FontSize',10,...
    'Position',[1005,91,40,18],'BackgroundColor',color_7,...
    'Callback',{@t_cal_Callback});


hplot = uicontrol('Style','pushbutton','String','Simulate & Plot',...
      'FontSize',10,'FontWeight','bold','Position',[1055,80,120,40],...
      'ForegroundColor',[1 0 0.3],'Callback',{@plotbutton_Callback});
function plotbutton_Callback(source,eventdata)
delete(ha);ha=uipanel('Unit','pixels','Position',[450,145,725,510]);


VCP=vcp_goal;
n_t=rho_t*v_t;
total_clono_cell=n_t*f_s;
```

```
delta_t=d_t/(60*24);
t_start=0;


tic;
IC=[]; GF=[]; TCP=[]; TD50=[]; BED=[];
Reox_time=[]; Reox_time2=[]; Treat_duration=[]; vec_leng=[];
comp_size(1)=0;      comp_size(2)=0;       comp_size(3)=0;
p_pre=[];  i_pre=[];   h_pre=[];
T_end=[];


wb = waitbar(0,'PLEASE   WAIT...');step=0;
switch type


    case 1 %Initial Distribution for various CLF and GF%
        k=0; for clf=clf_in; k=k+1;
            l=0; for gf=gf_in; l=l+1;
                % run the sub-routine for a specific CLF and GF
                run SubRoutine/SR_initial_distribution;
                % save the the number of cell into matrix
                IC(l,1,k)=comp_size(1);
                IC(l,2,k)=comp_size(2);
                IC(l,3,k)=comp_size(3);
                step=step+1;
                waitbar(step/(length(gf_in)*length(clf_in)));
            end % loop for GF
        end % loop for CLF
        close(wb);
        %%%%%%%%%%%%%%%%%%%%%%%%%%%%%%%%%%%%%%%%%%%%%%%%%%%%%%%%%%%%%%%%%%%%%%%
        if tcp_goal=='-'
            for m=1:1:length(clf_in)
                size_y=ceil(sqrt(length(clf_in)));
                size_x=ceil(length(clf_in)/size_y);
                subplot(size_x,size_y,m,'parent',ha);
                bar(gf_in,IC(:,:,m),'stack');
                title(['CLF = ',num2str(clf_in(m))],'FontSize',12,...
                    'fontweight','b','color','b');
                xlim([min(gf_in)-0.02 max(gf_in)+0.02]); ylim([0 n_t]);
                xlabel('Growth Fraction','FontSize',11,'fontweight','b');
                ylabel('Cells in each comp','FontSize',11,'fontweight','b');
            end
        else
            IC=IC*tumor_size*1000/v_t;
            for m=1:1:length(clf_in)
                size_y=ceil(sqrt(length(clf_in)));
                size_x=ceil(length(clf_in)/size_y);
                subplot(size_x,size_y,m,'parent',ha);
                bar(gf_in,IC(:,:,m),'stack');
                title(['CLF = ',num2str(clf_in(m))],'FontSize',12,...
                    'fontweight','b','color','b');
                xlim([min(gf_in)-0.02 max(gf_in)+0.02]);
                ylim([0 n_t*tumor_size*1000/v_t]);
                xlabel('Growth Fraction','FontSize',11,'fontweight','b');
                ylabel('Cells in each comp','FontSize',11,'fontweight','b');
            end
        end

        legend('P','I','H');
        %%%%%%%%%%%%%%%%%%%%%%%%%%%%%%%%%%%%%%%%%%%%%%%%%%%%%%%%%%%%%%%%%%%%%%%
        t_cal=toc;
        set(ht_cal_value,'String',num2str(t_cal,'%5.1f'));
```

```
    %%%%%%%%%%%%%%%%%%%%%%%%%%%%%%%%%%%%%%%%%%%%%%%%%%%%%%%%%%%%%%%%%%%%%%%

case 2 %Example plots for a specific GF,CLF and fx%
    clf=clf_in; gf=gf_in; d=fx_in;
    % run the sub-routine for the initial distribution
    run SubRoutine/SR_initial_distribution;
    % calculate until TD50 achieved
    no_pro=0;
    alpha_i=alpha_p/oer_i;beta_i=beta_p/(oer_i)^2;
    alpha_h=alpha_p/oer_h;beta_h=beta_p/(oer_h)^2;
    run SubRoutine/SR_RT;
    % Calculate TCP & TD50
    s=cell_dist(1)+cell_dist(3)+cell_dist(5);
    nsc=s*f_s;
    tcp=exp(-nsc);
    td50=j*d;
    % Find reoxygenation time
    run SubRoutine/SR_Reox_time;
    step=step+1;
    waitbar(step/(length(gf_in)*length(clf_in)));
    close(wb);
    %%%%%%%%%%%%%%%%%%%%%%%%%%%%%%%%%%%%%%%%%%%%%%%%%%%%%%%%%%%%%%%%%%%%%%%
    time=delta_t:delta_t:round(t*96)/96;
    if tcp_goal=='-'
        subplot(2,2,1,'parent',ha);
        bar(1:3,[comp_size(1),comp_size(2),comp_size(3)]);
        xlabel('Compartment (1=P, 2=I and 3=H)','FontSize',11,...
            'fontweight','b');
        ylabel('Initial number of cells','FontSize',11,'fontweight','b');
        subplot(2,2,2,'parent',ha);
        semilogy(time,cum_cell_dist(1,:),'r',time,cum_cell_dist(2,:),...
            'r:',time,cum_cell_dist(3,:),'b',...
            time,cum_cell_dist(4,:),'b:',time,cum_cell_dist(5,:),'g',...
            time,cum_cell_dist(6,:),'g:');
        xlim([0 ceil(t)]);
        ylim([10 2*max(sum(cum_cell_dist))]);
        xlabel('Time (Day)','FontSize',11,'fontweight','b');
        ylabel('Cells in each comp','FontSize',11,'fontweight','b');
        legend('P_v','P_d','I_v','I_d','H_v','H_d');
        subplot(2,2,3,'parent',ha);
        semilogy(time,sum(cum_cell_dist(1:6,:)),'r',...
            time,sum(cum_cell_dist(2:6,:)),'r:',...
            time,sum(cum_cell_dist(3:6,:)),'b',...
            time,sum(cum_cell_dist(4:6,:)),'b:',...
            time,sum(cum_cell_dist(5:6,:)),'g',...
            time,cum_cell_dist(6,:),'g:');
        xlim([0 ceil(t)]);
        ylim([10 2*max(sum(cum_cell_dist))]);
        xlabel('Time (Day)','FontSize',11,'fontweight','b');
        ylabel('Number of tumor cells','FontSize',11,'fontweight','b');
        text(t*0.3,1e-5*(sum(comp_size)),...
            ['t_R = ',num2str(reox_time2),',  ',num2str(reox_time)],...
            'FontSize',11,'fontweight','b');
        subplot(2,2,4,'parent',ha);
        semilogy(time,sum(cum_cell_dist([1 3 5],:)),'r',...
            time,sum(cum_cell_dist([3 5],:)),'b',...
            time,cum_cell_dist(5,:),'g');
        xlim([0 ceil(t)]);
        ylim([10 2*max(sum(cum_cell_dist))]);
        xlabel('Time (Day)','FontSize',11,'fontweight','b');
        ylabel('Number of viable cells','FontSize',11,'fontweight','b');
        text(t*0.3,0.5*(sum(comp_size)),...
```

```
        ['# of stem cells = ',num2str((cell_dist(1)+cell_dist(3)...
        +cell_dist(5))*f_s)],'FontSize',11,'fontweight','b');
    text(t*0.45,0.1*(sum(comp_size)),...
        ['VCP = ',num2str(exp(-(cell_dist(1)+cell_dist(3)+...
        cell_dist(5))*f_s))],'FontSize',11,'fontweight','b');
    text(t*0.45,0.02*(sum(comp_size)),...
     ['VCD50 = ',num2str(td50),' Gy'],'FontSize',11,...
     'fontweight','b');
else
    cum_cell_dist=cum_cell_dist*tumor_size*1000/v_t;
    comp_size(1)=comp_size(1)*tumor_size*1000/v_t;
    comp_size(2)=comp_size(2)*tumor_size*1000/v_t;
    comp_size(3)=comp_size(3)*tumor_size*1000/v_t;
    subplot(2,2,1,'parent',ha);
    bar(1:3,[comp_size(1),comp_size(2),comp_size(3)]);
    ylim([0 1.1*max([comp_size(1),comp_size(2),comp_size(3)])]);
    xlabel('Compartment (1=P, 2=I and 3=H)','FontSize',11,...
        'fontweight','b');
    ylabel('Initial number of cells','FontSize',11,'fontweight','b');
    subplot(2,2,2,'parent',ha);
    semilogy(time,cum_cell_dist(1,:),'r',...
        time,cum_cell_dist(2,:),'r:',time,cum_cell_dist(3,:),'b',...
        time,cum_cell_dist(4,:),'b:',time,cum_cell_dist(5,:),'g',...
        time,cum_cell_dist(6,:),'g:');
    xlim([0 ceil(t)]);
    ylim([10 2*max(sum(cum_cell_dist))]);
    xlabel('Time (Day)','FontSize',11,'fontweight','b');
    ylabel('Cells in each comp','FontSize',11,'fontweight','b');
    legend('P_v','P_d','I_v','I_d','H_v','H_d');
    subplot(2,2,3,'parent',ha);
    semilogy(time,sum(cum_cell_dist(1:6,:)),'r',...
        time,sum(cum_cell_dist(2:6,:)),'r:',...
        time,sum(cum_cell_dist(3:6,:)),'b',...
        time,sum(cum_cell_dist(4:6,:)),'b:',...
        time,sum(cum_cell_dist(5:6,:)),'g',...
        time,cum_cell_dist(6,:),'g:');
    xlim([0 ceil(t)]);
    ylim([10 2*max(sum(cum_cell_dist))]);
    xlabel('Time (Day)','FontSize',11,'fontweight','b');
    ylabel('Number of tumor cells','FontSize',11,'fontweight','b');
    text(t*0.3,1e-7*(sum(comp_size)),...
        ['t_R = ',num2str(reox_time2),',  ',num2str(reox_time)],...
        'FontSize',11,'fontweight','b');
    subplot(2,2,4,'parent',ha);
    semilogy(time,sum(cum_cell_dist([1 3 5],:)),'r',...
        time,sum(cum_cell_dist([3 5],:)),'b',...
        time,cum_cell_dist(5,:),'g');
    xlim([0 ceil(t)]);
    ylim([10 2*max(sum(cum_cell_dist))]);
    xlabel('Time (Day)','FontSize',11,'fontweight','b');
    ylabel('Number of viable cells','FontSize',11,'fontweight','b');
    text(t*0.3,0.5*(sum(comp_size)),['# of stem cells = ',...
        num2str((cell_dist(1)+cell_dist(3)+cell_dist(5))...
        *f_s*tumor_size/v_t*1000)],'FontSize',11,'fontweight','b');
    text(t*0.45,0.05*(sum(comp_size)),...
        ['TCP = ',num2str(exp(-(cell_dist(1)+cell_dist(3)+...
        cell_dist(5))*f_s)^(tumor_size/v_t*1000))],'FontSize',11,...
        'fontweight','b');
    text(t*0.45,0.005*(sum(comp_size)),...
        ['TCD50 = ',num2str(td50),' Gy'],'FontSize',11,...
        'fontweight','b');
end
%%%%%%%%%%%%%%%%%%%%%%%%%%%%%%%%%%%%%%%%%%%%%%%%%%%%%%%%%%%%%%%%%%%%%%%%%%%%
```

```
    t_cal=toc;
    set(ht_cal_value,'String',num2str(t_cal,'%5.1f'));
    %%%%%%%%%%%%%%%%%%%%%%%%%%%%%%%%%%%%%%%%%%%%%%%%%%%%%%%%%%%%%%%%%%%%%%%%%%%%

case 3 %TD50 vs. GF for various fx%
    clf=clf_in;
    k=0; for gf=gf_in; k=k+1;
        % run the sub-routine for the initial distribution
        run SubRoutine/SR_initial_distribution;
        l=0; for d=fx_in; l=l+1;
            % calculate until TD50 achieved
            no_pro=0;
            alpha_i=alpha_p/oer_i;beta_i=beta_p/(oer_i)^2;
            alpha_h=alpha_p/oer_h;beta_h=beta_p/(oer_h)^2;
            run SubRoutine/SR_RT;
            % Calculate TCP & TD50
            s=cell_dist(1)+cell_dist(3)+cell_dist(5);
            nsc=s*f_s;
            tcp=exp(-nsc);
            td50=j*d;
            % Output
            GF(k,l)=gf;
            NSC(k,l)=nsc;
            TCP(k,l)=tcp;
            TD50(k,l)=td50;
            Treat_duration(k,l)=j+add_time;
            step=step+1;waitbar(step/(length(gf_in)*length(fx_in)))
        end
    end
    close(wb);
    %%%%%%%%%%%%%%%%%%%%%%%%%%%%%%%%%%%%%%%%%%%%%%%%%%%%%%%%%%%%%%%%%%%%%%%%%%%%
    haxes = axes('parent',ha,'Units','Pixels','Position',...
        [55,50,640,430]);
    line=['-ks' '-ro' '-g^' '-bv' '-cd' '-m<'];
    for m=1:1:length(fx_in)
        plot(haxes,gf_in,TD50(:,m),line((3*m-2):3*m));
        hold on;
    end
    xlabel('Growth Fraction','FontSize',11,'fontweight','b');
    ylabel('TD50','FontSize',11,'fontweight','b');
    xlim([0 max(max(GF))+0.01]);
    ylim([min(min(TD50))-2 max(max(TD50))+10]);
    legend(strcat(num2str(fx_in'),' Gy/fx'));
    %%%%%%%%%%%%%%%%%%%%%%%%%%%%%%%%%%%%%%%%%%%%%%%%%%%%%%%%%%%%%%%%%%%%%%%%%%%%
    t_cal=toc;
    set(ht_cal_value,'String',num2str(t_cal,'%5.1f'));
    %%%%%%%%%%%%%%%%%%%%%%%%%%%%%%%%%%%%%%%%%%%%%%%%%%%%%%%%%%%%%%%%%%%%%%%%%%%%


case 4 %Reoxygenation time vs. GF for various fx%
    clf=clf_in;
    k=0; for gf=gf_in; k=k+1;
        % run the sub-routine for the initial distribution
        run SubRoutine/SR_initial_distribution;
        l=0; for d=fx_in; l=l+1;
            % calculate until TD50 achieved
            no_pro=0;
            alpha_i=alpha_p/oer_i;beta_i=beta_p/(oer_i)^2;
            alpha_h=alpha_p/oer_h;beta_h=beta_p/(oer_h)^2;
            run SubRoutine/SR_RT_reox;
            % Calculate TCP & TD50
            s=cell_dist(1)+cell_dist(3)+cell_dist(5);
```

```
            nsc=s*f_s;
            tcp=exp(-nsc);
            td50=j*d;
            % Output
            GF(k,l)=gf;
            NSC(k,l)=nsc;
            TCP(k,l)=tcp;
            TD50(k,l)=td50;
            Treat_duration(k,l)=j+add_time;
            % Find reoxygenation time
            run SubRoutine/SR_Reox_time;
            Reox_time(k,l)=reox_time;
            Reox_time2(k,l)=reox_time2;
            step=step+1;
            waitbar(step/(length(gf_in)*length(fx_in)));
        end
    end
    close(wb);
    %%%%%%%%%%%%%%%%%%%%%%%%%%%%%%%%%%%%%%%%%%%%%%%%%%%%%%%%%%%%%%%%%%%%%%%
    haxes = axes('parent',ha,'Units','Pixels',...
        'Position',[55,50,640,430]);
    line=['-ks' '-ro' '-g^' '-bv' '-cd' '-m<'];
    for m=1:1:length(fx_in)
        plot(haxes,gf_in,Reox_time(:,m),line((3*m-2):3*m));
        hold on;
    end
    xlabel('Growth Fraction','FontSize',11,'fontweight','b');
    ylabel('Reoxgenation time [day]','FontSize',11,'fontweight','b');
    xlim([0 0.31]);
    ylim([min(min(Reox_time))-2 max(max(Reox_time))+10]);
    legend(strcat(num2str(fx_in'),' Gy/fx'));
    %%%%%%%%%%%%%%%%%%%%%%%%%%%%%%%%%%%%%%%%%%%%%%%%%%%%%%%%%%%%%%%%%%%%%%%
    t_cal=toc;
    set(ht_cal_value,'String',num2str(t_cal,'%5.1f'));
    %%%%%%%%%%%%%%%%%%%%%%%%%%%%%%%%%%%%%%%%%%%%%%%%%%%%%%%%%%%%%%%%%%%%%%%


case 5 %TD50 vs. Treatment duration for various GF%
    clf=clf_in;
    k=0; for gf=gf_in; k=k+1;
        % run the sub-routine for the initial distribution
        run SubRoutine/SR_initial_distribution;
        j=0;add_time=0;
        l=0;
        terminated=0;
        d=50;
        while j+add_time<120
            if gf==0.1
                if d>1.15
                    d=d*0.99;
                else
                    d=d*0.999;
                end
            else
                d=d*0.99;
            end
            l=l+1;
            % calculate until TD50 achieved
            no_pro=0;
            alpha_i=alpha_p/oer_i;beta_i=beta_p/(oer_i)^2;
            alpha_h=alpha_p/oer_h;beta_h=beta_p/(oer_h)^2;
            run SubRoutine/SR_RT;
```

```
        % Calculate TCP & TD50
        s=cell_dist(1)+cell_dist(3)+cell_dist(5);
        nsc=s*f_s;
        tcp=exp(-nsc);
        td50=j*d;
        bed=j*d*(1+0.1*d);
        GF(k,l)=gf;
        NSC(k,l)=nsc;
        TCP(k,l)=tcp;
        TD50(k,l)=td50;
        BED(k,l)=bed;
        Treat_duration(k,l)=j+add_time;
        if rem(j,5)==0
            Treat_duration(k,l)=Treat_duration(k,l)-2;
        end
        waitbar(((k-1)*120+min(120,Treat_duration(k,l)))/...
            (120*length(gf_in)));
        if l>1
            if Treat_duration(k,l)==Treat_duration(k,l-1)
                if TD50(k,l)<TD50(k,l-1)
                    TD50(k,l-1)=TD50(k,l);
                end
                l=l-1;
            end
        end
    end
    if terminated~=1
        vec_leng(k)=l;
    else
        vec_leng(k)=l-1;
        TD50(k,l)=0;
        Treat_duration(k,l)=0;
    end
end
close(wb);


slope_sum=0;
for k=3:1:5
    linearCoef = polyfit(Treat_duration(k,vec_leng(k)-2:...
        vec_leng(k)),TD50(k,vec_leng(k)-2:vec_leng(k)),1);
    slope_sum=slope_sum+linearCoef(1);
end
slope=slope_sum/3;

%%%%%%%%%%%%%%%%%%%%%%%%%%%%%%%%%%%%%%%%%%%%%%%%%%%%%%%%%%%%%%%%%%%%%%%
haxes = axes('parent',ha,'Units','Pixels',...
    'Position',[55,50,640,430]);
line=['-k' '-b' '-g' '-m' '-r'];
for m=1:1:length(gf_in)
    plot(haxes,Treat_duration(m,1:vec_leng(m)),...
        TD50(m,1:vec_leng(m)),line((2*m-1):2*m),'LineWidth', 1.5);
    hold on;
end
xlim([0 120]); ylim([20 110]);
legend(strcat('GF=',num2str(gf_in')),'Location','NorthWest');
xlabel('Treatment duration (day)','FontSize',11,'fontweight','b');
ylabel('TD50 (Gy)','FontSize',11,'fontweight','b');
text(60,100,['Asymtotic line slope = ',num2str(slope)],...
    'FontSize',11,'fontweight','b');
%%%%%%%%%%%%%%%%%%%%%%%%%%%%%%%%%%%%%%%%%%%%%%%%%%%%%%%%%%%%%%%%%%%%%%%
t_cal=toc;
set(ht_cal_value,'String',num2str(t_cal,'%5.1f'));
```

```
    %%%%%%%%%%%%%%%%%%%%%%%%%%%%%%%%%%%%%%%%%%%%%%%%%%%%%%%%%%%%%%%%%%%%%%%%

case 6 %Tumor size vs. Time for various GF%
    clf=clf_in; d=fx_in;
    k=0;for gf=gf_in;k=k+1;
        % run the sub-routine for the initial distribution
        run SubRoutine/SR_initial_distribution;
        % calculate until TD50 achieved
        no_pro=0;
        alpha_i=alpha_p/oer_i;beta_i=beta_p/(oer_i)^2;
        alpha_h=alpha_p/oer_h;beta_h=beta_p/(oer_h)^2;
        run SubRoutine/SR_RT;
        % Calculate TCP & TD50
        s=cell_dist(1)+cell_dist(3)+cell_dist(5);
        nsc=s*f_s;
        tcp=exp(-nsc);
        td50=j*d;
        T_end(k)=t;

        step=step+1;
        waitbar(step/length(gf_in));
    end
    close(wb);
    clinical=6.4e7*(1-0.018.*(delta_t:delta_t:max(T_end)));
    if tcp_goal~='-'
        Total_cell=Total_cell*tumor_size*1000/v_t;
        clinical=clinical*tumor_size*1000/v_t;
    end
    %%%%%%%%%%%%%%%%%%%%%%%%%%%%%%%%%%%%%%%%%%%%%%%%%%%%%%%%%%%%%%%%%%%%%%%%
    haxes = axes('parent',ha,'Units','Pixels',...
        'Position',[55,50,640,430]);
    plot(delta_t:delta_t:round(T_end(1)),...
        Total_cell(1,1:uint16(round(T_end(1))/delta_t)),'r',...
        delta_t:delta_t:round(T_end(2)),...
        Total_cell(2,1:uint16(round(T_end(2))/delta_t)),'b',...
        delta_t:delta_t:round(T_end(3)),...
        Total_cell(3,1:uint16(round(T_end(3))/delta_t)),'g',...
        delta_t:delta_t:round(T_end(4)),...
        Total_cell(4,1:uint16(round(T_end(4))/delta_t)),'m',...
        delta_t:delta_t:round(T_end(5)),...
        Total_cell(5,1:uint16(round(T_end(5))/delta_t)),'c',...
        delta_t:delta_t:max(T_end),clinical,'k','LineWidth', 1.5);
    xlim([0 max(T_end)]); ylim([0 1.5*max(max(Total_cell))]);
    xlabel('Time (Day)','FontSize',11,'fontweight','b');
    ylabel('Total number of cells','FontSize',11,'fontweight','b');
    legend(strvcat(strcat('GF = ',num2str(gf_in')),'Clinical'));
    %%%%%%%%%%%%%%%%%%%%%%%%%%%%%%%%%%%%%%%%%%%%%%%%%%%%%%%%%%%%%%%%%%%%%%%%
    t_cal=toc;
    set(ht_cal_value,'String',num2str(t_cal,'%5.1f'));
    %%%%%%%%%%%%%%%%%%%%%%%%%%%%%%%%%%%%%%%%%%%%%%%%%%%%%%%%%%%%%%%%%%%%%%%%


case 7 % 7. Effect of proliferation and hypoxia
    clf=clf_in;
    d=fx_in;
    oer_i_in=oer_i;
    oer_h_in=oer_h;
    f_p_pro=f_p_pro_in;
    k=0; for cal_type=[1 2 3 4]; k=k+1;
        % run the sub-routine for the initial distribution
        l=0; for gf=gf_in; l=l+1;
            run SubRoutine/SR_initial_distribution;
```

```
            % calculate until TD50 achieved
            alpha_i=alpha_p/oer_i;beta_i=beta_p/(oer_i)^2;
            alpha_h=alpha_p/oer_h;beta_h=beta_p/(oer_h)^2;
            switch cal_type
                case 1
                    oer_i=1; oer_h=1;
                    alpha_i=alpha_p/oer_i; beta_i=beta_p/oer_i^2;
                    alpha_h=alpha_p/oer_h; beta_h=beta_p/oer_h^2;
                    no_pro=1;
                    run SubRoutine/SR_RT;
                case 2
                    oer_i=oer_i_in; oer_h=oer_h_in;
                    alpha_i=alpha_p/oer_i; beta_i=beta_p/oer_i^2;
                    alpha_h=alpha_p/oer_h; beta_h=beta_p/oer_h^2;
                    no_pro=1;
                    run SubRoutine/SR_RT;
                case 3
                    oer_i=1; oer_h=1;
                    alpha_i=alpha_p/oer_i; beta_i=beta_p/oer_i^2;
                    alpha_h=alpha_p/oer_h; beta_h=beta_p/oer_h^2;
                    no_pro=0;
                    run SubRoutine/SR_RT;
                case 4
                    oer_i=oer_i_in; oer_h=oer_h_in;
                    alpha_i=alpha_p/oer_i; beta_i=beta_p/oer_i^2;
                    alpha_h=alpha_p/oer_h; beta_h=beta_p/oer_h^2;
                    no_pro=0;
                    run SubRoutine/SR_RT;
            end
            % Calculate TCP & TD50
            s=cell_dist(1)+cell_dist(3)+cell_dist(5);
            nsc=s*f_s;
            tcp=exp(-nsc);
            td50=j*d;
            % Output
            GF(k,l)=gf;
            NSC(k,l)=nsc;
            TCP(k,l)=tcp;
            TD50(k,l)=td50;
            Treat_duration(k,l)=j+add_time;
            step=step+1;waitbar(step/(length(gf_in)*4))
        end
    end
    close(wb)
    %%%%%%%%%%%%%%%%%%%%%%%%%%%%%%%%%%%%%%%%%%%%%%%%%%%%%%%%%%%%%%%%%%%%%%%
    haxes = axes('parent',ha,'Units','Pixels',...
        'Position',[55,50,640,430]);
    plot(haxes,gf_in,TD50(1,:),'-ks',gf_in,TD50(2,:),'-g^',...
        gf_in,TD50(3,:),'-ro',gf_in,TD50(4,:),'-bv');
    xlabel('Growth Fraction','FontSize',11,'fontweight','b');
    ylabel('TD50','FontSize',11,'fontweight','b');
    xlim([0 max(max(GF))+0.01]);
    ylim([min(min(TD50))-2 max(max(TD50))+10]);
    legend('Neither Proliferation nor Hypoxia','Only Hypoxia',...
       'Only Proliferation', 'Both Proliferation and Hypoxia');
    %%%%%%%%%%%%%%%%%%%%%%%%%%%%%%%%%%%%%%%%%%%%%%%%%%%%%%%%%%%%%%%%%%%%%%%
    t_cal=toc;
    set(ht_cal_value,'String',num2str(t_cal,'%5.1f'));
    %%%%%%%%%%%%%%%%%%%%%%%%%%%%%%%%%%%%%%%%%%%%%%%%%%%%%%%%%%%%%%%%%%%%%%%


case 8 %Cell cycle dependent SF, alpha & OERs%
    clf=clf_in; gf=gf_in;
```

```
% run the sub-routine for a specific CLF and GF
run SubRoutine/SR_initial_distribution;
% save the the number of cell into matrix
f_p=comp_size(1)/sum(comp_size);
f_i=comp_size(2)/sum(comp_size);
f_h=comp_size(3)/sum(comp_size);
sf=[]; SF=[]; Alpha_eff=[]; OERI_eff=[]; OERH_eff=[];
for d=fx_in
    f=@(alpha_s)F_p_cyc(1)*exp(-Alpha_ratio_p_cyc(1)*alpha_s*2-...
        0.1*Alpha_ratio_p_cyc(1)*alpha_s*4)+...
    F_p_cyc(2)*exp(-alpha_s*2-0.1*alpha_s*4)+...
    F_p_cyc(3)*exp(-Alpha_ratio_p_cyc(2)*alpha_s*2-...
    0.1*Alpha_ratio_p_cyc(2)*alpha_s*4)-...
    exp(-alpha_p*2-0.1*alpha_p*4);

    Alpha_p_cyc(2)=fzero(f,0.3);
    Alpha_p_cyc(1)=Alpha_p_cyc(2)*Alpha_ratio_p_cyc(1);
    Alpha_p_cyc(3)=Alpha_p_cyc(2)*Alpha_ratio_p_cyc(2);

    Su_p=F_p_cyc(1)*exp(-Alpha_p_cyc(1)*d-0.1*Alpha_p_cyc(1)*d^2)...
        +F_p_cyc(2)*exp(-Alpha_p_cyc(2)*d-0.1*Alpha_p_cyc(2)*d^2)...
        +F_p_cyc(3)*exp(-Alpha_p_cyc(3)*d-0.1*Alpha_p_cyc(3)*d^2);
    alpha_p_eff=-log(Su_p)/(d*(1+0.1*d));
    beta_p_eff=0.1*alpha_p_eff;

    Su_i_2gy=exp(-alpha_p/oer_i*2-0.1*alpha_p/(oer_i^2)*2^2);
    oer_i_g1=(-(Alpha_p_cyc(1)*2)-sqrt((Alpha_p_cyc(1)*2)^2-...
        4*log(Su_i_2gy)*0.1*Alpha_p_cyc(1)*2^2))/(2*log(Su_i_2gy));
    Su_h_2gy=exp(-alpha_p/oer_h*2-0.1*alpha_p/(oer_h^2)*2^2);
    oer_h_g1=(-(Alpha_p_cyc(1)*2)-sqrt((Alpha_p_cyc(1)*2)^2-...
        4*log(Su_h_2gy)*0.1*Alpha_p_cyc(1)*2^2))/(2*log(Su_h_2gy));
    alpha_i=Alpha_p_cyc(1)/oer_i_g1;
    beta_i=0.1*Alpha_p_cyc(1)/(oer_i_g1^2);
    alpha_h=Alpha_p_cyc(1)/oer_h_g1;
    beta_h=0.1*Alpha_p_cyc(1)/(oer_h_g1^2);

    Su_i=exp(-alpha_i*d-beta_i*d^2);
    oer_i_eff=(-(alpha_p_eff*d)-sqrt((alpha_p_eff*d)^2-...
        4*log(Su_i)*beta_p_eff*d^2))/(2*log(Su_i));

    Su_h=exp(-alpha_h*d-beta_h*d^2);
    oer_h_eff=(-(alpha_p_eff*d)-sqrt((alpha_p_eff*d)^2-...
        4*log(Su_h)*beta_p_eff*d^2))/(2*log(Su_h));

    Su_p_g1=f_p*F_p_cyc(1)*exp(-Alpha_p_cyc(1)*d-0.1*...
        Alpha_p_cyc(1)*d^2);
    Su_p_s=f_p*F_p_cyc(2)*exp(-Alpha_p_cyc(2)*d-0.1*...
        Alpha_p_cyc(2)*d^2);
    Su_p_g2m=f_p*F_p_cyc(2)*exp(-Alpha_p_cyc(3)*d-0.1*...
        Alpha_p_cyc(3)*d^2);
    Su_i_g1=f_i*exp(-alpha_i*d-beta_i*d^2);
    Su_h_g1=f_h*exp(-alpha_h*d-beta_h*d^2);

    sf=[Su_p_g1;Su_p_s;Su_p_g2m;Su_i_g1;Su_h_g1];
    SF=[SF sf];
    Alpha_eff=[Alpha_eff alpha_p_eff];
    OERI_eff=[OERI_eff oer_i_eff];
    OERH_eff=[OERH_eff oer_h_eff];

    step=step+1;
    waitbar(step/length(fx_in));
end
close(wb);
```

```
        %%%%%%%%%%%%%%%%%%%%%%%%%%%%%%%%%%%%%%%%%%%%%%%%%%%%%%%%%%%%%%%%%%%%%%%
        subplot(2,2,1,'parent',ha);
        semilogy(fx_in,SF(1,:),'m:',fx_in,SF(2,:),'c:',fx_in,SF(3,:),...
            'y:',fx_in,sum(SF(1:3,:)),'r',fx_in,SF(4,:),'b',...
            fx_in,SF(5,:),'g',fx_in,sum(SF),'k','LineWidth', 1.5);
        ylim([0.0000001 1]);
        xlabel('Dose (Gy)','FontSize',11,'fontweight','b');
        ylabel('Survival Fraction','FontSize',11,'fontweight','b');
        legend('G1 in P','S in P','G2/M in P','P','I','H','Total');
        subplot(2,2,2,'parent',ha);
        plot(fx_in,Alpha_eff,'LineWidth', 1.5);
        xlabel('Dose (Gy)','FontSize',11,'fontweight','b');
        ylabel('\alpha of P (Gy^{-1})','FontSize',11,'fontweight','b');
        subplot(2,2,3,'parent',ha);
        plot(fx_in,OERI_eff,'LineWidth', 1.5);
        xlabel('Dose (Gy)','FontSize',11,'fontweight','b');
        ylabel('OER of I','FontSize',11,'fontweight','b');
        subplot(2,2,4,'parent',ha);
        plot(fx_in,OERH_eff,'LineWidth', 1.5);
        xlabel('Dose (Gy)','FontSize',11,'fontweight','b');
        ylabel('OER of H','FontSize',11,'fontweight','b');
        %%%%%%%%%%%%%%%%%%%%%%%%%%%%%%%%%%%%%%%%%%%%%%%%%%%%%%%%%%%%%%%%%%%%%%%
        t_cal=toc;
        set(ht_cal_value,'String',num2str(t_cal,'%5.1f'));
        %%%%%%%%%%%%%%%%%%%%%%%%%%%%%%%%%%%%%%%%%%%%%%%%%%%%%%%%%%%%%%%%%%%%%%%


    case 9 %Example for estimating model predicted EQD2%
        clf=clf_in; gf=gf_in;
        % run the sub-routine for a specific CLF and GF
        run SubRoutine/SR_initial_distribution;
        % save the the number of cell into matrix
        f_p=comp_size(1)/sum(comp_size);
        f_i=comp_size(2)/sum(comp_size);
        f_h=comp_size(3)/sum(comp_size);
        for d=fx_in
            Treat_day=schedule_in;

            f=@(alpha_s)F_p_cyc(1)*exp(-Alpha_ratio_p_cyc(1)*alpha_s*2-...
                0.1*Alpha_ratio_p_cyc(1)*alpha_s*4)+F_p_cyc(2)*...
                exp(-alpha_s*2-0.1*alpha_s*4)+F_p_cyc(3)*...
                exp(-Alpha_ratio_p_cyc(2)*alpha_s*2-0.1*...
                Alpha_ratio_p_cyc(2)*alpha_s*4)-exp(-alpha_p*2-0.1*...
                alpha_p*4);

            Alpha_p_cyc(2)=fzero(f,0.3);
            Alpha_p_cyc(1)=Alpha_p_cyc(2)*Alpha_ratio_p_cyc(1);
            Alpha_p_cyc(3)=Alpha_p_cyc(2)*Alpha_ratio_p_cyc(2);

            Su_p=F_p_cyc(1)*exp(-Alpha_p_cyc(1)*d-0.1*Alpha_p_cyc(1)*d^2)...
                +F_p_cyc(2)*exp(-Alpha_p_cyc(2)*d-0.1*Alpha_p_cyc(2)*d^2)...
                +F_p_cyc(3)*exp(-Alpha_p_cyc(3)*d-0.1*Alpha_p_cyc(3)*d^2);
            alpha_p_eff=-log(Su_p)/(d*(1+0.1*d));
            beta_p_eff=0.1*alpha_p_eff;

            Su_i_2gy=exp(-alpha_p/oer_i*2-0.1*alpha_p/(oer_i^2)*2^2);
            oer_i_g1=(-(Alpha_p_cyc(1)*2)-sqrt((Alpha_p_cyc(1)*2)^2-...
                4*log(Su_i_2gy)*0.1*Alpha_p_cyc(1)*2^2))/(2*log(Su_i_2gy));
            Su_h_2gy=exp(-alpha_p/oer_h*2-0.1*alpha_p/(oer_h^2)*2^2);
            oer_h_g1=(-(Alpha_p_cyc(1)*2)-sqrt((Alpha_p_cyc(1)*2)^2-...
                4*log(Su_h_2gy)*0.1*Alpha_p_cyc(1)*2^2))/(2*log(Su_h_2gy));
            alpha_i=Alpha_p_cyc(1)/oer_i_g1;
            beta_i=0.1*Alpha_p_cyc(1)/(oer_i_g1^2);
```

```
    alpha_h=Alpha_p_cyc(1)/oer_h_g1;
    beta_h=0.1*Alpha_p_cyc(1)/(oer_h_g1^2);

    alpha_p=alpha_p_eff;
    beta_p=beta_p_eff;

    % run the sub-routine for a specific CLF and GF
    run SubRoutine/SR_RT_sbrt;

    s_sbrt=cell_dist(1)+cell_dist(3)+cell_dist(5);
    sf_sbrt=s_sbrt/sum(comp_size);
    ntd2=length(Treat_day)*d*(1+d/10)/1.2;
    d_sbrt=d;
    n_frac_sbrt=length(Treat_day);
    duration_sbrt=max(Treat_day);
    t_sbrt=t;
    step=step+1;
    waitbar(step/2)

    % for EQD2 calculation
    d=2;
    alpha_p=0.35;       beta_p=0.035;
    alpha_i=0.35/2;     beta_i=0.035/(2^2);
    alpha_h=0.35/1.37;  beta_h=0.035/(1.37^2);

    run SubRoutine/SR_RT_eqd2

    s_eqd2=cell_dist(1)+cell_dist(3)+cell_dist(5);
    sf_eqd2=s_eqd2/sum(comp_size);
    eqd2=j*d;
    step=step+1;
    waitbar(step/2);
end
close(wb);


%%%%%%%%%%%%%%%%%%%%%%%%%%%%%%%%%%%%%%%%%%%%%%%%%%%%%%%%%%%%%%%%%%%%%%%%%%%%
time_sbrt=delta_t:delta_t:round(t_sbrt*96)/96;
time=delta_t:delta_t:round(t*96)/96;

if tcp_goal~='-'
    cum_cell_dist_sbrt=cum_cell_dist_sbrt*tumor_size*1000/v_t;
    cum_cell_dist=cum_cell_dist*tumor_size*1000/v_t;
    comp_size(1)=comp_size(1)*tumor_size*1000/v_t;
    comp_size(2)=comp_size(2)*tumor_size*1000/v_t;
    comp_size(3)=comp_size(3)*tumor_size*1000/v_t;
end
    subplot(2,2,1,'parent',ha);
    bar(1:3,[comp_size(1),comp_size(2),comp_size(3)]);
    xlabel('Compartment (1=P, 2=I and 3=H)','FontSize',11,...
        'fontweight','b');
    ylabel('Initial number of cells','FontSize',11,...
        'fontweight','b');
    subplot(2,2,3,'parent',ha);
    semilogy(time_sbrt,sum(cum_cell_dist_sbrt([1 3 5],:)),'r',...
        time_sbrt,sum(cum_cell_dist_sbrt([3 5],:)),'b',...
        time_sbrt,cum_cell_dist_sbrt(5,:),'g');
    xlim([0 ceil(t_sbrt)]);
    ylim([0.1 2*max(sum(cum_cell_dist_sbrt))]);
    xlabel('Time (Day)','FontSize',11,'fontweight','b');
    ylabel('Number of viable cells','FontSize',11,'fontweight','b');
    text(t_sbrt*0.6,0.5*(sum(comp_size)),...
        ['SF = ',num2str(sf_sbrt)],'FontSize',11,'fontweight','b');
```

```
        text(t_sbrt*0.5,0.05*(sum(comp_size)),...
            [num2str(d_sbrt),'Gy X ',num2str(n_frac_sbrt),'fx  in ',...
            num2str(duration_sbrt),' days'],'FontSize',11,...
            'fontweight','b');
        text(t_sbrt*0.6,0.005*(sum(comp_size)),...
            ['NTD2 = ',num2str(ntd2),' Gy'],'FontSize',11,...
            'fontweight','b');
        subplot(2,2,4,'parent',ha);
        semilogy(time,sum(cum_cell_dist([1 3 5],:)),'r',...
            time,sum(cum_cell_dist([3 5],:)),'b',...
            time,cum_cell_dist(5,:),'g');
        xlim([0 ceil(t)]);
        ylim([0.1 2*max(sum(cum_cell_dist))]);
        xlabel('Time (Day)','FontSize',11,'fontweight','b');
        ylabel('Number of viable cells','FontSize',11,'fontweight','b');
        text(t*0.5,0.5*(sum(comp_size)),...
            ['SF = ',num2str(sf_eqd2)],'FontSize',11,'fontweight','b');
        text(t*0.5,0.05*(sum(comp_size)),...
            ['EQD2 = ',num2str(eqd2),' Gy'],'FontSize',11,...
            'fontweight','b');
    %%%%%%%%%%%%%%%%%%%%%%%%%%%%%%%%%%%%%%%%%%%%%%%%%%%%%%%%%%%%%%%%%%%%%%%
    t_cal=toc;
    set(ht_cal_value,'String',num2str(t_cal,'%5.1f'));
    %%%%%%%%%%%%%%%%%%%%%%%%%%%%%%%%%%%%%%%%%%%%%%%%%%%%%%%%%%%%%%%%%%%%%%%


case 10 %Model predicted EQD2 vs. BED2%
    NTD2=[]; EQD2=[];
    clf=clf_in; gf=gf_in;
    % run the sub-routine for a specific CLF and GF
    run SubRoutine/SR_initial_distribution;
    % save the the number of cell into matrix
    f_p=comp_size(1)/sum(comp_size);
    f_i=comp_size(2)/sum(comp_size);
    f_h=comp_size(3)/sum(comp_size);
    q=0;for d=fx_in;q=q+1;
        Treat_day=schedule_in;

        f=@(alpha_s)F_p_cyc(1)*exp(-Alpha_ratio_p_cyc(1)*alpha_s*2-...
            0.1*Alpha_ratio_p_cyc(1)*alpha_s*4)+...
        F_p_cyc(2)*exp(-alpha_s*2-0.1*alpha_s*4)+...
        F_p_cyc(3)*exp(-Alpha_ratio_p_cyc(2)*alpha_s*2-...
        0.1*Alpha_ratio_p_cyc(2)*alpha_s*4)-...
        exp(-alpha_p*2-0.1*alpha_p*4);

        Alpha_p_cyc(2)=fzero(f,0.3);
        Alpha_p_cyc(1)=Alpha_p_cyc(2)*Alpha_ratio_p_cyc(1);
        Alpha_p_cyc(3)=Alpha_p_cyc(2)*Alpha_ratio_p_cyc(2);

        Su_p=F_p_cyc(1)*exp(-Alpha_p_cyc(1)*d-0.1*Alpha_p_cyc(1)*d^2)...
            +F_p_cyc(2)*exp(-Alpha_p_cyc(2)*d-0.1*Alpha_p_cyc(2)*d^2)...
            +F_p_cyc(3)*exp(-Alpha_p_cyc(3)*d-0.1*Alpha_p_cyc(3)*d^2);
        alpha_p_eff=-log(Su_p)/(d*(1+0.1*d));
        beta_p_eff=0.1*alpha_p_eff;

        Su_i_2gy=exp(-alpha_p/oer_i*2-0.1*alpha_p/(oer_i^2)*2^2);
        oer_i_g1=(-(Alpha_p_cyc(1)*2)-sqrt((Alpha_p_cyc(1)*2)^2-...
            4*log(Su_i_2gy)*0.1*Alpha_p_cyc(1)*2^2))/(2*log(Su_i_2gy));
        Su_h_2gy=exp(-alpha_p/oer_h*2-0.1*alpha_p/(oer_h^2)*2^2);
        oer_h_g1=(-(Alpha_p_cyc(1)*2)-sqrt((Alpha_p_cyc(1)*2)^2-...
            4*log(Su_h_2gy)*0.1*Alpha_p_cyc(1)*2^2))/(2*log(Su_h_2gy));
        alpha_i=Alpha_p_cyc(1)/oer_i_g1;
        beta_i=0.1*Alpha_p_cyc(1)/(oer_i_g1^2);
```

```
        alpha_h=Alpha_p_cyc(1)/oer_h_g1;
        beta_h=0.1*Alpha_p_cyc(1)/(oer_h_g1^2);

        alpha_p=alpha_p_eff;
        beta_p=beta_p_eff;

        % run the sub-routine for a specific CLF and GF
        run SubRoutine/SR_RT_sbrt;

        s_sbrt=cell_dist(1)+cell_dist(3)+cell_dist(5);
        n_frac_sbrt=length(Treat_day);
        duration_sbrt=max(Treat_day);
        ntd2=length(Treat_day)*d*(1+d/10)/1.2;
        NTD2=[NTD2 ntd2];


        % for EQD2 calculation
        d=2;
        alpha_p=0.35;       beta_p=0.035;
        alpha_i=0.35/2;     beta_i=0.035/(2^2);
        alpha_h=0.35/1.37;  beta_h=0.035/(1.37^2);

        run SubRoutine/SR_RT_eqd2

        eqd2=j*d;
        EQD2=[EQD2 eqd2];
        step=step+1;
        waitbar(step/length(fx_in));
    end
    close(wb);

    %%%%%%%%%%%%%%%%%%%%%%%%%%%%%%%%%%%%%%%%%%%%%%%%%%%%%%%%%%%%%%%%%%%%%%%
    haxes = axes('parent',ha,'Units','Pixels',...
        'Position',[55,50,640,430]);
    plot(haxes,NTD2,EQD2,'-r^',0:0.1:max(NTD2),0:0.1:max(NTD2),...
        'k',0:0.1:max(NTD2),0:0.05:(max(NTD2)/2),'k');
    xlabel('NTD2 (Gy)','FontSize',11,'fontweight','b');
    ylabel('Model Predicted EQD2 (Gy)','FontSize',11,'fontweight','b');
    xlim([0 max(NTD2)]); ylim([0 max(NTD2)]);
    text(20,0.8*max(NTD2),[num2str(n_frac_sbrt),...
        ' fx in ',num2str(duration_sbrt),' days'],'FontSize',14,...
        'fontweight','b');
    %%%%%%%%%%%%%%%%%%%%%%%%%%%%%%%%%%%%%%%%%%%%%%%%%%%%%%%%%%%%%%%%%%%%%%%
    t_cal=toc;
    set(ht_cal_value,'String',num2str(t_cal,'%5.1f'));
    %%%%%%%%%%%%%%%%%%%%%%%%%%%%%%%%%%%%%%%%%%%%%%%%%%%%%%%%%%%%%%%%%%%%%%%




case 11 %11. TD50 vs. FDG uptake%

    fdg_via=[];
    fdg_pro=[];
    fdg_hyp=[];
    fdg_mix=[];
    fdg_idst=[];
    td50=[];

    Via=zeros(min(length(gf_in),length(clf_in)));
    Pro=zeros(min(length(gf_in),length(clf_in)));
    Hyp=zeros(min(length(gf_in),length(clf_in)));
    Mix=zeros(min(length(gf_in),length(clf_in)));
```

```
Idst=zeros(min(length(gf_in),length(clf_in)));
TD50=zeros(min(length(gf_in),length(clf_in)));

d=fx_in;
k=0;for clf=clf_in;k=k+1;
    l=0;for gf=0.01:0.01:1/(2+clf);l=l+1;
        run SubRoutine/SR_initial_distribution;

        fdg_via=[fdg_via 0.5*comp_size(1)+0.5*comp_size(2)];
        fdg_pro=[fdg_pro 0.75*comp_size(1)+0.25*comp_size(2)];
        fdg_hyp=[fdg_hyp 0.25*comp_size(1)+0.75*comp_size(2)];
        fdg_mix=[fdg_mix 2/9*comp_size(1)+5/9*comp_size(2)+...
            2/9*comp_size(3)];
        fdg_idst=[fdg_idst comp_size(2)];

        no_pro=0;
        alpha_i=alpha_p/oer_i;beta_i=beta_p/(oer_i)^2;
        alpha_h=alpha_p/oer_h;beta_h=beta_p/(oer_h)^2;
        run SubRoutine/SR_RT;
        td50=[td50 j*d];


        Via(k,l)=0.5*comp_size(1)+0.5*comp_size(2);
        Pro(k,l)=0.75*comp_size(1)+0.25*comp_size(2);
        Hyp(k,l)=0.25*comp_size(1)+0.75*comp_size(2);
        Mix(k,l)=2/9*comp_size(1)+5/9*comp_size(2)+2/9*comp_size(3);
        Idst(k,l)=comp_size(2);
        TD50(k,l)=j*d;

        step=step+1;
        waitbar(step/(length(gf_in)*length(clf_in)));
    end
end
close(wb);

%%%%%%%%%%%%%%%%%%%%%%%%%%%%%%%%%%%%%%%%%%%%%%%%%%%%%%%%%%%%%%%%%%%%%%%
nor_fdg_via=fdg_via/max((fdg_via));
fit_via=polyfit(td50,nor_fdg_via,1);
line_via=polyval(fit_via,td50);
r_via=corrcoef(td50,nor_fdg_via);
R_sq_via=r_via(1,2)^2;

nor_fdg_pro=fdg_pro/max((fdg_pro));
fit_pro=polyfit(td50,nor_fdg_pro,1);
line_pro=polyval(fit_pro,td50);
r_pro=corrcoef(td50,nor_fdg_pro);
R_sq_pro=r_pro(1,2)^2;

nor_fdg_hyp=fdg_hyp/max((fdg_hyp));
fit_hyp=polyfit(td50,nor_fdg_hyp,1);
line_hyp=polyval(fit_hyp,td50);
r_hyp=corrcoef(td50,nor_fdg_hyp);
R_sq_hyp=r_hyp(1,2)^2;

nor_fdg_mix=fdg_mix/max((fdg_mix));
fit_mix=polyfit(td50,nor_fdg_mix,1);
line_mix=polyval(fit_mix,td50);
r_mix=corrcoef(td50,nor_fdg_mix);
R_sq_mix=r_mix(1,2)^2;

nor_fdg_idst=fdg_idst/max((fdg_idst));
fit_idst=polyfit(td50,nor_fdg_idst,1);
line_idst=polyval(fit_idst,td50);
```

```
r_idst=corrcoef(td50,nor_fdg_idst);
R_sq_idst=r_idst(1,2)^2;


subplot(2,2,1,'parent',ha);
plot(nor_fdg_via,td50,'o',line_via,td50,'r-');
title('Viable cells ','FontSize',12,'FontWeight','bold',...
    'color','b');
xlabel('Normalized FDG uptake ','FontSize',11,'fontweight','b');
ylabel('TD50 (Gy) ','FontSize',11,'fontweight','b');
xlim([min((nor_fdg_via))-0.02 1.02]);
text((0.9*min((nor_fdg_via))+0.1),(max(td50)),...
    ['R = ',num2str(r_via(1,2))],'FontSize',11,'Color','r',...
    'fontweight','b');
text((0.9*min((nor_fdg_via))+0.1),(max(td50))*0.97,...
    ['R^2 = ',num2str(R_sq_via)],'FontSize',11,'Color','r',...
    'fontweight','b');

subplot(2,2,2,'parent',ha);
plot(nor_fdg_pro,td50,'o',line_pro,td50,'r-');
title('Proliferation ','FontSize',12,'FontWeight','bold',...
    'color','b');
xlabel('Normalized FDG uptake ','FontSize',11,'fontweight','b');
ylabel('TD50 (Gy) ','FontSize',11,'fontweight','b');
xlim([min((nor_fdg_pro))-0.02 1.02]);
text((0.5*min((nor_fdg_pro))+0.5),max((td50)),...
    ['R = ',num2str(r_pro(1,2))],'FontSize',11,'Color','r',...
    'fontweight','b');
text((0.5*min((nor_fdg_pro))+0.5),max((td50))*0.97,...
    ['R^2 = ',num2str(R_sq_pro)],'FontSize',11,'Color','r',...
    'fontweight','b');

subplot(2,2,3,'parent',ha);
plot(nor_fdg_hyp,td50,'o',line_hyp,td50,'r-');
title('Hypoxia ','FontSize',12,'FontWeight','bold','color','b');
xlabel('Normalized FDG uptake ','FontSize',11,'fontweight','b');
ylabel('TD50 (Gy) ','FontSize',11,'fontweight','b');
xlim([min((nor_fdg_hyp))-0.02 1.02]);
text((0.9*min((nor_fdg_hyp))+0.1),max((td50)),...
    ['R = ',num2str(r_hyp(1,2))],'FontSize',11,'Color','r',...
    'fontweight','b');
text((0.9*min((nor_fdg_hyp))+0.1),max((td50))*0.97,...
    ['R^2 = ',num2str(R_sq_hyp)],'FontSize',11,'Color','r',...
    'fontweight','b');

subplot(2,2,4,'parent',ha);
plot(nor_fdg_mix,td50,'o',line_mix,td50,'r-');
title('hypoxia ','FontSize',12,'FontWeight','bold','color','b');
xlabel('Normalized FDG uptake ','FontSize',11,'fontweight','b');
ylabel('TD50 (Gy) ','FontSize',11,'fontweight','b');
xlim([min((nor_fdg_mix))-0.02 1.02]);
text((0.9*min((nor_fdg_mix))+0.1),max((td50)),...
    ['R = ',num2str(r_mix(1,2))],'FontSize',11,'Color','r',...
    'fontweight','b');
text((0.9*min((nor_fdg_mix))+0.1),max((td50))*0.97,...
    ['R^2 = ',num2str(R_sq_mix)],'FontSize',11,'Color','r',...
    'fontweight','b');

%%%%%%%%%%%%%%%%%%%%%%%%%%%%%%%%%%%%%%%%%%%%%%%%%%%%%%%%%%%%%%%%%%%%%%%%%%%%
t_cal=toc;
set(ht_cal_value,'String',num2str(t_cal,'%5.1f'));
%%%%%%%%%%%%%%%%%%%%%%%%%%%%%%%%%%%%%%%%%%%%%%%%%%%%%%%%%%%%%%%%%%%%%%%%%%%%
```

```
    end
end



%% File Export

file_name='';

color_8=[0.7 0.7 0.7];
hexport_title = uicontrol('Style','text','String','File name',...
    'FontSize',10,'Position',[865,53,180,18],...
    'BackgroundColor',color_7);
hexport_value = uicontrol('Style','edit','String',file_name,...
    'Position',[865,28,180,25],'FontSize',9,'BackgroundColor','white',...
    'Callback',{@export_value_Callback});
        function export_value_Callback(source,eventdata)
            file_name = get(source, 'String');
        end
hexport = uicontrol('Style','pushbutton','String','Export output',...
    'FontSize',10,'FontWeight','bold','Position',[1055,30,120,40],...
    'ForegroundColor',[0 0.3 1],'Callback',{@exportbutton_Callback});


function exportbutton_Callback(source,eventdata)
    str = get(ha_title, 'String');
    savefilename=strcat('Output/',num2str(type),'_',file_name,'.txt');
    fid = fopen(savefilename,'w');
    fprintf(fid,'    %s\n\n',str);
    fprintf(fid,'Computing time [sec]: %5.2f\n\n',t_cal);
    fprintf(fid,'Proliferation fraction of P compartment: %5.2f\n',...
        f_p_pro_in);
    fprintf(fid,'Cell death half time of H compartment [day]: %5.2f\n',...
        ht_loss);
    fprintf(fid,'Cell density [#/(mm^3)]: %7.2e\n',rho_t);
    fprintf(fid,'Voxel size [mm^3]: %5.2f\n',v_t);
    fprintf(fid,'Stem Cell Fraction: %5.2f\n',f_s);
    fprintf(fid,'Cell cycle time [day]: %5.2f\n',t_c);
    fprintf(fid,'Calculation time interval [min]: %5.2f\n',d_t);
    if type ~= 1 && type ~= 8
        fprintf(fid,'Mitotic death rate: %4.2f\n',k_m);
        fprintf(fid,'Lysis time [day]: %4.2f\n',ht_lys);
        fprintf(fid,'OER of I: %4.2f\n',oer_i);
        fprintf(fid,'OER of H: %4.2f\n',oer_h);
        if tumor_size~='-'
            fprintf(fid,'Simulated tumor size [cc]: %6.1f\n',tumor_size);
            fprintf(fid,'TCP goal: %7.5f\n',tcp_goal);
        end
        fprintf(fid,'VCP goal: %7.5f\n',vcp_goal);
    end


    switch type


        case 1 %Initial Distribution for various CLF and GF%
            for j=1:1:4;
                data = [gf_in; IC(:,:,j)'];
                fprintf(fid,'\n\nCLF = %3.1f\n\n',clf_in(j));
                fprintf(fid,' GF        P             I             H\n');
                fprintf(fid,'%4.2f  %12.6e  %12.6e  %12.6e\n',data);
            end
```

```
case 2 %Example plots for a specific GF,CLF and fx%
    fprintf(fid,'Cell loss factor: %4.2f\n',clf_in);
    fprintf(fid,'Growth fraction: %4.2f\n',gf_in);
    fprintf(fid,'Fraction size [Gy]: %4.2f\n',fx_in);
    fprintf(fid,'\n\nInitial \n\n');
    fprintf(fid,'     P            I            H\n');
    fprintf(fid,'%12.6e  %12.6e  %12.6e\n',...
        [comp_size(1) comp_size(2) comp_size(3)]);
    fprintf(fid,'\n\nEach compartment\n\n');
    data_each=[time;cum_cell_dist(1:7,:)];
    fprintf(fid,' time        Pv            Pd            Iv
     Id           Hv           Hd          Lysis\n');
    fprintf(fid,'%6.2f  %12.6e  %12.6e  %12.6e  %12.6e  %12.6e  %12.6e
     %12.6e\n',data_each);
    fprintf(fid,'\n\nCumulative\n\n');
    data_cum=[time;sum(cum_cell_dist(1:6,:));...
        sum(cum_cell_dist(2:6,:));sum(cum_cell_dist(3:6,:));...
        sum(cum_cell_dist(4:6,:));sum(cum_cell_dist(5:6,:));...
        cum_cell_dist(6,:)];
    fprintf(fid,' time        All         All-Pv         All-P
     All-P-Iv      All-P-I  All-P-I-Hv(Hd)\n');
    fprintf(fid,'%6.2f  %12.6e  %12.6e  %12.6e  %12.6e  %12.6e
     %12.6e\n',data_cum);
    fprintf(fid,'\n\nViable cumulative\n\n');
    data_vcum=[time;sum(cum_cell_dist([1 3 5],:));...
        sum(cum_cell_dist([3 5],:));cum_cell_dist(5,:)];
    fprintf(fid,' time       V_All       V_All-Pv  V_All-Pv-Iv(Hv)\n');
    fprintf(fid,'%6.2f  %12.6e  %12.6e  %12.6e\n',data_vcum);


case 3 %TD50 vs. GF for various fx%
    fprintf(fid,'Cell loss factor: %4.2f\n',clf_in);
    fprintf(fid,'Growth fraction: %4.2f ~ %4.2f\n',...
        gf_in(size(gf_in)));
    for j=1:1:6;
        data = [gf_in; TD50(:,j)'];
        fprintf(fid,'\n\nFx = %3.1f\n\n',fx_in(j));
        fprintf(fid,' GF   TD50\n');
        fprintf(fid,'%4.2f  %6.2f\n',data);
    end


case 4 %Reoxygenation time vs. GF for various fx%
    fprintf(fid,'Cell loss factor: %4.2f\n',clf_in);
    fprintf(fid,'Growth fraction: %4.2f ~ %4.2f\n',...
        gf_in(size(gf_in)));
    for j=1:1:length(fx_in);
        data = [gf_in; Reox_time(:,j)'; Reox_time2(:,j)'];
        fprintf(fid,'\n\nFx = %3.1f\n\n',fx_in(j));
        fprintf(fid,' GF   Reox_time  Reox_time2\n');
        fprintf(fid,'%4.2f   %6.2f    %6.2f\n',data);
    end


case 5 %TD50 vs. Treatment duration for various GF%
    fprintf(fid,'Cell loss factor: %4.2f\n',clf_in);
    fprintf(fid,'Fraction size: varies');
    A=[];
    for day=1:max(max(Treat_duration))
        for k=1:length(gf_in)
            for l=1:vec_leng(k)
                if Treat_duration(k,l)==day
```

```
                    A(k,day)=TD50(k,l);
                end
            end
        end
    end
    data = [1:max(max(Treat_duration)); A];
    fprintf(fid,'\n\nDuration     GF=0.01     GF=0.05     GF=0.10
     GF=0.20     GF=0.30\n');
    fprintf(fid,'%8.0f     %7.2f     %7.2f     %7.2f     %7.2f
     %7.2f\n',data);
    fprintf(fid,'\n\nAsymtotic line slope = %5.3f \n',slope);


case 6 %Tumor size vs. Time for various GF%
    fprintf(fid,'Cell loss factor: %4.2f\n',clf_in);
    fprintf(fid,'Fraction size [Gy]: %4.2f\n',fx_in);
    for j=1:1:5;
        data = [delta_t:delta_t:round(T_end(j)); ...
            Total_cell(j,1:round(T_end(j))/delta_t)];
        fprintf(fid,'\n\nGF = %4.2f\n\n',gf_in(j));
        fprintf(fid,'  Time    Total cells\n');
        fprintf(fid,'%7.4f  %12.6e\n',data);
    end


case 7 %Effect of proliferation and hypoxia%
    fprintf(fid,'Cell loss factor: %4.2f\n',clf_in);
    fprintf(fid,'Growth fraction: %4.2f ~ %4.2f\n',...
        gf_in(size(gf_in)))
    fprintf(fid,'Fraction size [Gy]: %4.2f\n',fx_in);
    data = [gf_in; TD50(1,:); TD50(2,:); TD50(3,:); TD50(4,:)];
    fprintf(fid,'\n GF   Neither  Hypoxia  Prolifer   Both\n');
    fprintf(fid,'%4.2f  %7.2f  %7.2f  %7.2f  %7.2f\n',data);


case 8 %Cell cycle dependent SF, alpha & OERs%
    fprintf(fid,'\n\nCell loss factor: %4.2f\n',clf_in);
    fprintf(fid,'Growth fraction: %4.2f\n',gf_in);
    fprintf(fid,'Fraction size: %4.2f ~ %4.2f\n',...
        fx_in(size(fx_in)));
    fprintf(fid,'Fraction of cells in each cycle in P\n');
    fprintf(fid,'  G1: %4.2f,  S: %4.2f,  G2/M: %4.2f\n',F_p_cyc);
    fprintf(fid,'Alpha ratio with respect to S phase\n');
    fprintf(fid,'  G1: %3.1f,  G2/M: %3.1f\n',Alpha_ratio_p_cyc);
    fprintf(fid,'\n\n   Dose    SF_P_G1    SF_P_S  SF_P_G2M  SF_P_tot
     SF_I_tot  SF_H_tot   Total\n');
    data=[fx_in;SF(1,:);SF(2,:);SF(3,:);sum(SF(1:3,:));SF(4,:);...
        SF(5,:);sum(SF)];
    fprintf(fid,'%8.5f %9.2e %9.2e %9.2e %9.2e %9.2e %9.2e
     %9.2e\n',data);
    fprintf(fid,'\n\n  Dose    Alpha of P\n');
    data=[fx_in; Alpha_eff];
    fprintf(fid,'%8.5f  %8.5f\n',data);
    fprintf(fid,'\n\n  Dose    OER of I\n');
    fprintf(fid,'%8.5f  %8.5f\n',[fx_in;OERI_eff]);
    fprintf(fid,'\n\n  Dose    OER of H\n');
    fprintf(fid,'%8.5f  %8.5f\n',[fx_in;OERH_eff]);


case 9 %Example for estimating model predicted EQD2%
    fprintf(fid,'Cell loss factor: %4.2f\n',clf_in);
    fprintf(fid,'Growth fraction: %4.2f\n',gf_in);
    fprintf(fid,'Fraction size [Gy]: %4.2f\n',fx_in);
```

```
        fprintf(fid,'Fraction of cells in each cycle in P\n');
        fprintf(fid,'  G1: %4.2f,  S: %4.2f,  G2/M: %4.2f\n',F_p_cyc);
        fprintf(fid,'Alpha ratio with respect to S phase\n');
        fprintf(fid,'  G1: %3.1f,  G2/M: %3.1f\n',Alpha_ratio_p_cyc);
        fprintf(fid,'\n\nInitial \n\n');
        fprintf(fid,'     P            I            H\n');
        fprintf(fid,'%12.6e  %12.6e  %12.6e\n',...
            [comp_size(1) comp_size(2) comp_size(3)]);
        fprintf(fid,'\n\nSBRT viable cumulative\n\n');
        data_vcum_sbrt=[time_sbrt;sum(cum_cell_dist_sbrt([1 3 5],:));...
            sum(cum_cell_dist_sbrt([3 5],:));cum_cell_dist_sbrt(5,:)];
        fprintf(fid,' time       V_All       V_All-Pv  V_All-Pv-Iv(Hv)\n');
        fprintf(fid,'%6.2f  %12.6e  %12.6e  %12.6e\n',data_vcum_sbrt);
        fprintf(fid,'\nSF = %9.3e\n',sf_sbrt);
        fprintf(fid,'NTD2 = %6.2f\n',ntd2);


        fprintf(fid,'\n\n2Gy/fx viable cumulative\n\n');
        data_vcum=[time;sum(cum_cell_dist([1 3 5],:));...
            sum(cum_cell_dist([3 5],:));cum_cell_dist(5,:)];
        fprintf(fid,' time       V_All       V_All-Pv  V_All-Pv-Iv(Hv)\n');
        fprintf(fid,'%6.2f  %12.6e  %12.6e  %12.6e\n',data_vcum);
        fprintf(fid,'\nSF = %9.3e\n',sf_eqd2);
        fprintf(fid,'EQD2 = %6.2f\n',eqd2);


    case 10 %Model predicted EQD2 vs. BED2%
        fprintf(fid,'Cell loss factor: %4.2f\n',clf_in);
        fprintf(fid,'Growth fraction: %4.2f\n',gf_in);
        fprintf(fid,'Fraction size: %4.2f ~ %4.2f\n',...
            fx_in(size(fx_in)));
        fprintf(fid,'Fraction of cells in each cycle in P\n');
        fprintf(fid,'  G1: %4.2f,  S: %4.2f,  G2/M: %4.2f\n',F_p_cyc);
        fprintf(fid,'Alpha ratio with respect to S phase\n');
        fprintf(fid,'  G1: %3.1f,  G2/M: %3.1f\n',Alpha_ratio_p_cyc);
        data=[NTD2;EQD2];
        fprintf(fid,'\n NTD2(Gy)  EQD2(Gy)\n');
        fprintf(fid,'  %6.2f    %6.2f\n',data);


    case 11 %TD50 vs. FDG uptake%
        fprintf(fid,'Cell loss factor: %4.2f ~ %4.2f\n',...
            clf_in(size(clf_in)));
        fprintf(fid,'Growth fraction: %4.2f ~ %4.2f\n',...
            gf_in(size(gf_in)));
        fprintf(fid,'Fraction size: %4.2f\n',fx_in);
        data=[td50;nor_fdg_via;nor_fdg_pro;nor_fdg_hyp;nor_fdg_mix;...
            nor_fdg_idst];
        fprintf(fid,'\nTD50(Gy)              Nor. FDG uptake  \n');
        fprintf(fid,'            viable    prolif   hypoxia     mixed    I
         comp\n');
        fprintf(fid,'  %6.2f    %6.4f    %6.4f    %6.4f    %6.4f
         %6.4f\n',data);
        fprintf(fid,'\nVia: R = %6.4f & R^2= %6.4f\n',...
            r_via(1,2),R_sq_via);
        fprintf(fid,'\nPro: R = %6.4f & R^2= %6.4f\n',...
            r_pro(1,2),R_sq_pro);
        fprintf(fid,'\nHyp: R = %6.4f & R^2= %6.4f\n',...
            r_hyp(1,2),R_sq_hyp);
        fprintf(fid,'\nMix: R = %6.4f & R^2= %6.4f\n',...
            r_mix(1,2),R_sq_mix);
        fprintf(fid,'\n  I: R = %6.4f & R^2= %6.4f\n',...
            r_idst(1,2),R_sq_idst);
```

```
    end

    fclose(fid);

end
end
```

A.5.2. Sub-routine for initial distribution (SR_initial_distribution.m)

```
%<<<<<<<<<<<<<<<<<<< for the initial st-st distribution >>>>>>>>>>>>>>>>>>%

% variables for the initial distribution
f_p_pro=f_p_pro_in;

comp_size(1)=gf/f_p_pro*n_t;
comp_size(2)=(1-gf*(1/f_p_pro_in+clf*ht_loss/t_c))*n_t;
comp_size(3)=clf*gf*ht_loss/t_c*n_t;

%<<<<<<<<<<<<<<<<<<<<<<<<<<<<<<<<<<<<<<<<<<<<<<<<<<<<<<<<<<<<<<<<<<<<<<<%
```

A.5.3. Sub-routine for fractionated radiation therapy (SR_RT.m)

```
%<<<<<<<<<<<<<<<<< RT fractional dose until TD50 achieved >>>>>>>>>>>>>>>>%

% Assign proliferating fraction to the initial value

f_p_pro=f_p_pro_in;

% Cell distribution in each compartment
% (1:Pv, 2:Pd, 3:Iv, 4:Id, 5:Hv, 6:Hd, 7:lysis)
% Initially all compartments are fully filled with viable cells
% "comp_size" is the size of each compartment (1:P, 2:I, 3:H)

cell_dist=[];
cell_dist(1)=comp_size(1);
cell_dist(2)=0;
cell_dist(3)=comp_size(2);
cell_dist(4)=0;
cell_dist(5)=comp_size(3);
cell_dist(6)=0;
cell_dist(7)=0;

% variables (t:time(day), j:# of fraction, add_time:additional time for
%           weekend break, cum_cell_dist: cumulative cell distribution for
%           each time increment)
t=0;
j=0;
add_time=0;
cum_cell_dist=[];


% Treat until VCP goal is achieved
while exp(-(cell_dist(1)+cell_dist(3)+cell_dist(5))*f_s)<VCP
```

```
% Change in f_p_pro (k_p) as blood supply improves
f_p_pro=1-0.5*(cell_dist(1)+cell_dist(2))/comp_size(1);


% RT fraction
if  t>(t_start+j+add_time-delta_t/2) && t<(t_start+j+add_time+delta_t/2)

    cell_dist(2)=cell_dist(2)+cell_dist(1)*(1-exp(-alpha_p*d-beta_p*d^2));
    cell_dist(1)=cell_dist(1)*exp(-alpha_p*d-beta_p*d^2);
    cell_dist(4)=cell_dist(4)+cell_dist(3)*(1-exp(-alpha_i*d-beta_i*d^2));
    cell_dist(3)=cell_dist(3)*exp(-alpha_i*d-beta_i*d^2);
    cell_dist(6)=cell_dist(6)+cell_dist(5)*(1-exp(-alpha_h*d-beta_h*d^2));
    cell_dist(5)=cell_dist(5)*exp(-alpha_h*d-beta_h*d^2);

    j=j+1;

    % Week-end break
    if rem(j,5)==0
        add_time=add_time+2;
    end

end

% Cell Proliferation & Death
if no_pro==0
cell_dist(1)=cell_dist(1)*(2)^(f_p_pro*delta_t/t_c);
end
h_pre=cell_dist(5)+cell_dist(6);
cell_dist(5)=cell_dist(5)*(0.5)^(delta_t/ht_loss);
cell_dist(6)=cell_dist(6)*(0.5)^(delta_t/ht_loss);
p_d_pre=cell_dist(2);
cell_dist(2)=cell_dist(2)*(2)^(f_p_pro*(2*k_m-1)*delta_t/t_c);


% Mitotically dead cell in 1 time step
md=p_d_pre-cell_dist(2)+(h_pre-cell_dist(5)-cell_dist(6));
cell_dist(7)=cell_dist(7)+md;
cell_dist(7)=cell_dist(7)*(0.5)^(delta_t/ht_lys);


% Recompartmentalization of the cell
if cell_dist(1)+cell_dist(2)>=comp_size(1)
    p_ex=(cell_dist(1)+cell_dist(2))-comp_size(1);
    p_ratio=cell_dist(1)/(cell_dist(1)+cell_dist(2));
    cell_dist(1)=comp_size(1)*p_ratio;
    cell_dist(2)=comp_size(1)*(1-p_ratio);
    cell_dist(3)=cell_dist(3)+p_ex*p_ratio;
    cell_dist(4)=cell_dist(4)+p_ex*(1-p_ratio);
else
    if cell_dist(3)+cell_dist(4)>0
        if cell_dist(3)+cell_dist(4)>comp_size(1)-...
                (cell_dist(1)+cell_dist(2))
            p_def=comp_size(1)-(cell_dist(1)+cell_dist(2));
            i_ratio=cell_dist(3)/(cell_dist(3)+cell_dist(4));
            cell_dist(1)=cell_dist(1)+p_def*i_ratio;
            cell_dist(2)=cell_dist(2)+p_def*(1-i_ratio);
            cell_dist(3)=cell_dist(3)-p_def*i_ratio;
            cell_dist(4)=cell_dist(4)-p_def*(1-i_ratio);
        else
            cell_dist(1)=cell_dist(1)+cell_dist(3);
            cell_dist(2)=cell_dist(2)+cell_dist(4);
            cell_dist(3)=0; cell_dist(4)=0;
```

```
                if cell_dist(5)+cell_dist(6)>0
                    if cell_dist(5)+cell_dist(6)>comp_size(1)-...
                            (cell_dist(1)+cell_dist(2))
                        p_def=comp_size(1)-(cell_dist(1)+cell_dist(2));
                        h_ratio=cell_dist(5)/(cell_dist(5)+cell_dist(6));
                        cell_dist(1)=cell_dist(1)+p_def*h_ratio;
                        cell_dist(2)=cell_dist(2)+p_def*(1-h_ratio);
                        cell_dist(5)=cell_dist(5)-p_def*h_ratio;
                        cell_dist(6)=cell_dist(6)-p_def*(1-h_ratio);
                    else
                        cell_dist(1)=cell_dist(1)+cell_dist(5);
                        cell_dist(2)=cell_dist(2)+cell_dist(6);
                        cell_dist(5)=0; cell_dist(6)=0;
                    end
                end
            end
        end
    end
    if cell_dist(3)+cell_dist(4)>=comp_size(2)
        i_ex=(cell_dist(3)+cell_dist(4))-comp_size(2);
        i_ratio=cell_dist(3)/(cell_dist(3)+cell_dist(4));
        cell_dist(3)=comp_size(2)*i_ratio;
        cell_dist(4)=comp_size(2)*(1-i_ratio);
        cell_dist(5)=cell_dist(5)+i_ex*i_ratio;
        cell_dist(6)=cell_dist(6)+i_ex*(1-i_ratio);
    else
        if cell_dist(5)+cell_dist(6)>0
            if cell_dist(5)+cell_dist(6)>comp_size(2)-...
                    (cell_dist(3)+cell_dist(4))
                i_def=comp_size(2)-(cell_dist(3)+cell_dist(4));
                h_ratio=cell_dist(5)/(cell_dist(5)+cell_dist(6));
                cell_dist(3)=cell_dist(3)+i_def*h_ratio;
                cell_dist(4)=cell_dist(4)+i_def*(1-h_ratio);
                cell_dist(5)=cell_dist(5)-i_def*h_ratio;
                cell_dist(6)=cell_dist(6)-i_def*(1-h_ratio);
            else
                cell_dist(3)=cell_dist(3)+cell_dist(5);
                cell_dist(4)=cell_dist(4)+cell_dist(6);
                cell_dist(5)=0; cell_dist(6)=0;
            end
        end
    end

    % time step increase and store the number of cells in each compartment
    t=t+delta_t;
    cum_cell_dist=[cum_cell_dist cell_dist'];
    if type==6
        Total_cell(k,uint16(t/delta_t))=sum(cell_dist);
    end

    if type==5
        if t>150
            cell_dist(1)=0; cell_dist(3)=0; cell_dist(5)=0;
            terminated=1;
        end
    end

end
%<<<<<<<<<<<<<<<<<<<<<<<<<<<<<<<<<<<<<<<<<<<<<<<<<<<<<<<<<<<<<<<<<<<<<<<<<<<<%
```

A.5.4. Sub-routine for SBRT (SR_RT_sbrt.m)

```
%<<<<<<<<<<<<<<<<< RT fractional dose for SBRT schedule >>>>>>>>>>>>>>>>%

% Assign proliferating fraction to the initial value

f_p_pro=f_p_pro_in;

% Cell distribution in each compartment
% (1:Pv, 2:Pd, 3:Iv, 4:Id, 5:Hv, 6:Hd, 7:lysis)
% Initially all compartments are fully filled with viable cells
% "comp_size" is the size of each compartment (1:P, 2:I, 3:H)

cell_dist=[];
cell_dist(1)=comp_size(1);
cell_dist(2)=0;
cell_dist(3)=comp_size(2);
cell_dist(4)=0;
cell_dist(5)=comp_size(3);
cell_dist(6)=0;
cell_dist(7)=0;

% variables (t:time(day), j:# of fraction, add_time:additional time for
%           weekend break, cum_cell_dist: cumulative cell distribution for
%           each time increment)
t=0;
j=0;
cum_cell_dist_sbrt=[];


% Treat for specific SBRT schedule
while t<t_start+(max(Treat_day)-1)+delta_t/2;

    % Change in f_p_pro (k_p) as blood supply improves
    f_p_pro=1-0.5*(cell_dist(1)+cell_dist(2))/comp_size(1);

    % RT fraction
    if  t>(t_start+(Treat_day(j+1)-1)-delta_t/2) &&...
            t<(t_start+(Treat_day(j+1)-1)+delta_t/2)

        cell_dist(2)=cell_dist(2)+cell_dist(1)*(1-exp(-alpha_p*d-beta_p*d^2));
        cell_dist(1)=cell_dist(1)*exp(-alpha_p*d-beta_p*d^2);
        cell_dist(4)=cell_dist(4)+cell_dist(3)*(1-exp(-alpha_i*d-beta_i*d^2));
        cell_dist(3)=cell_dist(3)*exp(-alpha_i*d-beta_i*d^2);
        cell_dist(6)=cell_dist(6)+cell_dist(5)*(1-exp(-alpha_h*d-beta_h*d^2));
        cell_dist(5)=cell_dist(5)*exp(-alpha_h*d-beta_h*d^2);

        j=j+1;
    end

    % Cell Proliferation & Death
    cell_dist(1)=cell_dist(1)*(2)^(f_p_pro*delta_t/t_c);
    h_pre=cell_dist(5)+cell_dist(6);
    cell_dist(5)=cell_dist(5)*(0.5)^(delta_t/ht_loss);
    cell_dist(6)=cell_dist(6)*(0.5)^(delta_t/ht_loss);
    p_d_pre=cell_dist(2);
    cell_dist(2)=cell_dist(2)*(2)^(f_p_pro*(2*k_m-1)*delta_t/t_c);


    % Mitotically dead cell in 1 time step
    md=p_d_pre-cell_dist(2)+(h_pre-cell_dist(5)-cell_dist(6));
```

```
cell_dist(7)=cell_dist(7)+md;
cell_dist(7)=cell_dist(7)*(0.5)^(delta_t/ht_lys);


% Recompartmentalization of the cell
if cell_dist(1)+cell_dist(2)>=comp_size(1)
    p_ex=(cell_dist(1)+cell_dist(2))-comp_size(1);
    p_ratio=cell_dist(1)/(cell_dist(1)+cell_dist(2));
    cell_dist(1)=comp_size(1)*p_ratio;
    cell_dist(2)=comp_size(1)*(1-p_ratio);
    cell_dist(3)=cell_dist(3)+p_ex*p_ratio;
    cell_dist(4)=cell_dist(4)+p_ex*(1-p_ratio);
else
    if cell_dist(3)+cell_dist(4)>0
        if cell_dist(3)+cell_dist(4)>comp_size(1)-...
                (cell_dist(1)+cell_dist(2))
            p_def=comp_size(1)-(cell_dist(1)+cell_dist(2));
            i_ratio=cell_dist(3)/(cell_dist(3)+cell_dist(4));
            cell_dist(1)=cell_dist(1)+p_def*i_ratio;
            cell_dist(2)=cell_dist(2)+p_def*(1-i_ratio);
            cell_dist(3)=cell_dist(3)-p_def*i_ratio;
            cell_dist(4)=cell_dist(4)-p_def*(1-i_ratio);
        else
            cell_dist(1)=cell_dist(1)+cell_dist(3);
            cell_dist(2)=cell_dist(2)+cell_dist(4);
            cell_dist(3)=0; cell_dist(4)=0;
            if cell_dist(5)+cell_dist(6)>0
                if cell_dist(5)+cell_dist(6)>comp_size(1)-...
                        (cell_dist(1)+cell_dist(2))
                    p_def=comp_size(1)-(cell_dist(1)+cell_dist(2));
                    h_ratio=cell_dist(5)/(cell_dist(5)+cell_dist(6));
                    cell_dist(1)=cell_dist(1)+p_def*h_ratio;
                    cell_dist(2)=cell_dist(2)+p_def*(1-h_ratio);
                    cell_dist(5)=cell_dist(5)-p_def*h_ratio;
                    cell_dist(6)=cell_dist(6)-p_def*(1-h_ratio);
                else
                    cell_dist(1)=cell_dist(1)+cell_dist(5);
                    cell_dist(2)=cell_dist(2)+cell_dist(6);
                    cell_dist(5)=0; cell_dist(6)=0;
                end
            end
        end
    end
end
if cell_dist(3)+cell_dist(4)>=comp_size(2)
    i_ex=(cell_dist(3)+cell_dist(4))-comp_size(2);
    i_ratio=cell_dist(3)/(cell_dist(3)+cell_dist(4));
    cell_dist(3)=comp_size(2)*i_ratio;
    cell_dist(4)=comp_size(2)*(1-i_ratio);
    cell_dist(5)=cell_dist(5)+i_ex*i_ratio;
    cell_dist(6)=cell_dist(6)+i_ex*(1-i_ratio);
else
    if cell_dist(5)+cell_dist(6)>0
        if cell_dist(5)+cell_dist(6)>comp_size(2)-...
                (cell_dist(3)+cell_dist(4))
            i_def=comp_size(2)-(cell_dist(3)+cell_dist(4));
            h_ratio=cell_dist(5)/(cell_dist(5)+cell_dist(6));
            cell_dist(3)=cell_dist(3)+i_def*h_ratio;
            cell_dist(4)=cell_dist(4)+i_def*(1-h_ratio);
            cell_dist(5)=cell_dist(5)-i_def*h_ratio;
            cell_dist(6)=cell_dist(6)-i_def*(1-h_ratio);
        else
            cell_dist(3)=cell_dist(3)+cell_dist(5);
```

```
                cell_dist(4)=cell_dist(4)+cell_dist(6);
                cell_dist(5)=0; cell_dist(6)=0;
            end
        end
    end


    % time step increase and store the number of cells in each compartment
    t=t+delta_t;
    cum_cell_dist_sbrt=[cum_cell_dist_sbrt cell_dist'];

end
%<<<<<<<<<<<<<<<<<<<<<<<<<<<<<<<<<<<<<<<<>>>>>>>>>>>>>>>>>>>>>>>>>>>>>>>>>>>>%
```

A.5.5. Sub-routine for the estimation of $EQD_{2,model}$ (SR_RT_eqd2.m)

```
%<<<<<<<<<<<<<<<<< RT fractional dose for EQD2 estimation >>>>>>>>>>>>>>>>%

% Assign proliferating fraction to the initial value

f_p_pro=f_p_pro_in;

% Cell distribution in each compartment
% (1:Pv, 2:Pd, 3:Iv, 4:Id, 5:Hv, 6:Hd, 7:lysis)
% Initially all compartments are fully filled with viable cells
% "comp_size" is the size of each compartment (1:P, 2:I, 3:H)

cell_dist=[];
cell_dist(1)=comp_size(1);
cell_dist(2)=0;
cell_dist(3)=comp_size(2);
cell_dist(4)=0;
cell_dist(5)=comp_size(3);
cell_dist(6)=0;
cell_dist(7)=0;

% variables (t:time(day), j:# of fraction, add_time:additional time for
%           weekend break, cum_cell_dist: cumulative cell distribution for
%           each time increment)
t=0;
j=0;
add_time=0;
cum_cell_dist=[];


% Treat until the SF becomes equivalent to SBRT regime
while (cell_dist(1)+cell_dist(3)+cell_dist(5))>s_sbrt

    % Change in f_p_pro (k_p) as blood supply improves
    f_p_pro=1-0.5*(cell_dist(1)+cell_dist(2))/comp_size(1);


    % RT fraction
    if  t>(t_start+j+add_time-delta_t/2) && t<(t_start+j+add_time+delta_t/2)

        cell_dist(2)=cell_dist(2)+cell_dist(1)*(1-exp(-alpha_p*d-beta_p*d^2));
        cell_dist(1)=cell_dist(1)*exp(-alpha_p*d-beta_p*d^2);
        cell_dist(4)=cell_dist(4)+cell_dist(3)*(1-exp(-alpha_i*d-beta_i*d^2));
        cell_dist(3)=cell_dist(3)*exp(-alpha_i*d-beta_i*d^2);
```

```
    cell_dist(6)=cell_dist(6)+cell_dist(5)*(1-exp(-alpha_h*d-beta_h*d^2));
    cell_dist(5)=cell_dist(5)*exp(-alpha_h*d-beta_h*d^2);

    j=j+1;

    % Week-end break
    if rem(j,5)==0
        add_time=add_time+2;
    end

end

% Cell Proliferation & Death
cell_dist(1)=cell_dist(1)*(2)^(f_p_pro*delta_t/t_c);
h_pre=cell_dist(5)+cell_dist(6);
cell_dist(5)=cell_dist(5)*(0.5)^(delta_t/ht_loss);
cell_dist(6)=cell_dist(6)*(0.5)^(delta_t/ht_loss);
p_d_pre=cell_dist(2);
cell_dist(2)=cell_dist(2)*(2)^(f_p_pro*(2*k_m-1)*delta_t/t_c);


% Mitotically dead cell in 1 time step
md=p_d_pre-cell_dist(2)+(h_pre-cell_dist(5)-cell_dist(6));
cell_dist(7)=cell_dist(7)+md;
cell_dist(7)=cell_dist(7)*(0.5)^(delta_t/ht_lys);


% Recompartmentalization of the cell
if cell_dist(1)+cell_dist(2)>=comp_size(1)
    p_ex=(cell_dist(1)+cell_dist(2))-comp_size(1);
    p_ratio=cell_dist(1)/(cell_dist(1)+cell_dist(2));
    cell_dist(1)=comp_size(1)*p_ratio;
    cell_dist(2)=comp_size(1)*(1-p_ratio);
    cell_dist(3)=cell_dist(3)+p_ex*p_ratio;
    cell_dist(4)=cell_dist(4)+p_ex*(1-p_ratio);
else
    if cell_dist(3)+cell_dist(4)>0
        if cell_dist(3)+cell_dist(4)>comp_size(1)-...
                (cell_dist(1)+cell_dist(2))
            p_def=comp_size(1)-(cell_dist(1)+cell_dist(2));
            i_ratio=cell_dist(3)/(cell_dist(3)+cell_dist(4));
            cell_dist(1)=cell_dist(1)+p_def*i_ratio;
            cell_dist(2)=cell_dist(2)+p_def*(1-i_ratio);
            cell_dist(3)=cell_dist(3)-p_def*i_ratio;
            cell_dist(4)=cell_dist(4)-p_def*(1-i_ratio);
        else
            cell_dist(1)=cell_dist(1)+cell_dist(3);
            cell_dist(2)=cell_dist(2)+cell_dist(4);
            cell_dist(3)=0; cell_dist(4)=0;
            if cell_dist(5)+cell_dist(6)>0
                if cell_dist(5)+cell_dist(6)>comp_size(1)-...
                        (cell_dist(1)+cell_dist(2))
                    p_def=comp_size(1)-(cell_dist(1)+cell_dist(2));
                    h_ratio=cell_dist(5)/(cell_dist(5)+cell_dist(6));
                    cell_dist(1)=cell_dist(1)+p_def*h_ratio;
                    cell_dist(2)=cell_dist(2)+p_def*(1-h_ratio);
                    cell_dist(5)=cell_dist(5)-p_def*h_ratio;
                    cell_dist(6)=cell_dist(6)-p_def*(1-h_ratio);
                else
                    cell_dist(1)=cell_dist(1)+cell_dist(5);
                    cell_dist(2)=cell_dist(2)+cell_dist(6);
                    cell_dist(5)=0; cell_dist(6)=0;
                end
```

```
                end
            end
        end
    end
    if cell_dist(3)+cell_dist(4)>=comp_size(2)
        i_ex=(cell_dist(3)+cell_dist(4))-comp_size(2);
        i_ratio=cell_dist(3)/(cell_dist(3)+cell_dist(4));
        cell_dist(3)=comp_size(2)*i_ratio;
        cell_dist(4)=comp_size(2)*(1-i_ratio);
        cell_dist(5)=cell_dist(5)+i_ex*i_ratio;
        cell_dist(6)=cell_dist(6)+i_ex*(1-i_ratio);
    else
        if cell_dist(5)+cell_dist(6)>0
            if cell_dist(5)+cell_dist(6)>comp_size(2)-...
                    (cell_dist(3)+cell_dist(4))
                i_def=comp_size(2)-(cell_dist(3)+cell_dist(4));
                h_ratio=cell_dist(5)/(cell_dist(5)+cell_dist(6));
                cell_dist(3)=cell_dist(3)+i_def*h_ratio;
                cell_dist(4)=cell_dist(4)+i_def*(1-h_ratio);
                cell_dist(5)=cell_dist(5)-i_def*h_ratio;
                cell_dist(6)=cell_dist(6)-i_def*(1-h_ratio);
            else
                cell_dist(3)=cell_dist(3)+cell_dist(5);
                cell_dist(4)=cell_dist(4)+cell_dist(6);
                cell_dist(5)=0; cell_dist(6)=0;
            end
        end
    end


    % time step increase and store the number of cells in each compartment
    t=t+delta_t;
    cum_cell_dist=[cum_cell_dist cell_dist'];

end

%<<<<<<<<<<<<<<<<<<<<<<<<<<<<<<<<<<<<<<<<>>>>>>>>>>>>>>>>>>>>>>>>>>>>>>>>>>>>%
```

A.5.6. Sub-routine for reoxygenation time (SR_Reox_time.m)

```
%<<<<<<<<<<<<<<<<<< Find reoxygenation times in two ways >>>>>>>>>>>>>>>>>>%

% variables for reox_time1
T=[];       reox_time=[];


% variables for reox_time2
time=[];    T1=[];      T2=[];      T3=[];
C=[];       C1=[];      C2=[];      C3=[];
a=[];       b=[];       c=[];
A=[];       crv=[];     abs_crv=[];
m=[];       reox_time2=[];


% Full reoxygenation time
T=find(cum_cell_dist(3,:)+cum_cell_dist(4,:)+cum_cell_dist(5,:)+...
    cum_cell_dist(6,:)==0);
if isempty(T)==1
    T=[inf];
```

```
end
reox_time=(T(1))*delta_t;


% Reoxygenation time by maximum curvature
time=delta_t:delta_t:round(t/delta_t)*delta_t;
T1=time(1:end-2);T2=time(2:end-1);T3=time(3:end);
C=log(cum_cell_dist(3,:)+cum_cell_dist(4,:)+cum_cell_dist(5,:)+...
    cum_cell_dist(6,:));
C1=C(1:end-2);C2=C(2:end-1);C3=C(3:end);
a=sqrt((T3-T2).^2+(C3-C2).^2);
b=sqrt((T1-T3).^2+(C1-C3).^2);
c=sqrt((T2-T1).^2+(C2-C1).^2);
A=1/2*(T1.*C2+T2.*C3+T3.*C1-T1.*C3-T2.*C1-T3.*C2);
crv=[0,4*A./(a.*b.*c),0];
abs_crv=abs(crv);


% to eliminate the noise in the curvature
for m=2:length(abs_crv)-1;
    if abs(abs_crv(m+1)-abs_crv(m))>0.15
        abs_crv(m+1)=abs_crv(m);
    end
end
if reox_time==inf
    reox_time2=inf;
else
    reox_time2=time(abs_crv==max(abs_crv));
    reox_time2=reox_time2(1);
end

%<<<<<<<<<<<<<<<<<<<<<<<<<<<<<<<<<<<<<<<<<<<<<<<<<<<<<<<<<<<<<<<<<<<<<<<<<<<<%
```

BIBLIOGRAPHY

Abramyuk, A., Tokalov, S., Zöphel, K., Koch, A., Szluha Lazanyi, K., Gillham, C., Herrmann, T. & Abolmaali, N., 2009, Is pre-therapeutical FDG-PET/CT capable to detect high risk tumor subvolumes responsible for local failure in non-small cell lung cancer? *Radiotherapy and Oncology*, 91(3), pp. 399-404.

Aerts, H.J.W.L., van Baardwijk, A.A.W., Petit, S.F., Offermann, C., Loon, J.V., Houben, R., Dingemans, A.M.C., Wanders, R., Boersma, L., Borger, J., Bootsma, G., Geraedts, W., Pitz, C., Simons, J., Wouters, B.G., Oellers, M., Lambin, P., Bosmans, G., Dekker, A.L.A.J. & Ruysscher, D.D., 2009, Identification of residual metabolic-active areas within individual NSCLC tumours using a pre-radiotherapy 18Fluorodeoxyglucose-PET-CT scan, *Radiotherapy and Oncology*, 91(3), pp. 386-92.

Agarwal, M., Brahmanday, G., Bajaj, S.K., Ravikrishnan, K.P. & Wong, C.Y.O., 2009, Revisiting the prognostic value of preoperative 18F-fluoro-2-deoxyglucose (18F-FDG) positron emission tomography (PET) in early-stage (I & II) non-small cell lung cancers (NSCLC), *European Journal of Nuclear Medicine and Molecular Imaging*, pp. 1-8.

Agren Cronqvist, A.K., Kallman, P., Turesson, I. & Brahme, A., 1995, Volume and heterogeneity dependence of the dose-response relationship for head and neck tumours, *Acta Oncologica*, 34(6), pp. 851-60.

Ahuja, V., Edward Coleman, R., Herndon, J. & Patz Jr, E.F., 1998, The prognostic significance of fluorodeoxyglucose positron emission tomography imaging for patients with nonsmall cell lung carcinoma, *Cancer*, 83(5), pp. 918-24.

Allal, A.S., Slosman, D.O., Kebdani, T., Allaoua, M., Lehmann, W. & Dulguerov, P., 2004, Prediction of outcome in head-and-neck cancer patients using the standardized uptake value of 2-[^{18}f]fluoro-2-deoxy-d-glucose, *International Journal of Radiation Oncology Biology Physics*, 59(5), pp. 1295-300.

Barker Jr, J.L., Garden, A.S., Ang, K.K., O'Daniel, J.C., Wang, H., Court, L.E., Morrison, W.H., Rosenthal, D.I., Chao, K.S.C., Tucker, S.L., Mohan, R. & Dong, L., 2004, Quantification of volumetric and geometric changes occurring during fractionated radiotherapy for head-and-neck cancer using an integrated CT/linear accelerator system, *International Journal of Radiation Oncology Biology Physics*, 59(4), pp. 960-70.

Been, L.B., Suurmeijer, A.J.H., Cobben, D.C.P., Jager, P.L., Hoekstra, H.J. & Elsinga, P.H., 2004, [18F]FLT-PET in oncology: Current status and opportunities, *European Journal of Nuclear Medicine and Molecular Imaging*, 31(12), pp. 1659-72.

Benedict, S.H., Yenice, K.M., Followill, D., Galvin, J.M., Hinson, W., Kavanagh, B., Keall, P., Lovelock, M., Meeks, S., Papiez, L., Purdie, T., Sadagopan, R., Schell, M.C., Salter, B., Schlesinger, D.J., Shiu, A.S., Solberg, T., Song, D.Y., Stieber, V., Timmerman, R., Tomé, W.A., Verellen, D., Wang, L. & Yin, F.F., 2010, Stereotactic body radiation therapy: the report of AAPM Task Group 101, *Medical physics*, 37(8), pp. 4078-101.

Bentzen, S.M., 1992, Steepness of the clinical dose-control curve and variation in the in vitro radiosensitivity of head and neck squamous cell carcinoma, *International Journal of Radiation Biology*, 61(3), pp. 417-23.

Bentzen, S.M., 2005, Theragnostic imaging for radiation oncology: Dose-painting by numbers, *Lancet Oncology*, 6(2), pp. 112-7.

Bentzen, S.M. & Thames, H.D., 1996, Tumor volume and local control probability: Clinical data and radiobiological interpretations, *International Journal of Radiation Oncology Biology Physics*, 36(1), pp. 247-51.

Bentzen, S.M., Johansen, L.V., Overgaard, J. & Thames, H.D., 1991, Clinical radiobiology of squamous cell carcinoma of the oropharynx, *International Journal of Radiation Oncology Biology Physics*, 20(6), pp. 1197-206.

Berry, R.J., Hall, E.J. & Cavanagh, J., 1970, Radiosensitivity and the oxygen effect for mammalian cells cultured in vitro in stationary phase, *Br J Radiol*, 43(506), pp. 81-90.

Biade, S., Stobbe, C.C. & Chapman, J.D., 1997, The intrinsic radiosensitivity of some human tumor cells throughout their cell cycles, *Radiat Res*, 147(4), pp. 416-21.

Biehl, K.J., Kong, F.M., Dehdashti, F., Jin, J.Y., Mutic, S., El Naqa, I., Siegel, B.A. & Bradley, J.D., 2006, 18F-FDG PET definition of gross tumor volume for radiotherapy of non-small cell lung cancer: Is a single standardized uptake value threshold approach appropriate? *Journal of Nuclear Medicine*, 47(11), pp. 1808-12.

Borkenstein, K., Levegrün, S. & Peschke, P., 2004, Modeling and computer simulations of tumor growth and tumor response to radiotherapy, *Radiat Res*, 162(1), pp. 71-83.

Borst, G.R., Belderbos, J.S.A., Boellaard, R., Comans, E.F.I., De Jaeger, K., Lammertsma, A.A. & Lebesque, J.V., 2005, Standardised FDG uptake: A prognostic factor for inoperable non-small cell lung cancer, *European Journal of Cancer*, 41(11), pp. 1533-41.

Bradley, J., Thorstad, W.L., Mutic, S., Miller, T.R., Dehdashti, F., Siegel, B.A., Bosch, W. & Bertrand, R.J., 2004, Impact of FDG-PET on radiation therapy volume delineation in non-small-cell lung cancer, *International Journal of Radiation Oncology Biology Physics*, 59(1), pp. 78-86.

Brenner, D.J., 1993, Dose, volume, and tumor-control predictions in radiotherapy, *International Journal of Radiation Oncology Biology Physics*, 26(1), pp. 171-9.

Brown, J.M., 1999, The hypoxic cell: A target for selective cancer therapy - Eighteenth Bruce F. Cain Memorial Award Lecture, *Cancer Research*, 59(23), pp. 5863-70.

Brown, J.M., 2002, Tumor microenvironment and the response to anticancer therapy, *Cancer biology & therapy*, 1(5), pp. 453-8.

Brown, J.M. & Koong, A.C., 2008, High-dose single-fraction radiotherapy: exploiting a new biology? *International journal of radiation oncology, biology, physics*, 71(2), pp. 324-5.

Brown, J.M. & Wilson, W.R., 2004, Exploiting tumour hypoxia in cancer treatment, *Nature Reviews Cancer*, 4(6), pp. 437-47.

Brown, J.M., Diehn, M. & Loo, B.W., 2010, Stereotactic ablative radiotherapy should be combined with a hypoxic cell radiosensitizer, *International journal of radiation oncology, biology, physics*, 78(2), pp. 323-7.

Bruechner, K., Bergmann, R., Santiago, A., Mosch, B., Yaromina, A., Hessel, F., Hofheinz, F., van den Hoff, J., Baumann, M. & Beuthien-Baumann, B., 2009, Comparison of [18F]FDG uptake and distribution with hypoxia and proliferation in FaDu human squamous cell carcinoma (hSCC) xenografts after single dose irradiation, *International journal of radiation biology*, 85(9), pp. 772-80.

Brun, E., Kjellén, E., Tennvall, J., Ohlsson, T., Sandell, A., Perfekt, R., Wennerberg, J. & Strand, S.E., 2002, FDG pet studies during treatment: Prediction of therapy outcome in head and neck squamous cell carcinoma, *Head and Neck*, 24(2), pp. 127-35.

Bucci, M.K., Bevan, A. & Roach Iii, M., 2005, Advances in radiation therapy: Conventional to 3D, to IMRT, to 4D, and beyond, *Ca-A Cancer Journal for Clinicians*, 55(2), pp. 117-34.

Buchmann, I., Haberkorn, U., Schmidtmann, I., Brochhausen, C., Buchholz, H.G., Bartenstein, P. & Hansen, T., 2008, Influence of cell proportions and proliferation rates on FDG uptake in squamous-cell esophageal carcinoma: a PET study, *Cancer Biother Radiopharm*, 23(2), pp. 172-80.

Buck, A.K., Halter, G., Schirrmeister, H., Kotzerke, J., Wurziger, I., Glatting, G., Mattfeldt, T., Neumaier, B., Reske, S.N. & Hetzel, M., 2003, Imaging proliferation in lung tumors with PET: 18F-FLT versus 18F-FDG, *Journal of Nuclear Medicine*, 44(9), pp. 1426-31.

Buffa, F.M. & Nahum, A.E., 2000, Monte Carlo dose calculations and radiobiological modelling: Analysis of the effect of the statistical noise of the dose distribution on the probability of tumour control, *Physics in Medicine and Biology*, 45(10), pp. 3009-23.

Buffa, F.M., Fenwick, J.D. & Nahum, A.E., 2000, An analysis of the relationship between radiosensitivity and volume effects in tumor control probability modeling, *Medical Physics*, 27(6), pp. 1258-65.

Buffa, F.M., West, C., Byrne, K., Moore, J.V. & Nahum, A.E., 2001, Radiation response and cure rate of human colon adenocarcinoma spheroids of different size: The significance of hypoxia on tumor control modelling, *International Journal of Radiation Oncology Biology Physics*, 49(4), pp. 1109-18.

Cairns, R.A., Kalliomaki, T. & Hill, R.P., 2001, Acute (cyclic) hypoxia enhances spontaneous metastasis of KHT murine tumors, *Cancer Research*, 61(24), pp. 8903-8.

Carlin, S., Pugachev, A., Sun, X., Burke, S., Claus, F., O'Donoghue, J., Ling, C.C. & Humm, J.L., 2009, In vivo characterization of a reporter gene system for imaging hypoxia-induced gene expression, *Nuclear Medicine and Biology*.

Carlone, M.C., Warkentin, B., Stavrev, P. & Fallone, B.G., 2006, Fundamental form of a population TCP model in the limit of large heterogeneity, *Medical Physics*, 33(6), pp. 1634-42.

Carlson, D.J., Keall, P.J., Loo, B.W., Chen, Z.J. & Brown, J.M., 2011, Hypofractionation results in reduced tumor cell kill compared to conventional fractionation for tumors with regions of hypoxia, *International journal of radiation oncology, biology, physics*, 79(4), pp. 1188-95.

Carlson, D.J., Stewart, R.D. & Semenenko, V.A., 2006, Effects of oxygen on intrinsic radiation sensitivity: A test of the relationship between aerobic and hypoxic linear-quadratic (LQ) model parameters, *Medical physics*, 33(9), pp. 3105-15.

Casali, C., Cucca, M., Rossi, G., Barbieri, F., Iacuzio, L., Bagni, B. & Uliano, M., 2009, The variation of prognostic significance of Maximum Standardized Uptake Value of [18F]-fluoro-2-deoxy-glucose positron emission tomography in different histological subtypes and pathological stages of surgically resected Non-Small Cell Lung Carcinoma, *Lung cancer (Amsterdam, Netherlands)*.

Caswell, H., 2001, *Matrix population models : construction, analysis, and interpretation,* Sinauer, Sunderland Mass.

Cárdenas-Navia, L.I., Mace, D., Richardson, R.A., Wilson, D.F., Shan, S. & Dewhirst, M.W., 2008, The pervasive presence of fluctuating oxygenation in tumors, *Cancer Research*, 68(14), pp. 5812-9.

Cerfolio, R.J., Bryant, A.S., Ohja, B. & Bartolucci, A.A., 2005, The maximum standardized uptake values on positron emission tomography of a non-small cell lung cancer predict stage, recurrence, and survival, *Journal of Thoracic and Cardiovascular Surgery*, 130(1), pp. 151-9.

Chan, N., Koch, C.J. & Bristow, R.G., 2009, Tumor hypoxia as a modifier of DNA strand break and cross-link repair, *Curr Mol Med*, 9(4), pp. 401-10.

Chan, N., Koritzinsky, M., Zhao, H., Bindra, R., Glazer, P.M., Powell, S., Belmaaza, A., Wouters, B. & Bristow, R.G., 2008, Chronic hypoxia decreases synthesis of homologous recombination proteins to offset chemoresistance and radioresistance, *Cancer Res*, 68(2), pp. 605-14.

Chang, B.K. & Timmerman, R.D., 2007, Stereotactic body radiation therapy: a comprehensive review, *American journal of clinical oncology*, 30(6), pp. 637-44.

Chang, D.T., Swaminath, A., Kozak, M., Weintraub, J., Koong, A.C., Kim, J., Dinniwell, R., Brierley, J., Kavanagh, B.D., Dawson, L.A. & Schefter, T.E., 2011, Stereotactic body radiotherapy for colorectal liver metastases: A pooled analysis, *Cancer*, 117(17), pp. 4060-9.

Chen, J.C., Huang, T.W., Cheng, Y.L., Chang, H., Tzao, C., Huang, W.S. & Lee, S.C., 2009, Prognostic value or 18-FDG uptake in early stage NSCLC, *Thoracic and Cardiovascular Surgeon*, 57(7), pp. 413-6.

Chen, W., Cloughesy, T., Kamdar, N., Satyamurthy, N., Bergsneider, M., Liau, L., Mischel, P., Czernin, J., Phelps, M.E. & Silverman, D.H.S., 2005, Imaging proliferation in brain tumors with 18F-FLT PET: Comparison with 18F-FDG, *Journal of Nuclear Medicine*, 46(6), pp. 945-52.

Chi, A., Tomé, W.A., Fowler, J., Komaki, R., Nguyen, N.P., Mehta, M.P. & Welsh, J.S., 2011, Stereotactic body radiation therapy in non-small-cell lung cancer: linking radiobiological modeling and clinical outcome, *American journal of clinical oncology*, 34(4), pp. 432-41.

Chvetsov, A.V., Dong, L., Palta, J.R. & Amdur, R.J., 2009, Tumor-volume simulation during radiotherapy for head-and-neck cancer using a four-level cell population model, *International journal of radiation oncology, biology, physics*, 75(2), pp. 595-602.

Chvetsov, A.V., Palta, J.J. & Nagata, Y., 2008, Time-dependent cell disintegration kinetics in lung tumors after irradiation, *Physics in medicine and biology*, 53(9), pp. 2413-23.

Daisne, J.F., Duprez, T., Weynand, B., Lonneux, M., Hamoir, M., Reychler, H. & Grégoire, V., 2004, Tumor volume in pharyngolaryngeal squamous cell carcinoma: Comparison at CT, MR imaging, and FDG PET and validation with surgical specimen, *Radiology*, 233(1), pp. 93-100.

Dang, C.V. & Semenza, G.L., 1999, Oncogenic alterations of metabolism, *Trends in Biochemical Sciences*, 24(2), pp. 68-72.

Das, S.K., Miften, M.M., Zhou, S., Bell, M., Munley, M.T., Whiddon, C.S., Craciunescu, O., Baydush, A.H., Wong, T., Rosenman, J.G., Dewhirst, M.W. & Marks, L.B., 2004, Feasebility of optimizing the dose distribution in lung tumors using fluorine-18-fluorodeoxyglucose positron emission tomography and single photon emission computed tomography guided dose prescriptions, *Medical Physics*, 31(6), pp. 1452-61.

Dawson, A. & Hillen, T., 2006, Derivation of the tumour control probability (TCP) from a cell cycle model, *Computational and Mathematical Methods in Medicine*, 7(2-3), pp. 121-41.

Deasy, B.M., Jankowski, R.J., Payne, T.R., Cao, B., Goff, J.P., Greenberger, J.S. & Huard, J., 2003, Modeling Stem Cell Population Growth: Incorporating Terms for Proliferative Heterogeneity, *Stem Cells*, 21(5), pp. 536-45.

Dehdashti, F., Grigsby, P.W., Lewis, J.S., Laforest, R., Siegel, B.A. & Welch, M.J., 2008, Assessing tumor hypoxia in cervical cancer by PET with 60Cu- labeled diacetyl-bis(N4-methylthiosemicarbazone), *Journal of Nuclear Medicine*, 49(2), pp. 201-5.

Dehdashti, F., Grigsby, P.W., Mintun, M.A., Lewis, J.S., Siegel, B.A. & Welch, M.J., 2003, Assessing tumor hypoxia in cervical cancer by positron emission tomography with 60Cu-ATSM: Relationship to therapeutic response - A preliminary report, *International Journal of Radiation Oncology Biology Physics*, 55(5), pp. 1233-8.

Dhital, K., Saunders, C.A.B., Seed, P.T., O'Doherty, M.J. & Dussek, J., 2000, [18F]Fluorodeoxyglucose positron emission tomography and its prognostic value in lung cancer, *European Journal of Cardio-thoracic Surgery*, 18(4), pp. 425-8.

Dierckx, R.A. & Van De Wiele, C., 2008, FDG uptake, a surrogate of tumour hypoxia? *European Journal of Nuclear Medicine and Molecular Imaging*, 35(8), pp. 1544-9.

Dionysiou, D.D., Stamatakos, G.S., Uzunoglu, N.K., Nikita, K.S. & Marioli, A., 2004, A four-dimensional simulation model of tumour response to radiotherapy in vivo: Parametric validation considering radiosensitivity, genetic profile and fractionation, *Journal of Theoretical Biology*, 230(1), pp. 1-20.

Downey, R.J., Akhurst, T., Gonen, M., Vincent, A., Bains, M.S., Larson, S. & Rusch, V., 2004, Preoperative F-18 fluorodeoxyglucose-positron emission tomography maximal standardized uptake value predicts survival after lung cancer resection, *Journal of Clinical Oncology*, 22(16), pp. 3255-60.

Evans, S.M., Hahn, S.M., Magarelli, D.P. & Koch, C.J., 2001, Hypoxic heterogeneity in human tumors: EF5 binding, vasculature, necrosis, and proliferation, *American Journal of Clinical Oncology: Cancer Clinical Trials*, 24(5), pp. 467-72.

Feng, M., Kong, F.M., Gross, M., Fernando, S., Hayman, J.A. & Ten Haken, R.K., 2009, Using Fluorodeoxyglucose Positron Emission Tomography to Assess Tumor Volume During Radiotherapy for Non-Small-Cell Lung Cancer and Its Potential Impact on Adaptive Dose Escalation and Normal Tissue Sparing, *International Journal of Radiation Oncology Biology Physics*, 73(4), pp. 1228-34.

Fowler, J.F., 1989, The linear-quadratic formula and progress in fractionated radiotherapy, *British Journal of Radiology*, 62(740), pp. 679-94.

Fowler, J.F. & Chappell, R., 1994, Local control versus dose or overall time: From coefficients to percentages, *British Journal of Radiology*, 67(803), pp. 1108-12.

Fowler, J.F., Tomé, W.A., Fenwick, J.D. & Mehta, M.P., 2004, A challenge to traditional radiation oncology, *International Journal of Radiation Oncology Biology Physics*, 60(4), pp. 1241-56.

Freyer, J.P., Jarrett, K., Carpenter, S. & Raju, M.R., 1991, Oxygen enhancement ratio as a function of dose and cell cycle phase for radiation-resistant and sensitive CHO cells, *Radiat Res*, 127(3), pp. 297-307.

Garcia-Barros, M., Paris, F., Cordon-Cardo, C., Lyden, D., Rafii, S., Haimovitz-Friedman, A., Fuks, Z. & Kolesnick, R., 2003, Tumor response to radiotherapy regulated by endothelial cell apoptosis, *Science*, 300(5622), pp. 1155-9.

Gatenby, R.A. & Gillies, R.J., 2004, Why do cancers have high aerobic glycolysis? *Nature Reviews Cancer*, 4(11), pp. 891-9.

Gillespie, C.J., Chapman, J.D., Reuvers, A.P. & Dugle, D.L., 1975, The inactivation of Chinese hamster cells by X rays: Synchronized and exponential cell populations, *Radiation Research*, 64(2), pp. 353-64.

Goitein, M., 2008, *Radiation Oncology: A Physicist's-Eye View,* Springer,.

Graeber, T.G., Osmanian, C., Jacks, T., Housman, D.E., Koch, C.J., Lowe, S.W. & Giaccia, A.J., 1996, Hypoxia-mediated selection of cells with diminished apoptotic potential in solid tumours, *Nature*, 379(6560), pp. 88-91.

Grigsby, P.W., Siegel, B.A., Dehdashti, F. & Mutch, D.G., 2003, Posttherapy surveillance monitoring of cervical cancer by FDG-PET, *International Journal of Radiation Oncology Biology Physics*, 55(4), pp. 907-13.

Grigsby, P.W., Siegel, B.A., Dehdashti, F., Rader, J. & Zoberi, I., 2004, Posttherapy [18F] fluorodeoxyglucose positron emission tomography in carcinoma of the cervix: Response and outcome, *Journal of Clinical Oncology*, 22(11), pp. 2167-71.

Gyllenberg, M. & Webb, G.F., 1989, Quiescence as an explanation of Gompertzian tumor growth, *Growth, Development and Aging*, 53(1-2), pp. 25-33.

Hall, E.J. & Giaccia, A.J., 2006, *Radiobiology for the radiologist,* Lippincott Williams & Wilkins, Philadelphia.

Hara, T., Bansal, A. & DeGrado, T.R., 2006, Effect of hypoxia on the uptake of [methyl-3H]choline, [1-14C] acetate and [18F]FDG in cultured prostate cancer cells, *Nuclear Medicine and Biology*, 33(8), pp. 977-84.

Heiden, M.G.V., Cantley, L.C. & Thompson, C.B., 2009, Understanding the warburg effect: The metabolic requirements of cell proliferation, *Science*, 324(5930), pp. 1029-33.

Hemmings, C., 2010, The elaboration of a critical framework for understanding cancer: The cancer stem cell hypothesis, *Pathology*, 42(2), pp. 105-12.

Hendry, J.H., Bentzen, S.M., Dale, R.G., Fowler, J.F., Wheldon, T.E., Jones, B., Munro, A.J., Slevin, N.J., Robertson, A.G. & Cowles, A., 1996, A modelled comparison of the effects of using different ways to compensate for missed treatment days in radiotherapy, *Clinical Oncology*, 8(5), pp. 297-307.

Heppner, G.H., 1984, Tumor heterogeneity, *Cancer Research*, 44(6), pp. 2259-65.

Hlatky, L., Sachs, R.K. & Alpen, E.L., 1988, Joint oxygen-glucose deprivation as the cause of necrosis in a tumor analog, *Journal of cellular physiology*, 134(2), pp. 167-78.

Hoogsteen, I.J., Marres, H.A., Bussink, J., van der Kogel, A.J. & Kaanders, J.H., 2007, Tumor microenvironment in head and neck squamous cell carcinomas: predictive value and clinical relevance of hypoxic markers. A review, *Head Neck*, 29(6), pp. 591-604.

Hoogsteen, I.J., Marres, H.A., Wijffels, K.I., Rijken, P.F., Peters, J.P., van den Hoogen, F.J., Oosterwijk, E., van der Kogel, A.J. & Kaanders, J.H., 2005, Colocalization of carbonic anhydrase 9 expression and cell proliferation in human head and neck squamous cell carcinoma, *Clinical cancer research : an official journal of the American Association for Cancer Research*, 11(1), pp. 97-106.

Hoos, A., Stojadinovic, A., Mastorides, S., Urist, M.J., Polsky, D., Di Como, C.J., Brennan, M.F. & Cordon-Cardo, C., 2001, High Ki-67 proliferative index predicts disease specific survival in patients with high-risk soft tissue sarcomas, *Cancer*, 92(4), pp. 869-74.

Höckel, M. & Vaupel, P., 2001a, Biological consequences of tumor hypoxia, *Seminars in Oncology*, 28(2 SUPPL. 8), pp. 36-41.

Höckel, M. & Vaupel, P., 2001b, Tumor hypoxia: Definitions and current clinical, biologic, and molecular aspects, *Journal of the National Cancer Institute*, 93(4), pp. 266-76.

Huang, Z., Mayr, N.A., Yuh, W.T., Lo, S.S., Montebello, J.F., Grecula, J.C., Lu, L., Li, K., Zhang, H., Gupta, N. & Wang, J.Z., 2010, Predicting outcomes in cervical cancer: a kinetic model of tumor regression during radiation therapy, *Cancer Res*, 70(2), pp. 463-70.

Ido, T., Wan, C.-N., Casella, V., Fowler, J.S., Wolf, A.P., Reivich, M. & Kuhl, D.E., 1978, Labeled 2-deoxy-D-glucose analogs. 18F-labeled 2-deoxy-2-fluoro-D-glucose, 2-deoxy-2-fluoro-D-mannose and 14C-2-deoxy-2-fluoro-D-glucose, *Journal of Labelled Compounds and Radiopharmaceuticals*, 14(2), pp. 175-83.

Ishida, T., Kaneko, S., Akazawa, K., Tateishi, M., Sugio, K. & Sugimachi, K., 1993, Proliferating cell nuclear antigen expression and argyrophilic nucleolar organizer regions as factors influencing prognosis of surgically treated lung cancer patients, *Cancer Research*, 53(20), pp. 5000-3.

Janssen, M.H.M., Aerts, H.J.W.L., Öllers, M.C., Bosmans, G., Lee, J.A., Buijsen, J., De Ruysscher, D., Lambin, P., Lammering, G. & Dekker, A.L.A.J., 2009, Tumor Delineation Based on Time-Activity Curve Differences Assessed With Dynamic Fluorodeoxyglucose Positron Emission Tomography-Computed Tomography in Rectal Cancer Patients, *International Journal of Radiation Oncology Biology Physics*, 73(2), pp. 456-65.

Jeong, H.J., Min, J.J., Park, J.M., Chung, J.K., Kim, B.T., Jeong, J.M., Lee, D.S., Lee, M.C., Han, S.K. & Shim, Y.S., 2002, Determination of the prognostic value of [18F]fluorodeoxyglucose uptake by using positron emission tomography in patients with non-small cell lung cancer, *Nuclear Medicine Communications*, 23(9), pp. 865-70.

Johnson, C.R., Thames, H.D., Huang, D.T. & Schmidt-Ullrich, R.K., 1995, The tumor volume and clonogen number relationship: Tumor control predictions based upon tumor volume estimates derived from computed tomography, *International Journal of Radiation Oncology Biology Physics*, 33(2), pp. 281-7.

Joiner, M. & Kogel, A.V.D., 2009, *Basic clinical radiobiology,* Hodder Arnold, London.

Keall, P.J. & Webb, S., 2007, Optimum parameters in a model for tumour control probability, including interpatient heterogeneity: Evaluation of the log-normal distribution, *Physics in Medicine and Biology*, 52(1), pp. 291-302.

Kelly, C.J., Smallbone, K., Roose, T. & Brady, M., 2007, Biomedical Imaging: From Nano to Macro, *A model to investigate the feasibility of FDG as a surrogate marker of hypoxia.* Arlington, VA, pp. 540-3.

Kennedy, A.S., Raleigh, J.A., Perez, G.M., Calkins, D.P., Thrall, D.E., Novotny, D.B. & Varia, M.A., 1997, Proliferation and hypoxia in human squamous cell carcinoma of the cervix: First report of combined immunohistochemical assays, *International Journal of Radiation Oncology Biology Physics*, 37(4), pp. 897-905.

Khrizman, P., Small, W., Dawson, L. & Benson, A.B., 2010, The use of stereotactic body radiation therapy in gastrointestinal malignancies in locally advanced and metastatic settings, *Clinical colorectal cancer*, 9(3), pp. 136-43.

Kidd, E.A., Siegel, B.A., Dehdashti, F. & Grigsby, P.W., 2007, The standardized uptake value for F-18 fluorodeoxyglucose is a sensitive predictive biomarker for cervical cancer treatment response and survival, *Cancer*, 110(8), pp. 1738-44.

Kim, J.J. & Tannock, I.F., 2005, Repopulation of cancer cells during therapy: An important cause of treatment failure, *Nature Reviews Cancer*, 5(7), pp. 516-25.

Kim, J.W. & Dang, C.V., 2006, Cancer's molecular sweet tooth and the warburg effect, *Cancer Research*, 66(18), pp. 8927-30.

Kim, S.Y., Roh, J.L., Mi, R.K., Jae, S.K., Choi, S.H., Soon, Y.N., Lee, S.W. & Kim, S.B., 2007, Use of ^{18}F-FDG PET for primary treatment strategy in patients with squamous cell carcinoma of the oropharynx, *Journal of Nuclear Medicine*, 48(5), pp. 752-7.

Kiran, K.L., Jayachandran, D. & Lakshminarayanan, S., 2009, Mathematical modelling of avascular tumour growth based on diffusion of nutrients and its validation, *The Canadian Journal of Chemical Engineering*, 87(5), pp. 732-40.

Kong, F.M.S., Frey, K.A., Quint, L.E., Ten Haken, R.K., Hayman, J.A., Kessler, M., Chetty, I.J., Normolle, D., Eisbruch, A. & Lawrence, T.S., 2007, A pilot study of [18F]fluorodeoxyglucose positron emission tomography scans during and after radiation-based therapy in patients with non-small-cell lung cancer, *Journal of Clinical Oncology*, 25(21), pp. 3116-23.

Kozusko, F. & Bajzer, Ž., 2003, Combining Gompertzian growth and cell population dynamics, *Mathematical Biosciences*, 185(2), pp. 153-67.

Krohn, K.A., Link, J.M. & Mason, R.P., 2008, Molecular imaging of hypoxia, *Journal of Nuclear Medicine*, 49(SUPPL.6).

Kropveld, A., Slootweg, P.J., Blankenstein, M.A., Terhaard, C.H.J. & Hordijk, G.J., 1998, Ki-67 and p53 in T2 laryngeal cancer, *The laryngoscope*, 108(10), pp. 1548-52.

Kunkel, M., Förster, G.J., Reichert, T.E., Kutzner, J., Benz, P., Bartenstein, P. & Wagner, W., 2003, Radiation response non-invasively imaged by [18F]FDG-PET predicts local tumor control and survival in advanced oral squamous cell carcinoma, *Oral Oncology*, 39(2), pp. 170-7.

Larsson, P., Roos, G., Stenling, R. & Ljungberg, B., 1993, Tumor-cell proliferation and prognosis in renal-cell carcinoma, *International Journal of Cancer*, 55(4), pp. 566-70.

Lee, Y., Auh, S.L., Wang, Y., Burnette, B., Wang, Y., Meng, Y., Beckett, M., Sharma, R., Chin, R., Tu, T., Weichselbaum, R.R. & Fu, Y.X., 2009, Therapeutic effects of ablative radiation on local tumor require CD8+ T cells: changing strategies for cancer treatment, *Blood*, 114(3), pp. 589-95.

Ljungkvist, A.S.E., Bussink, J., Kaanders, J.H.A.M., Rijken, P.F.J.W., Begg, A.C., Raleigh, J.A. & Van Der Kogel, A.J., 2005, Hypoxic cell turnover in different solid tumor lines, *International Journal of Radiation Oncology Biology Physics*, 62(4), pp. 1157-68.

Ljungkvist, A.S.E., Bussink, J., Kaanders, J.H.A.M., Wiedenmann, N.E., Vlasman, R. & Van Der Kogel, A.J., 2006, Dynamics of hypoxia, proliferation and apoptosis after irradiation in a murine tumor model, *Radiation Research*, 165(3), pp. 326-36.

Luk, C.K., Keng, P.C. & Sutherland, R.M., 1985, Regrowth and radiation sensitivity of quiescent cells isolated from EMT6/Ro-fed plateau monolayers, *Cancer Res*, 45(3), pp. 1020-5.

Machtay, M., Natwa, M., Andrel, J., Hyslop, T., Anne, P.R., Lavarino, J., Intenzo, C.M. & Keane, W., 2009, Pretreatment FDG-PET standardized uptake value as a prognostic factor for outcome in head and neck cancer, *Head and Neck*, 31(2), pp. 195-201.

Mac Manus, M.P., Hicks, R.J., Matthews, J.P., McKenzie, A., Rischin, D., Salminen, E.K. & Ball, D.L., 2003, Positron emission tomography is superior to computed tomography scanning for response-assessment after radical radiotherapy or chemoradiotherapy in patients with non-small-cell lung cancer, *Journal of Clinical Oncology*, 21(7), pp. 1285-92.

Mac Manus, M.P., Hicks, R.J., Matthews, J.P., Wirth, A., Rischin, D. & Ball, D.L., 2005, Metabolic (FDG-PET) response after radical radiotherapy/chemoradiotherapy for non-small cell lung cancer correlates with patterns of failure, *Lung cancer (Amsterdam, Netherlands)*, 49(1), pp. 95-108.

Madani, I., Duthoy, W., Derie, C., De Gersem, W., Boterberg, T., Saerens, M., Jacobs, F., Grégoire, V., Lonneux, M., Vakaet, L., Vanderstraeten, B., Bauters, W., Bonte, K., Thierens, H. & De Neve, W., 2007a, Positron emission tomography-guided, focal-dose escalation using intensity-modulated radiotherapy for head and neck cancer, *International journal of radiation oncology, biology, physics*, 68(1), pp. 126-35.

Madani, I., Duthoy, W., Derie, C., De Gersem, W., Boterberg, T., Saerens, M., Jacobs, F., Grégoire, V., Lonneux, M., Vakaet, L., Vanderstraeten, B., Bauters, W., Bonte, K., Thierens, H. & De Neve, W., 2007b, Positron Emission Tomography-Guided, Focal-Dose Escalation Using Intensity-Modulated Radiotherapy for Head and Neck Cancer, *International Journal of Radiation Oncology Biology Physics*, 68(1), pp. 126-35.

Madoc-Jones, H., 1964, Variations in radiosensitivity of a mammalian cell line with phase of the growth cycle, .

Martinive, P., Defresne, F., Bouzin, C., Saliez, J., Lair, F., Grégoire, V., Michiels, C., Dessy, C. & Feron, O., 2006, Preconditioning of the tumor vasculature and tumor cells by intermittent hypoxia: Implications for anticancer therapies, *Cancer Research*, 66(24), pp. 11736-44.

Marusic, M., Bajzer, Z., Freyer, J.P. & Vuk-Pavlovic, S., 1994, Analysis of growth of multicellular tumour spheroids by mathematical models, *Cell Proliferation*, 27(2), pp. 73-94.

Marusyk, A. & Polyak, K., 2009, Tumor heterogeneity: Causes and consequences, *Biochimica et Biophysica Acta - Reviews on Cancer*.

McAneney, H. & O'Rourke, S.F.C., 2007, Investigation of various growth mechanisms of solid tumour growth within the linear-quadratic model for radiotherapy, *Physics in Medicine and Biology*, 52(4), pp. 1039-54.

Mehta, M., Scrimger, R., Mackie, R., Paliwal, B., Chappell, R. & Fowler, J., 2001, A new approach to dose escalation in non-small-cell lung cancer, *International journal of radiation oncology, biology, physics*, 49(1), pp. 23-33.

Michiels, S., Le Maître, A., Buyse, M., Burzykowski, T., Maillard, E., Bogaerts, J., Vermorken, J.B., Budach, W., Pajak, T.F., Ang, K.K., Bourhis, J. & Pignon, J.P., 2009, Surrogate endpoints for overall survival in locally advanced head and neck cancer: meta-analyses of individual patient data, *The Lancet Oncology*, 10(4), pp. 341-50.

Minn, H., Lapela, M., Klemi, P.J., Grénman, R., Leskinen, S., Lindholm, P., Bergman, J., Eronen, E., Haaparanta, M. & Joensuu, H., 1997, Prediction of survival with fluorine-18-fluorodeoxyglucose and PET in head and neck cancer, *Journal of Nuclear Medicine*, 38(12), pp. 1907-11.

Müller, W., Schneiders, A., Meier, S., Hommel, G. & Gabbert, H.E., 1996, Immunohistochemical study on the prognostic value of MIB-1 in gastric carcinoma, *British Journal of Cancer*, 74(5), pp. 759-65.

Nahum, A.E., Movsas, B., Horwitz, E.M., Stobbe, C.C. & Chapman, J.D., 2003, Incorporating clinical measurements of hypoxia into tumor local control modeling of prostate cancer: Implications for the Î±/Î² ratio, *International Journal of Radiation Oncology Biology Physics*, 57(2), pp. 391-401.

Niemierko, A. & Goitein, M., 1993, Implementation of a model for estimating tumor control probability for an inhomogeneously irradiated tumor, *Radiotherapy and Oncology*, 29(2), pp. 140-7.

Nilsson, J., Lind, B.K. & Brahme, A., 2002, Radiation response of hypoxic and generally heterogeneous tissues, *International Journal of Radiation Biology*, 78(5), pp. 389-405.

Norton, L., 1988, A Gompertzian model of human breast cancer growth, *Cancer Research*, 48(24 I), pp. 7067-71.

O'Donoghue, J.A., 1997, The response of tumours with Gompertzian growth characteristics to fractionated radiotherapy, *International Journal of Radiation Biology*, 72(3), pp. 325-39.

Padhani, A., 2006, PET imaging of tumour hypoxia, *Cancer imaging : the official publication of the International Cancer Imaging Society*, 6.

Palcic, B. & Skarsgard, L.D., 1984, Reduced oxygen enhancement ratio at low doses of ionizing radiation, *Radiat Res*, 100(2), pp. 328-39.

Petit, S.F., Dekker, A.L., Seigneuric, R., Murrer, L., van Riel, N.A., Nordsmark, M., Overgaard, J., Lambin, P. & Wouters, B.G., 2009, Intra-voxel heterogeneity influences the dose prescription for dose-painting with radiotherapy: a modelling study, *Physics in medicine and biology*, 54(7), pp. 2179-96.

Pich, A., Chiusa, L. & Navone, R., 2004, Prognostic relevance of cell proliferation in head and neck tumors, *Annals of oncology : official journal of the European Society for Medical Oncology / ESMO*, 15(9), pp. 1319-29.

Popple, R.A., Ove, R. & Shen, S., 2002, Tumor control probability for selective boosting of hypoxic subvolumes, including the effect of reoxygenation, *International Journal of Radiation Oncology Biology Physics*, 54(3), pp. 921-7.

Pugachev, A., Ruan, S., Carlin, S., Larson, S.M., Campa, J., Ling, C.C. & Humm, J.L., 2005, Dependence of FDG uptake on tumor microenvironment, *International Journal of Radiation Oncology Biology Physics*, 62(2), pp. 545-53.

Quiet, C.A., Weichselbaum, R.R. & Grdina, D.J., 1991, Variation in radiation sensitivity during the cell cycle of two human squamous cell carcinomas, *International journal of radiation oncology, biology, physics*, 20(4), pp. 733-8.

Rajendran, J.G., Mankoff, D.A., O'Sullivan, F., Peterson, L.M., Schwartz, D.L., Conrad, E.U., Spence, A.M., Muzi, M., Farwell, D.G. & Krohn, K.A., 2004, Hypoxia and Glucose Metabolism in Malignant Tumors: Evaluation by [18F]Fluoromisonidazole and [18F]]Fluorodeoxyglucose Positron Emission Tomography Imaging, *Clinical Cancer Research*, 10(7), pp. 2245-52.

Rajendran, J.G., Schwartz, D.L., O'Sullivan, J., Peterson, L.M., Ng, P., Scharnhorst, J., Grierson, J.R. & Krohn, K.A., 2006, Tumor hypoxia imaging with [F-18] fluoromisonidazole positron emission tomography in head and neck cancer, *Clinical Cancer Research*, 12(18), pp. 5435-41.

Raybaud, H., Fortin, A., Bairati, I., Morency, R., Monteil, R.A. & Têtu, B., 2000, Nuclear DNA content, an adjunct to p53 and Ki-67 as a marker of resistance to radiation therapy in oral cavity and pharyngeal squamous cell carcinoma, *Int J Oral Maxillofac Surg*, 29(1), pp. 36-41.

Révész, L. & Palcic, B., 1985, Radiation dose dependence of the sensitization by oxygen and oxygen mimic sensitizers, *Acta radiologica. Oncology*, 24(3), pp. 209-17.

Roh, J.L., Pae, K.H., Choi, S.H., Kim, J.S., Lee, S., Kim, S.B., Nam, S.Y. & Kim, S.Y., 2007, 2-[18F]-Fluoro-2-deoxy-d-glucose positron emission tomography as guidance for primary treatment in patients with advanced-stage resectable squamous cell carcinoma of the larynx and hypopharynx, *European Journal of Surgical Oncology*, 33(6), pp. 790-5.

Roose, T., Chapman, S.J. & Maini, P.K., 2007, Mathematical models of avascular tumor growth, *SIAM Review*, 49(2), pp. 179-208.

Rothkamm, K., Kruger, I., Thompson, L.H. & Lobrich, M., 2003, Pathways of DNA double-strand break repair during the mammalian cell cycle, *Molecular and cellular biology*, 23(16), p. 5706.

Roti Roti, J.L. & Dethlefsen, L.A., 1975a, Matrix simulation of duodenal crypt cell kinetics. I. The steady state, *Cell Tissue Kinet*, 8(4), pp. 321-33.

Roti Roti, J.L. & Dethlefsen, L.A., 1975b, Matrix simulation of duodenal crypt cell kinetics. II. Cell kinetics following hydroxyurea, *Cell Tissue Kinet*, 8(4), pp. 335-53.

Sakata, K.I., Oouchi, A., Nagakura, H., Akiba, H., Tamakawa, M., Koito, K., Hareyama, M., Asakura, K., Satoh, M. & Ohtani, S., 2000, Accelerated radiotherapy for T1, 2 glottic carcinoma: Analysis of results with KI-67 index, *International Journal of Radiation Oncology Biology Physics*, 47(1), pp. 81-8.

Sanchez-Nieto, B. & Nahum, A.E., 1999, The delta-TCP concept: A clinically useful measure of tumor control probability, *International Journal of Radiation Oncology Biology Physics*, 44(2), pp. 369-80.

Sanchez-Nieto, B. & Nahum, A.E., 2000, Bioplan: Software for the biological evaluation of radiotherapy treatment plans, *Medical Dosimetry*, 25(2), pp. 71-6.

Sasaki, R., Komaki, R., Macapinlac, H., Erasmus, J., Allen, P., Forster, K., Putnam, J.B., Herbst, R.S., Moran, C.A., Podoloff, D.A., Roth, J.A. & Cox, J.D., 2005, [18F]fluorodeoxyglucose uptake by positron emission tomography predicts outcome of non-small-cell lung cancer, *Journal of Clinical Oncology*, 23(6), pp. 1136-43.

Schultheiss, T.E., Orton, C.G. & Peck, R.A., 1983, Models in radiotherapy: Volume effects, *Medical Physics*, 10(4), pp. 410-5.

Schwartz, D.L., Rajendran, J., Yueh, B., Coltrera, M.D., LeBlanc, M., Eary, J. & Krohn, K., 2004, FDG-PET prediction of head and neck squamous cell cancer outcomes, *Archives of Otolaryngology - Head and Neck Surgery*, 130(12), pp. 1361-7.

Schwarz, J.K., Siegel, B.A., Dehdashti, F. & Grigsby, P.W., 2007, Association of posttherapy positron emission tomography with tumor response and survival in cervical carcinoma, *Journal of the American Medical Association*, 298(19), pp. 2289-95.

Scigliano, S., Pinel, S., Poussier, S., Fouyssac, F., Plenat, F., Karcher, G. & Chastagner, P., 2008, Measurement of hypoxia using invasive oxygen-sensitive electrode, pimonidazole binding and 18F-FDG uptake in anaemic or erythropoietin-treated mice bearing human glioma xenografts, *International journal of oncology*, 32(1), pp. 69-77.

Semenza, G.L., 2003, Targeting HIF-1 for cancer therapy, *Nature Reviews Cancer*, 3(10), pp. 721-32.

Semenza, G.L., 2008, Tumor metabolism: Cancer cells give and take lactate, *Journal of Clinical Investigation*, 118(12), pp. 3835-7.

Shibamoto, Y., Ike, O., Mizuno, H., Fukuse, T., Hitomi, S. & Takahashi, M., 1998, Proliferative activity and micronucleus frequency after radiation of lung cancer cells as assessed by the cytokinesis-block method and their relationship to clinical outcome, *Clinical cancer research : an official journal of the American Association for Cancer Research*, 4(3), pp. 677-82.

Shields, A.F., Grierson, J.R., Dohmen, B.M., Machulla, H.J., Stayanoff, J.C., Lawhorn-Crews, J.M., Obradovich, J.E., Muzik, O. & Mangner, T.J., 1998, Imaging proliferation in vivo with [F-18]FLT and positron emission tomography, *Nature Medicine*, 4(11), pp. 1334-6.

Sinclair, W.K. & Morton, R.A., 1966, X-ray sensitivity during the cell generation cycle of cultured Chinese hamster cells, *Radiat Res*, 29(3), pp. 450-74.

Skarsgard, L.D. & Harrison, I., 1991, Dose Dependence of the Oxygen Enhancement Ratio (OER) in Radiation Inactivation of Chinese Hamster V79-171 Cells, *Radiation Research*, 127(3), pp. 243-7.

Sonveaux, P., Végran, F., Schroeder, T., Wergin, M.C., Verrax, J., Rabbani, Z.N., De Saedeleer, C.J., Kennedy, K.M., Diepart, C., Jordan, B.F., Kelley, M.J., Gallez, B., Wahl, M.L., Feron, O. & Dewhirst, M.W., 2008, Targeting lactate-fueled respiration selectively kills hypoxic tumor cells in mice, *Journal of Clinical Investigation*, 118(12), pp. 3930-42.

Soto, D.E., Kessler, M.L., Piert, M. & Eisbruch, A., 2008, Correlation between pretreatment FDG-PET biological target volume and anatomical location of failure after radiation therapy for head and neck cancers, *Radiotherapy and Oncology*, 89(1), pp. 13-8.

South, C.P., Partridge, M. & Evans, P.M., 2008, A theoretical framework for prescribing radiotherapy dose distributions using patient-specific biological information, *Medical Physics*, 35(10), pp. 4599-611.

Stavreva, N.A., Stavrev, P.V., Warkentin, B. & Fallone, B.G., 2003, Investigating the effect of cell repopulation on the tumor response to fractionated external radiotherapy, *Medical Physics*, 30(5), pp. 735-42.

Steel, G.G., 1977, *Growth kinetics of tumours : Cell population kinetics in relation to the growth and treatment of cancer,* Clarendon Press, Oxford.

Suit, H., Skates, S., Taghian, A., Okunieff, P. & Efird, J.T., 1992, Clinical implications of heterogeneity of tumor response to radiation therapy, *Radiotherapy and Oncology*, 25(4), pp. 251-60.

Sura, S., Greco, C., Gelblum, D., Yorke, E.D., Jackson, A. & Rosenzweig, K.E., 2008, 18F-Fluorodeoxyglucose Positron Emission Tomography-Based Assessment of Local Failure Patterns in Non-Small-Cell Lung Cancer Treated With Definitive Radiotherapy, *International Journal of Radiation Oncology Biology Physics*, 70(5), pp. 1397-402.

Søvik, Malinen, E., Bruland, S., Bentzen, S.M. & Olsen, D.R., 2007, Optimization of tumour control probability in hypoxic tumours by radiation dose redistribution: A modelling study, *Physics in Medicine and Biology*, 52(2), pp. 499-513.

Thames, H.D., Bentzen, S.M., Turesson, I., Overgaard, M. & Van den Bogaert, W., 1990, Time-dose factors in radiotherapy: A review of the human data, *Radiotherapy and Oncology*, 19(3), pp. 219-35.

Thorwarth, D., Eschmann, S.M., Paulsen, F. & Alber, M., 2007, Hypoxia Dose Painting by Numbers: A Planning Study, *International Journal of Radiation Oncology Biology Physics*, 68(1), pp. 291-300.

Thorwarth, D., Eschmann, S.M., Scheiderbauer, J., Paulsen, F. & Alber, M., 2005, Kinetic analysis of dynamic 18F-fluoromisonidazole PET correlates with radiation treatment outcome in head-and-neck cancer, *BMC Cancer*, 5.

Thorwarth, D., Soukup, M. & Alber, M., 2008, Dose painting with IMPT, helical tomotherapy and IMXT: A dosimetric comparison, *Radiotherapy and Oncology*, 86(1), pp. 30-4.

Timmerman, R., Papiez, L., McGarry, R., Likes, L., DesRosiers, C., Frost, S. & Williams, M., 2003, Extracranial stereotactic radioablation: results of a phase I study in medically inoperable stage I non-small cell lung cancer, *Chest*, 124(5), pp. 1946-55.

Tinnemans, M.M., Schutte, B., Lenders, M.H., Ten Velde, G.P., Ramaekers, F.C. & Blijham, G.H., 1993, Cytokinetic analysis of lung cancer by in vivo bromodeoxyuridine labelling, *British journal of cancer*, 67(6), pp. 1217-22.

Titz, B. & Jeraj, R., 2008, An imaging-based tumour growth and treatment response model: Investigating the effect of tumour oxygenation on radiation therapy response, *Physics in Medicine and Biology*, 53(17), pp. 4471-88.

Tomé, W.A. & Fowler, J.F., 2000, Selective boosting of tumor subvolumes, *International Journal of Radiation Oncology Biology Physics*, 48(2), pp. 593-9.

Tomé, W.A. & Fowler, J.F., 2003, On the inclusion of proliferation in tumour control probability calculations for inhomogeneously irradiated tumours, *Physics in Medicine and Biology*, 48(18).

Torizuka, T., Tanizaki, Y., Kanno, T., Futatsubashi, M., Naitou, K., Ueda, Y. & Ouchi, Y., 2009, Prognostic Value of l8F-FDG PET in patients with head and neck squamous cell cancer, *American Journal of Roentgenology*, 192(4).

Travis, E.L. & Tucker, S.L., 1987, Isoeffect models and fractionated radiation therapy, *International Journal of Radiation Oncology Biology Physics*, 13(2), pp. 283-7.

Tubiana, M., 1989, Tumor cell proliferation kinetics and tumor growth rate, *Acta Oncologica*, 28(1), pp. 113-21.

Tucker, S.L., Thames, H.D. & Taylor, J.M.G., 1990, How well is the probability of tumor cure after fractionated irradiation described by poisson statistics? *Radiation Research*, 124(3), pp. 273-82.

Valera, V., Yokoyama, N., Walter, B., Okamoto, H., Suda, T. & Hatakeyama, K., 2005, Clinical significance of Ki-67 proliferation index in disease progression and prognosis of patients with resected colorectal carcinoma, *British Journal of Surgery*, 92(8), pp. 1002-7.

van Baardwijk, A., Baumert, B.G., Bosmans, G., van Kroonenburgh, M., Stroobants, S., Gregoire, V., Lambin, P. & De Ruysscher, D., 2006, The current status of FDG-PET in tumour volume definition in radiotherapy treatment planning, *Cancer Treatment Reviews*, 32(4), pp. 245-60.

van Baardwijk, A., Dooms, C., van Suylen, R.J., Verbeken, E., Hochstenbag, M., Dehing-Oberije, C., Rupa, D., Pastorekova, S., Stroobants, S., Buell, U., Lambin, P., Vansteenkiste, J. & Ruysscher, D.D., 2007, The maximum uptake of 18F-deoxyglucose on positron emission tomography scan correlates with survival, hypoxia inducible factor-1α and GLUT-1 in non-small cell lung cancer, *European Journal of Cancer*, 43(9), pp. 1392-8.

Vanderstraeten, B., Duthoy, W., Gersem, W.D., Neve, W.D. & Thierens, H., 2006, [18F]fluoro-deoxy-glucose positron emission tomography ([18F]FDG-PET) voxel intensity-based intensity-modulated radiation therapy (IMRT) for head and neck cancer, *Radiotherapy and Oncology*, 79(3), pp. 249-58.

van Loon, J., Grutters, J., Wanders, R., Boersma, L., Oellers, M., Dingemans, A.M., Bootsma, G., Geraedts, W., Pitz, C., Simons, J., Fatah, S.A., Snoep, G., Hochstenbag, M., Lambin, P. & De Ruysscher, D., 2009, Follow-up with 18FDG-PET-CT after radical radiotherapy with or without chemotherapy allows the detection of potentially curable progressive disease in non-small cell lung cancer patients: A prospective study, *European Journal of Cancer*, 45(4), pp. 588-95.

Vansteenkiste, J.F., Stroobants, S.G., Dupont, P.J., De Leyn, P.R., Verbeken, E.K., Deneffe, G.J., Mortelmans, L.A. & Demedts, M.G., 1999, Prognostic importance of the standardized uptake value on 18F-fluoro- 2-deoxy-glucose-positron emission tomography scan in non-small-cell lung cancer: An analysis of 125 cases, *Journal of Clinical Oncology*, 17(10), pp. 3201-6.

Varia, M.A., Calkins-Adams, D.P., Rinker, L.H., Kennedy, A.S., Novotny, D.B., Fowler Jr, W.C. & Raleigh, J.A., 1998, Pimonidazole: A novel hypoxia marker for complementary study of tumor hypoxia and cell proliferation in cervical carcinoma, *Gynecologic Oncology*, 71(2), pp. 270-7.

Vaupel, P. & Mayer, A., 2007, Hypoxia in cancer: Significance and impact on clinical outcome, *Cancer and Metastasis Reviews*, 26(2), pp. 225-39.

Vesselle, H., Freeman, J.D., Wiens, L., Stern, J., Nguyen, H.Q., Hawes, S.E., Bastian, P., Salskov, A., Vallières, E. & Wood, D.E., 2007, Fluorodeoxyglucose uptake of primary non-small cell lung cancer at positron emission tomography: New contrary data on prognostic role, *Clinical Cancer Research*, 13(11), pp. 3255-63.

Vesselle, H., Salskov, A., Turcotte, E., Wiens, L., Schmidt, R., Jordan, C.D., Vallières, E. & Wood, D.E., 2008, Relationship between non-small cell lung cancer FDG uptake at PET, tumor histology, and Ki-67 proliferation index, *Journal of Thoracic Oncology*, 3(9), pp. 971-8.

Vesselle, H., Schmidt, R.A., Pugsley, J.M., Li, M., Kohlmyer, S.G., Vallieres, E. & Wood, D.E., 2000, Lung cancer proliferation correlates with [F-18]fluorodeoxyglucose uptake by positron emission tomography, *Clinical Cancer Research*, 6(10), pp. 3837-44.

Viberti, L., Papotti, M., Abbona, G.C., Celano, A., Filosso, P.L. & Bussolati, G., 1997, Value of Ki-67 immunostaining in preoperative biopsies of carcinomas of the lung, *Human Pathology*, 28(2), pp. 189-92.

Volm, M., Mattern, J., Sonka, J., Vogt-Schaden, M. & Wayss, K., 1985, DNA distribution in non-small-cell lung carcinomas and its relationship to clinical behavior, *Cytometry*, 6(4), pp. 348-56.

Wallen, C.A., Ridinger, D.N. & Dethlefsen, L.A., 1985, Heterogeneity of X-ray cytotoxicity in proliferating and quiescent murine mammary carcinoma cells, *Cancer Res*, 45(7), pp. 3064-9.

Wang, J.Z., Li, X.A. & Mayr, N.A., 2006, Dose escalation to combat hypoxia in prostate cancer: A radiobiological study on clinical data, *British Journal of Radiology*, 79(947), pp. 905-11.

Wang, W., Georgi, J.C., Nehmeh, S.A., Narayanan, M., Paulus, T., Bal, M., O'Donoghue, J., Zanzonico, P.B., Schmidtlein, C.R., Lee, N.Y. & Humm, J.L., 2009, Evaluation of a compartmental model for estimating tumor hypoxia via FMISO dynamic PET imaging, *Physics in Medicine and Biology*, 54(10), pp. 3083-99.

Warburg, O., 1956, On the origin of cancer cells, *Science*, 123(3191), pp. 309-14.

Webb, S. & Nahum, A.E., 1993, A model for calculating tumour control probability in radiotherapy including the effects of inhomogeneous distributions of dose and clonogenic cell density, *Physics in Medicine and Biology*, 38(6), pp. 653-66.

Webb, S., Evans, P.M., Swindell, W. & Deasy, J.O., 1994, A proof that uniform dose gives the greatest TCP for fixed integral dose in the planning target volume, *Physics in Medicine and Biology*, 39(11), pp. 2091-8.

West, C.M.L., Keng, P.C. & Sutherland, R.M., 1988, Growth phase related variation in the radiation sensitivity of human colon adenocarcinoma cells, *International Journal of Radiation Oncology* Biology* Physics*, 14(6), pp. 1213-9.

Wijffels, K.I., Marres, H.A., Peters, J.P., Rijken, P.F., van der Kogel, A.J. & Kaanders, J.H., 2008, Tumour cell proliferation under hypoxic conditions in human head and neck squamous cell carcinomas, *Oral Oncol*, 44(4), pp. 335-44.

Wilson, G.D., Saunders, M.I., Dische, S., Daley, F.M., Buffa, F.M., Richman, P.I. & Bentzen, S.M., 2006, Pre-treatment proliferation and the outcome of conventional and accelerated radiotherapy, *European Journal of Cancer*, 42(3), pp. 363-71.

Withers, H.R., Taylor, J.M.G. & Maciejewski, B., 1988, The hazard of accelerated tumor clonogen repopulation during radiotherapy, *J Acta Oncologica*, 27(2), pp. 131-46.

Wouters, B.G. & Brown, J.M., 1997, Cells at intermediate oxygen levels can be more important than the "hypoxic fraction" in determining tumor response to fractionated radiotherapy, *Radiat Res*, 147(5), pp. 541-50.

Xie, P., Yue, J.B., Zhao, H.X., Sun, X.D., Kong, L., Fu, Z. & Yu, J.M., 2009, Prognostic value of 18F-FDG PET-CT metabolic index for nasopharyngeal carcinoma, *Journal of Cancer Research and Clinical Oncology*, pp. 1-7.

Xue, F., Lin, L.L., Dehdashti, F., Miller, T.R., Siegel, B.A. & Grigsby, P.W., 2006, F-18 fluorodeoxyglucose uptake in primary cervical cancer as an indicator of prognosis after radiation therapy, *Gynecologic Oncology*, 101(1), pp. 147-51.

Yamamoto, Y., Nishiyama, Y., Ishikawa, S., Nakano, J., Chang, S.S., Bandoh, S., Kanaji, N., Haba, R., Kushida, Y. & Ohkawa, M., 2007, Correlation of 18F-FLT and 18F-FDG uptake on PET with Ki-67 immunohistochemistry in non-small cell lung cancer, *European Journal of Nuclear Medicine and Molecular Imaging*, 34(10), pp. 1610-6.

Zaider, M. & Minerbo, G.N., 2000, Tumour control probability: A formulation applicable to any temporal protocol of dose delivery, *Physics in Medicine and Biology*, 45(2), pp. 279-93.

Zhong, X., Yu, J., Zhang, B., Mu, D., Zhang, W., Li, D., Han, A., Song, P., Li, H., Yang, G., Kong, F.M. & Fu, Z., 2009, Using 18F-Fluorodeoxyglucose Positron Emission Tomography to Estimate the Length of Gross Tumor in Patients With Squamous Cell Carcinoma of the Esophagus, *International Journal of Radiation Oncology Biology Physics*, 73(1), pp. 136-41.

Zimny, M., Gagel, B., DiMartino, E., Hamacher, K., Coenen, H.H., Westhofen, M., Eble, M., Buell, U. & Reinartz, P., 2006, FDG - A marker of tumour hypoxia? A comparison with [18F] fluoromisonidazole and pO2-polarography in metastatic head and neck cancer, *European Journal of Nuclear Medicine and Molecular Imaging*, 33(12), pp. 1426-31.

Zips, D. 2009, Tumor growth and response to radiation, in M Joiner & A van der Kogel (eds), *Basic clinical radiobiology,* Hodder Arnold, London,.

Zölzer, F. & Streffer, C., 2002, Increased radiosensitivity with chronic hypoxia in four human tumor cell lines, *International journal of radiation oncology, biology, physics*, 54(3), pp. 910-20.

VITA

Jeho Jeong was born in Anyang, South Korea, on March 30th, 1977. After graduating from Shinsung high school in Anyang, he was further educated at the Hanyang University in Seoul, S. Korea, where he received a Bachelor of Science in Nuclear Engineering in February 2003 and a Master of Science in Nuclear Engineering in February 2005. After receiving a Doctor of Philosophy in Nuclear Engineering at the University of Missouri - Columbia in May 2012, he will be joining the Memorial Sloan-Kettering Cancer Center in New York as a postdoctoral researcher, where his dissertation advisor, Dr. Deasy, is employed as a chair of the medical physics department.